

# Optimizing Range Aware Localization in Wireless Sensor Networks (WSNs)

by

Hemat Kumar Maheshwari

Submitted in accordance with the requirements for the degree of  
Doctor of Philosophy

The University of Leeds  
School of Electronic and Electrical Engineering

June, 2011

The candidate confirms that the work submitted is his own and that appropriate credit has been given where reference has been made to the work of others.

The copy has been supplied on the understanding that it is copyright material and that no quotation from the thesis may be published without proper acknowledgement.

# Acknowledgements

Like any research project, this work would not have been possible without the great support of my supervisor Dr. Andrew Kemp. I owe deepest gratitude to him for his contagious assistance and regular supervision meetings, which provided me the freedom to explore the new ideas. I would like to thank Prof. JMH Elmirghani and Dr. Ian Glover for their constructive feedback towards my research. I appreciate Colin Faulkner and Ivan Lawrow from NXP (Jennic) Ltd for their support during this research.

My four years at University of Leeds were simply remarkable and for that I would like to thank my WSN research group members. It was great to share my setbacks and successes with friends inside and outside the professional environment. I also extend my thanks to Mrs. A De Jong for her friendly assistance and making things simpler.

Here, I would mention one person whose care and encouragement made my restless days and weekends simple and easy during the whole period of my research, my wife Raj Kumari. Thank you so much Raj, especially for your thoughtful attitude, delicious cooking, and wonderful company during all the trips and above all your trust and patience provided me a constant source of motivation.

Finally, I would especially like to thank my dearest grandparents, Dad and Mom for their endless support, blessings and teaching me values that are precious, irrespective of time and place. Special thanks and love to my brothers, sisters and in-laws for their encouragement and well wishes. They provide a constant source of motivation in my life.

*To My Beautiful Mom & Dad*

*&*

*lovely wife Raj Kumari.*

***Thanks for such a wonderful family!***

# Abstract

The adoption of wireless sensor networks (WSNs) in numerous emerging applications have prevailed us to realize that *smart living is no longer an imagination, it already exists*. In emerging applications, localization is an essential function so that all the sensed information can be responded carefully. Among the range free and range aware localization, range aware localization has been the most promising for fine-grained accuracy. Range aware localization has two phases, ranging and localization. Location errors always exist no matter which ranging or localization technique is used. Therefore, there is a need to optimize range aware localization for better performance.

Firstly, this thesis investigates the performance of time-of-flight (ToF) and received signal strength (RSS) based ranging using IEEE 802.15.4 compliant WSNs nodes in outdoor and indoor for both line-of-sight (LOS) and non-line-of-sight (NLOS) paths. The fundamental Cramér-Rao lower bound (CRLB) on ToF and RSS ranging performance is compared with the performance limits of IEEE 802.15.4 compliant modules. The experimental results for both outdoor and indoor LOS path demonstrated that RSS is a good candidate for range estimation at ranges less than 7m. Further analysis over long range demonstrates that ToF is a good candidate for range estimation at greater than 7m.

In addition to the ranging error, another well-known error mechanism is the poor geometric anchors placement, which can significantly degrade localization performance. In the Global Positioning System (GPS) community, geometric dilution of precision (GDOP) is a well-known problem which illustrates the geometric configuration impacting localization accuracy. To analyse the impact of anchor placement

on localization, performance of three lateration based approaches is compared in a cooperative fashion. Through results, It is confirmed that lateration based approaches presents a trade-off for complex computation, thus energy consumption and accuracy. It provided the needed motivation to investigate and optimize the anchor placement for better localization accuracy. The impact of anchor placement for quality reliable localization has been limited to 3-4 anchors with respect to a single subject node for 2-D. Therefore, to model reality most clearly, it makes sense to step beyond the easy and secure reach of unrealistic and mostly researched 2-dimensional representations to the pragmatic world in 3-dimensional visualization. In addition, previous work for optimal anchors placement has been limited to only additive noise. To the best of our knowledge, there is no study of optimization of anchor placement with respect to the multiplicative noise. Therefore, the optimal anchor placements are determined for both signal models based on minimum mean CRLB (m-CRLB). It is confirmed that optimal anchor placement for both signal models is different and have a serious impact on localization accuracy. The optimal anchor placement is further verified by developing a new Range Aware Localization System (RALS) using IEEE 802.15.4 compliant devices.

In LOS, quality reliable localization performance can be achieved but as propagation criteria change from LOS to NLOS, localization performance also changes. In an indoor environment, localization performance degrades significantly due to multipath components. To overcome, a new 3-D scheme named *Range Estimate Threshold* (RET) is proposed which exploits field dimensions based on the signal model and optimal anchor placement to define a *threshold*. Based on the defined threshold, RET mitigates the poor range estimates from *Measured Estimation* (ME) for better localization accuracy. The ramification of RET on ME is explored through additive, multiplicative and log-normal shadowing models. It is confirmed that localization based on RET compared to ME showed improved accuracy.

# Contents

Acknowledgements	i
Dedication	ii
Abstract	iii
List of Figures	xi
List of Tables	xxii
Abbreviations	xxiii
Symbols	xxvii
<b>1 Introduction</b>	<b>1</b>
1.1 Introduction . . . . .	1
1.2 Localization for Wireless Sensor Networks . . . . .	3
1.3 Scope and Motivations . . . . .	4
1.4 Contributions of the Dissertation . . . . .	9
1.5 Outline of the Dissertation . . . . .	10
1.6 Publications . . . . .	13
<b>2 Background and Related Work</b>	<b>15</b>
2.1 Introduction . . . . .	15
2.2 Localization in WSNs . . . . .	16
2.3 Classification of Localization . . . . .	17
2.3.1 Range Estimation Phase . . . . .	17

## CONTENTS

---

2.3.1.1	Angle of Arrival (AoA) . . . . .	17
2.3.1.2	Complexity and Error Concerns using AoA . . . . .	18
2.3.1.3	Time Difference of Arrival (TDoA) . . . . .	18
2.3.1.4	Time of Flight (ToF) . . . . .	19
2.3.1.5	Received Signal Strength (RSS) . . . . .	19
2.3.2	Position Computation Phase . . . . .	21
2.3.3	Localization Algorithms . . . . .	21
2.4	Localization Techniques and Optimization . . . . .	26
2.4.1	Maximum Likelihood algorithm (ML) . . . . .	28
2.4.2	Approximate Maximum Likelihood algorithm (AML) . . . . .	29
2.5	Performance metric . . . . .	30
2.5.1	Accuracy . . . . .	30
2.5.2	Precision . . . . .	31
2.5.3	Complexity . . . . .	31
2.5.4	Robustness . . . . .	33
2.5.5	Scalability . . . . .	33
2.5.6	Cost . . . . .	33
2.6	Localization Systems . . . . .	33
2.6.1	Active Badge, 1992 . . . . .	33
2.6.2	Active Bat, 1999 . . . . .	34
2.6.3	Cricket, 2000 . . . . .	34
2.6.4	RADAR, 2000 . . . . .	35
2.6.5	Horus, 2005 . . . . .	35
2.6.6	SpotON, 2001 . . . . .	35
2.7	Applications . . . . .	35
2.7.1	Kid-Spotter . . . . .	36
2.7.2	Freight containers Positioning . . . . .	36
2.7.3	Asset Tracking and Management . . . . .	36
2.7.4	Aid to fire-fighters and police . . . . .	37
2.7.5	Detecting and Locating Radiation Levels . . . . .	37
2.7.6	Smart and Interactive Gaming . . . . .	37
2.7.7	Habitat Monitoring and Wildlife Tracking . . . . .	37
2.8	Conclusion . . . . .	38

## CONTENTS

---

<b>3</b>	<b>Performance Analysis of Ranging with IEEE 802.15.4 Compliant WSN Devices</b>	<b>39</b>
3.1	Overview . . . . .	39
3.2	Introduction . . . . .	40
3.3	Sources of Ranging Error . . . . .	42
3.3.1	Systematic Parameter . . . . .	42
3.3.2	Radio Propagation . . . . .	43
3.3.2.1	Large Scale Fading Models . . . . .	43
3.3.3	Small Scale Fading Models . . . . .	44
3.3.3.1	Effect of Frequency Channel on Multipath Performance . . . . .	45
3.3.4	Thermal Noise . . . . .	46
3.4	Experimental Infrastructure . . . . .	47
3.4.1	Antenna Models . . . . .	48
3.4.1.1	Integrated Folded Mono-pole Antenna . . . . .	49
3.4.2	Experimental Setup for Ranging . . . . .	49
3.4.2.1	Outdoor Experimental Setup . . . . .	50
3.4.2.2	Indoor Experimental Setup . . . . .	51
3.5	Round-Trip Time-of-Flight (RT-ToF) . . . . .	51
3.5.1	Principle of Operation . . . . .	54
3.5.2	RT-ToF Range Resolution . . . . .	55
3.5.3	Cramér-Rao Lower Bound of ToF . . . . .	56
3.6	RSS: Principle of Operation . . . . .	59
3.6.1	Cramér-Rao Lower Bound of RSS . . . . .	61
3.7	Site Survey and Analysis . . . . .	62
3.7.1	Successful ToF . . . . .	62
3.7.2	Remote Time Value Invalid . . . . .	63
3.7.3	Local Time Value Invalid . . . . .	63
3.7.4	No Acknowledgement . . . . .	63
3.7.5	No Data From Remote Node . . . . .	63
3.8	Experimental Results and Analysis . . . . .	66
3.8.1	Cross-over Range ( $C_R$ ) . . . . .	76
3.9	Conclusion . . . . .	77

## CONTENTS

---

<b>4</b>	<b>Localization using Optimal and Sub-Optimal Multi-lateration</b>	<b>79</b>
4.1	Overview . . . . .	79
4.2	Introduction . . . . .	80
4.3	Signal Model . . . . .	81
4.4	Sub-Optimal Blind Trilateration (SBT) . . . . .	83
4.4.1	Least Squares Solution . . . . .	85
4.5	Geometric Dilution of Precision (GDOP) . . . . .	90
4.5.1	Simulation Results and Analysis . . . . .	99
4.6	Modified Sub-Optimal Blind Trilateration (MSBT) . . . . .	102
4.7	Optimal Multi-lateration (OML) . . . . .	106
4.8	Performance Analysis and Results . . . . .	111
4.8.1	Impact of Ranging Error . . . . .	113
4.8.2	Impact of Node Density . . . . .	116
4.8.3	Impact of Anchor Nodes on Localization Accuracy . . . . .	117
4.8.4	Analysis of Computational Complexity . . . . .	119
4.9	Discussion . . . . .	122
4.10	Summary . . . . .	122
<b>5</b>	<b>The Optimization of Range Derived Localization in 2D and 3D WSNs</b>	<b>124</b>
5.1	Overview . . . . .	124
5.2	Introduction . . . . .	125
5.3	Signal Models . . . . .	126
5.3.1	Multiplicative Noise Model . . . . .	128
5.4	Lower Bounds On Localization Error . . . . .	129
5.5	Optimal Anchor Placement for Minimum CRLB . . . . .	131
5.5.1	Two-Dimensional (2-D Case) . . . . .	131
5.5.2	Three-Dimensional (3-D Case) . . . . .	133
5.6	Optimal Anchor Placements . . . . .	136
5.6.1	Two-Dimensional (2-D) Case . . . . .	137
5.6.1.1	Optimal Anchor Placement for Additive Noise Model	140
5.6.1.2	Optimal Anchor Placement for Multiplicative Noise Model . . . . .	146

## CONTENTS

---

5.6.1.3	CRLB Analysis of Anchor Node Constraints in 2-D	152
5.6.2	Three-Dimensional (3-D) Case . . . . .	155
5.6.2.1	Optimal Anchor Placement for Additive Noise Model	155
5.6.2.2	Optimal Anchor Placement for Multiplicative Noise Model . . . . .	159
5.6.2.3	CRLB Analysis of Anchor Node Constraints in 3D	162
5.7	Discussion . . . . .	163
5.8	Conclusion . . . . .	165
<b>6</b>	<b>Localization Performance at Optimized Anchor Placement</b>	<b>166</b>
6.1	Introduction . . . . .	166
6.2	2-D Case: Additive and Multiplicative Noise Model . . . . .	170
6.3	3-D Case: Additive and Multiplicative Noise Model . . . . .	175
6.4	Conclusion . . . . .	179
<b>7</b>	<b>Experiencing RALS</b>	<b>181</b>
7.1	Introduction . . . . .	181
7.2	Principle of Operation . . . . .	182
7.3	Experimental Infrastructure and Setup . . . . .	183
7.3.1	Indoor Setup . . . . .	184
7.4	Localization Performance Analysis . . . . .	186
7.4.1	Arbitrary Anchor Placement . . . . .	190
7.5	Summary . . . . .	191
<b>8</b>	<b>Range Aware 3-D Localization in Indoor WSNs</b>	<b>192</b>
8.1	Introduction . . . . .	192
8.2	Geometric Dilution of Precision Test for 3-D Setup . . . . .	195
8.3	Received Signal Strength . . . . .	199
8.4	Calibration of Path loss Exponent . . . . .	201
8.4.1	Training Phase . . . . .	202
8.4.1.1	Experimental Infrastructure and setup . . . . .	202
8.4.1.2	Formulation of Lookup Table . . . . .	206
8.4.2	Estimation Phase . . . . .	208
8.5	Range Estimate Threshold (RET) . . . . .	208

## CONTENTS

---

8.5.1	RET Algorithm Description . . . . .	212
8.6	Results and Analysis . . . . .	216
8.6.1	Simulation Case 1 : Lab-262b . . . . .	217
8.6.2	Simulation Case 2: Lab-160 . . . . .	226
8.7	Conclusion . . . . .	230
<b>9</b>	<b>Conclusions and Future Research</b>	<b>232</b>
9.1	Conclusions . . . . .	232
9.2	Future Research and Improvements . . . . .	236
9.2.1	Cooperative Localization (Extension to chapter 4) . . . . .	236
9.2.2	Additive/Multiplicative noise model . . . . .	237
9.2.3	Gaussianity assumption . . . . .	237
9.2.4	Path loss Exponent ( $\eta$ ) . . . . .	238
9.2.5	Optimal anchor placement . . . . .	238
9.2.6	Experiencing RALS . . . . .	239
9.3	Sectorization Using Optimal Anchor Placement . . . . .	239
	<b>References</b>	<b>242</b>

# List of Figures

1.1	Fig. 1.1(a). Smart Sensor Architecture [1]. Fig. 1.1(b). JN5148 Micro-controller and sensor board [1]. . . . .	2
2.1	Location Stack [2] . . . . .	17
2.2	Fig. 2.2(a). Subject node with 3 in-range anchor nodes with actual ranging. Fig. 2.2(b). Subject node with 3 in-range anchor nodes with noise range. . . . .	27
2.3	Precision and Accuracy analysis for randomly selected data: Fig. 2.3(a). High accuracy with high precision, Fig. 2.3(b). High accuracy with low precision, Fig. 2.3(c). Low accuracy with high precision, Fig. 2.3(d). High accuracy with low precision. . . . .	32
3.1	Integrated Folded Mono-pole antenna measurement planes [3]. Fig. (a). XY-Plane Fig. (b). XZ-Plane Fig. (c). YZ-Plane . . . . .	49
3.2	Measured antenna radiation pattern [3]. Fig. 3.2(a). XY-plane radiation pattern polar plot, Fig. 3.2(b). XZ-plane radiation pattern polar plot and Fig. 3.2(c). YZ-plane radiation pattern polar plot . . . . .	50
3.3	Outdoor experimental setup with two nodes, tripods and data logger laptop for range measurements. . . . .	51
3.4	Indoor experimental setup with two nodes, tripods and data logger laptop for range measurements. . . . .	52
3.5	Time-of-Flight (ToF) measurement. . . . .	53
3.6	RT-Time-of-Flight Process . . . . .	55

## LIST OF FIGURES

---

3.7	Impact of SNR and $\beta$ on the fundamental CRLB for ToF ranging using IEEE 802.15.4 and UWB. . . . .	57
3.8	The Fundamental CRLB and measured performance limit of Jennic JN5148 series ranging module for ToF ranging . . . . .	58
3.9	RSS versus range for measured data and path loss model. Fig. 3.9(a). Outdoor LOS at antenna height of 1.5m. Fig. 3.9(b). Indoor LOS at antenna height of 1.5m. . . . .	61
3.10	The fundamental CRLB limit and measured performance limit of Jennic JN5148 series ranging module for RSS. . . . .	62
3.11	Comparison of failed ToF polls taking quiet and busy channel in the account for indoor and outdoor LOS environment (height=1.5 m). (a, b). Quiet Channel in Outdoor and Indoor. respectively (c, d). Busy Channel in Outdoor and Indoor respectively. . . . .	65
3.12	Fig. (a). ToF estimated range in outdoor LOS path for different antenna heights. Fig. (b). ToF estimated range in indoor LOS path for different antenna heights. . . . .	67
3.13	Fig. (a). RSS estimated range in outdoor LOS path for different antenna heights. Fig. (b). RSS estimated range in indoor LOS path for different antenna heights. . . . .	68
3.14	ToF versus RSS estimated range in outdoor and indoor LOS path for antenna height of 1.5m . . . . .	68
3.15	ToF versus RSS estimated range in outdoor and indoor NLOS path for antenna height of 1.5m . . . . .	70
3.16	ToF estimated range in outdoor and indoor over long range for antenna height of 1.5m . . . . .	70
3.17	RSS estimated range in outdoor and indoor for antenna height of 1.5m . . . . .	71
3.18	ToF and RSS: MMRE percentage in outdoor and indoor for LOS and NLOS paths over short range with antenna height of 1.5m. . . . .	72
3.19	ToF and RSS: MMRE percentage in outdoor and indoor for LOS and NLOS paths over long range with antenna height of 1.5m. . . . .	73
3.20	PDF and Q-Q plot across ToF measurements over short range for outdoor LOS. . . . .	74

## LIST OF FIGURES

---

3.21	PDF and Q-Q plot across RSS measurements over short range for outdoor LOS. . . . .	74
3.22	PDF and Q-Q plot across all of the ToF and RSS measurements over short range for outdoor NLOS. . . . .	75
3.23	Cross-over Range using experimental parameters. . . . .	77
4.1	Subject node with 3 in-range anchor nodes . . . . .	84
4.2	Subject node with 3 in-range anchor nodes . . . . .	85
4.3	Fig. 4.3(a). Subject node with 3 in-range collinear anchor nodes. Fig. 4.3(b). Subject node with 2 in-range anchor nodes, where 3 anchor nodes are co-incident. . . . .	89
4.4	Fig. 4.4(a). Anchor combinations, where $A_1, A_2$ are fixed anchors and anchor $A_3$ is changed from $A_3$ to $A_{13}$ . Fig. 4.4(b). $E_{\text{RMS}}$ associated with the position estimate for different anchor geometries as shown in Fig. 4.4(a). Fig. 4.4(c) - Fig. 4.4(h). First 6 anchor combinations from Fig. 4.4(a), where $A_1, A_2$ are fixed anchors and anchor $A_3$ is changed from $A_3$ to $A_8$ respectively. . . . .	91
4.5	Simulation Flow chart for SBT . . . . .	92
4.6	Subject node with 24 in-range anchors/pseudo-anchors, where $A_1, A_2$ are fixed and $A_3$ is changed from $A_3$ to $A_{24}$ . . . . .	100
4.7	Comparison of GDOP and $E_{\text{RMS}}$ for 24 in-range anchor nodes, where $A_1, A_2$ are fixed and $A_3$ is changed from $A_3$ to $A_{24}$ as shown in Fig. 4.6. . . . .	100
4.8	Subject node with 3 in-range anchors/pseudo-anchors, where $A_1, A_2, A_3$ are fixed and $s_j$ is changed from $s_1$ to $s_{10}$ . . . . .	101
4.9	Comparison of HDOP and $E_{\text{RMS}}$ for 3 in-range anchor nodes, where $A_1, A_2, A_3$ are fixed and $s_j$ is changed from $s_1$ to $s_{10}$ as shown in Fig. 4.8. . . . .	102
4.10	Subject node with 3 in-range anchor nodes, where $A_1, A_2, A_3$ are fixed and $s_j$ is changed from $s_1$ to $s_{21}$ . . . . .	103
4.11	Comparison of GDOP and $E_{\text{RMS}}$ for 3 in-range anchor nodes, where $A_1, A_2, A_3$ are fixed and $s_j$ is changed from $s_1$ to $s_{21}$ as shown in Fig. 4.10. . . . .	103

## LIST OF FIGURES

---

4.12	Subject node with 5 in-range anchor/pseudo-anchor nodes. . . . .	106
4.13	Possible anchor/pseudo-anchor node combinations. . . . .	107
4.14	Simulation Flow chart for MSBT. . . . .	108
4.15	Comparison of HDOP and $E_{\text{RMS}}$ for all anchor combinations as shown in Fig. 4.13. . . . .	109
4.16	Optimal multi-lateration, where 8 anchor/pseudo-anchor nodes are in-range of a subject node. . . . .	109
4.17	HDOP and $E_{\text{RMS}}$ for OML, where 8 anchor/pseudo-anchor nodes are in-range of a subject node as shown in Fig. 4.16. . . . .	111
4.18	Simulation Flow chart for OML. . . . .	112
4.19	Fig. 4.19(a). Example of simulation setup for 3 anchors (red squares), subject nodes (blue circles). Fig. 4.19(b). Example of simulation setup for 3 anchors (red squares), subject nodes (blue circles), and estimated subject nodes (yellow, pink, cyan and green squares) from each localization phase. . . . .	114
4.20	Impact of ranging error on average $E_{\text{RMS}}$ for 400 randomly deployed nodes. . . . .	115
4.21	Impact of node density on average $E_{\text{RMS}}$ at $\sigma^2 = 0.5\text{m}$ . . . . .	116
4.22	Average number of Anchors/Pseudo-Anchors with respect to Node Density ( $\sigma^2 = 0.5\text{m}$ ). . . . .	117
4.23	Impact of the number of Anchors/Pseudo-Anchors on average $E_{\text{RMS}}$ ( $\sigma^2 = 5\text{m}$ ) in 200m by 200m network. . . . .	118
4.24	Impact of the number of Anchors/Pseudo-Anchors on average $E_{\text{RMS}}$ ( $\sigma^2 = 10\text{m}$ ) in 200m by 200m network. . . . .	118
4.25	Impact of possible combinations of anchors/pseudo-anchors on average RMS location error for 100 randomly deployed nodes (transmission range = 40m, $\sigma^2 = 0.5\text{m}$ ) for MSBT. . . . .	119
4.26	Average simulation time for single iteration of computation in 400m by 400m network with transmission range of 100m . . . . .	120
4.27	Impact of possible combinations of anchors/pseudo-anchors on average computation time for 100 randomly deployed nodes (transmission range = 40m, $\sigma^2 = 0.5\text{m}$ ) for MSBT. . . . .	121

## LIST OF FIGURES

---

5.1	Fig. 5.1(a). Effects of additive noise model on the estimated range at noise variance of 2 and 4. Fig. 5.1(b). Effects of additive noise model on the estimated range at noise variance of 6 and 8. . . . .	127
5.2	Effects of Multiplicative noise model on the estimated range. Fig. 5.2(a). For $\kappa=0.005$ , $\eta=2$ and 2.4. Fig. 5.2(b). For $\kappa=0.005$ , $\eta=2.8$ and 3.2. Fig. 5.2(c). For $\kappa=0.5$ , $\eta=2$ and 2.4. Fig. 5.2(d). For $\kappa=0.8$ , $\eta=2.8$ and 3.2. . . . .	130
5.3	Geometric relationship between two nodes in 2-D space. . . . .	131
5.4	Geometric relationship between two nodes in 3-D space. . . . .	133
5.5	Fig. 5.5(a) Relationship between possible combinations of anchor placements and $3 \times 3$ field dimensions. Fig. 5.5(b). Relationship between possible combinations of anchor placements and $4 \times 4$ field dimensions. . . . .	138
5.6	m-CRLB Flow Chart. . . . .	139
5.7	CRLB of all possible anchor combinations (placements) for a single subject location. . . . .	140
5.8	Optimal anchor placement for additive noise model in a $11 \times 11$ 2-D plane for 3 to 8 anchors. . . . .	141
5.9	Optimal anchor placement and corresponding m-CRLB for additive noise model using 3 to 8 anchor nodes as shown in Fig. 5.8(a) - Fig. 5.8(f) for deployed subject nodes on a $11 \times 11$ 2-D plane. Fig. 5.9(a). Impact of anchor nodes on m-CRLB. Fig. 5.9(b) - Fig. 5.9(g). contour plots for 3 to 8 anchors in 2-D for $\sigma^2 = 2$ . . .	142
5.10	Optimal anchor placement for 8 anchor nodes for three different scales. Fig. 5.10(a). For $21 \times 21$ . Fig. 5.10(b). For $31 \times 31$ . Fig. 5.10(c). For $41 \times 41$ . . . . .	143
5.11	Worst anchor placement for additive noise model in a $11 \times 11$ 2-D plane for 3 to 8 anchors. . . . .	144
5.12	Contour plot of worst anchor placement and corresponding m-CRLB for additive noise model for 3 to 8 anchor nodes. . . . .	145

## LIST OF FIGURES

---

5.13	Arbitrary anchor placement and corresponding minimum m-CRLB for multiplicative noise model using 3 - 8 Anchor nodes as shown in Fig. 5.8(a) - Fig. 5.8(f) (optimal for additive noise model) for deployed subject nodes on a $11 \times 11$ 2-D space for $\eta = 2$ and $\kappa = 0.001$ . . . . .	146
5.14	m-CRLB for multiplicative noise model as a function of the number of anchor nodes placed at the optimal positions for additive noise model. . . . .	147
5.15	Optimal anchor placement for multiplicative noise model in a $4 \times 4$ 2-D plane for 3 to 8 anchors, where $\kappa = 0.001$ and $\eta = 4$ . . . . .	148
5.16	Optimal anchor placement for multiplicative noise model in a $4 \times 4$ 2-D plane for 3 to 8 anchors, where $\kappa = 0.005$ and $\eta = 2$ . . . . .	150
5.17	Fig. 5.17(a)-Fig. 5.17(c). Optimal anchor placement for multiplicative noise model in a $5 \times 5$ 2-D plane for 3 to 6 anchors, where $\kappa = 0.001$ and $\eta = 4$ . Fig. 5.17(d)-Fig. 5.17(f). Optimal anchor placement for multiplicative noise model in a $6 \times 6$ 2-D plane for 3 to 6 anchors, where $\kappa = 0.001$ and $\eta = 2$ . . . . .	151
5.18	Optimal anchor placement and corresponding minimum m-CRLB at $\kappa = 0.001$ and $\eta = 4$ for multiplicative noise model using 3-5 anchor nodes for deployed subject nodes on $11 \times 11$ 2-D plane. . .	151
5.19	Optimal anchor placement and corresponding minimum m-CRLB at $\kappa = 0.001$ and $\eta = 4$ for multiplicative noise model using 5 anchor nodes for deployed subject nodes on $21 \times 21$ , $31 \times 31$ and $41 \times 41$ 2-D space. . . . .	152
5.20	Worst anchor placement for multiplicative noise model in a $4 \times 4$ 2-D plane for 3 to 8 anchors, where $\kappa = 0.001$ and $\eta = 4$ . . . . .	153
5.21	Fig. 5.21(a). CRLB for 3 anchor nodes in 2-D, when anchor nodes are in a straight line ( $\sigma^2 = 2$ for all anchors). Fig. 5.21(b). CRLB for 3 anchor nodes in 2-D, when two of the anchor nodes are coincident ( $\sigma^2 = 2$ for all anchors). . . . .	154
5.22	Optimal anchor placement for additive noise model in $3 \times 3 \times 3$ 3-D space for 4 to 6 anchors. . . . .	155

## LIST OF FIGURES

---

5.23	Optimal anchor placement for additive noise model in $11 \times 11 \times 11$ 3-D space for 4 to 8 anchors. . . . .	156
5.24	Optimal anchor placement and corresponding minimum m-CRLB for additive noise model for 4 to 8 Anchor nodes as shown in Fig. 5.23(a) - Fig. 5.23(e) for deployed subject nodes in $11 \times 11 \times 11$ 3-D space for $\sigma^2 = 2$ . . . . .	157
5.25	Optimal anchor placement for 8 anchor nodes in 3-D for two different scales. Fig. 5.25(a) for $5 \times 5 \times 5$ scale. Fig. 5.25(b) for $12 \times 12 \times 12$ scale. . . . .	158
5.26	Suboptimal anchor placement and corresponding minimum m-CRLB for multiplicative noise model using 4 - 8 Anchor nodes as shown in Fig. 5.23(a) - Fig. 5.23(e) for deployed subject nodes on a $11 \times 11 \times 11$ 3-D space for $\kappa = 0.001$ and $\eta = 4$ . . . . .	160
5.27	Optimal anchor placement for multiplicative noise model in $3 \times 3 \times 3$ 3-D space for 4 to 6 anchors. Fig. 5.27(a) - Fig5.27(c). For $\kappa = 0.005$ and $\eta = 2$ . Fig. 5.27(d) - Fig5.27(f). For $\kappa = 0.001$ and $\eta = 4$ .	161
5.28	CRLB for 4 anchor nodes in 3-D, where anchor nodes are placed on a single plane. . . . .	162
6.1	Fig. 6.1(a). Simulation setup in 2-D plane. Fig. 6.1(b). Simulation setup in 3-D space. . . . .	167
6.2	Arbitrary anchor placement 1 in $10 \times 10$ 2-D space for 3 to 8 anchors.	168
6.3	Arbitrary anchor placement 2 in $10 \times 10$ 2-D space for 3 to 8 anchors.	168
6.4	Arbitrary anchor placement 3 in $10 \times 10$ 2-D space for 3 to 8 anchors.	169
6.5	Performance of the LS method for additive noise model at optimal and arbitrary anchor placement and comparison with m-CRLB. . . . .	171
6.6	Performance of the AML method for additive noise model at optimal and arbitrary anchor placement and comparison with m-CRLB.	171
6.7	Performance comparison of LS and AML method for additive noise model at optimal and arbitrary anchor placement. . . . .	172
6.8	Performance comparison of LS and AML method for multiplicative noise model at additive's optimal placement with arbitrary anchor placement. . . . .	173

## LIST OF FIGURES

---

6.9	Performance of the LS and AML method for multiplicative noise model for $\kappa = 0.001$ and $\eta = 4$ at optimal and arbitrary anchor placement and comparison with m-CRLB. Fig. 6.9(b). For $5 \times 5$ , where optimal placement for multiplicative noise model is as shown in Fig. 5.17(a) - Fig. 5.17(c). Fig. 6.9(a). For $11 \times 11$ , where optimal placement for multiplicative is as shown in Fig. 5.18. . . .	174
6.10	Arbitrary anchor placement 1 in $10 \times 10 \times 10$ 3-D space for 4 to 8 anchors. . . . .	175
6.11	Arbitrary anchor placement 2 in $10 \times 10 \times 10$ 3-D space for 4 to 8 anchors. . . . .	176
6.12	Arbitrary anchor placement 3 in $10 \times 10 \times 10$ 3-D space for 4 to 8 anchors. . . . .	176
6.13	Performance of the LS method for additive noise model at optimal and arbitrary anchor placement and comparison with m-CRLB. .	177
6.14	Performance of the AML method for additive noise model at optimal and arbitrary anchor placement and comparison with m-CRLB.	178
6.15	Performance comparison of LS and AML method for additive noise model at optimal and arbitrary anchor placement. . . . .	178
7.1	Flow Chart for PAN Coordinator node. . . . .	183
7.2	Flow Chart for Anchor nodes. . . . .	184
7.3	Flow Chart for Subject nodes. . . . .	185
7.4	Fig. 7.4(a). Localization testbed in a Lecture Theatre, where three anchors are optimally placed, whereas subject node is placed in the centre. Fig. 7.4(b). Jennic JN5148 controller board and LCD splash screen on the subject node. . . . .	186
7.5	Estimated subject coordinates and $E_{RMS}$ in cm, when anchors are optimally placed and subject node is placed at [3m,3m] as shown in Fig. 7.4(a). . . . .	187
7.6	Fig. 7.6(a). Estimated subject coordinates and $E_{RMS}$ in cm, when anchors are optimally placed and subject node is placed at [3m,0m]. Fig. 7.6(b). Estimated subject coordinates and $E_{RMS}$ in cm, when anchors are optimally placed and subject node is placed at [0m,3m].	188

## LIST OF FIGURES

---

7.7	Fig. 7.7(a). Three anchors are optimally placed, whereas subject node is placed at [3m,9m] outside of the triangle. Fig. 7.7(b). Corresponding $E_{\text{RMS}}(\text{cm})$ . . . . .	189
7.8	Fig. 7.8(a). Subject node estimated coordinates and $E_{\text{RMS}}$ when three anchors are placed at arbitrary placement, whereas subject node is placed in the centre of the field ([3m,3m]). . . . .	190
8.1	7 different 3-D anchor placements according to the dimensions of Wireless Sensor Networks Research Group lab (262b) at University of Leeds. . . . .	197
8.2	Simulation setup for anchor placement 1 as shown in Fig. 8.1. . .	197
8.3	Impact of noise variance and anchor node placements on PDOP in 3-D context. . . . .	198
8.4	Impact of noise variance and anchor node arrangements on $E_{\text{RMS}}$ in 3-D context (based on 3-D trilateration using LS method for 7 different anchor combinations and 50 randomly deployed subject nodes.) . . . . .	198
8.5	Profiling an area of interest by exploiting the link information (face diagonal) between pair of anchors in 3-D, where 4 anchors are optimally placed. . . . .	201
8.6	Fig. 8.6(a). Wireless Sensor Networks Research Group Lab (Lab-262b) in the School of Electronic and Electrical Engineering at the University of Leeds. Fig. 8.6(b). Computer Cluster Lab (Lab-160 in the School of Electronic and Electrical Engineering at the University of Leeds. Fig. 8.6(c). Node mounted on a tripod and connected to laptop via UART. Fig. 8.6(d). Node mounted with multi-purpose tac around the corner of the wall. Fig. 8.6(e). Experimental setup along with anchor nodes arrangement 1. . . . .	203
8.7	Node placement for calibration of path loss exponent in Lab-262b.	204
8.8	Node placement for calibration of path loss exponent in Lab-160. .	205
8.9	Path loss exponent calibration process for $A_i$ where $i = 1, \dots, N$ .	205
8.10	RSSI ranging samples between each anchor and subject node 1 as shown in Fig. 8.7 (lab-262b). . . . .	207

## LIST OF FIGURES

---

8.11	Fig. 8.11(a). Lab-262b lookup table mapping using $\eta_{A_i}$ and $\eta_\mu$ as shown in table 8.1 for each anchor node. Fig. 8.11(a). Lab-160 lookup table mapping using $\eta_{A_i}$ and $\eta_\mu$ as shown in table 8.1 for each anchor node. . . . .	208
8.12	Subject node estimation using calibrated path loss exponent with respect to each anchor node $A_i$ for $i = 1, \dots, N$ . . . . .	209
8.13	Space and face diagonal between anchor $A_i$ and subject $s_j$ nodes in 3-D for RET. . . . .	210
8.14	Fig. 8.14(a). RET for additive noise model where $\sigma^2 = 1, 3, 5, 7,$ and 9. Fig. 8.14(b). RET for multiplicative noise model where $\kappa = 0.001, 0.003, 0.005, 0.007,$ and 0.009. . . . .	212
8.15	Fig. 8.15(a). Space and face diagonals between anchors and subject nodes in 3-D for RET of Lab-160. Fig. 8.15(b). RET for additive noise model where $\sigma^2 = 1, 3, 5, 7,$ and 9. Fig. 8.15(c). RET for multiplicative noise model where $\kappa = 0.001, 0.003, 0.005, 0.007,$ and 0.009. . . . .	213
8.16	Extraction of poor range estimates ( $\hat{d}_{ij}^p$ ) based on RET defined by using lab262b field dimensions and signal models. Fig. 8.16(a). Additive noise model. Fig. 8.16(b). Multiplicative noise model using $\eta_\mu$ . Fig. 8.16(c). Multiplicative noise model using $\eta_{A_i}$ . Fig. 8.16(d). RSS path loss model. . . . .	218
8.17	CDF comparison of ME and RET for additive and multiplicative noise models. . . . .	220
8.18	Comparison of ME and RET for additive and multiplicative noise models. Fig. 8.18(a). Additive noise model. Fig. 8.18(b). Multiplicative noise model. Fig. 8.18(c). CDF comparison of ME and RET based on all samples at $\sigma^2 = 1, 3, 5, 7,$ and 9 for additive and $\kappa = 0.001, 0.003, 0.005, 0.007,$ and 0.009 for multiplicative noise model from Fig. 8.17(a) - Fig. 8.17(e) for both additive and multiplicative noise models. . . . .	221
8.19	$E_{\text{RMS}}$ comparison for each node index for additive noise model. Fig. 8.19(a) and Fig. 8.19(b) at $\sigma^2 = 1$ and 7 respectively. . . . .	222

## LIST OF FIGURES

---

8.20	$E_{\text{RMS}}$ comparison for each node index for multiplicative noise model. Fig. 8.20(a) and Fig. 8.20(b). Using $\eta_\mu$ at $\kappa = 0.001$ and $0.007$ respectively. Fig. 8.20(c) and Fig. 8.20(d). Using $\eta_{A_i}$ at $\kappa = 0.001$ and $0.007$ respectively. . . . .	223
8.21	CDF comparison of ME and RET for CE based RSS localization using $\eta_{A_i}$ and $\eta_\mu$ in lab-262-b. . . . .	224
8.22	$E_{\text{RMS}}$ comparison for each node index for RSS path loss model based on CE. Fig. 8.22(a) and Fig. 8.22(b). Using $\eta_\mu$ and $\eta_{A_i}$ respectively. . . . .	225
8.23	Extraction of poor range estimates ( $\hat{d}_{ij}^p$ ) based on RET defined by using lab169 field dimensions and signal models. Fig. 8.16(a). Additive noise model. Fig. 8.16(b). Multiplicative noise model using $\eta_\mu$ . Fig. 8.16(c). Multiplicative noise model using $\eta_{A_i}$ . Fig. 8.16(d). RSS path loss model. . . . .	226
8.24	Comparison of ME and RET using additive and multiplicative noise models for lab-160 dimensions. Fig. 8.24(a). Additive noise model. Fig. 8.24(b). Multiplicative noise model. Fig. 8.24(c). CDF comparison of ME and RET based on all samples at $\sigma^2 = 1, 3, 5, 7,$ and $9$ for additive and $\kappa = 0.001, 0.003, 0.005, 0.007,$ and $0.009$ for multiplicative noise model. . . . .	227
8.25	CDF comparison of ME and RET for CE based RSS localization using $\eta_{A_i}$ and $\eta_\mu$ in lab-160. . . . .	229
8.26	$E_{\text{RMS}}$ comparison for each node index for RSS path loss model based on CE. Fig. 8.26(a) and Fig. 8.26(b). Using $\eta_\mu$ and $\eta_{A_i}$ respectively. . . . .	229
9.1	Fig. 9.1(a) - Fig. 9.1(c). Sectorization of localization field with respect to 3, 4 and 5 optimally placed anchor nodes for multiplicative noise model. Fig. 9.1(d). Simulation setup for sectorization with respect to 4 optimal placed anchors for multiplicative noise model. . . . .	241

# List of Tables

3.1	Specification of IEEE 802.15.4 Compliant Devices . . . . .	48
3.2	Approximated Propagation Parameters . . . . .	60
3.3	Site Survey Results . . . . .	64
3.4	Site Survey Results . . . . .	66
3.5	Experimental Results: ToF Vs RSS . . . . .	69
4.1	Geometric Dilution of Precision Quality Rank . . . . .	93
4.2	Network Simulation Parameters for SBT, MSBT and OML . . . . .	113
6.1	Network Simulation Parameters to analyse the anchor placement.	167
8.1	Calibrated Propagation Parameters . . . . .	206
8.2	Simulation Parameters for indoor scenario . . . . .	216

## List of Abbreviations

ACK	Acknowledgement
AML	Approximate Maximum Likelihood
API	Application Programming Interface
APIT	Approximate Point In Triangulation
AWGN	Additive White Gaussian Noise
CCA	Clear Channel Assessment
CDF	Cumulative Distribution Function
CE	Calibrated Estimation
CRLB	Cramér-Rao Lower Bound
CSMA-CA	Carrier Sense Multiple Access with Collision Avoidance
DoD	Department of Defence
DOP	Dilution of Precision
DSSS	Direct Sequence Spread Spectrum
ED	Energy Detection
FCC	Federal Communications Commission
FIM	Fisher Information Matrix
GDOP	Geometric Dilution of Precision
GLONASS	Global Navigation Satellite System
GPS	Global Positioning System

## LIST OF ABBREVIATIONS

---

GPRS	<b>G</b> eneral <b>P</b> acket <b>R</b> adio <b>S</b> ervice
HDOP	<b>H</b> orizontal <b>D</b> ilution of <b>P</b> recision
HSPA	<b>H</b> igh <b>S</b> peed <b>P</b> acket <b>A</b> ccess
ID	<b>D</b> istinctive <b>I</b> dentification
IEEE	Institute of <b>E</b> lectrical and <b>E</b> lectronics <b>E</b> ngineers
IETF	<b>I</b> nternet <b>E</b> ngineering <b>T</b> ask <b>F</b> orce
ISM	<b>I</b> ndustrial, <b>S</b> cientific and <b>M</b> edical
LBS	<b>L</b> ocation <b>B</b> ased <b>S</b> ervice
LCD	<b>L</b> iquid <b>C</b> rystal <b>D</b> isplay
LoP	<b>L</b> ine of <b>P</b> osition
LOS	<b>L</b> ine-of- <b>S</b> ight
LS	<b>L</b> east <b>S</b> quares
LTE	<b>L</b> ong- <b>T</b> erm- <b>E</b> volution
m-CRLB	<b>M</b> ean <b>C</b> ramér- <b>R</b> ao <b>L</b> ower <b>B</b> ound
MAC	<b>M</b> edium <b>A</b> ccess <b>L</b> ayer
MATLAB	<b>M</b> atrix <b>L</b> aboratory
ME	<b>M</b> easured <b>E</b> stimation
MEMS	<b>M</b> icro- <b>E</b> lectro- <b>M</b> echanical <b>S</b> ystem
ML	<b>M</b> aximum <b>L</b> ikelihood
MLME	<b>M</b> edia <b>A</b> ccess <b>C</b> ontrol ( <b>M</b> AC) <b>S</b> ublayer <b>M</b> anagement <b>E</b> ntity
MMRE	<b>M</b> agnitude of <b>M</b> ean <b>R</b> ange <b>E</b> rror
MP	<b>M</b> ultipath <b>P</b> ropagation
MSBT	<b>M</b> odified <b>S</b> ub- <b>O</b> ptimal <b>B</b> lind <b>T</b> rilateration
MSE	<b>M</b> ean <b>S</b> quare <b>E</b> rror

## LIST OF ABBREVIATIONS

---

NLOS	<b>N</b> on- <b>L</b> ine-of- <b>S</b> ight
O-QPSK	<b>O</b> ffset <b>Q</b> uadrature <b>P</b> hase <b>S</b> hift <b>K</b> eying
OML	<b>O</b> ptimal <b>M</b> ulti-lateration
PCB	<b>P</b> rinted <b>C</b> ircuit <b>B</b> oard
PDF	<b>P</b> robability <b>D</b> ensity <b>F</b> unction
PDOP	<b>P</b> osition <b>D</b> ilution of <b>P</b> recision
PN	<b>P</b> seudo-noise
PSD	<b>P</b> ower <b>S</b> pectral <b>D</b> ensity
QoS	<b>Q</b> uality of <b>S</b> ervice
Q-Q	<b>Q</b> uantile- <b>Q</b> uantile
RALS	<b>R</b> ange <b>A</b> ware <b>L</b> ocalization <b>S</b> ystem
RBW	<b>R</b> esolution <b>B</b> and <b>W</b> idth
RET	<b>R</b> ange <b>E</b> stimate <b>T</b> hreshold
RF	<b>R</b> adio <b>F</b> requency
RISC	<b>R</b> educed <b>I</b> nstruction <b>S</b> et <b>C</b> omputing
RSS	<b>R</b> eceived <b>S</b> ignal <b>S</b> trength
RSR	<b>R</b> oot <b>S</b> election <b>R</b> outine
RT-ToF	<b>R</b> ound- <b>T</b> rip - <b>T</b> ime of <b>F</b> light
RTLS	<b>R</b> eal <b>T</b> ime <b>L</b> ocation <b>S</b> ystem
SBT	<b>S</b> ub- <b>O</b> ptimal <b>B</b> lind <b>T</b> rilateration
SeRLoc	<b>S</b> ecure <b>R</b> ange- <b>I</b> ndependent <b>L</b> ocalization
SNR	<b>S</b> ignal-to- <b>N</b> oise <b>R</b> atio
TDOA	<b>T</b> ime <b>D</b> ifference of <b>A</b> rrival
TEU	<b>T</b> wenty-foot <b>E</b> quivalent <b>U</b> nit

## LIST OF ABBREVIATIONS

---

TLS	<b>T</b> aylor <b>S</b> eries <b>E</b> xpansion
ToF	<b>T</b> ime <b>o</b> f <b>F</b> light
TRET	<b>T</b> amper <b>R</b> esistant <b>E</b> mbedded <b>C</b> ontroller
UART	<b>U</b> niversal <b>A</b> synchronous <b>R</b> eceiver <b>T</b> ransmitter
USB	<b>U</b> niversal <b>S</b> erial <b>B</b> us
UWB	<b>U</b> ltra- <b>W</b> ide- <b>B</b> and
VDOP	<b>V</b> ertical <b>D</b> ilution <b>o</b> f <b>P</b> recision
VHF	<b>V</b> ery <b>H</b> igh <b>F</b> requency
WiMAX	<b>W</b> orldwide <b>I</b> nteroperability for <b>M</b> icrowave <b>A</b> ccess
WLAN	<b>W</b> ireless <b>L</b> ocal <b>A</b> rea <b>N</b> etwork
WPAN	<b>W</b> ireless <b>P</b> ersonal <b>A</b> rea <b>N</b> etwork
WSN	<b>W</b> ireless <b>S</b> ensor <b>N</b> etwork

## List of Symbols

Symbol	Definition
$\alpha$	Orientation (Angle)
$\beta$	Bandwidth
$\delta$	Dirac Delta Function
$\eta$	Path Loss Exponent
$\eta_{A_i}$	Path Loss Exponent for Anchor $i$
$\eta_\mu$	Averaged Path Loss Exponent
$\epsilon_o$	Standard Normal Random Variable
$\sigma^2$	Noise Variance
2-D	2 Dimensions
3-D	3 Dimensions
$A^t$	Path Amplitudes
$A_i$	$i^{th}$ Anchor Node
$A_N$	Number of Anchor/Pseudo-Anchor
$A_c$	Anchor Combinations
$\hat{A}_c$	Selected Anchor Combination
$A_{ir}$	Number of in-range Anchor/Pseudo-anchor Nodes
$c$	Speed of Light

## LIST OF SYMBOLS

---

Symbol	Definition
$C_{AP}$	Collinear Anchor Placement
cm	Centimetre
$C_R$	Cross-over range
dBm	Decibels related to 1 milliwatt
$d_{ij}$	Distance between $i^{th}$ anchor and $j^{th}$ subject node
$\hat{d}_{ij}$	Estimated Distance $i^{th}$ anchor and $j^{th}$ subject node
$dx_i$	Direction Cosines
$dy_i$	Direction Cosines
$E_{RMS}$	Root-Mean-Square-Error
$E_{RMS}^{Loc}$	Root-Mean-Square-Error for Localization
$E_{RMS}^r$	Root-Mean-Square-Error for Ranging
$f_s$	Clock Rate
$G_r$	Receiver antenna gain
$G_t$	Transmit antenna gain
$G_M$	Geometry Matrix
h	Height
$h_r$	Receiver antenna height
$h_t$	Transmit antenna height
Hz	Hertz
I	Fisher Information Matrix

## LIST OF SYMBOLS

---

Symbol	Definition
$\ell_i$	NLOS bias
$l$	Length
$J$	Objective function (AML)
$k$	Number of iterations
$k_B$	Boltzmann's constant
$K_p$	Multiple paths
$L$	System loss factor
$M$	Number of subject nodes
$m$	Metre
MSs	Mobile Stations
$M_{PL}$	Maximum Possible Locations
$N$	Number of anchor nodes
$N_o$	Noise power spectral density
$N_p$	Noise power
$n$	Error Function of Ranging System
$P_r$	Receive power
$P_t$	Transmit power
$\mathcal{R}_c$	Chip Rate
$s$	Second
$\hat{s}$	Estimated subject node
$s_j$	Subject node
$\mathcal{S}_m$	Symbol

## LIST OF SYMBOLS

---

Symbol	Definition
$\text{SNR}_m$	Measured Signal-to-Noise-Ratio
$\mathcal{S}_r$	Symbol rate
$\tau$	Propagation Delay
T	Matrix transpose
$T$	System temperature (Kelvin)
$\mathcal{T}_c$	Chip period
$T_{\text{cor}}$	Correlation time estimate
$T_{\text{tof}}$	Total Time-of-Flight
$T_{\text{tot}}$	Total measure time
$T_{\text{tat}}$	Total turn-around time
$T_{\text{rx}}$	Receive delay
$\mathcal{T}_s$	Symbol duration Time
$T_{\text{tx}}$	Transmit delay
w	Width
$x$	x coordinated
$y$	y coordinated
$z$	z coordinated

# Chapter 1

## Introduction

### 1.1 Introduction

The last couple of decades have seen a tremendous development in micro-electro-mechanical-systems (MEMS), data communication and electronics. In 2002, it allowed researchers from Intel and UC Berkeley as a part of famous Great Duck Island project to monitor dozens of petrel's nesting burrows with small devices called *motes* [4]. Each mote is about the size of its power source—a pair AA batteries (energy source), capable of performing some processing (equipped with processor), gathering sensory information (small memory), sensing and monitoring environment (light, humidity, pressure, and heat sensors). Above all, there was also a radio transceiver just powerful enough to cooperatively communicate with other connected neighbour motes in the network and to transmit monitored data. The motes, equipped with five main components as shown in figure 1.1(a), reflect a future composed by networks of battery powered wireless sensors that monitor our environment, our machines and even us [4]. Fig. 1.1(b) shows 2.4GHz IEEE 802.15.4 and ZigBee PRO compliant JN5148 micro-controller and sensor board. It integrates an extremely powerful 32-bit RISC CPU with cumulative memory inside amounts to 256 kbyte, and, combined with efficient code utilization. This is enough for a full ZigBee PRO stack and to provide space for applications [1].

WSNs are very application specific networks and composed of a large number of tiny sensors, which can be deployed over a vicinity of interest. Based on the type and purpose like continuous sensing and control, event detection and

## 1.1 Introduction

---

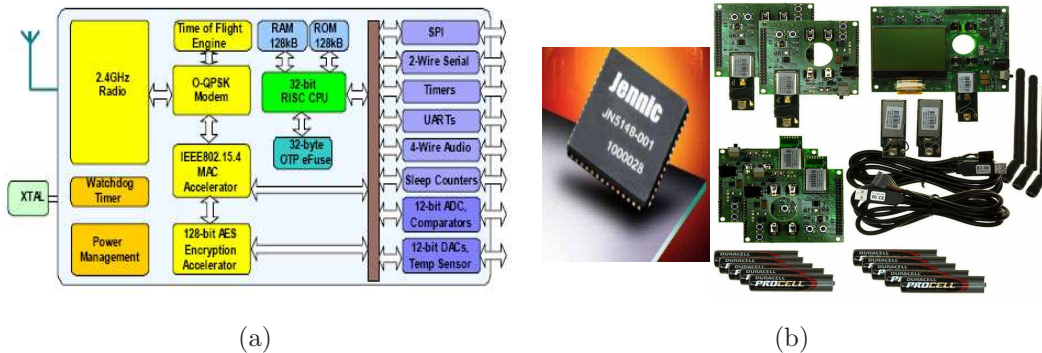


Figure 1.1: Fig. 1.1(a). Smart Sensor Architecture [1]. Fig. 1.1(b). JN5148 Micro-controller and sensor board [1].

identification, monitoring and surveillance they can be deployed in small scale or large scale networks. The deployment can be with the static constraint of nodes or considering the mobility based indoor or outdoor with unpredictable environmental factors. These sensor devices exhibit several limitations in terms of energy consumption, restricted computation capability, storage capability, signal processing and short range radio communication [5]. Furthermore, WSNs differ from traditional wired and wireless networks in terms of the node density (i.e. large number of sensor nodes in a vicinity), sensor nodes deployment (i.e. unattainable or remote vicinities), dynamic and unpredictable node mobility (i.e. may leave or join the network) and node failure (i.e. due to lack of battery power). Therefore, to address these limitations, there is a need of efficient and optimized processing, which can reduce the communication cost.

Based on different characteristics as discussed above and application specific nature of WSNs, the field of WSNs exhibits many challenges. A detailed survey of different challenges is discussed in [5]. These challenges include, optimization of localization, energy efficient geographic routing, location aware security, data storage, location aware inter-node cooperation, data-dissemination incorporating localization, fault detection and tolerance and others. However, localization of nodes in such networks exhibit new challenges due to its integration with many emerging applications and system functionalities.

## 1.2 Localization for Wireless Sensor Networks

According to Technology Review magazine published by Massachusetts Institute of Technology (MIT), WSNs are one of the top ten technologies, which will change the world and the way we live our lives [4]. A wide variety of emerging applications are considered under the umbrella of WSNs such as, intelligent transport, biodiversity mapping, robotic land-mine detection, battlefield surveillance, precision farming, disaster recovery operations, intelligent buildings, monitoring the flow of glaciers, critical coastal ecosystems, detect alpha, beta and gamma radiation and others. In many of these applications, determining the position of sensors is one of the top priorities. Since, WSNs are application oriented networks, the ultimate aim of location aware WSNs is to optimize the reliability and precision of location information for location based services (LBS). It is because that without the knowledge of geographic information, data passed by sensors is meaningless or without having the knowledge of location of an event it will be quite useless for LBS to reply in response to data received from the sensors. In addition, energy efficient geographic routing has shown great interest, where accurate and reliable localization is the first basic requirement [6]. Furthermore, system functionalities like network coverage checking and location-based information querying are dependent on the reliable localization [7]. It previews that; optimized localization can be further incorporated to optimize the communication mechanism in WSNs.

Localization is used to solve the problem of determining the positions of nodes or objects. Localization in fact can be used to represents the relationship between different objects based on the coordination system. Due to the application specific nature and its integration with many systems functionalities, the localization approaches in WSNs are classified as range-free [8–10] and range-based approaches [11–13]. The former is based on the topological relationship and does not utilize range estimation for localization. One of the main problems with range-free localization is that this type of localization is suitable for relative location instead of fixed location as they use proximity information to estimate the location of the nodes in a WSN, and thus have limited precision. The latter approach (geometrical) is based on using angle estimates [14, 15], or accurate range measurements, which can be derived from measuring point-to-point propagation time [16, 17] or

## 1.3 Scope and Motivations

---

using received signal strength [14]. This thesis addresses the challenge of range aware localization in WSNs.

## 1.3 Scope and Motivations

This section states the scope and impetus behind this research in WSNs with respect to each chapter.

- **Motivation 1 - [Chapter 3]:** The swift growth of wireless networking in our daily life has forced the division of wireless applications into different standardization directions. One direction getting a lot of attention is the IEEE 802.15.4/Zigbee [18] global standard for short range, low-data-rate, low-power, and low-cost applications, which is intended to serve and be adopted by industrial, scientific and medical (ISM) applications. These features, differentiate IEEE 802.15.4/Zigbee standard with other standards such as Wireless Local Area Networks (WLAN), the ubiquitous Bluetooth devices, different versions of Worldwide Interoperability for Microwave Access (WiMAX) such as, fixed WiMAX (802.16d) for faster Wi-Fi style ISP networks, mobile WiMAX (802.16e) for use as a 3G/HSPA replacement by mobile phone operators and recently approved WiMAX2/WirelessMAN-Advanced (802.16m) standard for high-speed wide area wireless networking and Long Term Evolution (LTE) technology, which are expected to become the next major global wireless technology. However, all of these networks focused to achieve high data throughput and high quality of services (QoS) and it makes IEEE 802.15.4/Zigbee standard an ideal choice for WSNs research community for a wide range of applications as discussed above. In many of these applications, determining the position of sensors is one of the top priorities. An alternate to IEEE 802.15.4/Zigbee standard for location aware application is Ultra-Wide-Band (UWB), which is developed by IEEE 802.15.4a Task Group [19] to meet sub-metre accuracy. However, UWB is limited in operational range ( $< 100\text{m}$ ) because of the Federal Communications Commission (FCC) regulation on transmission power [20]. The UWB air interface, which is between 3.1GHz and 10.6GHz, has

### 1.3 Scope and Motivations

---

attracted many wireless communication areas, including WSNs due to its lower power consumption, an increased data rate over comparatively short range, large bandwidth (minimum of 500MHz), superior performance in multipath environments, and realization of an ultra-low power with simple and easy to design transmitters [21]. The poor ranging performance of non-coherent UWB receivers [22] (i.e. lack of synchronization, channel estimation and pulse shape estimation, energy detection, and interference) diverted research towards the fully coherent reception of UWB signals [23]. The performance of these coherent receivers is the result of relatively high computation and processing requirements, and hardware complexity [21].

The most common technique in locating a wireless device is the so called trilateration method. In the first phase of this technique, anchor nodes perform ranging individually with the subject node and based on this range information, the second phase (localization phase) estimates the subject nodes coordinates. It suggests that ranging accuracy is an important aspect to consider because a localization system obtains position estimates using range estimates. Inaccurate range estimation may lead to unacceptable localization errors. Hence, for efficient localization, it is imperative to understand the performance limits of ranging in realistic environments. Two widely used methods for range estimation are the time-of-flight (ToF) and the received signal strength (RSS). Recently, commercial products have been released by several vendors such as Jennic [24], Dust Networks (winner of the best technical development of a WSN/RTLS device, May 2011, by DTechEx Energy Harvesting and WSN Awards) [25], Texas Instruments [26], Freescale semiconductor [27], and Atmel [28]. In late 2009, Jennic introduced IEEE 802.15.4 compliant devices with built-in ToF engine and RSS capability to revolutionize LBSs. It encouraged us to address the performance limits of ToF and RSS based ranging for IEEE 802.15.4 compliant devices in realistic environments. The indoor and outdoor experimental results provided a platform to understand and demonstrate the performance behaviour of IEEE 802.15.4 ToF based ranging.

### 1.3 Scope and Motivations

---

- **Motivation 2 - [Chapter 4, 5 and 6]:** The last couple of decades have seen tremendous interest in research towards subject localization, where the subject position is to be determined from a set of noisy measurements. This work is mainly focused on range aware localization, where a set of measurement used to locate the subject node are range estimates between the subject and a set of fixed nodes (aka *anchors*). The range estimates can be obtained via time-of-flight (ToF) or received signal strength (RSS). Location errors always exist no matter which ranging technique is used. In addition to the ranging error (as discussed above), another well-known error source is the geometric placement of anchor nodes, which can significantly degrade the quality of position estimate based any localization technique. In NAVSTAR/Global Positioning System (GPS), and Global Navigation Satellite System (GLONASS) community, geometric dilution of precision (GDOP) is a well-known problem [29–36] which illustrates the geometric configuration impacting location estimation accuracy of a localization system. Previous work has shown that poor anchor placement can lead to a substantial degradation in the performance of any range aware localization technique in terms of accuracy. Although, several schemes and fixes have been proposed to mitigate the impact of anchor placement on range derived localization. However, there is little or limited work on the optimization of anchor nodes placement. The impact of anchor placement for precise and accurate localization have been limited to 3-4 anchor nodes with respect to a single subject node for 2-dimensions, hence no optimization of optimal sensor placement. Moreover, there is a comparatively little extension available for optimal anchor placement in 3-dimensions. In addition to that, in terms of the signal model, previous work for geometric placement of anchors has been limited to only additive noise model. To the best of our knowledge, there is no study of geometric placement of anchor nodes with respect to the multiplicative noise model. The observation above encouraged us to investigate the optimization of optimal anchor placement for both additive and multiplicative noise models, moreover for both 2-D and 3-D scenarios. In addition, the above observation also motivates to obtain the understand-

### 1.3 Scope and Motivations

---

ing of the impact of location error due to the geographic anchor placement for range derived localization in WSNs.

To understand the impact of geometric placement of anchor nodes, chapter 4 presents the performance analysis of three localization methods. Different geometric anchor placements have shown the different impact on localization accuracy. Particularly, extensive simulations try to discover the impact of anchors/pseudo-anchors geometry by varying the number of anchor nodes, node density and communication range. The study is expected to extend the finding of other studies, and also give new insight into optimal anchor placement. This comparative performance analysis of localization using optimal and sub-optimal lateration provided the needed motivation to optimize the anchor placement in order to enhance the performance of range aware localization.

Various techniques have been developed to solve the trilateration distance equations. These include the LS methods [37], the weighted LS method [38] and the maximum likelihood (ML) approach [39]. The performance of these algorithms is bounded by the Cramér-Rao lower bound (CRLB) which is dependent on the geometry of the anchors and the target node. The limit on performance calculated in [40] is based on the additive noise model while a modified CRLB based on the multiplicative noise model is proposed in [41]. Noticeably, work in this area [42, 43] has not considered the minimum mean CRLB (m-CRLB) to optimize the anchor placement. So it is believed that, it is the first study which takes minimum m-CRLB into consideration for both additive and multiplicative noise models for optimization of anchor placement in 2-D as well as in 3-D. It exposes new findings and problems, which have not been previously discovered or have been miss understood before due to the widely studied and focused additive signal model.

- **Motivation 3 - [Chapter 7]:**

The last couple of decades have seen tremendous interest in the implementation of real time localization system (RTLS) using wireless sensor nodes, due to the fact that GPS cannot be connected with every single piece of

### 1.3 Scope and Motivations

---

sensor node. An added challenge is the fact that in practice the real world is 3-D, which adds more complexity but on the same time demands for high accuracy. The localization systems that are implemented using wireless sensor networks (WSNs) are beacon-based localization [8], RSSI based SpotON [44], and RF and acoustic signal based Calamari [45]. However, these implemented wireless sensor networks are limited to 2-D. These systems are further discussed in chapter 2. The real sign of motivation here is to understand the practical issues while deploying a real time location system, differentiation between the practical deployment and simulation world and moreover, to verify the impact of optimal anchor placement on a real time location system, which are derived in chapter 5. The range aware localization system (RALS) uses Jennic's JN148 compliant devices with built-in RT-ToF ranging to locate a subject node in 3-D as well as in 2-D.

- **Motivation 4 - [Chapter 8]:** In recent years, there has been a great interest in research towards positioning of wireless devices in confined areas. The Global Positioning System (GPS) [29] provides an excellent worldwide lateration framework for determining geographic position. GPS solution is famous for outdoor applications. However, this solution has several limitations, the major is of course the dependency on LOS reception, together with the high power requirement and hardware complexity from satellites. With such limitations GPS typically fails in harsh environments (i.e. inside homes, offices, shopping malls, underground and between heavy vegetative cover) and exhibits suboptimal performance for WSNs. To overcome these limitations and to enhance localization accuracy, indoor positioning systems, based on the use of Global Navigation Satellite System (GNSS) repeaters [46], CarpetLAN [47] which is an indoor broadband-positioning system, infrared based active-badge system [48], or ultrasounds [49], have been developed. An overview on indoor application can be found in [50], which conclude that there is no optimal solution for positioning yet.

While GNSS have become the dominating system for open-sky, several systems share the indoor market; each having its own drawbacks, such as low accuracy, sophisticated infrastructures, limited coverage area or inadequate

## 1.4 Contributions of the Dissertation

---

acquisition costs [50]. However, their complexity, their power consumption, and their deployment costs are enduring problems [51]. To overcome, WSNs have found their way into a wide range of location based services (LBS) including indoor localization. Indoor localization has been a great interest in research because a reliable and accurate localization in harsh environments is an integral part of many emerging applications including logistics, medical services (i.e. neonatal monitoring, patient tracking), enclosed indoor rescue operations (i.e. tunnels, caves, buildings), home automation, and others. In addition, efficient localization in confined areas helps to enhance geographic routing and data dissemination for rescue operations. In ideal conditions (i.e. LOS case), quality reliable localization performance can be achieved but as propagation criteria change from ideal LOS to non-line-of-sight (NLOS), localization performance also changes. The localization performance degrades significantly in indoor environment, where range measurements include NLOS errors due to the excess path length caused by multipath propagation [52]. The estimated error in such harsh environments is assumed to have a large positive bias that causes range estimates to be greater than the actual range. Such indoor environments fail a localization system to mark the required accuracy and therefore, highlight the indoor localization as a challenging problem. The observation above encouraged us to present an attempt along this direction by proposing a new 3-D scheme named *Range Estimate Threshold* (RET). The proposed scheme defines a RET based on the 3-D field dimensions and the signal noise model to mitigate the poor range estimates ( $\hat{d}_{ij}^p$ ) from *Measured Estimation* (ME) to optimize range estimates.

## 1.4 Contributions of the Dissertation

The thesis focuses on the optimization of range aware localization in WSNs. The main novel contributions of this thesis are listed below and further explained in section 1.5:

## 1.5 Outline of the Dissertation

---

- Performance analysis of round-trip time-of-flight (RT-ToF) and received signal strength (RSS) for point to point range estimation using 2.4GHz IEEE 802.15.4 compliant transceivers (Chapter 3)
- Performance analysis of localization using sub-optimal blind lateration (SBT), optimal multi-lateration (OML), and modified sub-optimal blind trilateration (MSBT) based on knowledge of geometric dilution of precision (GDOP) in cooperative fashion (Chapter 4)
- Optimal and worst anchor placements for additive and multiplicative noise model in 2-D based on minimum mean *Cramér-Rao Lower Bound* (m-CRLB) (Chapter 5)
- Optimal and worst anchor placements for additive and multiplicative noise model in 3-D based on minimum mean *Cramér-Rao Lower Bound* (m-CRLB) (Chapter 5)
- Localization performance for additive and multiplicative noise model at different scales in 2-D and 3-D and their comparison with the lower bound for optimal, worst and arbitrary anchor placements (Chapter 6)
- Implementation of real time localization system 2.4GHz on Jennic's JN5147 IEEE 802.15.4 compliant transceivers (Chapter 7)
- A new 3-D scheme named *Range Estimate Threshold* (RET) for indoor localization (Chapter 8), which exploits the 3-D field dimensions and noise model information (Additive noise model, multiplicative noise model for ToF and log-normal shadowing model for RSS).

## 1.5 Outline of the Dissertation

This thesis comprises nine chapters as follows:

- **Chapter 2:** Chapter two presents the localization background study.

## 1.5 Outline of the Dissertation

---

- **Chapter 3:** Chapter three reports on round-trip time-of-flight (RT-ToF) and received signal strength (RSS) for point to point range estimation using 2.4GHz IEEE 802.15.4 compliant transceivers. Firstly, the performance limits for RT-ToF and RSS based range measurements are compared with the fundamental *Cramér-Rao Lower Bound* (CRLB). Secondly the range where the error for RSS ranging is expected to be greater than the error for ToF ranging is considered. We term this the ‘*cross-over*’ range ( $C_R$ ) of RSS and ToF ranging, where ToF ranging becomes more accurate than the RSS ranging. Thirdly, using a site survey application, a series of experiments have been conducted in different environments to make it possible to determine which parameters of the system lead to improved performance and successful ranging polls. Performance results and channel parameters have been obtained in outdoor and indoor for the LOS and NLOS environments. Both indoor and outdoor experimental results and analysis are presented.
- **Chapter 4:** Chapter four compares methods of two-dimensional (2-D) localization in order to try and reduce the processing overhead of optimal multi-lateration whilst still achieving a closer accuracy. Three methods of localization are examined, firstly sub-optimal blind trilateration (SBT) which randomly selects the minimum feasible number of anchors. This defines the lower processing limit. Secondly modified sub-optimal blind trilateration (MSBT) which selects anchor nodes based on geometric dilution of precision (GDOP). Thirdly we compare these with optimal multi-lateration (OML), which provides the benchmark in terms of accuracy achievable. A MATLAB based simulation platform is developed to analyse the lateration schemes in a cooperative fashion.

item **Chapter 5:** Chapter five investigates the problem of optimal placement of anchor nodes to optimize the range derived localization. The objective is to minimize the estimate of location uncertainty error by exploiting the geometric placement of the minimum number of anchor nodes required to perform the localization in 2-dimensional (2-D) and 3-dimensional (3-D) scenarios. The localization Cramér-Rao lower bound (CRLB) is derived for a 3-D case, which in previous work has only been limited to a 2-D plane.

## 1.5 Outline of the Dissertation

---

Conventionally, deploying a large number anchor node reduces localization inaccuracy; however this holds true only if the anchors are sub-optimally placed. The optimal and worst anchor positions are determined through extended simulation by comparing their mean Cramér-Rao lower bound (m-CRLB). Furthermore, the ramification of additive and multiplicative noise models on the minimum m-CRLB is explored.

- **Chapter 6:** Chapter six presents the performance analysis of optimized anchor placement (as determined and discussed in chapter 5). The least squares (LS) and approximate maximum likelihood (AML) methods for localization are used and its performance is compared with the m-CRLB for optimal and arbitrary anchor placements. It is concluded that the geometry of anchors and subject node have a serious impact on the localization process. In addition, the important question analysed in this chapter is: *If an optimal geometric placement of the minimum required anchor nodes can optimize the location estimate of subject nodes then why distribute a large number of arbitrary placed anchor nodes which will increase the complexity and processing in a resource constrained WSNs?* Further, it is also demonstrated that the optimal anchor placement of the minimum number of anchors outperforms the degraded deployment of many nodes.
- **Chapter 7:** Chapter seven presents the implementation of real time localization testbed on JN5148 IEEE compliant devices, where a device (i.e. subject) capable of performing the localization using LS method using the estimated RT-ToF measurements.
- **Chapter 8:** Chapter eight presents an indoor localization by proposing a new 3-dimensional (3-D) scheme named *Range Estimate Threshold* (RET). The proposed scheme defines a RET based on the 3-D field dimensions and the signal noise model to mitigate the poor range estimates ( $\hat{d}_{ij}^p$ ) from *Measured Estimation* (ME) to optimize range estimates. The ramification of RET on ME for indoor localization is explored through additive, multiplicative and log-normal shadowing models.

## 1.6 Publications

---

- **Chapter 9:** Chapter nine concludes the thesis with the promising future research directions.

## 1.6 Publications

The research papers published during this study are listed as follows:

1. **Maheshwari, H.K., Kemp, A.H.**, “Performance Analysis of Ranging with IEEE 802.15.4 Compliant WSN Devices”, soon to be published in *Ad Hoc & Sensor Wireless Networks: An International Journal (AHSWN)*, 2011
2. N. Salman, **Maheshwari, H.K.**, Kemp, A.H, M. Ghogho, “Effects of anchor placement on mean-CRB for localization”, *The 10th IFIP Annual Mediterranean Ad Hoc Networking Workshop*, 2011, 12-16 June, Italy
3. **Maheshwari, H.K.**, Kemp, A.H, “On the Enhanced Ranging Performance for IEEE 802.15.4 Compliant WSN Devices”, *Third International workshop on Wireless Sensor Networks - theory and practice, 2011*, 07-10 February 2011
4. **Maheshwari, H.K.**, Kemp, A.H., Peng, B,. “Localization Performance Comparison using optimal and suboptimal lateration in WSNs,” *Asia Pacific Conference on Communications (APCC 2009)*, 8th-10th October 2009
5. **Maheshwari, H.K.**, Kemp, A.H., “Comparative Performance analysis of Localization using optimal and suboptimal lateration in WSNs,” *Next Generation Mobile Applications, Services and Technologies (NGMAST 2009)*, *IEEE Communication Society*, 15th-18th September 2009
6. **Maheshwari, H.K.**, Kemp, A.H., Zeng, Q. (2008). “Range based real time localization in wireless sensor networks,” *International Multi Topic Conference, IMTIC 2008 Jamshoro, Pakistan*, vol. 20 of Communications in Computer and Information Science, 422432, Springer, April 11-12, 2008

## 1.6 Publications

---

7. I. Rasool., **Maheshwari, H. K.**, Kemp, A.H., “Error Distribution of Range Measurements in Wireless Sensor Networks (WSNs),” *21st Annual IEEE International Symposium on Personal, Indoor and Mobile Radio Communications (PIMRC 2010)*, 26-29 September 2010
8. Peng, B., Kemp, A.H., **Maheshwari, H.K.**, “Impact of Location Errors on Energy-Efficient Geographic Routing in Wireless Sensor Networks,” *Asia Pacific Conference on Communications (APCC 2009)*, 8th-10th October 2009
9. Peng, B., Kemp, A.H., **Maheshwari, H.K.**, “Power-saving Geographic Routing in the Presence of Location Errors,” *IEEE International Conference on Communications (ICC 2009)*, 14-18 June 2009.

# Chapter 2

## Background and Related Work

### 2.1 Introduction

Throughout history man has always been curious to know where things are; from navigation by looking at stars to modern techniques such as local positioning service (LPS) and the global positioning system (GPS), locating objects has invariably been of great interest and commercial value. As with most technologies, localization in wireless networks started in the military circles. Interest in navigation systems for the military use dates back to world war II when the Decca and Loran systems were implemented. Later on the new systems such as Transit, Timation, the Omega navigation system, Global Positioning System (GPS), Global Navigation Satellite System (GLONASS) were developed. GPS is a space-based global navigation satellite system (GNSS) with 24 operational satellites in the orbit, providing worldwide positioning coverage. Based on the *trilateration* principle, GPS is the most widely used navigation system that provides three-dimensional (3-D) positioning information at all times, all over the world. It has a wide range of applications including surveying, vehicle tracking, cellular positioning, and aircraft tracking. GPS is an accurate satellite system, initially developed in the late 1970 by the department of defence (DoD) and declared as fully operational in 1994 [53]. GPS solution is famous for outdoor applications. However, this solution has several limitations, the major is of course the dependency on line-of-sight (LOS) reception, together with relatively high power requirement and hardware complexity from satellites. With such limitations GPS

## 2.2 Localization in WSNs

---

typically fails in harsh environments (i.e. inside homes, offices, shopping malls, underground and between heavy vegetative cover) and exhibits suboptimal performance for WSN applications. In the last two decades, WSNs have become very popular and localization of nodes in such networks present new challenges. A list of current location technologies can be found in [54].

## 2.2 Localization in WSNs

Based on a detailed survey, a seven layer location stack as shown in Fig. 2.1 was presented in [2]. Layer 1 (*Sensors*) of location stack defines the sensor nodes capability to sense a variety of physical and logical phenomena including the infrared badges, barcode scanners or ToF engine (JN5148). It results in raw data samples such as RF ToF measurements. Layer 2 (*Measurements*) uses the different schemes to convert the raw data from layer 1 into the canonical form (e.g. proximities, distance and angles) along with an uncertainty that is associated with the task that generated the information [2, 55]. For example, ToF engine produces the range measurements with respective uncertainty models based on the characteristics of the radio and environment. The basic techniques available used for the canonical form are time-of-flight (ToF), received signal strength (RSS), angle-of-arrival (AoA), time-difference-of-arrival (TDoA). Based on the data fusion algorithms, Layer 3 (*Fusion*) joints all the available data to determine the position estimation through different localization strategies such as *lateration schemes, proximity sensing, fingerprinting, calibrating, and hybrid approaches* [14, 55]. It can be observed that layer 2 ‘*measurements*’ and layer 3 ‘*fusion*’ of the location stack are important for a robust, reliable and accurate location system. Layer 4 (*Arrangements*) interrelate the estimated target positions by converting their coordinates according to a relative coordinate system (i.e. absolute position or relative position). Layer 5 – 7 (*contextual fusion, activities and intentions*) are the elements of application layer. Layer 5 *contextual fusion* relates the location information with other contextual information such as temperature in the office, fire in the forest. Layer 6 *activities* follow the contextual information to monitor and analyse the environment. Layer 7 *intentions* follow the activities from layer 6 to prepare the system for actions to be taken.

## 2.3 Classification of Localization

---

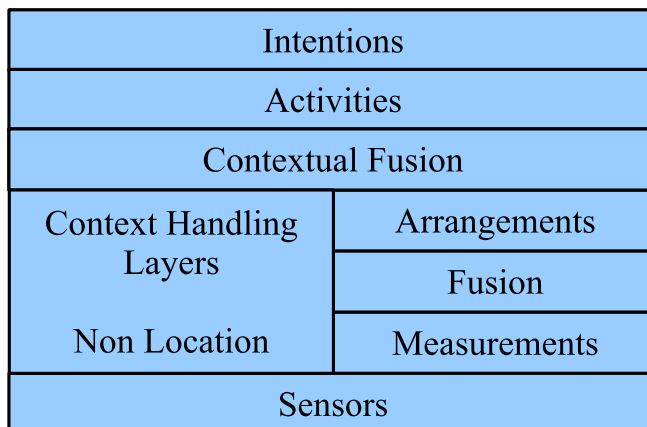


Figure 2.1: Location Stack [2]

## 2.3 Classification of Localization

Localization systems can be classified into the different approaches due to application specific aspects such as signalling scheme, accuracy, infrastructure, deployment, position estimation scheme, scalability, environment, and security. However, in general, almost all the sensor network localization algorithms share three main phases; 1) range estimation, 2) position computation and 3) localization algorithm [4, 56].

### 2.3.1 Range Estimation Phase

The techniques to measure distance and/or angle information comes under the range estimation phase and are the output of the measurement layer as defined by the location stack [55]. Range based localization schemes rely on the availability of range estimation. The precision of such estimation, however, is the focus to the transmission medium and surrounding environment. The commonly considered ranging techniques are:

#### 2.3.1.1 Angle of Arrival (AoA)

The AoA is a method to measure the angle at which an incoming signal arrives at the receiver (anchor node), hence its measures the angle between two nodes.

## 2.3 Classification of Localization

---

There are a couple of ways that sensors measure AoA. One category is phase interferometry, where an angle is estimated by phase differences in the signal received by two or more individual sensors (microphones for acoustic signals or antennas for RF signals) [57, 58]. Another category is based on the varying signal strength, where AoA estimation uses the RSS ratio between two (or more) directional antennas located on the sensor [59, 60]. Two directional antennas pointed in different directions, such that their main beams overlap, can be used to estimate the AoA from the ratio of their individual RSS values [59].

### 2.3.1.2 Complexity and Error Concerns using AoA

- The accuracy of AoA measurements is limited by the directivity of the antenna, by shadowing and by multipath reflections. A multipath component may appear as a signal arriving from an entirely different direction and can lead to very large errors in AoA measurements [14, 15, 59].
- The AoA is not a favourable localization approach for low cost IEEE Zigbee transceivers as use of directional antenna arrays increases the system cost and complexity. Furthermore, angle estimation improves at the cost of additional antennas.

### 2.3.1.3 Time Difference of Arrival (TDoA)

Conventionally, one-way ToF range measurement requires highly synchronized clock among the subject and anchors. To overcome this synchronization problem, TDoA was proposed. TDoA technique can be implemented in two different possible modes, uplink and downlink [55]. In the uplink mode, subject nodes broadcast a signal, which arrives at multiple measuring anchor nodes. This difference in the arrival of time can be treated as a hyperbola, which has two receiving anchors at its focii. Three anchor nodes are required in 2-D positioning. The target node is located at the intersection of two hyperbolas. An alternative mode downlink, where the anchors broadcast the signal simultaneously while the subject node receives it with different delays. In both cases, the anchor clocks should be accurately synchronized which are often wired to guarantee synchronization. The synchronization of the subject node and anchors in this case is however not

## 2.3 Classification of Localization

---

mandatory. In TDoA location estimation is the intersection of all hyperbolas (hyperboloids in 3-D). Unlike ToF where localization is the intersection of all circles (spheres in 3-D). This method is also known as hyperbolic localization method. Some famous TDoA based systems are Cricket (RF and ultrasound) [49], Active Bat (RF and ultrasound) [48].

### Complexity and Error Concerns using TDoA

- It requires highly synchronized clocks at each of the anchor nodes as precision of the location engine is directly proportional to the clock accuracy.
- Similar to AoA and ToA, TDoA is also affected by strong multipath components, which results in inaccurate range estimation (i.e. intersection of hyperbolas).

#### 2.3.1.4 Time of Flight (ToF)

In ToF ranging, measurements based on propagation time are used to estimate the distance between neighbouring devices. ToF is classified as either one-way propagation time or two-way propagation time measurement based on the number of packet transmission for range estimation. One-way ToF is less attractive in WSNs due to size and cost of precise clocks for synchronization between transmitter and receiver. In one-way, the node A transmits the time-stamped signal at  $t_1$  and is received at node B at  $t_2$ , the distance between the nodes is given by the equation  $d = c \times \text{ToF}_2 - \text{ToF}_1$ . As compared to one-way ToF, where two highly synchronized clocks are needed, in two-way ToF the same clock is used to calculate the round-trip time [16, 17]. Consequently synchronization between different clocks is not necessary. ToF is further discussed in chapter 3.

#### 2.3.1.5 Received Signal Strength (RSS)

The Received Signal Strength Indicator (RSSI) of a radio channel provides a feasible way of estimating distance between sensor nodes. It is preferred to use this distance measurement technique because the sensor nodes do not require any additional hardware but only a radio transceiver. Both medium characteristics

## 2.3 Classification of Localization

---

and node hardware consistency influences RSS measurement results. Existing distance-estimation based techniques for localization rely on a log-normal radio propagation model [61] to estimate inter-sensor distances from RSS measurements. The path loss exponent ( $\eta$ ) is a key parameter in the log-normal model which characterizes the transmission media and accurate knowledge of this factor is required in order to obtain an accurate estimate from RSS measurements. Hence to reduce the ranging error for localization, a calibration method (aka fingerprinting) to map the channel information (i.e.  $\eta$ , shadowing variance, frequency selective fading) has been considered to model an appropriate path loss model [11, 12, 61].

Most of the previous work is limited to 2-D, and in addition to that optimal anchor placement is not considered in order to calibrate the channel parameters [12, 61–63]. However, in practical systems, these calibrated channel parameters may become impractical due to the nuisance in the channel such as, the background noise and some other environmental factors, such as temperature, humidity, weather conditions and obstacles to the transmission. In addition, the hardware device characteristics include the wireless communication part (the node transmitting power, receiver sensitivity) and antenna (antenna directivity and antenna gains) [64]. It is therefore, in addition to the prior knowledge of channel parameters, knowledge of a confined area (indoor environment) can be utilized to enhance the RSS based localization. RSS is further experimentally analysed in chapter 3, and a proposed scheme for indoor localization is discussed in chapter 8.

Due to the complexity and error concerns posed by AoA and TDoA, ToF and RSS are mainly focused (chapter 3). Round-trip ToF overcomes the major problem of synchronization, faced by the one-way ToF, hence it reduces the complexity and system cost as compared to TDoA and AoA. Whereas, received signal strength (RSS) is one of the standard parameters available on most of the wireless devices.

## 2.3 Classification of Localization

---

### 2.3.2 Position Computation Phase

The second step after achieving accurate range estimate is to find the position of the subject nodes. Depending on the method used for ranging in phase 1, an appropriate localization technique is applied in the second phase. A detailed survey of these approaches can be found in [14, 55, 65]. However, a detailed analysis of lateration schemes is provided in chapter 4 titled “Localization using Optimal and Sub-Optimal Multi-lateration.” The main reason to analyse lateration scheme is to understand the impact of geometric placement of anchor nodes on location accuracy.

- **Geometrical Approaches:**
  - Lateration (Trilateration, Bounded Intersection, Multilateration)
  - Hyperbolic localization
  - Angulation
  - Bounding box
- **RSS Based Approaches**
  - Fingerprinting
  - Probabilistic approach
- **Hybrid Approaches**
  - Hybrid angulation and lateration
  - Hybrid angulation and hyperbolic localization

### 2.3.3 Localization Algorithms

In WSNs, the localization algorithm has been categorized into different categories based on the limited resource and application requirements. A list of such categories for localization algorithms is listed below [65].

## 2.3 Classification of Localization

---

- **Single-hop or Multi-hop localization:**

A direct communication link between two nodes is commonly referred to as a *hop*. Networks where there is only a single link between nodes for location purposes are called single-hop. GPS is an example of a single-hop positioning systems. On the other hand, if the node that is desired to be localized is out of range of an anchor or BS, a communication link using intermediate nodes is established, this is known as multi-hop. Single hop algorithms are simple and accurate but are not scalable, multi-hop algorithms are more scalable due to their distributed nature. The problem of scalability in single-hop localization can be minimized by the cooperative localization, where to cover the entire field (i.e. subject nodes), localized nodes can behave as the pseudo-anchor nodes. This scheme is further discussed and analysed in chapter 4.

- **Centralized or Distributed Algorithms:**

Centralized algorithms [12, 48, 66] are based on the central unit, which collects, process and sent back the processed data in a centralized manner. In such algorithms, the major problem is the scalability, intrinsic delay, however the accuracy stay better as they are less prone to error propagation but inefficiency increases as the network size increases, hence more communication cost and intrinsic delay.

On the other hand, distributed systems [49, 67, 68] can allow the processing to be performed at each node. Generally, distributed algorithms are more robust and energy capable since each node determines its position under the infrastructure (anchor based) or infrastructure less (connectivity based) networks, without the requirement of sending and receiving location information to and from a centralized unit. However, distributed algorithms are more complicated to implement due to the limited computational capabilities of sensor nodes. Distributed solutions tend to distribute and increase the error, cumulatively. This is because in multi-hop execution, there can be a considerable number of subject nodes that cannot directly communicate with any anchor node [65] and accumulate error while being localized using pseudo-anchor nodes in a cooperative way.

## 2.3 Classification of Localization

---

- **With Infrastructure or Without Infrastructure:**

Further classification of localization is based on the systems with infrastructure and without infrastructure. Infrastructure based systems are those which are based on the anchor nodes (aka reference nodes). Anchor nodes are the special capability nodes who know their position usually either through a GPS receiver installed on them or through pre-programmed configuration. Other unknown subject nodes use these anchor nodes to calculate the location. One of the common examples of infrastructure based system is GPS. One of the most important factors to consider in infrastructure based networks is the anchors geometry, which strongly affect the quality of the localization. In GPS community, this problem has been studied extensively with respect to the Geometric Dilution of Precision (GDOP) [30–32, 35] metric but extendible to any range based localization system [55]. However, in the context of the WSN, GDOP study has been limited [69–71]. GDOP metric along with the lateration schemes is analysed thoroughly in chapter 4. In [42] it is concluded that *the one-hop distance-based localization mechanism has geometry as its foundation*. However, the analysis was limited to 2-D as well as Cramér-Rao lower bound (CRLB) metric is only used at different angles just to analyse the impact of 3 anchors geometry on localization accuracy [42, 43]. Furthermore, the analysis was limited to the additive noise model and no optimal placement is suggested. A marginal degree of research has been done on optimal anchor placement. In [72, 73], the authors obtained an analytical solution for the optimal anchor placement based on the CRLB. Where authors achieve optimality condition for 3 and 4 anchors only. The relation between lower bound and the Fisher Information Matrix (FIM) is given as (2.1):

$$\sigma^2(\hat{s}) \geq [\mathbf{I}(s)]_{jj}^{-1} \quad (2.1)$$

where,

## 2.3 Classification of Localization

---

where  $\sigma^2(\hat{s})$  can be given as  $\sigma^2(\hat{s}) = E \{(\hat{s}_j - s_j)(\hat{s}_j - s_j)^T\}$ ,  $(\mathbf{I}(s)^{-1})_{jj}$  is the lower bound on the variance of  $(\hat{s})$  and  $\mathbf{I}(s)$  is the (FIM) and is defined as [72]:

$$\mathbf{I}(s) = \begin{bmatrix} \sum_{i=1}^N \frac{\cos^2(\alpha_{ij})}{\sigma_{ij}^2} & \sum_{i=1}^N \frac{\cos(\alpha_{ij}) \sin(\alpha_{ij})}{\sigma_{ij}^2} \\ \sum_{i=1}^N \frac{\cos(\alpha_{ij}) \sin(\alpha_{ij})}{\sigma_{ij}^2} & \sum_{i=1}^N \frac{\sin^2(\alpha_{ij})}{\sigma_{ij}^2} \end{bmatrix} \quad (2.2)$$

Minimizing the inverse of the FIM is equivalent to maximizing its determinant. The determinant is given as:

$$\det [\mathbf{I}(s)] = \frac{1}{4\sigma_{ij}^2} \left[ N^2 - \left( \sum_{i=1}^N \cos(2\alpha_{ij}) \right)^2 - \left( \sum_{i=1}^N \sin(2\alpha_{ij}) \right)^2 \right] \quad (2.3)$$

The upper bound can be bounded by  $\frac{N^2}{4\sigma_{ij}^2}$ , which is only achieved when:

$$\sum_{i=1}^N \cos(2\alpha_{ij}) = 0, \sum_{i=1}^N \sin(2\alpha_{ij}) = 0 \quad (2.4)$$

As a consequence, the optimal anchor placement for 3 and 4 anchors is obtained if:

$$\beta_{ij} = \beta_{ij} = \frac{2}{N}\pi \quad (2.5)$$

where  $N$  is the number of anchors and  $\beta_{ij}$  is the angle subtended at the target by two anchors. Thus in order to minimize the localization error (i.e.

## 2.3 Classification of Localization

---

MSE) for 3 and 4 anchors, each anchor should subtended the same angle on the target. For  $N > 5$  anchors, the optimal anchor geometry is not unique. Furthermore, in both [72, 73], the authors limited the analytical and simulation to 3 and 4 anchors with their own choice, i.e. without exploiting all possible combinations. The same approach is applied to TDoA [72] and RSS [74].

### **Without Infrastructure:**

On the other hand, infrastructures less networks are those, which are without the anchor nodes. The communication in such systems is based on the connectivity with in-range nodes; hence they provide the location of sensor node relative to neighbour nodes. The nodes in the infrastructure less systems show more complexity due to the fact that each node has to communicate in hop count manner, hence nodes are required to have some way to access, prioritize the sequence of communication in order to provide quality of service (QoS).

- **Range based or range free:**

Range based approaches are discussed above under the process of range estimation phase in section 2.3.1, whereas range free approach is discussed below:

This course of localization systems is cost effective because it eliminates the need of high cost specialized hardware on each sensor node. The calculation in these systems is based on the radio connectivity information among neighbouring nodes and sensing capabilities (as they use the number of hops between a node pair as a distance metric) that each sensor node posses [10, 56, 65]. One of the main problems with range-free localization is that, this type of localization is suitable for relative location instead of absolute location tracking. Example of range free localization schemes are approximate point in triangulation (APIT) [75], Secure Range-Independent Localization for Wireless Sensor Networks (SeRLoc) [76]. The accuracy of range-free methods is less than the range-based ones but they satisfy the requirements for many applications. Because of the hardware limitations of WSN devices, solutions in range-free localization are being pursued as a

## 2.4 Localization Techniques and Optimization

---

simple and cost-effective alternative to range-based approaches. The most obvious disadvantage of this scheme is the fact that it performs poorly [65].

## 2.4 Localization Techniques and Optimization

Consider a 2-D network, consisting of  $N$  anchor nodes whose locations  $A_i = [x_i, y_i]^T$  for  $i = 1, \dots, N$  are known, this can be achieved by placing these anchors at predefined points or their position can be determined via GPS. Considering the  $M$  number of unknown subject nodes whose true locations are denoted as  $s_j = [x_j, y_j]^T$  for  $j = 1, \dots, M$ , where  $.^T$  is the matrix transpose operation. It is desired to determine the location of a subject node  $s_j$ . In practice, actual distance  $d_{ij}$  based on ToF is corrupted by the various factors discussed in Chapter 3, hence the estimate distance ( $\hat{d}_{ij}$ ) between anchor and subject node can be given as:

$$\hat{d}_{ij} = d_{ij} + n_{ij} \quad (i = 1, \dots, N) \quad (2.6)$$

where  $d_{ij}$  is the true distance between anchor  $i$  and subject node  $j$ , given as  $d_{ij} = \sqrt{(x_i - x_j)^2 + (y_i - y_j)^2}$ . If the noise for each measurement is considered to be independent zero mean Gaussian random variable with variance  $\sigma_{ij}^2$  ( $n_{ij} \sim \mathcal{N}(0, \sigma_{ij}^2)$ ). In vector form to include estimated distances from  $N$  anchors can be given as  $\hat{\mathbf{d}}_{ij} = [\hat{d}_{1j}, \hat{d}_{2j}, \dots, \hat{d}_{Nj}]^T$ .

In general, the range estimates ( $d_{ij}$ ) are not accurate due to the noisy measurements and NLOS bias. Due to the inaccurate range estimates, the lateration technique yields line of positions (LoPs), which provide a region of uncertainty instead of a single point as shown in Fig. 2.2(b), resulting in  $N$  inconsistent equations in the form of  $\hat{d}_{ij} = \sqrt{(x_i - x_j)^2 + (y_i - y_j)^2}$  for  $i = 1, 2, \dots, N$ . In this case there will be no unique solution and subject node could be located within any point in the uncertainty region.

In literature, many localization techniques were proposed to estimate the subject position from  $N$  inconsistent equations, such as:

- **Direct Method:** Direct method can be used by directly solving a set of simultaneous equations based on the range estimates.

## 2.4 Localization Techniques and Optimization

---

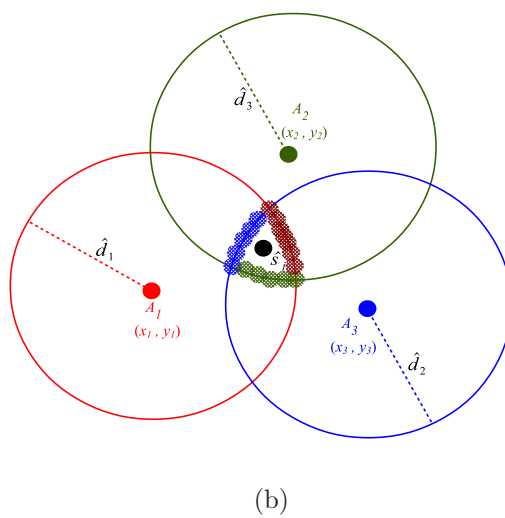
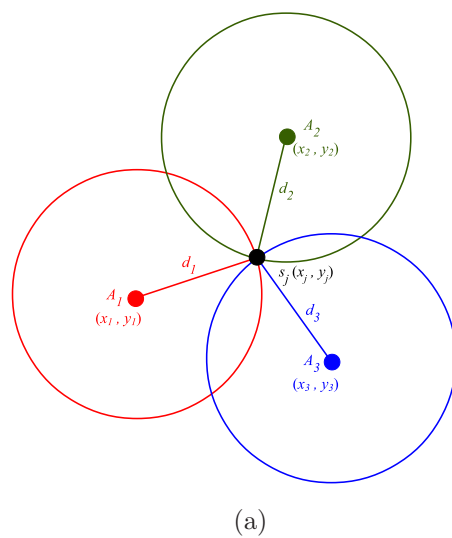


Figure 2.2: Fig. 2.2(a). Subject node with 3 in-range anchor nodes with actual ranging. Fig. 2.2(b). Subject node with 3 in-range anchor nodes with noise range.

## 2.4 Localization Techniques and Optimization

---

- **Iterative Method:** The iterative methods perform the location estimation iteratively. These iterative methods are based on the predefined threshold/criteria and only stops when the predefined criteria is satisfied. Some famous iterative methods are Taylor series, gradient decent method, and Approximate Maximum Likelihood (AML).

However, to analyse the impact of optimal anchor placements and their impact on the location accuracy, Least Squares (LS) and Approximate Maximum Likelihood (AML) are used for position estimation. The LS is explained in chapter 4 with lateration schemes and AML is explained below.

### 2.4.1 Maximum Likelihood algorithm (ML)

The estimated distance can be give by Eq. (2.6), where  $i = 1, \dots, N$ ,  $N$  is the number of anchor nodes, while  $d_{ij}$  is the true distance between anchor  $i$  and subject node  $j$ , given as  $d_{ij} = \sqrt{(x_i - x_j)^2 + (y_i - y_j)^2}$ . In vector form to include actual distances from  $N$  anchors can be given as  $\mathbf{d}_{ij} = [d_{1j}, d_{2j}, \dots, d_{Nj}]^T$ , and in vector form to include estimated distances from  $N$  anchors can be given as  $\hat{\mathbf{d}}_{ij} = [\hat{d}_{1j}, \hat{d}_{2j}, \dots, \hat{d}_{Nj}]^T$ . Its covariance vector is given as [77]:

$$\mathbf{Q} = E \{ n_{ij} n_{ij}^T \} = \begin{bmatrix} \sigma_{ij}^2 & \cdots & 0 \\ \vdots & \ddots & \vdots \\ 0 & \cdots & \sigma_{ij}^2 \end{bmatrix} \quad (2.7)$$

If the noise for each measurement is considered to be independent zero mean Gaussian random variable, then the p.d.f of  $d_{ij}$  is given as Eq. (2.8) [77]:

$$p(\hat{\mathbf{d}}_{ij} | s) = \prod_{i=1}^N \frac{1}{\sqrt{2\pi\sigma_{ij}^2}} \exp \left( -\frac{(\hat{d}_{ij} - d_{ij})^2}{2\sigma_{ij}^2} \right) \quad (2.8)$$

$$p(\hat{\mathbf{d}}_{ij} | s) = \frac{1}{\sqrt{(2\pi)^N \det(\mathbf{Q})}} \exp \left\{ -\frac{\mathbf{J}}{2} \right\} \quad (2.9)$$

where  $\mathbf{J} = [\hat{\mathbf{d}}_{ij} - \mathbf{d}_{ij}]^T \mathbf{Q}^{-1} [\hat{\mathbf{d}}_{ij} - \mathbf{d}_{ij}]$ . The ML solution would be  $x$  that maximize the *probability density function* (PDF) or alternatively minimize the  $\mathbf{J}$ . To

## 2.4 Localization Techniques and Optimization

---

find the minimum of  $J$ , taking the gradient of  $J$  with respect to  $x_j$  and  $y_j$  ( $\frac{d_j J}{dx_j} = 0$  and  $\frac{d_j J}{dy_j} = 0$ ). The ML solution is given as [77]:

$$\frac{d_j J}{dx_j} = 0 = \sum_{i=1}^N \frac{(d_{ij} - \hat{d}_{ij})(x_j - x_i)}{d_{ij}} \quad (2.10)$$

$$\frac{d_j J}{dy_j} = 0 = \sum_{i=1}^N \frac{(d_{ij} - \hat{d}_{ij})(y_j - y_i)}{d_{ij}} \quad (2.11)$$

Since the Eq. (2.10) and Eq. (2.11) are not linear and both depend on the  $d_{ij}$  which is unknown, thus an approximate ML solution is required. A solution based on the approximate Maximum Likelihood algorithm is given below.

### 2.4.2 Approximate Maximum Likelihood algorithm (AML)

An approximate maximum likelihood solution (AML) is proposed in [77] which start with ML and converts the ML equations into the linear equation with unknown  $(x_j, y_j)$ , whose coefficients are also dependent on  $(x_j, y_j)$ . In order to solve it, it starts with the initial guess of  $(x_j, y_j)$ , and updates  $(x_j, y_j)$  iteratively. After  $n$  number of updates, AML checks the ML cost function with  $(x_j, y_j)$  for each update, and selects the minimum as the estimated location. By substituting  $\frac{d_{ij}^2 - \hat{d}_{ij}^2}{d_{ij} + \hat{d}_{ij}}$  [77]:

$$\sum_{i=1}^N \frac{(d_{ij}^2 - \hat{d}_{ij}^2)(x_j - x_i)}{d_{ij}(d_{ij} + \hat{d}_{ij})} = 0 \quad (2.12)$$

$$\sum_{i=1}^N \frac{(d_{ij}^2 - \hat{d}_{ij}^2)(y_j - y_i)}{d_{ij}(d_{ij} + \hat{d}_{ij})} = 0 \quad (2.13)$$

Writing Eq. (2.12) and Eq. (2.13) in matrix form [77]:

$$2 \begin{bmatrix} \sum_{i=1}^N g_i x_i & \sum_{i=1}^N g_i y_i \\ \sum_{i=1}^N h_i x_i & \sum_{i=1}^N h_i y_i \end{bmatrix} \begin{bmatrix} x \\ y \end{bmatrix} = \begin{bmatrix} \sum_{i=1}^N g_i (s + k_i + \hat{d}_{ij}^2) \\ \sum_{i=1}^N h_i (s + k_i + \hat{d}_{ij}^2) \end{bmatrix} \quad (2.14)$$

## 2.5 Performance metric

---

where

$$\begin{aligned} g_{ij} &= \frac{x_j - x_i}{d_{ij} (d_{ij} + \hat{d}_{ij})} \\ h_{ij} &= \frac{y_j - y_i}{d_{ij} (d_{ij} + \hat{d}_{ij})} \end{aligned} \quad (2.15)$$

The equation (2.15) is treated as linear by the ML in terms of  $s$ . It is solved by first giving it an initial guess value of  $x_j$  and  $y_j$  to obtain the values of  $g_i$  and  $h_i$ . The LS solution will result in quadratic in  $s = x_j^2 + y_j^2$ , with two roots  $r1$  and  $r2$ . By using root selection routing (RSR) and selecting positive roots, a new value of  $x_j$  and  $y_j$  will be obtained for next iteration. If both roots are positive, the root giving minimum J is selected. However if both the roots are negative, the absolute values are taken. Compute the cost function J for this new value of  $x_j$  and  $y_j$ . The procedure is repeated a fixed number of iteration and the  $(x_j, y_j)$  giving the minimum value of J, hence closest estimated location is chosen [77]. AML approaches CRLB in many scenarios, such as, when there are three anchors on a straight line, AML gives better location estimate, hence avoiding the dilution of precision problem. It is further verified in chapter 5 when compared with the LS method for optimal placement of 3 anchors based on multiplicative noise model.

## 2.5 Performance metric

Accuracy of a location system is not the only benchmark of its performance; there are other criterion's that should also be taken into consideration. The performance of a positioning system can be determined by the following yardsticks.

### 2.5.1 Accuracy

Accuracy is the most important criterion for a location system. Accuracy can be defined as the degree of perfection of a measured or calculated quantity to its true value [78]. Accuracy of a system can be achieved by considering the overall estimate of the errors including systematic errors. It shows the quality of the physical measured data by matching it with true measurement. As mentioned

## 2.5 Performance metric

---

above, accuracy is also connected with the systematic errors, it can be increased by proper calibration or making adjustment to the internal system.

### 2.5.2 Precision

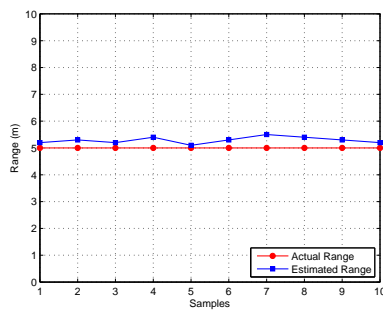
Precision (aka repeatability or reproducibility) can be defined as the measurement stability of the system. It gives the indication of intrinsic variability in the measurements [79]. The requirement and degree of precision may vary application to application. Fig. 2.3(c) shows the estimated range with high precision but low accuracy. The average estimated error of 4m over all repeated samples provide low accuracy but high precision (i.e. 92% average precision). This is because of the consistence range estimates in all iterations for the same input signal. The accuracy and precision are considered as two crucial parameters to describe the result of a localization system. The concept of accuracy and precision is further illustrated in Fig. 2.3. In Fig. 2.3(a), an estimated range that is 0.2 to 0.5m displaced from its actual range in all repeated samples is considered as a measure of high accuracy and high precision. Whereas, Fig. 2.3(d) shows high accuracy with low precision due to its high degree of error and large variations in estimated range. A good positioning system apart from being accurate should be persistent in estimating accurate localization. If two systems have equal accuracy, the system, which is more precise, is chosen. This decision is normally based on the *cumulative distribution function* (CDF) of the distance error, systems with high precision have steeper CDF graphs. Usually, the precision is measured in percentile.

### 2.5.3 Complexity

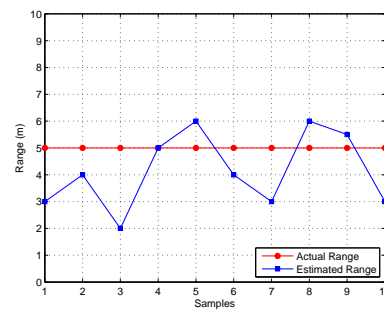
Localization in low power networks (such as sensor networks) is desired to be of low complexity. Nodes in such networks have lower computation power and algorithms requiring low processing are preferred. Other systems, where the calculations are carried out by an external base station can of course afford high complexity algorithms. The complexity of the system is normally measured in terms of the time taken by the network to localize a node.

## 2.5 Performance metric

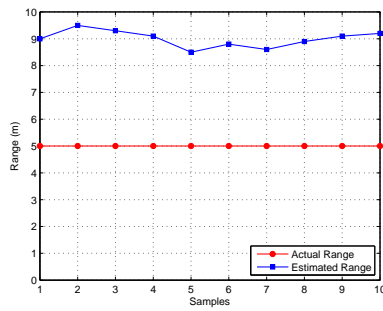
---



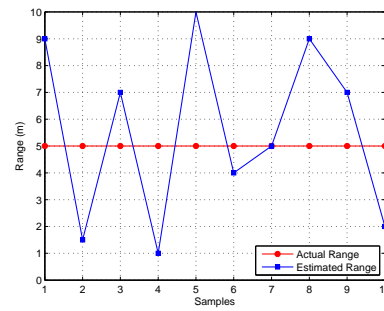
(a)



(b)



(c)



(d)

Figure 2.3: Precision and Accuracy analysis for randomly selected data: Fig. 2.3(a). High accuracy with high precision, Fig. 2.3(b). High accuracy with low precision, Fig. 2.3(c). Low accuracy with high precision, Fig. 2.3(d). High accuracy with low precision.

## 2.6 Localization Systems

---

### 2.5.4 Robustness

Systems that perform well in harsh conditions (i.e. highly cluttered environments) are preferred compared to systems, which perform well only in accommodating scenarios. Thus, systems, which are able to perform localization with incomplete information, are more robust.

### 2.5.5 Scalability

The scalability of a system can be measured in terms of geography and density. A system is geographically scalable if it can perform localization at longer distance; generally, the performance of a system degrades as the distance between the nodes increases. On the other hand, the density of a network refers to the number of nodes per unit area/ volume. The performance of systems deteriorates as more nodes are added into the network (due to multi-user interference MUI). Furthermore, scalability also can be assessed whether a system can localize in two dimensions (2-D) or three dimensions (3-D).

### 2.5.6 Cost

Another important factor in choosing a positioning system is the cost. Cost can be in terms of money, energy consumption, size and weight. It might be desired to install low power and cheap positioning systems with little maintenance requirement. Such needs cannot be fulfilled by GPS and low cost systems are generally preferred.

## 2.6 Localization Systems

### 2.6.1 Active Badge, 1992

Active Badge localization system introduced by AT&T Cambridge [66] is a centralized system. This indoor tracking system uses the infrared transmitters (objects to be located) to periodically transmit the distinctive identification (ID) every 10s or on demand. The fixed receiver receives this identifier, which is then collected by centralized server for absolute location information (i.e. room or

## 2.6 Localization Systems

---

office). It is limited within a room on fixed locations due to the short range of infrared.

### 2.6.2 Active Bat, 1999

Active Bat [48] an extension to Active Badge, was introduced by AT&T uses the TDoA. This centralized system uses an ultrasound ToF to estimate the distance and multi-lateration technique to provide the more accuracy than Active Badge [66]. In this system, users or objects carry a transmitter (Active Bat tag). The system starts, when a controller sends a short radio pulse to the tags. At the same time, systems sends a reset signal to the ceiling mounted receivers (anchors) using a wired network. The tag emits an ultrasonic pulse to the grid of the ceiling-mounted receivers. Each receiver calculates the time interval from reset to ultrasonic pulse arrival and computes its distance from a tag and reports back to a central server for multi-lateration. The reported accuracy is 9cm with 95% precision (i.e. out of 100 samples, 95 samples are within the accuracy of 9cm)in 3-D. Due to the limited ceiling grid deployment, it requires complex infrastructure throughout the ceiling, calculation of orientation and deployment overhead, which increases the system cost and reduces the scalability. Furthermore, Active Bat employs centralized system architecture and requires a large number of precisely positioned ultrasonic receivers.

### 2.6.3 Cricket, 2000

Cricket [49], equipped with the ultrasound transceiver with frequency of 40kHz is a first distributed (decentralized) 2-D indoor localization support system, where devices perform their own calculations. Cricket measures the distance using TDOA (first detect RF wave and then detect the ultrasound) and then calculate the coordinates using triangulation. The reported accuracy to locate  $4 \times 4$  region (absolute location) is with 100% precision in 2-D. However, as addressed by [50], the ultrasound is sensitive to temperature variations and multipath signals.

## 2.7 Applications

---

### 2.6.4 RADAR, 2000

RADAR [12], introduced by the Microsoft Research group, is a centralized indoor system for locating and tracking users based on IEEE 802.11 standard. It is based on the RSSI for location awareness between transmitter and receiver. This system works on different phases. In the first phase, it collects the multiple RF signal strength from a base station during off-line (i.e. scene analysis phase). In the second phase, the collected samples are compared with a set of signal strength measurements at a centralized system for best match. In third phase, a metric is measured and compared. As it is based on the scene analysis, predefined signal strength database should be according to the environment.

### 2.6.5 Horus, 2005

Horus [80], based on the IEEE 802.11 standard is similar to RADAR. It is also based on the off-line and on-line phases. The system uses the signal strength observed for frames transmitted by the access points to infer the user location. Since the wireless cards measure the signal strength information of the received frames as part of their normal operation, this makes the Horus system a software solution on top of the wireless network infrastructure.

### 2.6.6 SpotON, 2001

SpotON, introduced by the Intel Research and University of Washington, is a RSSI based 3-D locating system. The device to be located holds a SpotON tag, which measures RSSI to a reader upon hearing the beacons. SpotON, works on the idea of ad-hoc location sensing to localize the wireless devices relative to one another rather than to fixed base stations. To enhance the accuracy, it is based on the calibrated mapping between reader and the tag.

## 2.7 Applications

The number and variety of WSN applications continues to broaden. Some of the applications are given below:

## 2.7 Applications

---

### 2.7.1 Kid-Spotter

During the trips and visits, the tourist agents and parents can track customers and children from being lost or to track the location of these, whether they are within the building or outside the building, either they are within the range of the tourist point or out of the range through locating with the help of WSNs. In this type of application tourists, parents and children are moving all around the vicinity and thus changing geographic position. Apart from the mobility, the propagation environment (background noise, interference, LOS problem beneath heavy foliage) is also responsible for the frequent change in location information. In this situation, GPS however deteriorates to achieve the desired accuracy. KidSpotter [81], is one of the world's first indoor and outdoor tracking system designed for safety conscious venues. For outdoor, it requests its position on the planet through GPS satellites, whereas in indoor it asks the Zigbee network for information on its position [81].

### 2.7.2 Freight containers Positioning

Today, shipping and cargo in any country have a very important responsibility to improve financial conditions. As the number of twenty-foot equivalent units (TEU) is increasing throughout the world, the percentage of containers which are misplaced or delivered to the wrong destination is also increasing. Localization and retrieval of freight containers in a port is a challenging problem. One of the GPS based application is Tamper Resistant Embedded Controller (TREC) [82]. However, in a harsh environment, when the containers are stacked under other containers, GPS cannot provide the correct position because its GPS antenna cannot communicate with enough satellites. Here, low power sensor network localization can enhance the localization performance with cheaper system cost.

### 2.7.3 Asset Tracking and Management

Recent advancement in WSNs not only revolutionizes the way we live out live but also the way we identify the things. It helps to identify, track, manage and monitor the important assets. In addition, safety being a major concern

## 2.7 Applications

---

motivating building owners to deploy a system, which can track any movement within certain area of the building. Visitors can be tagged before entering the building, this will limit their movement. The tags can report to security when they are taken to a restricted area.

### 2.7.4 Aid to fire-fighters and police

Sensor network localization can be used for detection of fire-fighters in a building on fire. Positioning of individuals in such situations is imperative, as visibility in a smoked filled building is extremely low. Fire-fighters could locate each other and can also be monitored from an external station. Similarly, police dogs trained to find explosives in a building could be located by tagging them with sensor-equipped collars.

### 2.7.5 Detecting and Locating Radiation Levels

Recent nuclear disaster in Fukushima after the unfortunate earthquake and tsunami struck Japan motivated researchers towards a new application of WSNs. To detect the radiation level, battery powered Geiger Counter [83] have been created which can read the radiation levels automatically and send the information in real time using wireless technologies like ZigBee and GPRS [83].

### 2.7.6 Smart and Interactive Gaming

Advancement in technology also opened the doors for the gaming industry. Kinect XBox 360 [84] is the latest example for this type of application. With the help of a motion sensor, Kinect track the ones entire body. Furthermore, with the help of sensors, it creates the fingerprints to map the digital skeleton by tracking the movements. Advancements in this industry reflect the future with more advance game consoles with location sensors without the LOS constraint.

### 2.7.7 Habitat Monitoring and Wildlife Tracking

Keeping track of wildlife [85–87] has been of interest to zoologist, knowledge of animal movement over time can indicate animal behaviour with other species and

## 2.8 Conclusion

---

interaction with their own kind. The systems that are employed for such purposes are either using very high frequency (VHF) collars or using GPS chips. Since such observations are recorded over a long period, regular battery replacement in the collars becomes impractical. Low power sensor network localization will improve battery life and guarantee little human interaction with the animals.

## 2.8 Conclusion

WSNs have received increased attention recently, among different issues, localization has been recognized as a very challenging task due to the number of unique characteristics discussed. In this chapter, several different approaches and problems currently being faced by WSN localization research are reviewed. In the next chapter 3, the lateration schemes (sub-optimal, optimal multi-lateration and lateration incorporating Geometric Dilution of Precision (GDOP) metric) are analysed in detail in order to observe the impact of anchor placement on localization accuracy and its trade-off.

## Chapter 3

# Performance Analysis of Ranging with IEEE 802.15.4 Compliant WSN Devices

### 3.1 Overview

Recently the area of wireless sensor networks (WSNs) has gained a lot of momentum and has become increasingly attractive for many emerging applications due to its low cost, small size, light weight, and potential to be deeply embedded into the environment for a variety of applications. In many of these applications, localization has been an active area of research due to the fact that without the knowledge of sensor location, data passed by sensors will be meaningless. Here, determining the physical location of subject nodes will provide additional information in order to quantify the measured data. One of the important tasks for real time localization in WSNs is the precision and accuracy of range measurement. Hence, for efficient localization, it is imperative to understand the performance limits of ranging in realistic environments.

This chapter reports on round-trip time-of-flight (RT-ToF) and received signal strength (RSS) for point to point range estimation using 2.4GHz IEEE 802.15.4 compliant transceivers. Firstly, the performance limits for RT-ToF and RSS based range measurements are compared with the fundamental *Cramér-Rao Lower Bound* (CRLB). Secondly the range where the error for RSS ranging is expected

## 3.2 Introduction

---

to be greater than the error for ToF ranging is considered. We term this the ‘*cross-over*’ range ( $C_R$ ) of RSS and ToF ranging, where ToF ranging becomes more accurate than the RSS ranging. Thirdly, using a site survey application, a series of experiments has been conducted in different environments to make it possible to determine which parameters of the system lead to improved performance and successful ranging polls. Performance results and channel parameters have been obtained in outdoor and indoor for the line-of-sight (LOS) and non-line-of-sight (NLOS) environments. Both indoor and outdoor experimental results and analysis are presented. Based on the experimental results for outdoor and indoor unobstructed (LOS) environment over short range, it is demonstrated that RSS is a good candidate for range estimation at ranges less than 7m. Uncertainty in RSS based range estimation increases with distance and beyond 7m severely limits RSS performance. Further analysis over long range (i.e. up-to 100m) demonstrate that ToF is a good candidate for range estimation at greater than 7m.

## 3.2 Introduction

Localization is mainly categorized into range-free and range-based localization schemes, that differ in what kind of geometric information they use to estimate locations. The former is based on the radio connectivity information, where each node estimates the location based on the information received from the neighbour nodes. The accuracy of range free localization depends on assumption that nodes in a dense network with radio connectivity are typically in close proximity. However, node density negatively effects traffic overhead [10]. The latter approach is based on using angle estimates [14], or range measurements, which can be derived from measuring point-to-point propagation time [16, 17] or using RSS [14]. In range-based localization, the process to determine the physical location of sensor nodes consists of two main phases. During the first phase of localization, a sensor node performs range estimation to a set of anchor nodes, whose positions are known. Sensor nodes are typically equipped with extra hardware capable of estimating distance or angle [14, 88]. The second phase uses the range estimation

## 3.2 Introduction

---

as an input to determine the position estimation through different localization strategies such as *trilateration*, *multi-lateration* and *triangulation* [55].

For the first phase of localization, literature has focused on two classes of ranging techniques: RF based ranging and acoustic ranging [89, 90]. The RF method is more cost effective than acoustic signal based ranging schemes, as it does not require ultrasonic transducers [90]. The basic RF-based techniques available for the first phase of localization are angle-of-arrival (AoA) [14], time-difference-of-arrival (TDoA) [91], time-of-flight (ToF) [90, 92], and received signal strength (RSS) [12, 93].

The RSS is a standard parameter available on most wireless devices [94]. It is a popular method of ranging because it does not require additional hardware which makes it cheap as compared to other methods. Due to the complex behaviour of RF signal propagation (reflection, diffraction, refraction and scattering) and different application environments, there are several propagation models developed to predict signal decay with distance. It is a challenge to set up a model to predict RSS appropriate to the environment in which the system will be used. The RSS measurement model and principle of operation is discussed in section 3.6.

In ToF ranging, measurements based on propagation time are used to estimate the distance between neighbouring devices. ToF is classified as either one way propagation time or two-way propagation time measurement based on the number of packet transmission for range estimation. In one way, the node A transmits the time-stamped signal at  $t_1$  and is received at node B at  $t_2$ , the distance between the nodes is given by the equation  $d = c \times \text{ToF}_2 - \text{ToF}_1$ . As compared to one-way ToF, where two highly synchronized clocks are needed, in two-way ToF the same clock is used to calculate the round-trip time [16, 17]. Consequently synchronization between different clocks is not necessary. The ToF principle of operation is discussed in section 3.5.1. In the context of WSNs, range based techniques are more suitable due to the requirement of high accuracy and simple measurement hardware. The two most widely used and accepted techniques in wireless networks are ToF and RSS [90]. These two techniques have shown great potential for numerous emerging WSN applications, so are the focus of this chapter.

### 3.3 Sources of Ranging Error

---

This chapter is organized as follows. Section 3.2 followed by the sources of ranging errors in section 3.3. Section 3.4.2 describes the experimental infrastructure and test beds used for point-to-point ranging. In section 3.5 and 3.6 respectively, the principle of operation for ToF and RSS is discussed. Section 3.8.1 explains the cross-over range whereas results and analysis from site survey are presented in section 3.7. Finally, experimental results and conclusions are provided in section 3.8 and 3.9 respectively.

## 3.3 Sources of Ranging Error

Ranging accuracy is an important aspect to consider because a localization system obtains position estimates using range estimates. An inaccurate range estimation may lead to unacceptable localization errors. This section categorizes the thermal noise, systematic parameters and multipath propagation as the main sources of ranging errors.

### 3.3.1 Systematic Parameter

One of the crucial factors to consider in time-based ranging is precision of timing between nodes. *Clock Offset* is the difference between the time reported by the clock and the real time. Using the speed of propagation to measure distance will mean a  $0.1\mu\text{s}$  timing error results in a 30m range error. In reality it is not possible to have perfectly aligned clocks at the transceiver due to tolerances of quartz oscillators, temperature variations, and environmental changes and this result in *clock offset*. The clock frequency mismatch can be significant in the context of WSNs, where high-precision oscillators do not comply with cost and size constraints. Higher clock inaccuracy will not only increase the estimation error but also the energy consumption [95] by corrupting the ability to correctly determine the back-off boundaries of the slotted CSMA/CA mechanism (which requires a precise clock). The impact of this parameter (clock offset) on ranging accuracy can be mitigated by high-precision oscillators (which however compromises the constraints of WSNs) or tight synchronization techniques at the physical layer and averaging of a large number of measurement samples [96]. In addition to this,

### 3.3 Sources of Ranging Error

---

due to discrete values (clock quantification) of time-based ranging, the measured ToF is usually higher than the actual one.

#### 3.3.2 Radio Propagation

Due to the unpredictable nature of the wireless medium i.e. space and time variation, a ranging system may fail to mark the expected accuracy. The unpredictable behaviour of RF signal propagation can be attributed to reflection, diffraction, refraction and scattering. It has always been a challenge to set up a model to predict radio propagation appropriate to the environment in which the system will be used. Therefore, several propagation models have been developed that envisage mechanism of RF propagation. To overcome unpredictable RF characteristics in different environments, channel models are broadly classified as *large scale and small scale fading models* [94].

##### 3.3.2.1 Large Scale Fading Models

Large scale fading (a.k.a slow fading or shadowing) is a deterministic process caused by the buildings, mountains, hills, vegetations and other surrounding objects in outdoor environment. Large scale fading is further categorised into different models. The most commonly use models are [94]:

- Inverse-square law based model
- Two-ray Ground Model

The model based on inverse-square law considers the ideal environment and can be given as Eq. (3.1) [94],

$$P_r(d) = \frac{P_t G_t G_r \lambda^2}{(4\pi)^2 d^2 L} \quad (3.1)$$

where  $P_r(d)$  is the received power at distance  $d$ ,  $P_t$  is the transmit power,  $\lambda$  is the wavelength,  $G_r$  and  $G_t$  are the receiver and transmitter antenna gains respectively and  $L$  is the system loss factor [94].

### 3.3 Sources of Ranging Error

---

However the above mentioned model is an ideal case and does not consider an obstructed environment. A two-ray ground model (direct and ground reflected) adds the unavoidable *reflection* to the inverse-square model, when the WSN nodes are deployed close to the ground [97]. In this case, received power at distance  $d$  for both the direct path and a ground reflection path can be predicted as  $P_r(d) = \frac{P_t \lambda^2}{(4\pi d)^2} [2 \sin(\frac{2\pi}{\lambda} \frac{h_t h_r}{d})]^2 G_t G_r$  [98], where  $h_t$  and  $h_r$  are the heights of the transmit and receive antennas respectively.

Comparing with the free-space model, signal power in two-ray propagation model decays at a faster rate ( $d^4$ ) as the distance increases. However in practice, both the free space and the two-ray model do not correctly predict the received power strength due to the complex nature of real propagation. The relationship between distance and path loss exponent in Eq. (3.1) does not consider the harsh environment, that may experience different propagation at two different positions with same distance between transmitter and receiver. To overcome this, a *log-normal shadowing model* (Eq. (3.2)) is considered, which states that with a specific value of  $d_{ij}$ , the  $\eta$  at particular location is random and distributed as lognormally (normal in dB) about the mean distance-dependent value [98, 99].

$$P_r(d)[dBm] = \Psi[dBm] - 10\eta \log_{10} \frac{d}{d_0} + \varepsilon_{dB} \quad (3.2)$$

where  $\Psi$  is received power at a reference distance  $d_0$ ,  $\eta$  is the path loss exponent based on the propagation environment (normally taken between 2 and 6) and  $\varepsilon$  is the shadow fading (zero mean Gaussian distributed random variable in dB with standard deviation  $\sigma$ ) [98]. In practice, the  $\eta$  will be different in each environment. Therefore, it is important to approximate this unit-less constant analytically or experimentally.

#### 3.3.3 Small Scale Fading Models

As opposed to wired channels, the received signal from the wireless channel suffers from strong amplitude fluctuations that cause fading in the received signal. In a multipath environment, it is a common to have multiple independent components

### 3.3 Sources of Ranging Error

---

at a receiver. Each component shows independent nature with its own amplitude and phase (due to reflections, scattering etc). Without any mitigation technique, a receiver deals with the summation of these multiple signals in a constructive or destructive manner (depending on the relative phase shift). It causes the signal to arrive at the receiver by  $K_p$  multiple paths with  $A_k^t$  different path amplitudes and associated delay  $\tau_k$ . Assume that the receiver is static, then the received signal can be given as:

$$r(t) = \sum_{k=1}^{K_p} A_k^t s(t - \tau_k) \quad (3.3)$$

Further, Eq. (3.3) can be presented as Eq. (3.4), which represent the phase difference between multiple paths.

$$r(t) = \sum_{k=1}^{K_p} A_k^t \cos 2\pi f_c t + \theta_k \quad (3.4)$$

Small scale fading is stochastic and caused by the movement of transmitter or receiver, hence it reflects a change in the amplitude of the received signal. Small scale fading is further statistically categorised as *Rayleigh* and *Rician* distributions. When a signal arrives at the receiver without any dominant path (i.e. no line-of-sight path between Transmitter-Receiver (T-R)), the envelope of the signal is *Rayleigh* distributed. An addition of a LOS component (non-zero mean) to the Rayleigh distribution, results the received signal envelope into *Rician* distribution. Rician becomes Gaussian distribution at large value of rice factor (ratio of the power of LoS to power of diffuse components).

#### 3.3.3.1 Effect of Frequency Channel on Multipath Performance

A change in frequency will change the fading characteristic. The effect of frequency channel is related to the Coherence bandwidth ( $B_c$ ). Coherence bandwidth is a measure of how much the frequency can be changed while experiencing

### 3.3 Sources of Ranging Error

---

a similar fading environment and can be given by Eq. (3.5) [100]. ( $B_w < C_c$  i.e. narrowband)

$$B_c = \frac{1}{2\pi T_m} \text{ (Hz)} \quad (3.5)$$

where  $T_m$  is the delay spread. The coherence bandwidth can be used to classify the channels as flat or frequency selective fading channels.

If all frequency components in the transmitted signal are affected by the same random attenuation and phase shift, then the channel will be considered as the frequency flat channel. In this type of the channel, the bandwidth of the transmitted signal is smaller than the channel's coherence bandwidth, hence minimal inter-symbol interference (ISI) (i.e. narrowband). On the other hand, frequency selective fading considers that the frequency components of the transmitted signal are affected by the different amplitude gains and phase shifts. In this case, the bandwidth of the transmitted signal is bigger than the channel coherence bandwidth ( $B_w > C_c$  i.e. wideband), hence significant ISI. In spread spectrum, when the signal bandwidth increases it becomes sufficiently larger than the coherence bandwidth. Hence, It is possible that a portion of the signal spectrum may experience a different fading environment.

Considering an delay spread of 70ns in an indoor environment [100], Eq. (3.5) provide the  $B_c$  of 2.3MHz. Now if the receiver is in deep fade, a shift of 1MHz in carrier frequency will hold the receiver in deep face. However, a shift of 10MHz in carrier frequency will allow the receiver to experience a different fading environment and can have a better chance of receiving the signal [100].

#### 3.3.4 Thermal Noise

Thermal noise (or *Gaussian*) will be generated within devices because of agitation of electrons in a conductor. The power contained within thermal noise is dependent on the temperature, and operating signal bandwidth [101]. This unwanted intrinsic noise is responsible for introducing errors into precise measurements so reducing it improves performance. With the context of digital receivers, noise is

### 3.4 Experimental Infrastructure

---

typically measured by the single-sided noise power spectral density (PSD) given by Eq. (3.6) [102]:

$$N_0 = k_B T \text{ [W/Hz]} \quad (3.6)$$

where  $k_B$  is Boltzmann's constant which is  $\sim 1.381 \times 10^{-23}$  J/K,  $T$  is the system temperature in kelvin. The thermal noise is additive, that is, the received signal can be represented as a sum of the transmitted signal and the noise signal as given by Eq. (3.7) [102].

$$r_{ij}(t) = s_t + n_{ij}(t) \quad (3.7)$$

where  $n(t)$  has Gaussian distribution with zero mean and finite variance  $\sigma^2$ .

### 3.4 Experimental Infrastructure

The Jennic JN5148 series IEEE 802.15.4 transceiver, including ZigBee PRO (ZigBee Compliant Platform) is an ultra low power, low cost wireless micro-controller that operates in 2.4GHz ISM band ( $\lambda = 0.125\text{m}$ ) [1]. It uses 2MSps direct sequencing spread spectrum (DSSS) with each symbol mapped to a 32 – *chip* PN sequence. The 32 – *chip* sequence represents each data symbol and therefore chip rate can be given as 32 times the symbol rate (62.5 kSps), and symbol duration is given as  $1/\text{symbol rate} = 16 \mu\text{s}$ . The bandwidth of Zigbee is 2 MHz. A built-in ranging engine based on Time of Flight (ToF) calculates the time-of-flight of a radio signal between two wireless nodes using the two-way (round trip) ToF ranging. Its integrated power control system enables the system power consumption to be controlled carefully using different modes (i.e., active processing mode, sleep mode, deep sleep mode) to maximise battery life, hence network life. A 32-bit load and store RISC processor help to minimise the power consumption

### 3.4 Experimental Infrastructure

---

for battery powered application and implementation of protocols with high performance and high level efficient programming. Table 3.1 lists the specification of IEEE 802.15.4 Compliant Device [19, 24].

Parameter	Notation	Value
Radio Frequency	RF	2.4GHz
Spread Spectrum	$S_s$	DSSS
Data Rate	$D_r$	250kbps
Transmit Power	$P_t$	0dBm (1mW)
Modulation Scheme	$M_s$	OQPSK
Chip Spreading Sequence	PN	32 chips
Symbol	$S_m$	PN = 32 chips
Symbol Rate	$S_r$	62.5 kHz (ksymbols/s)
Symbol Duration Time	$T_s$	$1/S_r=16\mu s$
Chip Rate	$R_c$	$S_r \times 32 = 2$ Mchip/s
Chip Period	$T_c$	$\frac{1}{R_c} = 500$ ns
Clock Rate (JN5148)	$f_s$	16MHz
Antenna Type		Folded-monopole

Table 3.1: Specification of IEEE 802.15.4 Compliant Devices

#### 3.4.1 Antenna Models

Anisotropy is a common and non-negligible phenomenon in wireless networks caused by different factors such as, antenna type, antenna gain, and environment dependant path loss [94, 98]. In the age of compact devices, a light weight, small-sized and inexpensive antenna plays a important role to overcome the deployment concerns of external mounted antennas. There are many situations in which small size is important (particular in hand-held equipment). There are two different variants of Jennic’s wireless modules: modules with an integrated antenna and modules with an external antenna. Experimental results discussed in this work are based on the Jennic wireless modules those with an integrated antenna. The JN5148 modules with integrated antenna are based on a folded-monopole, omnidirectional characteristic [1]. Integrated antenna are useful for many application (i.e. child locating solution, where a sensor node as wristband with integrated

### 3.4 Experimental Infrastructure

---

antenna can be secured on the wrist of the child, tracking expensive items in a super market) where mounting an external antenna is not feasible due to the much required space or volume.

#### 3.4.1.1 Integrated Folded Mono-pole Antenna

The Jennic experimental units include an antenna with a folded-monopole, omnidirectional characteristic [1]. The main radiating lobe of this 2.4GHz ISM band antenna is projected at right-angles to the PCB ground plane. Fig. 3.1 shows the measurement planes for the folded mono-pole antenna [3], whereas Fig. 3.2 shows the radiation pattern of the three measurement planes [3]. In order to optimize the received power, it is important to match the polarization for both receiver and transmitter antennas particularly when there is a LOS or directional antenna in use. Considering the fact that antenna polarization is more dynamic for mobile nodes, a static and approximately aligned configuration is considered between nodes.

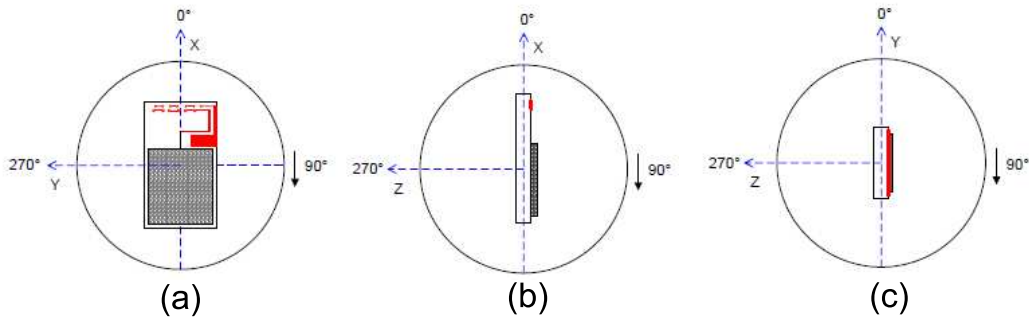


Figure 3.1: Integrated Folded Mono-pole antenna measurement planes [3]. Fig. (a). XY-Plane Fig. (b). XZ-Plane Fig. (c). YZ-Plane

#### 3.4.2 Experimental Setup for Ranging

The experiments have been performed in an indoor and outdoor environment with both LOS and NLOS conditions. For each condition three different sets of experiments have been performed with the transceiver nodes mounted on a

### 3.4 Experimental Infrastructure

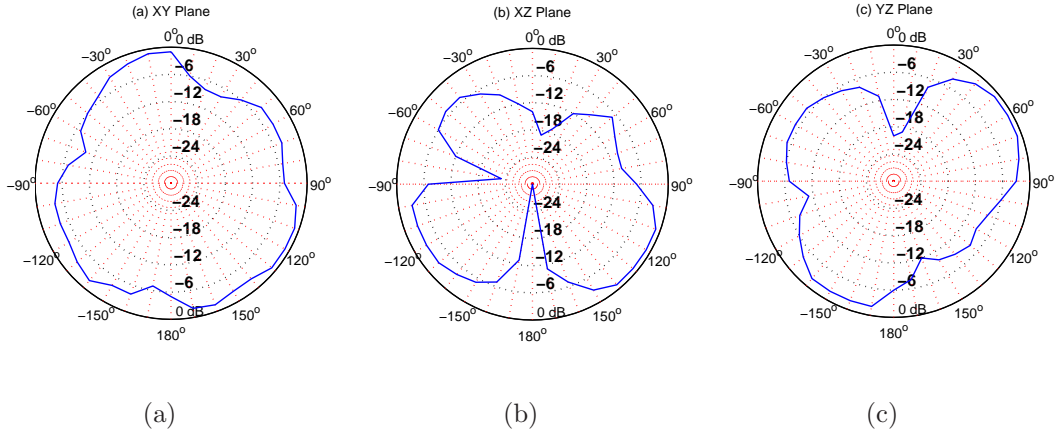


Figure 3.2: Measured antenna radiation pattern [3]. Fig. 3.2(a). XY-plane radiation pattern polar plot, Fig. 3.2(b). XZ-plane radiation pattern polar plot and Fig. 3.2(c). YZ-plane radiation pattern polar plot

tripod at one of 3 specified heights of 0.5m, 1.0m, 1.5m. A *Coordinator node* was fixed (connected to laptop) at one side of the field whereas an *End device* is fixed at variable distances (i.e. 1m, 2m,  $\dots$  15m). The actual distance between the nodes was measured using Leica Disto A5 laser distance meter [103]. For each separation and height between sensor nodes, a total of 700 ranging samples were collected (a total of 10,500 for all separations). A coordinator node was used to capture, process and save the data on a laptop.

#### 3.4.2.1 Outdoor Experimental Setup

The left side of Figure 3.3 illustrates the outdoor test site setup for LOS path. The outdoor experiments were performed in Hyde Park situated just beside the University of Leeds. For all LOS ranging samples, a clear LOS is maintained on a plane open grassy field with no trees or obstacles between or near the transceivers. The NLOS outdoor experiments are executed in the same park at a location where the direct LOS was completely blocked for each height with trees and wooden benches. The obstructions e.g. trees, were of the order of 1m thick so no LOS existed. The dimensions of the field are 120m $\times$ 200m.

### 3.5 Round-Trip Time-of-Flight (RT-ToF)

---

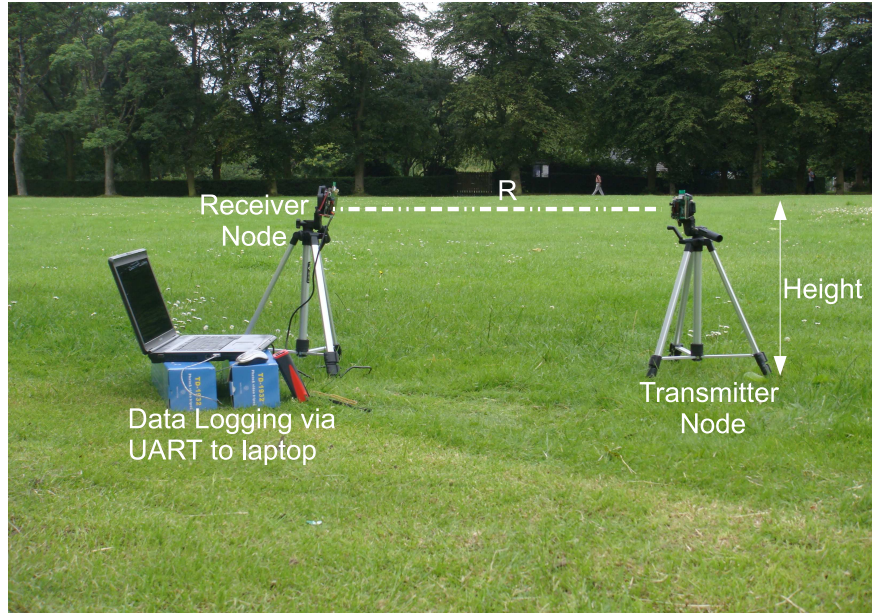


Figure 3.3: Outdoor experimental setup with two nodes, tripods and data logger laptop for range measurements.

#### 3.4.2.2 Indoor Experimental Setup

The indoor experimental setup is illustrated on the right of Figure 3.4. The indoor experiments were performed in a corridor at Edward Boyle library at the University of Leeds. The dimensions of the corridor are  $\sim 3.5 \text{ m} \times 110\text{m}$  and floor to ceiling height is 2.5m. For LOS experiments the transceiver were kept in a straight line in the centre of the corridor. The NLOS experiments were executed in the extreme left of the corridor where the direct LOS was blocked by the side concrete walls, furniture and people.

## 3.5 Round-Trip Time-of-Flight (RT-ToF)

The ToF method used in JN5148 IEEE 802.15.4 compliant device is based on *round-trip time* ( $T_{\text{RTT}}$ ) which overcomes the major problem of clock synchronization between the nodes for range measurement. The ranging scheme involves measuring the total duration from sending an outgoing request to receiving an incoming acknowledgement. The estimated delays in each node are subtracted

### 3.5 Round-Trip Time-of-Flight (RT-ToF)

---



Figure 3.4: Indoor experimental setup with two nodes, tripods and data logger laptop for range measurements.

from the total duration to obtain the round trip time of flight and hence the inter-nodal distance. The ToF measurement begins with *Node 1* transmitting a poll at a known time within the *Node 1* device time-scale, but essentially an arbitrary time with respect to the *Node 2*. The poll transmitted by the *Node 1* has a transmit delay  $T_{tx1}$  and propagation time  $T_{tof}$  between the *Node 1* and *Node 2*. However, as the *Node 2* is not synchronised to the *Node 1* the offset it measures is denoted received delay in *Node 2*  $T_{rx2}$ , correlation time estimate in *Node 2* ( $T_{cor2}$ ), turn-around time measured in *Node 2* ( $T_{tat2}$ ) and transmit delay ( $T_{tx2}$ ) in *Node 2*. The *Node 2* sends a ACK to the *Node 1* exactly after the delay information equivalent to  $T_{rx2} + T_{cor2} + T_{tat2} + T_{tx2}$ . The ACK received by the *Node 1* has a received delay  $T_{rx1}$  and correlation time estimate  $T_{cor1}$ . Fig. 3.5 shows the ToF measurement between two nodes, where *Node 1* measures the total time ( $T_{tot}$ ) from sending a poll to receiving the ACK. The RT-ToF is obtained by subtracting the  $\tau_{delay}$  recorded by both nodes from the  $T_{tot}$ . Eq. (3.8) indicates half the RT-ToF, that is the ToF on the assumption that the delay in each direction took an equal amount of time.

### 3.5 Round-Trip Time-of-Flight (RT-ToF)

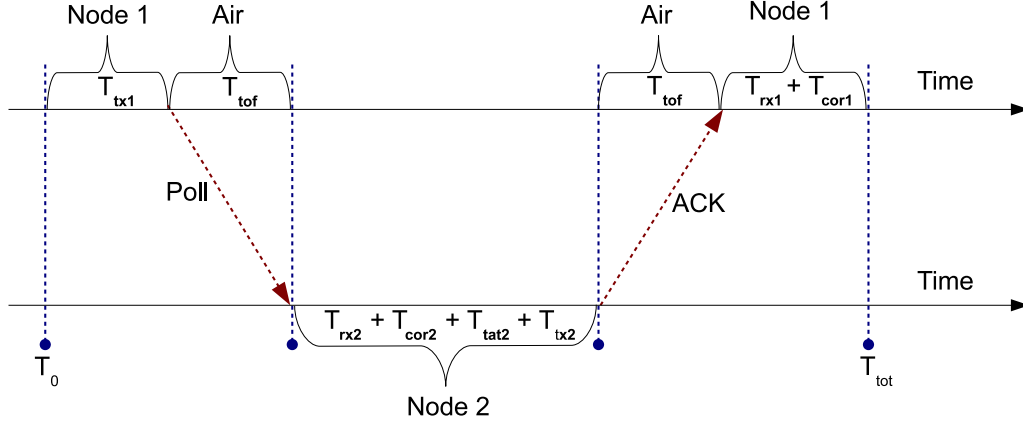


Figure 3.5: Time-of-Flight (ToF) measurement.

$$T_{tof} = (T_{tot} - \tau_{delay})/2 \quad (3.8)$$

where  $T_{tot}$  is total time measured by *node 1* and  $\tau_{delay}$  can be given by Eq. (3.9):

$$\tau_{delay} = T_{tx1} + T_{rx1} + T_{cor1} + T_{tx2} + T_{rx2} + T_{cor2} + T_{tat2} \quad (3.9)$$

where  $T_{tx1}$  and  $T_{tx2}$  are transmit delays,  $T_{rx1}$  and  $T_{rx2}$  are receive delays in *Node 1* and *2* respectively,  $T_{cor1}$  and  $T_{cor2}$  are the correlation time estimate (representing the processing to obtain received signal correlation peaks within an observation window) in *Node 1* and *2* respectively, and  $T_{tat2}$  is turn around time measured in *Node 2* using accurate hardware timers running at the system clock frequency.

Given  $T_{tot}$  from Eq. (3.8) and knowing that the radio signal travel at the speed of light  $c$ , the range estimated between two nodes can be given as Eq. (3.10):

$$\hat{d}_{ij} = c \times T_{tof} \quad (3.10)$$

### 3.5 Round-Trip Time-of-Flight (RT-ToF)

---

Since the ToF based ranging can be affected by clock frequency offsets and multipath, hence it relies on the measurement of time at *Node 1* and *Node 2*. Knowing the fact that error of 1ns in  $T_{\text{tof}}$  leads to ranging error of 0.3m, hence it is required to reduce the ranging error mechanisms. To reduce the impact of clock frequency offsets and multipath propagation, ranging results obtained through forward (*Node 1* to *Node 2*) and reverse (*Node 2* to *Node 1*) direction can be averaged.

#### 3.5.1 Principle of Operation

To perform the ToF measurement, two nodes (i.e. *Node 1* and *Node 2*) must follow the interface for the request and confirm association primitives as per IEEE 802.15.4 standard [19]. In order to join a network, a device (i.e. *Node 2*) must first find a Co-ordinator (*Node 1*) by conducting an active channel scan. The *Node 2* can then send an association request to the *Node 1*, which acknowledges the request and then determines whether it has sufficient resources to add the device to its network [24]. The *Node 1* will then accept or reject the association request. Once both the nodes are successfully associated, nodes can perform the RT-ToF process as described below.

- The ToF process starts when a *Node 1* (i.e. subject node) sends a packet to the *Node 2* (i.e. anchor node). In response to this packet from *Node 1*, *Node 2* performs two sequences. In first sequence, it transmits an acknowledgement (ACK) to *Node 1* and then initializes the ToF engine in second sequence.
- On receiving the ACK from *Node 2*, *Node 1* initializes the ToF engine and transmits a packet for ToF measurement. It then waits for an ACK from *Node 2*.
- When *Node 2* receives a ToF measurement packet from *Node 1*, it starts time measurement and transmits ACK to *Node 1*, then stops the time measurement by disabling the ToF engine and preserves the timing information. During this process, *Node 2* does not need clock synchronization with respect to *Node 1*.

### 3.5 Round-Trip Time-of-Flight (RT-ToF)

- On receiving the ACK from *Node 2*, *Node 1* also disables its ToF engine. By this stage, both nodes have disabled ToF engine. *Node 1* and *Node 2* process the correlation data. On the same time, *Node 2* calculates the delay information.
- On request from *Node 1* for delay information, *Node 2* transmits the delay information.
- On receiving the delay information from *Node 2*, *Node 1* responds to DATA packet by transmitting an ACK back to *Node 2*. *Node 1* calculates the ToF and writes the result over the UART. Once ToF calculation is finished, *Node 1* and *Node 2* are then ready for another ToF measurement. In case of multiple measurements (i.e.  $n$  polls), the whole process repeats for  $n$  times.

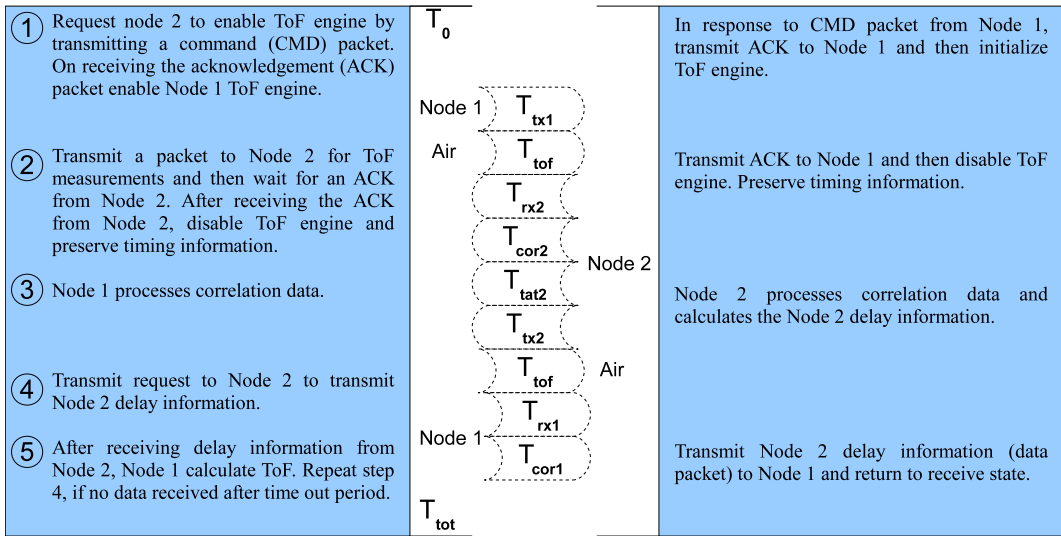


Figure 3.6: RT-Time-of-Flight Process

#### 3.5.2 RT-ToF Range Resolution

One of the factor that bounds the ranging accuracy is the resolution, which is proportionally bounded by the time quantization introduced by the sampling period [90]. Thus, increasing the sampling period ( $\frac{1}{f_s}$ ) can improve the achievable accuracy. RT-ToF ranging resolution can be given by Eq. (3.11):

### 3.5 Round-Trip Time-of-Flight (RT-ToF)

---

$$R_{\text{Res}} = \frac{c}{2f_s} \quad (3.11)$$

where  $R_{\text{Res}}$  is the RT-ToF ranging resolution,  $c$  is the speed of light,  $f_s$  is sampling rate and factor of 2 is due to the forward and backward averages.

Jennic's JN5148 measures the total time  $T_{\text{TOT}}$  using accurate hardware timers running at system clock frequency 16MHz, where a single clock cycle corresponds to 62.5ns (that is going to be divided by two due to the round-trip). Hence, 31.25ns (9.37m) is sampling period of the received signal. It can be observed that, in order to enhance the ranging resolution, higher clock frequency is required. For example, in order to have a ranging resolution of 1.67ns (0.5m), accurate hardware timers running at system clock frequency 300MHz are required. For resource constraint WSNs applications, such high frequency system clock is not ideal.

#### 3.5.3 Cramér-Rao Lower Bound of ToF

The CRLB sets a limit on the mean square error variance of an unbiased estimator of unknown parameters [59]. The best achievable accuracy of a set of range estimates derived from narrowband ToF measurements in single path channels satisfies the following inequality [90]:

$$\sigma_{T_{\text{tof}}}^2 \geq \frac{1}{8\pi^2 \text{SNR} \beta^2} \quad (3.12)$$

where SNR is the signal-to-noise-ratio and  $\beta^2$  is the mean square effective bandwidth. The effective bandwidth (also known as the Gabor bandwidth [104]) is given by (3.13) [59], where  $S(f)$  is the Fourier transform of transmitted signal  $s(t)$ .

$$\beta \Delta \left[ \frac{\int_{-\infty}^{\infty} f^2 |S(f)|^2 df}{\int_{-\infty}^{\infty} |S(f)|^2 df} \right]^{1/2} \quad (3.13)$$

### 3.5 Round-Trip Time-of-Flight (RT-ToF)

---

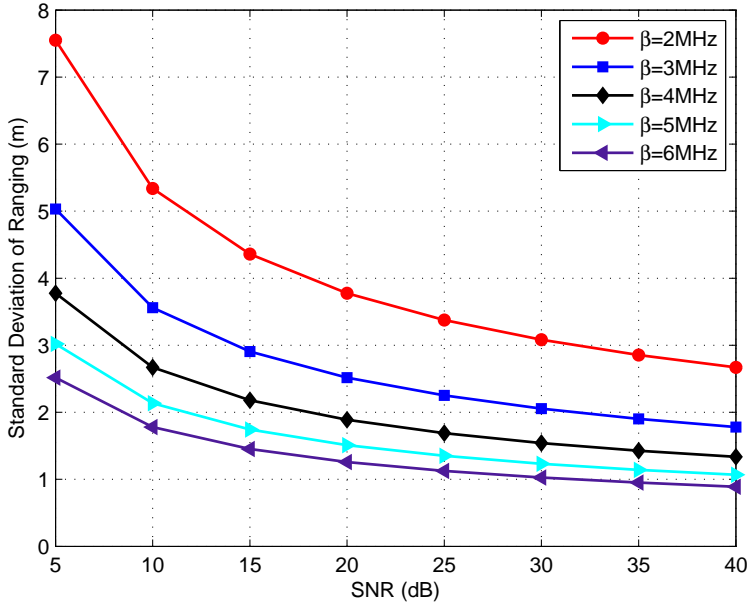


Figure 3.7: Impact of SNR and  $\beta$  on the fundamental CRLB for ToF ranging using IEEE 802.15.4 and UWB.

Eq. (3.12) shows that increasing the  $\beta$  and SNR reduce the lower bound, hence improving the ranging precision. This is because the ranging precision is related to the achievable time resolution. Figure 3.7 illustrates the bound on ranging performance for different  $\beta$  values using Eq. (3.12). Ranging performance for UWB which occupies the effective bandwidth  $\geq 500\text{MHz}$  yields a CRLB of below 1m. As shown, increasing the effective bandwidth and SNR improves the CRLB, hence ranging precision. This is because the ranging precision is related to the spread signal bandwidth (i.e. chip rate) and SNR. It reflects the advantage offered by the UWB over IEEE 802.15.4 in ranging precision. But as discussed in section 3.2, high ranging precision is the result of high computation, processing requirement, hardware complexity, hence an increased power requirement.

To evaluate the lower bound on the variance of spread spectrum ToF estimation, Eq. (3.12) can be used by specifying the required parameters as given by Eq. (3.14) [92].

### 3.5 Round-Trip Time-of-Flight (RT-ToF)

---

$$\sigma_{T_{\text{tof}}}^2 = \frac{1}{8\pi^2 \text{SNR} \beta^2 \sqrt{\alpha} N} \quad (3.14)$$

where  $N$  is the number of chips in the PN sequence and  $\alpha$  is the number of repetitions of each sequence element. IEEE 802.15.4 uses one of 16 ‘*nearly orthogonal*’ 32-chip long PN sequences to represent one of 16 symbols [19]. The sequence is oversampled by a factor of 8 so each sequence element is repeated and this enhances the processing gain achievable.

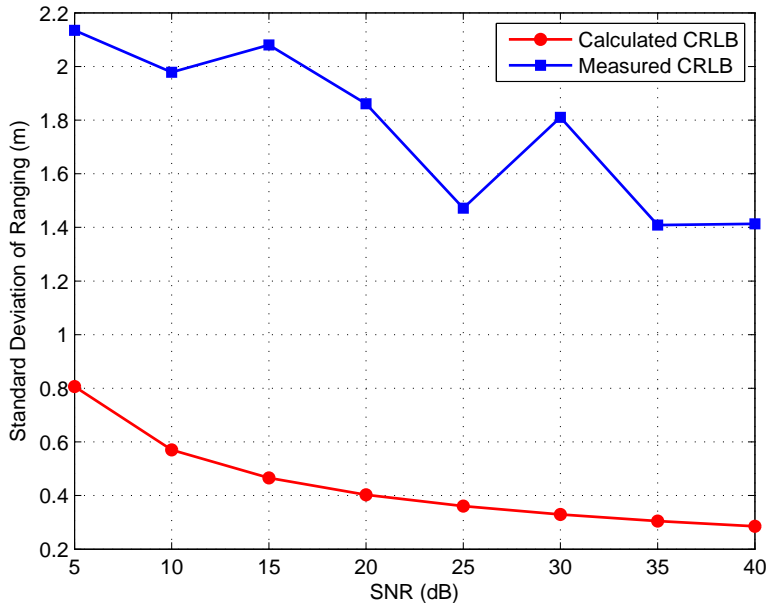


Figure 3.8: The Fundamental CRLB and measured performance limit of Jennic JN5148 series ranging module for ToF ranging

The lower bound for the system using Eq. (3.14) is compared with the measured variance of range estimate derived from ToF estimation. This theoretical bound is compared with outdoor LOS experimental results to verify the theoretical calculated bound and measured bound. Our test setup is designed with two JN514x nodes mounted on a tripod and an *HP-8593E* series spectrum analyzer. In order to avoid the impact of multipath, a clear LOS existed between *Node 1*, the controller, and *Node 2*. Figure 3.8 shows the fundamental calculated CRLB

### 3.6 RSS: Principle of Operation

---

(Eq. (3.14)) along with the measured variance of ToF ranging measurements for varying SNR. The required SNR of a signal for a given signal quality was measured using Eq. (3.15) [105], where  $(S + N)_m$  dBm is the combined signal and noise value and  $N_m$  dBm is the noise floor after measurements. The power of the signal is measured by considering the power of the band where the signal was located. Then, by terminating the input, the power of the noise of the instrument is measured with same attenuation and resolution bandwidth (RBW) of 100kHz [21].

$$\text{SNR}_m = (S + N)_m - N_m \text{ dB} \quad (3.15)$$

The measured  $\sigma^2$  of ToF measurements is the result of 700 iterations for each SNR value. Each correlation is performed using the last 31-chips of each received 32-chip spreading sequence. The correlation is 248-samples in length and operates at the full receive system sampling clock rate of 16MHz i.e. each of the 31-chips are oversampled by a factor of 8. It can be seen that the measured performance limit of Jennic JN5148 series ranging module overstepped the fundamental CRLB for ToF ranging. A higher sampling rate would be required in order to achieve the performance limit that meets theoretical performance.

### 3.6 RSS: Principle of Operation

The maximum value of RSS which can be reported by Jennic for JN – 5148 is 108dB whereas minimum is 20dB, limited by the intrinsic noise floor of the radio receiver. Hence the dynamic range of RSS for JN – 5148 is 88dB. The RSS value can be converted in to  $P_r$  by using the Eq. (3.16), where  $RSS(\text{dB})$  is the measured RSS value relative to 1dB resolution. The obtained RSS value is the average of RSS measurements from local and remote node for the same radio link. A local node sends a command to a remote node to get the RSS value. After receiving the remote RSS, the local node reads out the local RSS. The average of remote and local RSS is the measured RSS value.

### 3.6 RSS: Principle of Operation

---

$$P_r(\text{dBm}) = \text{RSS}(\text{dB}) - 108(\text{dBm}) \quad (3.16)$$

The calculated  $P_r(\text{dBm})$  can be converted into the distance by using Eq. (3.2). In this work, constant  $\Psi$  is approximated using experimental results at a reference distance of 1m outdoor and indoor and later used to approximate the  $\eta$  and variance of the shadowing ( $\sigma_{sh}^2$ ) using empirical data. The value of  $\eta$  and  $\sigma_{sh}^2$  outdoor and indoor is calculated using a minimum mean-square error (MMSE) fit to experimented measurements, in a similar manner to [98]. The empirical values of  $\Psi$  which are used for the LOS and NLOS path are shown in Table 3.2.

Case	$\Psi$ dBm $d_0=1$	$\eta$	$\sigma_{sh}^2$ dB	$\sigma$ dB
Short Range				
RSS: Outdoor LOS	-42.06	2.12	14.6	3.82
RSS: Indoor LOS	-42.06	1.87	14.3	3.78
RSS: Outdoor NLOS	-38.14	2.71	14.6	3.82
RSS: Indoor NLOS	-38.14	2.59	15.4	3.92
Long Range				
RSS: Outdoor LOS	-42.06	2.3	14.1	3.75
RSS: Indoor LOS	-42.06	2.1	14.6	3.79
RSS: Outdoor NLOS	-38.14	3.2	14.7	3.84
RSS: Indoor NLOS	-38.14	2.92	14.6	3.83

Table 3.2: Approximated Propagation Parameters

Figure 3.9 presents the RSS versus range for the empirical data and path loss model based on the approximated propagation parameters as shown in table 3.2. The vertical bars in Fig. 3.9(a) for outdoor LOS and Fig. 3.9(b) for indoor LOS show the distribution of measured  $P_r$ ; whereas the dashed line indicates the average  $P_r$  at each range. Average  $P_r$  is compared with fitted path loss model, calculated with respective  $\eta$  (as shown in Fig. 3.9) and  $d_0=1\text{m}$ . Fig. 3.9 shows that at ranges less than  $\sim 7\text{m}$ , the average  $P_r$  is comparable to fitted propagation model. However, an increase in distance shows higher decay in RSS for outdoor and indoor LOS at antenna height of 1.5m.

### 3.6 RSS: Principle of Operation

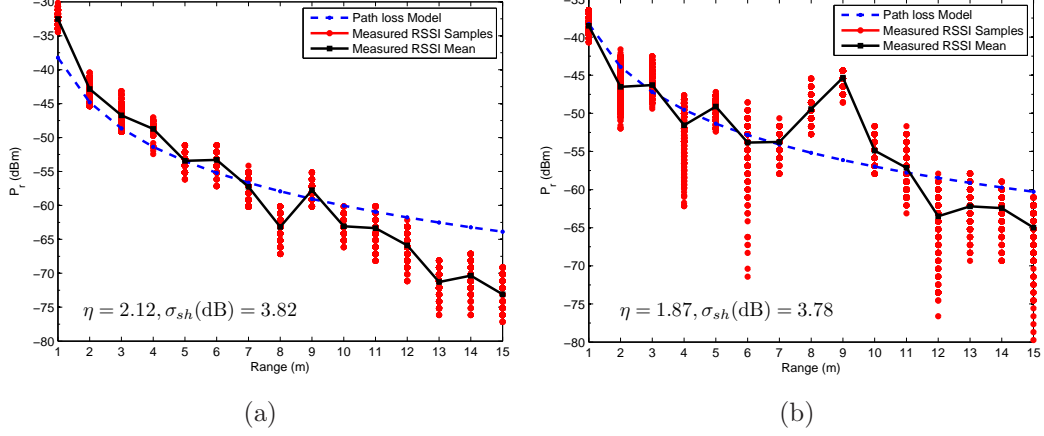


Figure 3.9: RSS versus range for measured data and path loss model. Fig. 3.9(a). Outdoor LOS at antenna height of 1.5m. Fig. 3.9(b). Indoor LOS at antenna height of 1.5m.

#### 3.6.1 Cramér-Rao Lower Bound of RSS

In [100], the CRLB for a range estimate derived from RSS measurements is:

$$\sqrt{\text{var}(\hat{d})} \geq \left( \frac{\ln 10}{10} \frac{\sigma_{sh}}{\eta} d \right) \quad (3.17)$$

where  $\sigma_{sh}^2$  is the variance of Gaussian variable  $\mathcal{N}(0, \sigma_{sh}^2)$  representing log-normal shadowing and  $\eta$  is the environment based distance-power gradient and  $d$  is the distance. Compared with Eq. (3.12), Eq. (3.17) shows that RSS measurement does not depend on the bandwidth ( $\beta$ ).

Figure 3.10 compares the measured RSS performance with the CRLB for RSS in outdoor and indoor (LOS) environment. The calculated CRLB is based on the average  $\eta$  and  $\sigma_{sh}^2$  calculated from measurements using MMSE, as discussed above. It is apparent that the  $\sqrt{\text{var}}$  of the RSS estimates is above the calculated CRLB. From (3.17), it is observed that lower bound of RSS estimates increases with an increase of  $\sigma_{sh}^2$  and decreases with larger  $\eta$ .

### 3.7 Site Survey and Analysis

---

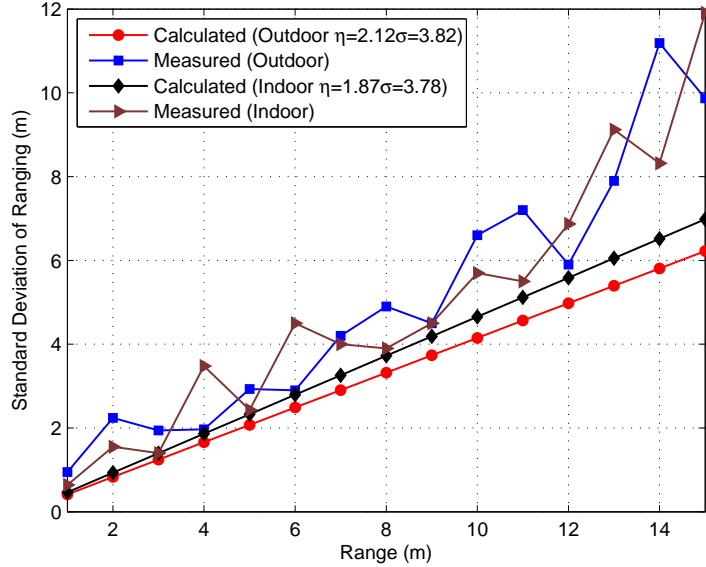


Figure 3.10: The fundamental CRLB limit and measured performance limit of Jennic JN5148 series ranging module for RSS.

## 3.7 Site Survey and Analysis

Before commencing a series of experiments, a site survey was carried out to discover the traffic on each channel. Based on this activity, two different channels with maximum and minimum traffic were selected for the experiments. Within the ToF API timings are calculated at each end of the link - such as the time of arrival of a packet, or the time between sending a packet and receiving the ACK. The ToF measurements are performed without retries enabled. This means that there is a chance that some packets or ACKs will get corrupted on air and not be correctly received. During these calculations, a single ToF poll may result in one of five ToF status categories as discussed below.

### 3.7.1 Successful ToF

MAC-ToF-SUCCESS status results when a ToF poll successfully receives the ACK and DATA packet from a remote node. On a successful poll, it returns the measured ToF in pico seconds (*ps*), which can then be equated to a distance.

## 3.7 Site Survey and Analysis

---

### 3.7.2 Remote Time Value Invalid

MAC-ToF-RT (Remote Time Value Invalid) status results due to an invalid time sequence in the remote node (i.e. *Node 2* in Figure . If the calculation of ToF, or the time between sending a packet and receiving the ACK results in a negative time then MAC-ToF-RT will return this error code.

### 3.7.3 Local Time Value Invalid

MAC-TOF-LT (Local Time Value Invalid) status results due to an invalid time sequence in a local node (i.e. *Node 1* in Figure 3.6).

### 3.7.4 No Acknowledgement

MAC-ToF-NO-ACK (No Acknowledgement) status results when a local node fails to receive any ACK for one of the ToF measurement packets from a remote node.

### 3.7.5 No Data From Remote Node

MAC-ToF-NO-DATA (No Data From Remote Node) status results when a local node fails to receive any DATA packet from a remote node. If the remote node identifies that a packet has been lost then it will report a MAC-ToF-DATA-ERROR.

Table 3.3 shows results for two channels (13 and 26) in the indoor LOS path. At each range from 2m to 14m, 765 ToF polls were collected (i.e. 5,355 in total). As shown in table 3.3, for channel 13 results, the number of successful polls is 5,047 (94.25%) and 5.74% polls failed due to the 4 reasons listed above. Of the failed polls 72.18% are due to the condition where a local node failed to receive the *ACK* and 16.23% due to the channel being noisy with other traffic (clear channel assessment (CCA) failure). The results in on air corruption of a packet causing the arrival time correlators to give a false reading. CCA/CSMA is used for all packets, this helps to reduce the chance of this type of corruption - but it does not completely eliminate it.

Figure 3.11 illustrates the comparison of two channels in an indoor and outdoor environment. Comparing the channel 13 with channel 26, it is observed that

### 3.7 Site Survey and Analysis

---

Transceiver Height=1.5m, Indoor LoS, <b>Channel Number=13 and 26</b> Ranging Polls at each Range (m) = 765									
<b>Poll Status</b>	<b>Ch:</b>	<b>2</b>	<b>4</b>	<b>6</b>	<b>8</b>	<b>10</b>	<b>12</b>	<b>14</b>	<b>Total</b>
<b>Successful</b>	<b>13</b>	760	760	712	753	714	684	664	5047
	<b>26</b>	760	760	761	762	760	755	761	5319
<b>RT Invalid</b>	<b>13</b>	3	3	3	7	8	1	8	33
	<b>26</b>	0	0	3	0	0	1	1	5
<b>LT Invalid</b>	<b>13</b>	2	0	1	3	6	5	3	20
	<b>26</b>	5	5	0	3	5	9	3	30
<b>No ACK</b>	<b>13</b>	0	2	19	2	37	55	90	205
	<b>26</b>	0	0	1	0	0	0	0	1
<b>No Data</b>	<b>13</b>	0	0	30	0	0	20	0	50
	<b>26</b>	0	0	0	0	0	0	0	0
Channel 13 - Successful ToF Polls (for all ranges) = 5047 (94.25%)									
Channel 13 - Failed ToF Polls (for all ranges) = 308 (5.65%)									
Channel 26 - Successful ToF Polls (for all ranges) = 7319 (99.33%)									
Channel 26 - Failed ToF Polls (for all ranges) = 36 (0.67%)									

Table 3.3: Site Survey Results

### 3.7 Site Survey and Analysis

the percentage of failed polls reduced from 5.74% to 0.67% (99.33% successful). A similar trend was observed for the outdoor environment where successful ToF reported as 99.24%, about 6.79% higher than the busy channel on the site. Based on the experimental results, it is observed that operating on the noisy channel generates a noticeable number of failed polls and effects the RSS estimated range more erroneously as compared to ToF. It is also observed that indoor path is more adversely affected by the noisy channel. Based on these observations, further experimental results were conducted on a quiet channel for enhanced performance.

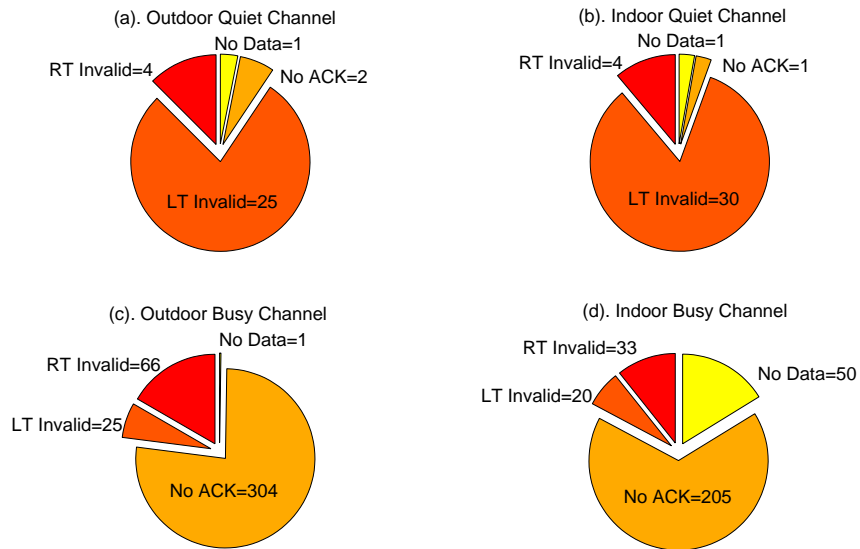


Figure 3.11: Comparison of failed ToF polls taking quiet and busy channel in the account for indoor and outdoor LOS environment (height=1.5 m). (a, b). Quiet Channel in Outdoor and Indoor. respectively (c, d). Busy Channel in Outdoor and Indoor respectively.

As seen above, a noisy channel generates a noticeable number of failed polls. Table 3.7.5 shows the magnitude of mean range error (MMRE) and standard deviation ( $\sigma$ ) for both ToF and RSS for indoor and outdoor LOS environments. It is observed that RSS estimated range is more erroneously affected by the noisy channel as compared to ToF. Furthermore, it is noticed that outdoor environment is more affected as compared to indoor.

### 3.8 Experimental Results and Analysis

---

RT-ToF and RSS estimated Range (m)					
Transceiver Height=1.5 m					
		MMRE (m)		$\sigma$ (m)	
Ranging	Environment	Ch 13	Ch 26	Ch 13	Ch 26
RT-ToF	Outdoor LOS	8.54	7.09	8.34	5.38
RSS	Outdoor LOS	39.7	21.10	29.9	18.8
RT-ToF	Indoor LOS	8.97	9.18	8.16	6.36
RSS	Indoor LOS	29.2	12.36	18.8	10.5

Table 3.4: Site Survey Results

## 3.8 Experimental Results and Analysis

In this section, point-to-point experimental data obtained to assess the performance in outdoor and indoor environments are analysed and compared. The experimental setup is discussed above in section 3.4.2 and measurements were performed using an integrated folded mono-pole antenna. The transmit power level is 0 dBm for all ranging measurements. The ranging measurements were done on two different scales. First going from 1 m to 15 m in increments of 1 m and then 10 m to 100 m in 10 m increments. In the descriptions which follow these are described as *short range* ( $S_R$ ) and *long range* ( $L_R$ ) respectively. The transmit and receive antennas were approximately aligned for maximum received power. In Figures, actual range represent the range without error, and it shows the comparison with estimated range.

Figure 3.12a and Figure 3.12b show the ToF ranging accuracy performance for the 3 different antenna heights in an unobstructed outdoor and indoor site respectively. Based on the initial site survey, a low noise channel was selected to reduce the range measurement errors [106]. Figure 3.12 shows the variation in the performance of ToF estimated range at all 3 different antenna heights. However, at antenna height of 1.5m the magnitude of mean range error (MMRE) for outdoor LOS is found to be lowest 3.41m for 1.5m height compared to 4.48m and 3.64m at heights of 1.0m and 0.5m respectively. Similarly, the MMRE for indoor LOS is found to be lowest at 2.83m compared to 3.04m and 4.36m at heights of 1.0m and 0.5m respectively. Based on the experimental results, it is observed that at short range ToF range estimates are not significantly effected

### 3.8 Experimental Results and Analysis

by the antenna heights.

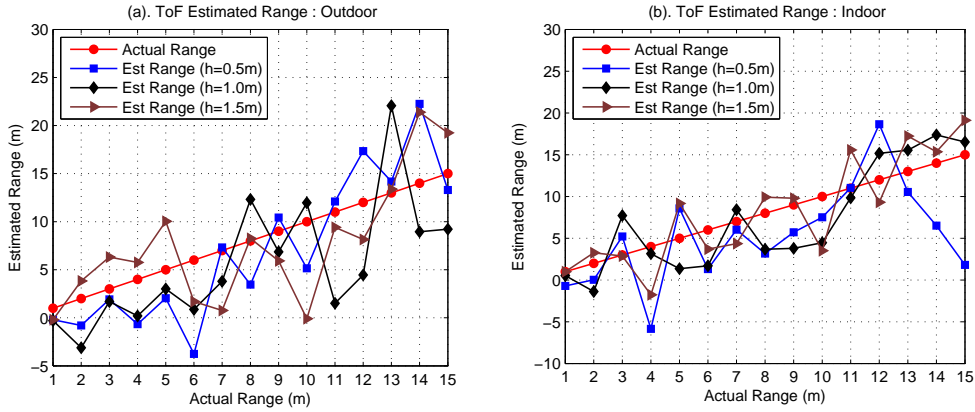


Figure 3.12: Fig. (a). ToF estimated range in outdoor LOS path for different antenna heights. Fig. (b). ToF estimated range in indoor LOS path for different antenna heights.

Figure 3.13a and Figure 3.13b show the RSS ranging accuracy performance for the 3 different antenna heights in an unobstructed outdoor and indoor site respectively. It is observed that both outdoor and indoor range estimates are more adversely affected by the antenna height as the range increases; this is attributed to ground reflection. Results shown in Figure 3.13 indicate that antenna height of 1.5m gives better ranging performance at short range as compared to heights of 0.5m and 1.0m. Beyond 5-7m, RSS ranging performance is seen to be poor for all 3 device heights. However, based on the experimental results, it is observed that the open outdoor environment effects the RSS estimated range more erroneously as compared to indoor environment.

Figure 3.14a and Figure 3.14b shows the performance comparison between ToF and RSS estimated range in outdoor and indoor LOS paths respectively for antenna height of 1.5m. At ranges of less than 7m, ranging performance for both environments is seen to be almost the same. Beyond 7m, average ranging performance in indoor LOS becomes more accurate as compared to the outdoor. Statistics from the experimented results are provided in table 3.5 which shows that uncertainty in RSS based estimated range increases with distance and beyond 7m presents severe limitations in using RSS.

### 3.8 Experimental Results and Analysis

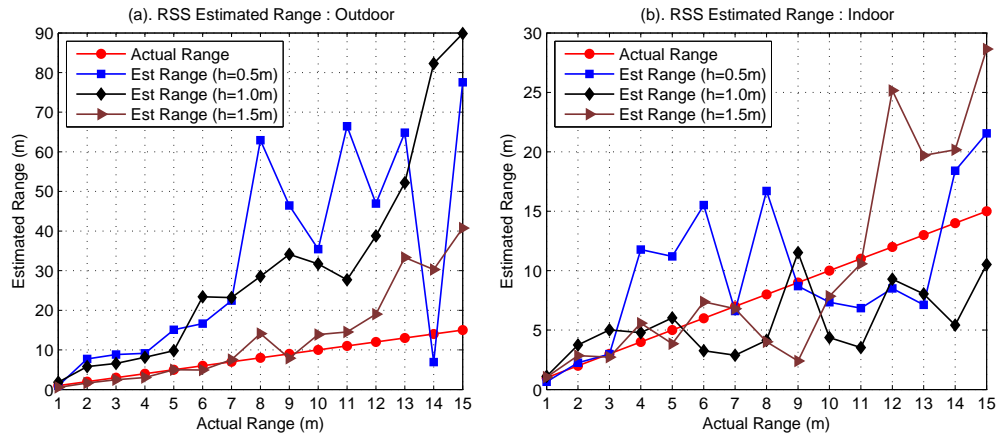


Figure 3.13: Fig. (a). RSS estimated range in outdoor LOS path for different antenna heights. Fig. (b). RSS estimated range in indoor LOS path for different antenna heights.

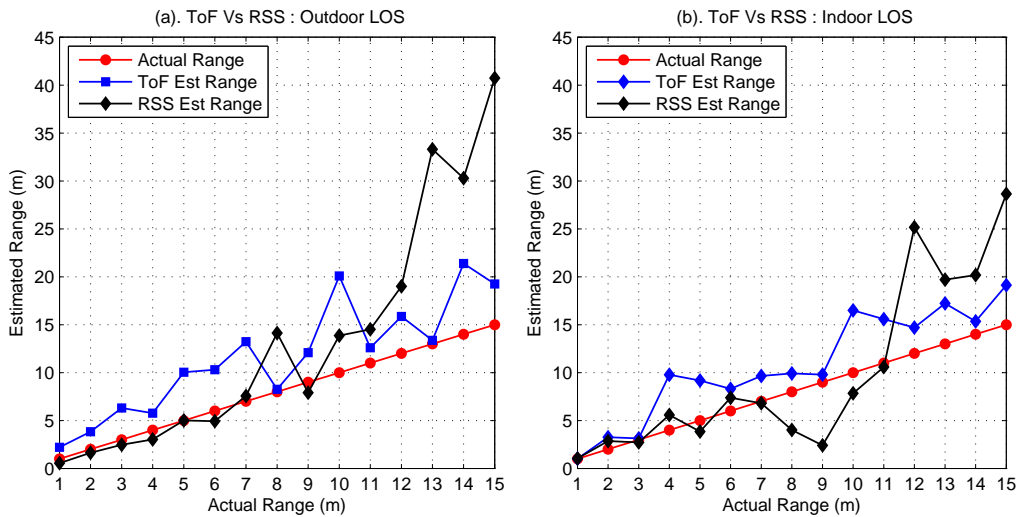


Figure 3.14: ToF versus RSS estimated range in outdoor and indoor LOS path for antenna height of 1.5m

### 3.8 Experimental Results and Analysis

---

Antenna Heights=1.5m, Channel Number=26, (R=Range)								
Outdoor LOS=OL, Indoor LOS=IL, Outdoor NLOS=ONL, Indoor NLOS=INL								
Parameter	Mean Error Magnitude (m)				Mean Standard Deviation (m)			
	R=1-6	R=7-15	R=1-15	R=10-100	R=1-6	R=7-15	R=1-15	R=10-100
ToF OL	2.91	4.12	3.41	2.74	2.04	2.37	2.24	3.20
RSS OL	0.56	9.39	5.86	18.5	0.29	3.86	2.43	5.33
ToF IL	2.27	3.20	2.83	5.3	1.70	2.92	2.43	3.06
RSS IL	0.88	5.89	3.89	15.4	1.52	5.27	3.77	6.40
ToF ONL	9.19	7.13	7.54	6.67	6.52	9.46	8.7	11.2
RSS ONL	7.14	9.36	8.84	21.3	2.91	3.85	4.48	2.94
ToF INL	4.01	5.35	4.82	4.17	5.29	5.78	5.59	5.01
RSS INL	5.72	5.40	5.31	16.25	2.32	2.74	2.57	4.51

Table 3.5: Experimental Results: ToF Vs RSS

Figure 3.15a and Figure 3.15b shows the performance comparison between ToF and RSS estimated range in outdoor and indoor NLOS paths respectively for antenna height of 1.5m. The experimental results indicate that at short range where no LOS exists both ToF and RSS provide poor ranging. This is attributed to the fact that multipath environment not only changes  $\eta$  and  $\sigma_{sh}$  dynamically to effect the amplitude of the received signal but also introduces the larger delays over a direct LOS path. Therefore, the estimated distance at short range based on ToF and RSS is very unreliable. There is a huge requirement to compensate this unreliability with more complex mitigation techniques.

Figure 3.16a and Figure 3.16b show the ToF ranging accuracy performance over a long range for LOS and NLOS paths respectively. It is observed that ToF gives better ranging accuracy over a long range as compared to the short range (as shown in Figure 3.12). In the case of outdoor and indoor LOS paths, source and remote nodes were able to perform range estimation over a range of 100m. This maximum radio communication range reduces to 70m for the case of NLOS paths. Based on our experimental results, it is confirmed that increase of distance between source and remote node does not effect ToF ranging error (i.e. no increase in the ranging error with the increase of distance). It establishes that ToF ranging is a good candidate for long range estimation.

### 3.8 Experimental Results and Analysis

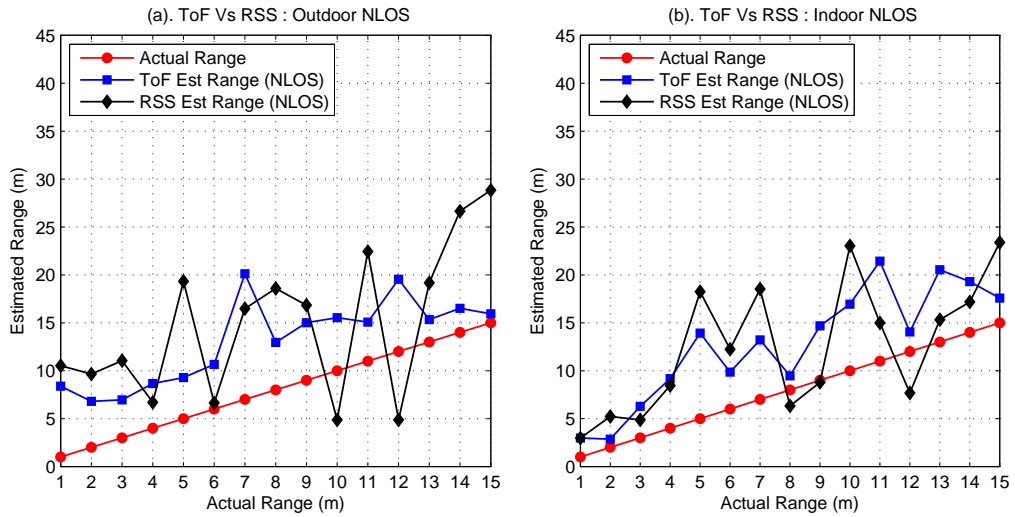


Figure 3.15: ToF versus RSS estimated range in outdoor and indoor NLOS path for antenna height of 1.5m

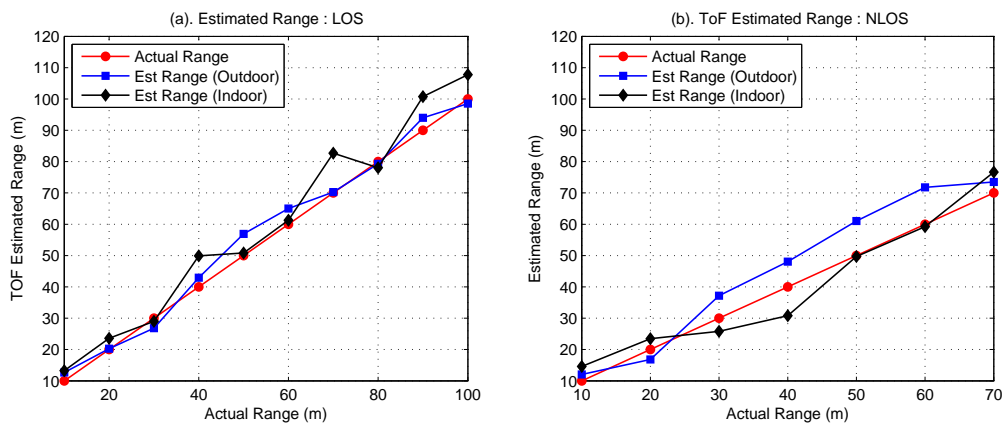


Figure 3.16: ToF estimated range in outdoor and indoor over long range for antenna height of 1.5m

### 3.8 Experimental Results and Analysis

Figure 3.17a and Figure 3.17b show the RSS ranging accuracy performance over a long range for LOS and NLOS paths respectively. It is observed that RSS gives poor ranging accuracy over a long range as compared to ToF as shown in Figure 3.16. Similar to ToF ranging, the communication range is reduced to 70m in the case of outdoor and indoor NLOS paths. The experimental results indicate that RSS ranging is a poor candidate for long range due to the fact that ranging error increases with distance.

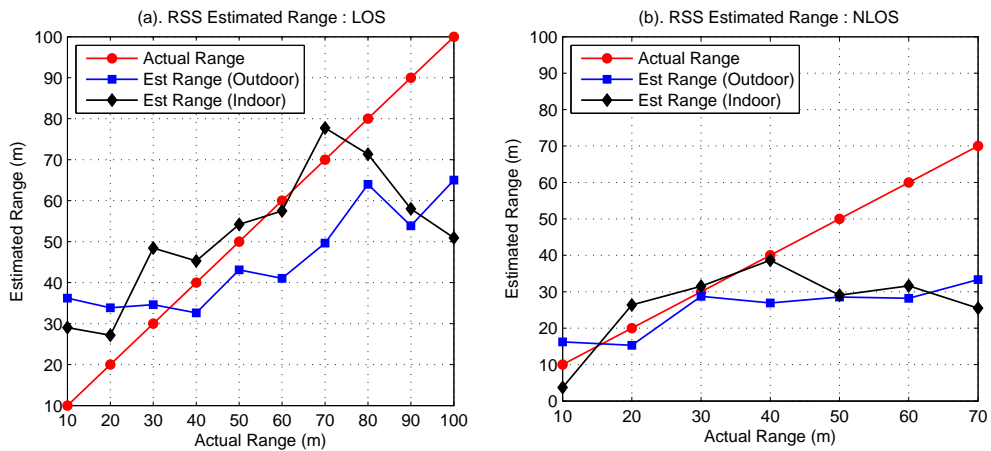


Figure 3.17: RSS estimated range in outdoor and indoor for antenna height of 1.5m

Figure 3.18a Figure 3.18b compare the percentage of MMRE for ToF and RSS. As shown in Figure 3.18a, approximately 78%-88% of the LOS ToF measurements are accurate to within 6m for outdoor and indoor LOS respectively. Comparing with the ToF measurements, a variation in the percentage of MMRE is observed for RSS measurements. Observing the indoor LOS path, result indicated that approximately 80% of the RSS measurements are accurate to within 6m, reducing to 70% for outdoor environment.

In the case of outdoor and indoor LOS channels Figure 3.18a shows, approximately 30% to 40% of the ToF measurements are accurate to within 2m MMRE. RSS ranging is seen to be good with 50% and 55% are accurate to within 2m for indoor and outdoor LOS respectively. As RSS showed good ranging accuracy at ranges less than  $\sim 7$ m for outdoor and indoor unobstructed paths, approximately 32%-38% of the LOS RSS measurements are accurate to within 1m.

### 3.8 Experimental Results and Analysis

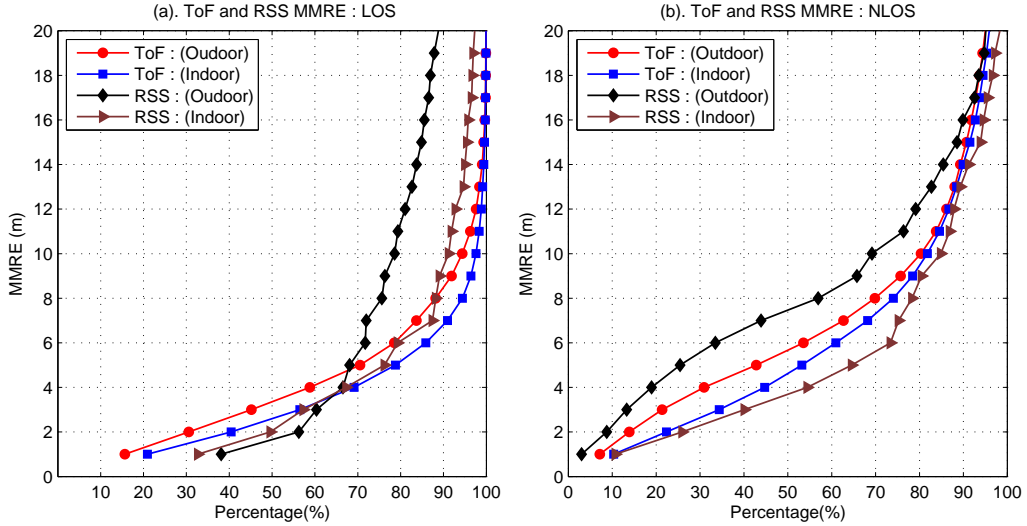


Figure 3.18: ToF and RSS: MMRE percentage in outdoor and indoor for LOS and NLOS paths over short range with antenna height of 1.5m.

In the case of outdoor and indoor NLOS channels Figure 3.18b show, approximately 15% to 22% of the ToF measurements are accurate to within 2m MMRE. RSS ranging is seen to be poor with only 10% are accurate to within 2m for outdoor whereas indoor NLOS showed better ranging performance. In indoor NLOS,  $\sim 15\%$  results are more accurate to within 2m as compared to outdoor NLOS. A close percentage of accurate results is observed between ToF and RSS for indoor NLOS, which also showed more accurate ranging as compared to the outdoor NLOS. As compared to indoor NLOS environment, outdoor NLOS environment showed considerable signal attenuation even at short ranges, where LOS is blocked by trees and wooden benches.

Figure 3.19a Figure 3.19b compare the percentage of MMRE for ToF and RSS over long range. As shown in Figure 3.19a, approximately 55%-70% of the LOS ToF measurements are accurate to within 5m for outdoor and indoor LOS. Compared with the ToF measurements, a huge variation in the percentage of MMRE is observed for RSS measurements. Observing the indoor LOS path, results indicated that approximately 25% of the RSS measurements are accurate to within 5m, reducing to 10% for outdoor environment. In the case of outdoor and indoor NLOS channels (Figure 3.19b), approximately 40% to 45% of the

### 3.8 Experimental Results and Analysis

ToF measurements are accurate to within 5m MMRE respectively. RSS ranging is seen to be poor with only 20% and 25% accurate to within 5m for outdoor and indoor NLOS.

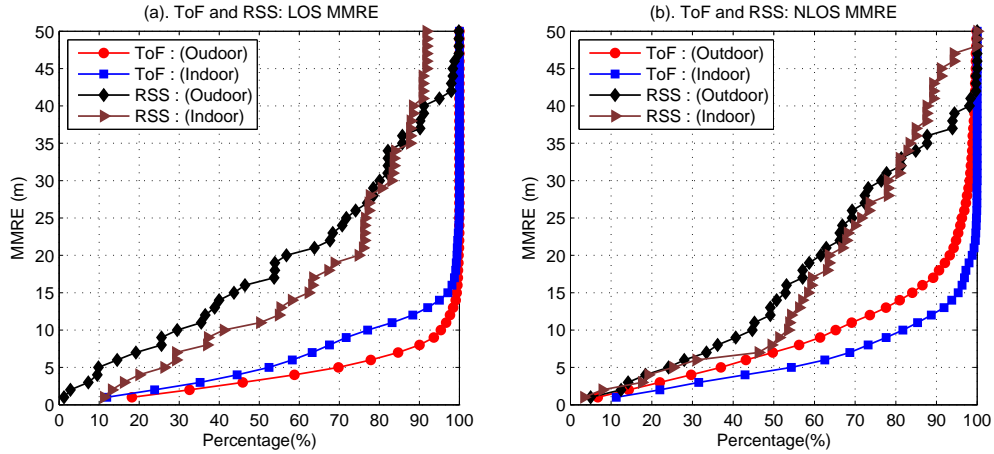


Figure 3.19: ToF and RSS: MMRE percentage in outdoor and indoor for LOS and NLOS paths over long range with antenna height of 1.5m.

Figure 3.20(a-c) presents the probability distribution plot for 3 individual ToF estimated ranges over a short range in the outdoor LOS environment. The respective quantile-quantile (Q-Q) plots are shown in Figure 3.20(d-f). As shown in Figure 3.20(a-c) distribution plots, average results are approximately distributed according to a normal distribution. Results shown in Figure 3.20(d-f) demonstrate a correlation where the plotted points fall approximately along the straight line proving the range estimated to be Gaussian distributed.

Figure 3.21(a-c) presents the probability distribution plot for 3 individual RSS estimated ranges over a short range in outdoor LOS environment. The respective quantile-quantile (Q-Q) plots are shown in Figure 3.21(d-f). Figure 3.21(a-c) shows less points due to the overlapping of data points. As shown in Figure 3.21(a) average results are approximately distributed according to a normal distribution and its correlation is shown in Figure 3.21(d). Results shown in Figure 3.21(e) and Figure 3.21(f) demonstrate a low correlation where the plotted points deviate from the straight line, which corresponds to the best-fitting normal distribution. It indicates that some of the RSS ranging results are not normally distributed.

### 3.8 Experimental Results and Analysis

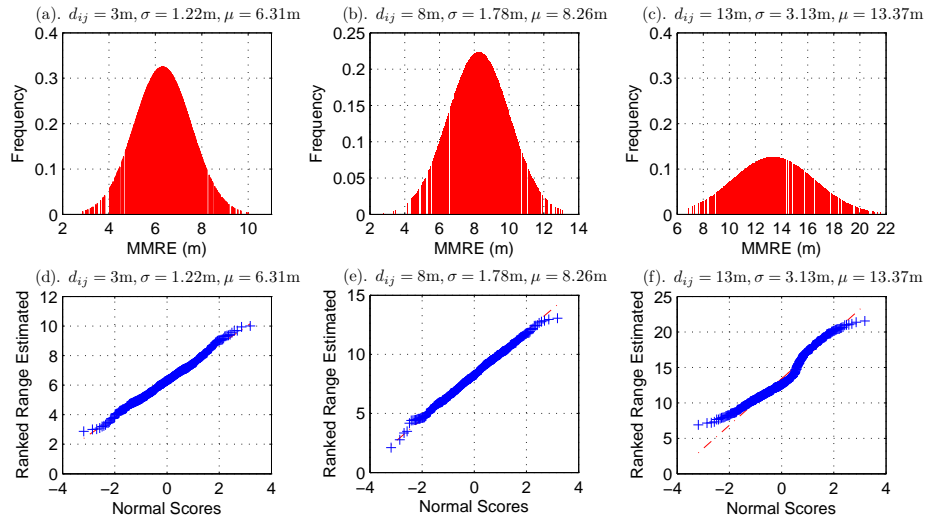


Figure 3.20: PDF and Q-Q plot across ToF measurements over short range for outdoor LOS.

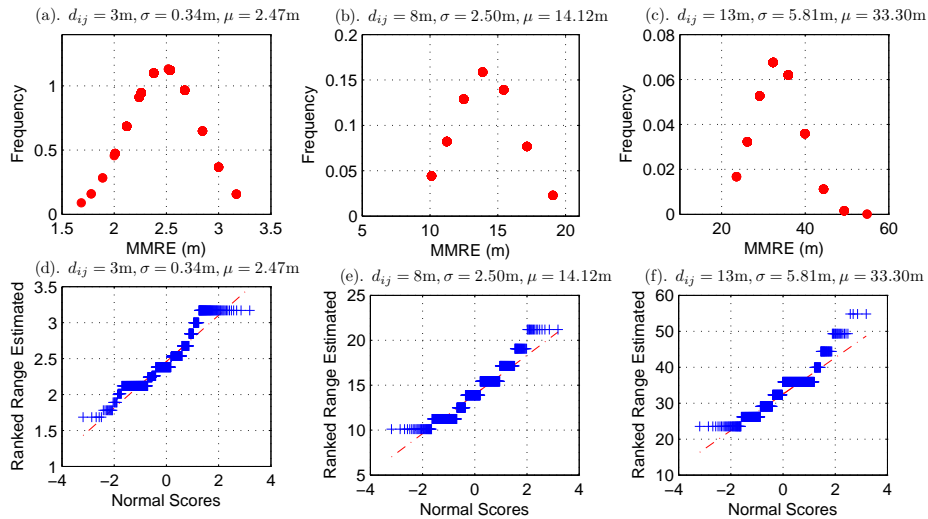


Figure 3.21: PDF and Q-Q plot across RSS measurements over short range for outdoor LOS.

### 3.8 Experimental Results and Analysis

Figure 3.22(a) and Figure 3.22(c) shows the distribution across all of the ToF and RSS measurements over short range for outdoor NLOS case, whereas Figure 3.22(b) and Figure 3.22(d) are respective Q-Q plots. Figure 3.22(a-b) indicates a strong correlation and the plotted points fall approximately along the straight line showing the range estimates to be Gaussian distributed. In the case of RSS, where plotted points deviate from the straight line, indicate that average of all RSS measurements over NLOS short range is not normally distributed. A very similar trend is observed across all of the ToF and RSS measurements over short range for indoor NLOS case.

It is further analysed through the moments (*skewness and kurtosis*) of the distribution. The skewness of 0.57 which is close to the 0 and kurtosis of 2.29 which is near the expected value of 3 are observed in the case of ToF. It indicates ToF measurements over a short range is normally distributed. In the case of RSS, skewness of 1.15 and kurtosis of 1.99 are deviated from the expected value, hence shows RSS measurements over a short range is not normally distributed.

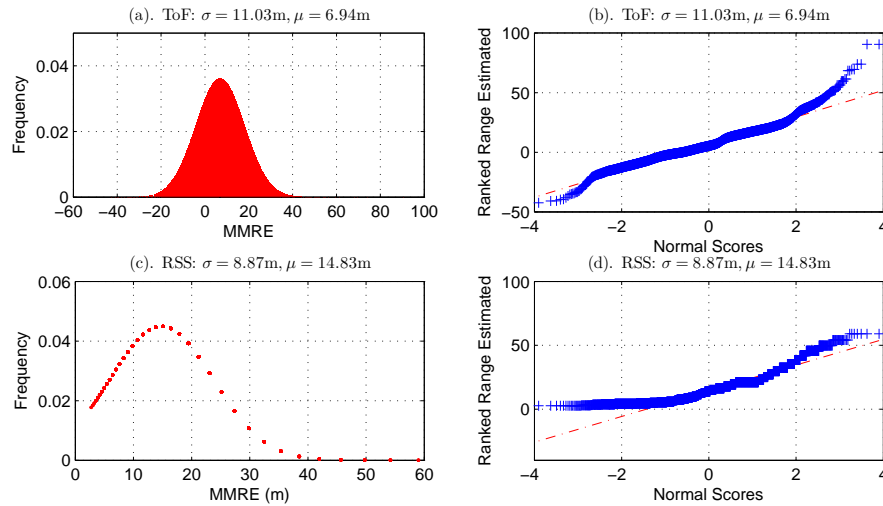


Figure 3.22: PDF and Q-Q plot across all of the ToF and RSS measurements over short range for outdoor NLOS.

## 3.8 Experimental Results and Analysis

---

### 3.8.1 Cross-over Range ( $C_R$ )

As observed through results and analysis in section 3.8, the variation in RSS tends to level off after about  $\sim 7\text{m}$ , it is difficult to resolve the distances based on RSSI as the distance increases above this range. It is therefore observed, RSS ranging system may fail to achieve the required accuracy mark. Unlike RSS, as the distance increases RT-ToF ranges estimates become better than the RSSI range estimates. Based on the analysis and looking at the effect of the mean error, it is crucial to have a cross-over range ( $C_R$ ) where the error of RSS ranging is known to becomes greater then the error for ToF ranging. To enhance the ranging performance for localization system, a ranging system based on  $C_R$  can be considered, which incorporates both RSS and RT-ToF based on the cross-over point. In order to compare the experimental  $C_R$  with theoretical  $C_R$  based on IEEE 802.15.4 specification, Eq. (3.14) and Eq. (3.17) can be exploited by equating as Eq. (3.18) [107]:

$$\frac{c^2}{8\pi^2\text{SNR}\beta^2\sqrt{\alpha}N} = \left( \frac{(\ell n 10)^2 \sigma_{sh}^2 d^2}{10^2 \eta^2} \right) \quad (3.18)$$

$$C_R = \frac{10c}{2\sqrt{2}\pi\sqrt{\Upsilon}\sqrt{N}\alpha^{1/4}\beta} \frac{\eta}{\ell n 10 \sigma_{sh}} \quad (3.19)$$

where the channel parameters  $\eta$  and  $\sigma_{sh}$  are calculated using the experimental data. Figure 3.23 shows the  $C_R$  for 4 different channel parameters ( $\eta$  and  $\sigma_{sh}$ ) for outdoor and indoor LOS case as shown in table 3.2. It can be observed that, the  $C_R$  is dependant on the SNR and the channel parameters. At  $\sim 6\text{dB} - 10\text{dB}$ , based on the LOS channel parameters, the  $C_R$  is  $\sim 7\text{m}$ . Experimental results discussed in section 3.8 indicate the  $\sim 5\text{-}7\text{m}$  as a  $C_R$ , Hence it suggests that above  $C_R$  RSS method should be outperformed by RT-ToF. Knowledge of this  $C_R$  can be used to devise a range aware joint (RAJ) estimation scheme to enhance range estimation hence the localization performance to get the accurate position estimate.

### 3.9 Conclusion

---

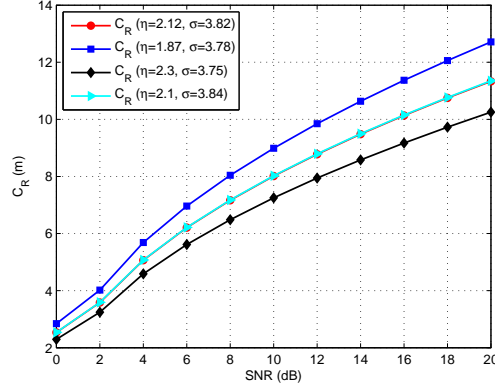


Figure 3.23: Cross-over Range using experimental parameters.

### 3.9 Conclusion

This chapter analyse the performance limits of RT-ToF and RSS based ranging using Jennic’s JN5148, IEEE 802.1.5.4 compliant WSNs. This chapter starts off with the RT-ToF, where range resolution is explained and fundamental CRLB is calculated and compared with the measured CRLB. Later on in the chapter, RSS propagation model is discussed and principle of operation is explained. The fundamental CRLB on ToF and RSS ranging performance is compared with the performance limits of JN5148 series ranging modules. The results indicate that the measured performance limits of ToF and RSS based range measurement approaches the theoretical CRLB. In addition to that, cross-over range is calculated for RSS, which suggest that RSS is a good candidate for short range.

The experimental infrastructure is demonstrated to analyse the performance of ToF and RSS based ranging using Jennic’s JN5148, IEEE 802.1.5.4 compliant WSNs nodes in outdoor and indoor environments for both LOS and NLOS paths. The fundamental CRLB on ToF and RSS ranging performance is compared with the performance limits of *JN-514x* series ranging modules. The results indicate that the measured performance limits of ToF and RSS based range measurement approaches the theoretical CRLB. Using a site survey tool prior to measuring ToF and RSS over different lower noise channels helped not only to improve the confidence in a burst of readings but also improved accuracy.

### 3.9 Conclusion

---

The results over a short range demonstrate that RSS is a good candidate for range estimation at ranges less than  $\sim 7\text{m}$  for outdoor and indoor unobstructed paths. The experimental results are compared with the calculated  $C_r$  to validate the point that RSS provides better ranging accuracy at short range. This can help to improve the range accuracy at a short range by alleviating the need for ToF calculation. Uncertainty in RSS based range estimation increases with distance and beyond 7m, presents severe limitations in using RSS. Further investigating NLOS paths, RSS ranging is found to be too erratic to be used in realistic location systems as compared to ToF at any range.

Comparing ToF on LOS paths for different antenna heights in outdoor and indoor environment, ToF measurements are seen to be largely independent of antenna height. However, at antenna height of 1.5m the MMRE is found to be lowest. As compared to ToF, RSS is found to be more dependent on antenna heights as range increases. However, antenna height of 1.5m showed better ranging accuracy at range less than  $\sim 7\text{m}$ . Comparing with the outdoor for both LOS and NLOS measurements, outdoor NLOS environment showed considerable signal attenuation even at short ranges, where LOS is blocked by trees and wooden benches.

# Chapter 4

## Localization using Optimal and Sub-Optimal Multi-lateration

### 4.1 Overview

This chapter compares methods of two-dimensional (2-D) localization in order to try and reduce the processing overhead of optimal multi-lateration whilst still achieving a closer accuracy. Three methods of localization are examined, firstly sub-optimal blind trilateration (SBT) which randomly selects the minimum feasible number of anchors. This defines the lower processing limit. Secondly modified sub-optimal blind trilateration (MSBT) which selects anchor nodes based on geometric dilution of precision (GDOP). Thirdly we compare these with optimal multi-lateration (OML), which provides the benchmark in terms of accuracy achievable. A Matlab based simulation platform is developed to analyse the lateration schemes. By exploiting the geometric relationship between nodes, our analysis and results show that performance of these lateration based approaches presents a trade-off for complex computation, thus energy consumption and accuracy.

## 4.2 Introduction

Accurate positioning of nodes in sensor networks is a key requirement for many applications. In the last decade many researchers have shown great interest in the efficient positioning of nodes. Satellite based localization such as the global positioning system (GPS) provides an excellent worldwide lateration framework for determining geographic position [53] but cannot fulfil the requirements of WSN localization due to its high power requirement and line of sight (LOS) constraints. Localization in WSNs is a very challenging task and there are significant device constraints which impact upon the design objectives for any practical localization scheme. One of the important device constraint is simple measurement hardware for both cost-effectiveness and device size miniaturization [14, 108]. With respect to this device constraint, range-based localization schemes are far more suitable than bearing-based approaches as they mandate either little or no additional hardware requirement to support the small form-factor of WSNs [108]. Hence, this chapter focuses the range-based localization.

Due to development in micro-electro-mechanical-systems (MEMS), data communication and electronics, deployment in large scale WSNs is rapidly becoming possible. Where large number of sensor nodes can coordinate with each other to perform challenging tasks, including localization, search and recovery operation, monitoring for buildings and bridges, medical, precision farming and environmental monitoring [56, 88]. In a typical localization scenario, a subject node ( $s_j$ ) can have a number of in-range anchor/pseudo-anchor<sup>1</sup> nodes ( $A_i$ ). Here, acquiring ranging information from all in-range anchors/pseudo-anchors and using this whole ranging information to calculate the optimal position estimate of a node ( $s_j$ ) is termed as ‘*optimal multi-lateration*’ (OML) [109]. Selection of anchor nodes to perform localization differentiates optimal ‘*multi-lateration*’ and sub-optimal ‘*trilateration*’. By randomly choosing just three of the in-range nodes with known estimated position and using them without an associated quality fig-

---

<sup>1</sup>Once a sensor node ( $s_j$ ) is localized using optimal multi-lateration or sub-optimal blind trilateration, it can be used as a pseudo-anchor node in the next iteration to localize other subject nodes. We term such nodes pseudo-anchors since we range from them as we do anchors but they will have a location error associated with them.

### 4.3 Signal Model

---

ure (describing the position error probability of nodes) to calculate the position estimate of the subject node ( $s_j$ ) is ‘sub-optimal *blind* trilateration’ (SBT) [56].

Localization error in the sensor network context is a result of several mechanisms each with different error patterns [68, 110, 111]. These different error patterns are due to inaccurate ranging, propagation of errors due to pseudo-anchors [17] and bad geometry of anchors [30–32, 91]. Ranging accuracy is an important aspect to consider because a localization system obtains position estimates using range estimates. Inaccurate range estimation may lead to unacceptable localization errors. Time based ranging is highly influenced by the systematic parameters such as clock offset, frequency offset and thermal noise. In addition to these systematic parameters, environmental condition corrupts ToF ranging samples. In reality it is not possible to have perfectly aligned clocks at the transmitter and receiver due to tolerances of quartz oscillators, temperature variations, and environmental changes and these results in *clock offset*. The clock frequency mismatch can be significant in the context of WSNs, where high-precision oscillators do not comply with the constraints.

In addition to the ranging accuracy, when using a lateration scheme, the localization accuracy is highly influenced by poor geometry of anchor nodes, hence the geometry of anchor nodes is an important source of error. The accuracy of location estimate can vary depending on anchors geometry and which anchors are used for the range measurement because different anchor geometries can enhance or reduce the localization accuracy. To consider the anchors geometry and its impact of localization accuracy, the well-known dimensionless metric, geometric dilution of precision (GDOP) [30–32, 35] can be used to design the location system. The GDOP metric is exposed for anchors selection by exploiting the geometric relation between the number of in-range anchor nodes. In order to facilitate the performance analysis of SBT, MSBT and OML approaches, the additive signal model is considered as discussed below.

### 4.3 Signal Model

To estimate a subject location in 2-D, a subject node requires minimum of three anchor nodes. Individual distance between each anchor and the subject node is

### 4.3 Signal Model

---

represented by a circle or line of position (LoP). Consider a field of dimensions with length( $l$ ) and width ( $w$ ) for a 2-D network, consisting of  $N$  anchor nodes whose locations  $A_i = [x_i, y_i]^T$  for  $i = 1, \dots, N$  are known, this can be achieved by placing these anchors at predefined points or their position can be determined via GPS. Considering the  $M$  number of unknown subject nodes whose true locations are denoted as  $s_j = [x_j, y_j]^T$  for  $j = 1, \dots, M$ , where  $.^T$  is the matrix transpose operation. It is desired to determine the location of a subject node  $s_j$ . In practice, actual distance  $d_{ij}$  based on ToF and RSS is corrupted by the various factors discussed in Chapter 3. The signal received at the subject node from the  $i^{th}$  anchor can be given Eq. (4.1) [102]:

$$r_{ij}(t) = A_{ij}^t s(t - \tau_{ij}) + n_{ij}(t) \quad (4.1)$$

where  $A_{ij}^t$  is the amplitude or attenuation of the signal,  $\tau_{ij}$  is the propagation delay,  $n_{ij}(t)$  is the ranging error that accounts for ToF errors due to the noisy measurement. The delay  $\tau_{ij}$  that is dependant on the distance between the anchor and the subject node is given by Eq.(4.2):

$$\tau(x, y, \ell) = \frac{1}{c} \sqrt{(x_i - x_j)^2 + (y_i - y_j)^2 + \ell_i} \quad (4.2)$$

where  $c$  is the speed of the electromagnetic wave ( $c \simeq 3 \times 10^8$  m/s) and  $\ell_i$  is non-line-of-sight (NLOS) bias. When dealing with the LOS case, the NLOS bias is 0 ( $\ell = 0$ ).

From Eq. (4.2), we note that the distance between  $i^{th}$  anchor and the  $j^{th}$  subject node is given by Eq. (4.3):

$$d_{ij} = c\tau_{ij} \quad (4.3)$$

In vector form to include distances from  $N$  anchors can be given as  $\mathbf{d}_{ij} = [d_{1j}, d_{2j}, \dots, d_{Nj}]^T$ . Thus the estimated distance  $\hat{d}_{ij}$  is given as Eq. (4.4)

#### 4.4 Sub-Optimal Blind Trilateration (SBT)

---

$$\hat{d}_{ij} = \sqrt{(x_i - x_j)^2 + (y_i - y_j)^2} + n_{ij}, \quad (i = 1, \dots, N) \quad (4.4)$$

where  $\hat{d}_{ij}$  is the estimated distance between node  $i$  and  $j$ ,  $N$  is the number of anchor nodes. To provide a generic idea of localization errors, it is considered that  $n_{ij} \sim \mathcal{N}(0, \sigma_{ij}^2)$  is the additive white Gaussian noise with constant standard deviation  $\sigma$ , that is independent of  $d_{ij}$ .

#### 4.4 Sub-Optimal Blind Trilateration (SBT)

Sub-optimal blind trilateration in a 2-D case requires a minimum of three anchor nodes. Individual distance between each anchor and the subject node is represented by a circle or line of position (LoP). The point of intersection of these circles is the subject node location whereas the centres of these circles are the locations of anchor nodes as shown in Fig. 4.1. Fig. 4.1 shows an example where a subject node ( $s_j$ ) with coordinates  $s_j = [x_j, y_j]^T$  is surrounded by 3 in-range anchor nodes whose locations  $A_i = [x_i, y_i]^T$  for  $i = 1, \dots, 3$  are known. This can be achieved by placing these anchors at predefined points or their position can be determined via global positioning system (GPS). The true distances ( $d_{ij}$ ) between the anchors and the subject nodes are the radii of the individual LoP and from the Pythagoras theorem, the set of equations can be given as:

$$d_{ij} = \sqrt{(x_i - x_j)^2 + (y_i - y_j)^2} \quad (1, \dots, 3) \quad (4.5)$$

where  $i$  is the number of anchor nodes.

In SBT, 3 anchors in-range of a subject node will result in 3 equations in the form of Eq. (4.5), which leads the following set of equations (Eq. (4.5), for  $i = 1, \dots, 3$ ) expressed in matrix form as given by Eq. (4.6):

$$\begin{bmatrix} (x_1 - x_j)^2 + (y_1 - y_j)^2 \\ (x_2 - x_j)^2 + (y_2 - y_j)^2 \\ (x_3 - x_j)^2 + (y_3 - y_j)^2 \end{bmatrix} = \begin{bmatrix} d_1^2 \\ d_2^2 \\ d_3^2 \end{bmatrix} \quad (4.6)$$

#### 4.4 Sub-Optimal Blind Trilateration (SBT)

---

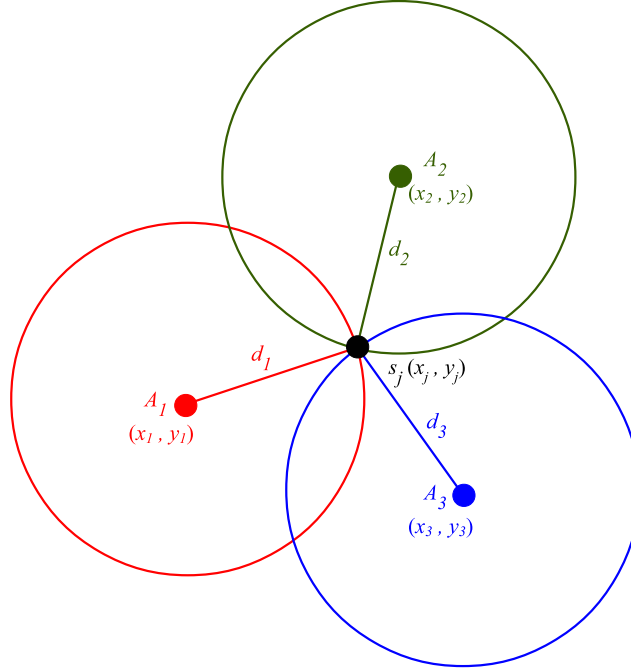


Figure 4.1: Subject node with 3 in-range anchor nodes

Eq. (4.6) is a set of three independent non-linear simultaneous equations with two unknowns  $[x_j, y_j]^T$ . Since there are more equations than unknowns, the system is overdetermined, and in general there is not a unique solution [102]. However, there is a least squares solution. Optimization techniques for the non linear equations will involve iterative and extensive complicated algorithms [43, 77]. Different approaches have been proposed to obtain an approximate location estimation in the previous studies [69, 77, 112, 113]. The Taylor series expansion (TSE) method was utilized in [112] to acquire the location estimation from the time measurements. The scheme requires iterative processes to obtain the location estimate from a linearised system. The major drawback of the TSE method is that it may suffer from the convergence problem due to an incorrect initial guess of the MSs position [69]. Since, the set of equation (Eq. (4.6)) is quadratic, many cases of sign would have to be considered. However, if the set of sub-optimal trilateration equation is linearised, then a simpler linear calculation can be used to obtain the subject node location.

## 4.4 Sub-Optimal Blind Trilateration (SBT)

---

### 4.4.1 Least Squares Solution

In general, the range estimates ( $d_{ij}$ ) are not accurate due to the noisy measurements and NLOS bias, as given by Eq. (4.4), where  $\hat{d}_{ij}$  is the estimated range. Due to the inaccurate range estimates, the trilateration technique yields LoPs, which provide a region of uncertainty instead of a single point, hence no unique solution and subject node could be located within any point in the uncertainty region as shown in Fig. 4.2 with dotted circles (red, green and blue). Due to non-linearity, to solve  $N$  equations, it is required to resort to an optimization scheme to estimate the location. Least-squares method are often used for solving such optimization problems. In the least squares method, a range estimate is computed that minimizes the squared error between it and all the calculated ranges. By removing the the quadratic terms  $x_j$  and  $y_j$ , the set of 3 equations can be written as linear equation [102, 114]. This can be achieved by subtracting the Eq. (4.5) for  $i = 3$  from  $i = 1$  and  $i = 2$ . The resulting two equations can be given as Eq. (4.7) and Eq. (4.8):

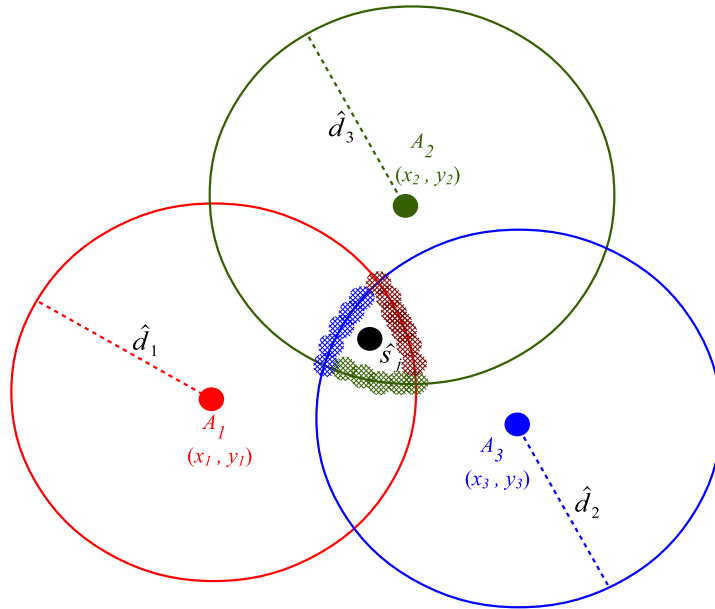


Figure 4.2: Subject node with 3 in-range anchor nodes

#### 4.4 Sub-Optimal Blind Trilateration (SBT)

---

$$(x_3 - x_j)^2 - (x_3 - x_j)^2 + (y_1 - y_j)^2 - (y_3 - x_j)^2 = d_1^2 - d_3^2 \quad (4.7)$$

$$(x_2 - x_j)^2 - (x_3 - x_j)^2 + (y_2 - y_j)^2 - (y_3 - x_j)^2 = d_2^2 - d_3^2 \quad (4.8)$$

Further, Eq. (4.7) and Eq. (4.8) can be expanded as Eq. (4.9) and Eq. (4.10) respectively:

$$\begin{aligned} & (x_1^2 - 2x_1x_j + x^2) - (x_3^2 - 2x_3x_j + x^2) + \\ & (y_1^2 - 2y_1y_j + y^2) - (y_3^2 - 2y_3y_j + y^2) = d_1^2 - d_3^2 \end{aligned} \quad (4.9)$$

$$\begin{aligned} & (x_2^2 - 2x_1x_j + x^2) - (x_3^2 - 2x_3x_j + x^2) + \\ & (y_2^2 - 2y_1y_j + y^2) - (y_3^2 - 2y_3y_j + y^2) = d_2^2 - d_3^2 \end{aligned} \quad (4.10)$$

rearranging the terms in Eq. (4.9) and Eq. (4.10) results in Eq. (4.11) and Eq. (4.12):

$$2(x_3 - x_1)x_j + 2(y_3 - y_1)y_j = (d_1^2 - d_3^2) - (x_1^2 - x_3^2) - (y_1^2 - y_3^2) \quad (4.11)$$

$$2(x_3 - x_2)x_j + 2(y_3 - y_2)y_j = (d_2^2 - d_3^2) - (x_2^2 - x_3^2) - (y_2^2 - y_3^2) \quad (4.12)$$

Following set of equations (Eq. (4.11) and Eq. (4.12)) can be extended to a matrix form as below:

#### 4.4 Sub-Optimal Blind Trilateration (SBT)

---

$$As = b \quad (4.13)$$

where  $A$  is a function of the coordinates of the anchor nodes as given by Eq. (4.14),  $s$  is the subject node location as given by Eq. (4.15) and matrix  $b$  is a function of the distance between the anchor nodes to the subject nodes and the coordinates of the anchor nodes as given by Eq. (4.16). As Eq. (4.14) is a function of the coordinates of the anchor nodes, therefore it remains same.

$$A = \begin{bmatrix} x_2 - x_1 & y_3 - y_1 \\ x_3 - x_1 & y_3 - y_1 \end{bmatrix} \quad (4.14)$$

$$s = \begin{bmatrix} x_j \\ y_j \end{bmatrix} \quad (4.15)$$

$$b = \frac{1}{2} \begin{bmatrix} (d_1^2 - d_2^2) + (x_2^2 - x_1^2) + (y_2^2 - y_1^2) \\ (d_1^2 - d_3^2) + (x_3^2 - x_1^2) + (y_3^2 - y_1^2) \end{bmatrix} \quad (4.16)$$

Eq. (4.13) assumes a system with unique solution, but as mentioned above, in practice, the range estimates are not perfect and a unique solution will not result:

$$As - b \neq 0 \quad (4.17)$$

As a resort to an optimization technique to determine the location estimation consider the optimization parameter as Eq. (4.18):

$$As = b - \hat{s} \quad (4.18)$$

Here an optimization parameter vector ( $\hat{s} = [\hat{x}^2, \hat{y}^2]^T$ ) is the quantity to be minimized. Here minimizing Eq. (4.19) is to minimize the mean square error by taking derivative with respect to  $\hat{s}$  and setting equal to zero [115], as given below by Eq. (4.19) and Eq. (4.20):

#### 4.4 Sub-Optimal Blind Trilateration (SBT)

---

$$\begin{aligned}
\hat{s} &= \arg \min_s \|b - As\|^2 \\
&= [b - A\hat{s}]^T [b - A\hat{s}] \\
&= b^T b - b^T A\hat{s} - A^T \hat{s}^T b + A^T \hat{s}^T A\hat{s}
\end{aligned} \tag{4.19}$$

$$\begin{aligned}
\hat{s} &= \partial\theta(\hat{s}) = 0 - A^T b - A^T b + 2A^T A\hat{s} \\
&= 2A^T A\hat{s} - 2A^T b = 0
\end{aligned} \tag{4.20}$$

This leads us to the determined system of the linear equations as given by Eq. (4.21), for which the unique solution exists under certain conditions (i.e.  $A$  has to have full rank) [102, 115, 116]:

$$\hat{s} = (A^T A)^{-1} A^T b \tag{4.21}$$

where  $T$  is transpose, and  $\hat{s}$  is the estimated subject node. Eq. (4.21) is called normal equation and a solution will exist for the set of  $N - 1$  linear equations if the number of equations is at least equal to the number of unknowns. In the case of SBT,  $N - 1$  must be 2, so at least 3 non-collinear anchor nodes are required to perform 2-D trilateration.

As mentioned above, when using a lateration scheme, the localization accuracy is highly influenced by poor anchor geometry. When using SBT, no unique solution exists under the following two conditions [117]:

1. If all the anchor nodes involved in trilateration are collinear as shown in Fig. 4.3(a). In this case, It will be impossible to differentiate which side of the reference line the subject node is located at due to the symmetry about the line.
2. If two of the anchor nodes involved to perform trilateration are co-incident as shown in Fig. 4.3(b).

#### 4.4 Sub-Optimal Blind Trilateration (SBT)

---

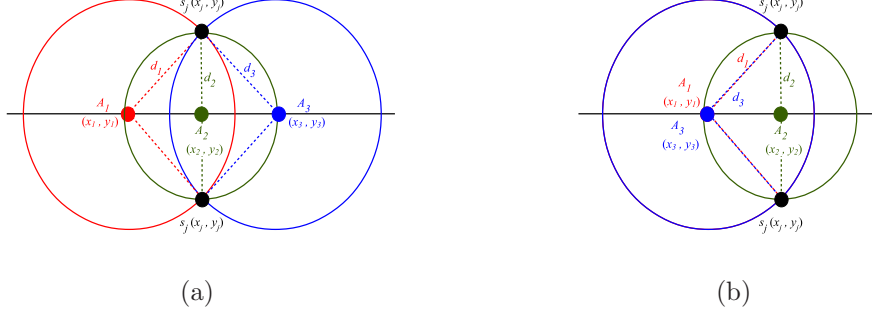


Figure 4.3: Fig. 4.3(a). Subject node with 3 in-range collinear anchor nodes. Fig. 4.3(b). Subject node with 2 in-range anchor nodes, where 3 anchor nodes are co-incident.

In addition to these two exceptions, the geometric placement of anchor nodes may result in a high degree of error, and make sub-optimal blind trilateration an impractical solution for a scalable network. As a metric to evaluate the lateration schemes, the root-mean-square error ( $E_{\text{RMS}}$ ) of the location estimate obtained from  $N$  anchors can be given by Eq. (4.22) as below:

$$E_{\text{RMS}} = \sqrt{\frac{\sum_{m=1}^k (s_j - \hat{s}_j^m)(s_j - \hat{s}_j^m)^T}{k}} \quad (4.22)$$

where  $k$  is the number of iterations selected for a lateration scheme. It provides an indication of how well the measured distances converge on the estimated subject node location. In practices, it shows an estimate of the location uncertainty due to ranging errors (e.g. background noise, multipath components and interference) along with distorted anchor placement.

Fig. 4.4 shows an estimate of the location error for different anchor combinations along with the ranging errors (e.g. background noise, multipath components and interference). Fig. 4.4(a) shows the different anchor combinations, where  $A_1$ ,  $A_2$  are considered as fixed anchors and  $A_3$  is changed from  $A_3$  to  $A_{13}$ . For each combination, the corresponding  $E_{\text{RMS}}$  is calculated at noise variance of 2, 4, and 6 and for each combination 1000 samples are collected as shown in Fig. 4.4(b).

## 4.5 Geometric Dilution of Precision (GDOP)

---

Fig. 4.4(c) shows the lowest uncertainty in location error, where  $A_1$ ,  $A_2$  and  $A_3$  are well separated. An increase in  $E_{\text{RMS}}$  is observed when an anchor nodes move from  $A_3$  to  $A_7$ . This is because of the angle between the anchor nodes which reduces as third anchor moves towards  $A_1$  and  $A_2$  (i.e. reduces the sides of the triangle). Fig. 4.4(g) shows the high uncertainty in location error where  $A_1$ ,  $A_2$  and  $A_7$  are almost collinear. There is no solution available for combination 6 as shown in Fig. 4.4(b), which is in accord with the fact that all the three anchors ( $A_1$ ,  $A_2$  and  $A_8$ ) are collinear (i.e. angle between the anchors is zero). Furthermore, as anchor node moves from  $A_9$  to  $A_{13}$ , it shows a decrease  $E_{\text{RMS}}$  because of the increases in angle between anchor nodes. The area within an error equates to a contour of probability for the estimated location of a subject node. This varies significantly with anchor selection for sub-optimal blind trilateration. A large error of a localized node will have a disastrous impact on subsequent phases of localization, if this node is subsequently used as an anchor, i.e. it becomes a pseudo-anchor. Fig. 4.5 shows the flow chart for SBT.

As discussed above, SBT selects only three of the in-range anchors/pseudo-anchors without an associated quality figure to calculate the position estimate of the subject node. In order to overcome the blind selection of anchor/pseudo-anchor, SBT is combined with GDOP as MSBT to exploit the geometric configuration between the anchor/pseudo-anchors to reduce the impact of bad geometry on localization accuracy. In a dense network<sup>1</sup>, where a subject sensor node may have choices on the selection of anchor nodes to perform SBT, a candid choice of anchors geometry based on the knowledge of GDOP can reduce the location error. GDOP metric is discussed in section 4.5 and a location refinement process using for MSBT using GDOP is discussed in 4.6

## 4.5 Geometric Dilution of Precision (GDOP)

In NAVSTAR/Global Positioning System (GPS), and Global Navigation Satellite System (GLONASS), DOP is a well known problem [29–36] which illustrates

---

<sup>1</sup>A dense environment, where sensor nodes are closely packed due to low sensing range or due to a large number of deployed nodes in a limited sensing field. In our case, a large number of nodes reflect a dense environment. This is scalable depending on transmission power.

## 4.5 Geometric Dilution of Precision (GDOP)

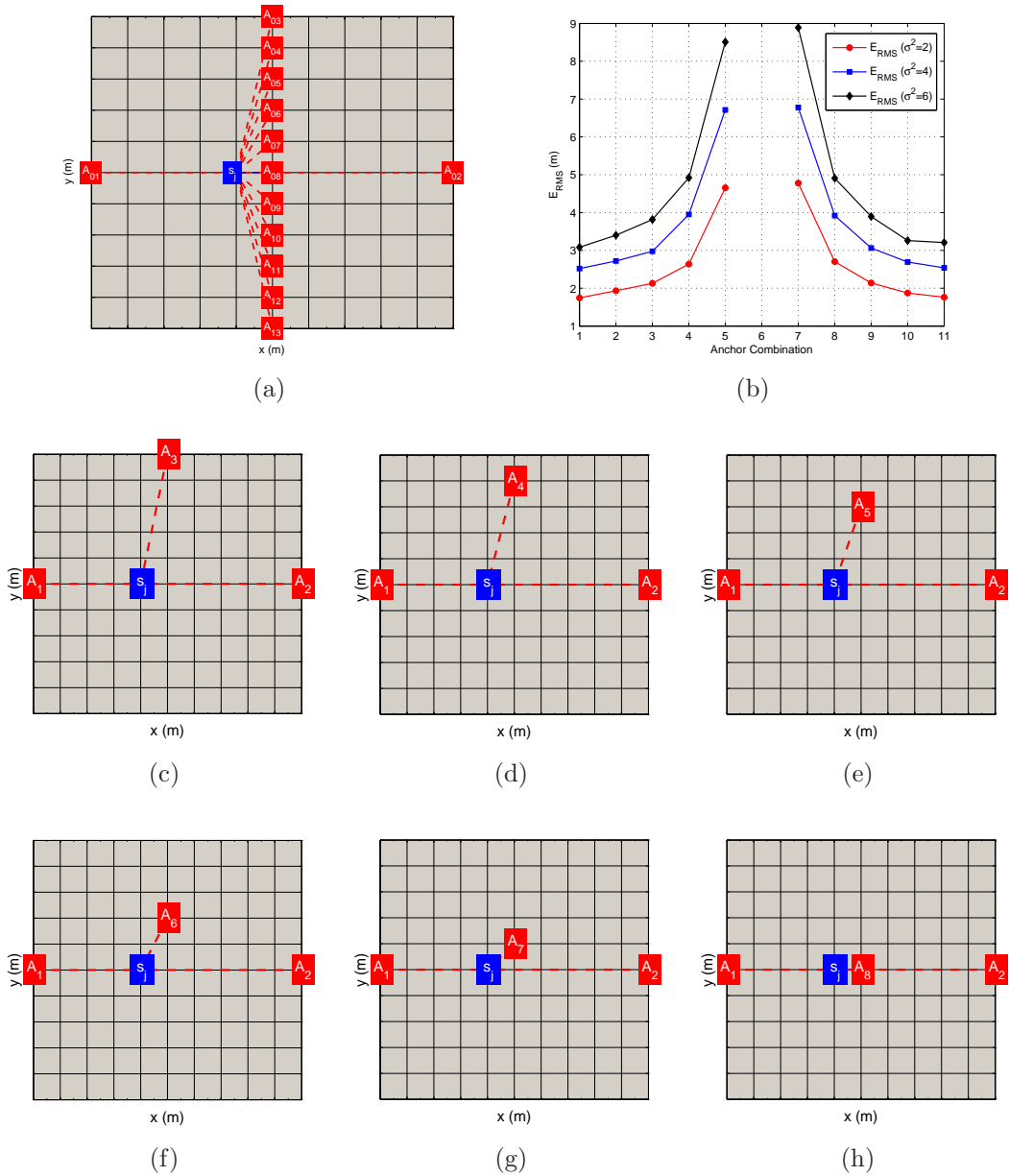


Figure 4.4: Fig. 4.4(a). Anchor combinations, where  $A_1$ ,  $A_2$  are fixed anchors and anchor  $A_3$  is changed from  $A_3$  to  $A_{13}$ . Fig. 4.4(b).  $E_{\text{RMS}}$  associated with the position estimate for different anchor geometries as shown in Fig. 4.4(a). Fig. 4.4(c) - Fig. 4.4(h). First 6 anchor combinations from Fig. 4.4(a), where  $A_1$ ,  $A_2$  are fixed anchors and anchor  $A_3$  is changed from  $A_3$  to  $A_8$  respectively.

## 4.5 Geometric Dilution of Precision (GDOP)

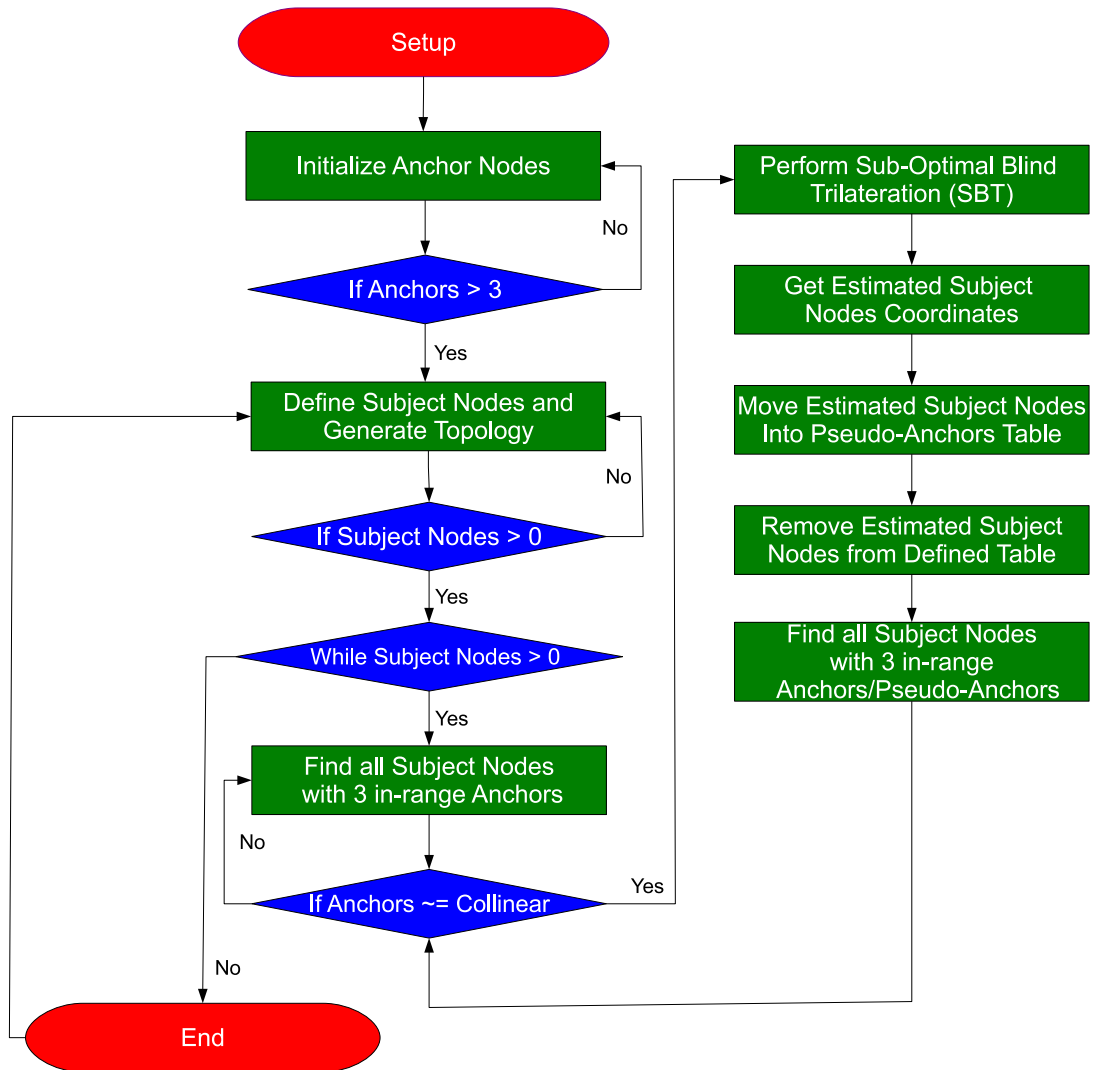


Figure 4.5: Simulation Flow chart for SBT

## 4.5 Geometric Dilution of Precision (GDOP)

---

geometric configuration impacting location estimation accuracy of a localization system. As discussed above, in order to locate a subject node, at least 3 range measurements (i.e. anchors) are required in 2-D. Here, the accuracy of the estimated subject node heavily depends on the geometry of the anchor nodes, which is characterized by the DOP. To reduce the degree of location error, anchor/pseudo-anchors nodes must be selected with optimal geometry. This dimensionless value is divided into various quality ranks for qualitative comparison of diverse geometric configurations. The smallest GDOP value reflects the strong geometric configuration whereas higher value reflects poor geometry. Table 4.1 shows the different quality ranks for GDOP [29, 91].

Quality Rank	Geometric Configuration
1	Ideal
2-4	Excellent
4-6	Good
6-8	Moderate
8-20	Fair
20-50	Poor

Table 4.1: Geometric Dilution of Precision Quality Rank

The computation of DOP metric can be defined by relating the expected value of the positional error to expected ranging error as given by Eq. (4.23) [30, 114]:

$$\text{GDOP} = \frac{E_{\text{RMS}}^{\text{loc}}}{E_{\text{RMS}}^r} \quad (4.23)$$

where,  $E_{\text{RMS}}^{\text{loc}}$  and  $E_{\text{RMS}}^r$  is the root-mean-square-error of the estimated subject node and estimated ranges respectively, and assumed to be uncorrelated, Gaussian random variables. The  $E_{\text{RMS}}^{\text{loc}}$  and  $E_{\text{RMS}}^r$  can be given by Eq. (4.24) and Eq. (4.25) respectively.

## 4.5 Geometric Dilution of Precision (GDOP)

---

$$E_{\text{RMS}}^{\text{loc}} = \sqrt{\frac{\sum_{m=1}^k (s_j - \hat{s}_j^m)(s_j - \hat{s}_j^m)^T}{k}} \quad (4.24)$$

where  $k$  is the number of iterations selected for a lateration scheme.

$$E_{\text{RMS}}^r = \sqrt{\frac{\sum_{i=1}^N \sum_{m=1}^k (d_{ij} - \hat{d}_{ij}^m)^2}{N \times k}} \quad (4.25)$$

where  $i$  is the number of anchor nodes selected for a lateration scheme and  $k$  is the number of the range estimates ( $\hat{d}_{ij}$ ) performed between an anchor and subject node. In GPS technology,  $E_{\text{RMS}}^r$  is known as User Equivalent Range Error (EURE) [31, 32].

When using lateration,  $N$  anchors/pseudo-anchors in-range of a subject node will result in  $N$  equations in the form of Eq. (4.4). By using the subject estimate  $(\hat{x}_j, \hat{y}_j)$ , an approximate range estimate can be given by Eq. (4.26):

$$\hat{d}_{ij} = \sqrt{(x_i - \hat{x}_j)^2 + (y_i - \hat{y}_j)^2}; \quad (i = 1, 2, 3) \quad (4.26)$$

Defining  $\hat{d}_{ij}$  as  $d_{ij}$  at  $(\hat{x}_j, \hat{y}_j)$  the positioning difference can be given as  $\Delta x_j = x_j - \hat{x}_j$  and  $\Delta y_j = y_j - \hat{y}_j$ . The computation of GDOP is based on a geometry matrix ( $G_M$ ) which can be formed by linearising the set of equations Eq. (4.26) by using truncated Taylor series around the approximate subject position  $(\hat{x}_j, \hat{y}_j)$  [53]. The Taylor series at first order by truncating high order terms can be given as:

$$d_{ij} = \hat{d}_{ij} + \frac{\partial \hat{d}_{ij}}{\partial \hat{x}_j} (x_j - \hat{x}_j) + \frac{\partial \hat{d}_{ij}}{\partial \hat{y}_j} (y_j - \hat{y}_j); \quad (i = 1, 2, 3) \quad (4.27)$$

## 4.5 Geometric Dilution of Precision (GDOP)

---

$$d_{ij} - \hat{d}_{ij} = \frac{\partial \hat{d}_{ij}}{\partial \hat{x}_j}(x_j - \hat{x}_j) + \frac{\partial \hat{d}_{ij}}{\partial \hat{y}_j}(y_j - \hat{y}_j); \quad (i = 1, 2, 3) \quad (4.28)$$

for ( $i = 1, 2$ , and  $3$ ), Eq. (4.28) can be simplified as below:

$$\begin{pmatrix} \Delta d_{1j} \\ \Delta d_{2j} \\ \Delta d_{3j} \end{pmatrix} = \begin{pmatrix} dx_1 \Delta x_j + dy_1 \Delta y_j \\ dx_2 \Delta x_j + dy_2 \Delta y_j \\ dx_3 \Delta x_j + dy_3 \Delta y_j \end{pmatrix} \quad (4.29)$$

Eq. (4.29) can be rearranged and simplified as Eq. (4.30):

$$\Delta d = G_M \Delta \rho \quad (4.30)$$

where,

$$\Delta d = \begin{bmatrix} \Delta d_{1j} \\ \Delta d_{2j} \\ \Delta d_{3j} \end{bmatrix}, G_M = \begin{bmatrix} dx_1 & dy_1 \\ dx_2 & dy_2 \\ dx_3 & dy_3 \end{bmatrix}, \Delta \rho = \begin{bmatrix} \Delta x_j \\ \Delta y_j \end{bmatrix} \quad (4.31)$$

Here  $G_M$  is  $3 \times 2$  geometry matrix, since at least 3 anchors are required to locate a subject node in 2-D. The  $3 \times 2$  geometry matrix for  $N$  anchors in 2-D case can be given as Eq. (4.32):

$$G_M = \begin{bmatrix} dx_i & dy_i \\ \dots & \dots \\ \vdots & \vdots \\ dx_N & dy_N \end{bmatrix} \quad (4.32)$$

## 4.5 Geometric Dilution of Precision (GDOP)

---

where, elements  $dx_i$ , and  $dy_i$  defines the direction cosines for subject to  $i^{th}$  anchor nodes can be given as Eq. (4.33) using Eq. (4.31):

$$\begin{pmatrix} dx_i \\ dy_i \end{pmatrix} = \begin{pmatrix} \frac{\partial d_{ij}}{\partial \hat{x}_j} \\ \frac{\partial d_{ij}}{\partial \hat{y}_j} \end{pmatrix} = \begin{pmatrix} \frac{\hat{x}_j - x_i}{\hat{d}_{ij}} \\ \frac{\hat{y}_j - y_i}{\hat{d}_{ij}} \end{pmatrix}; \quad (i = 1, 2, 3) \quad (4.33)$$

where,  $\hat{x}_j$  and  $\hat{y}_j$  are the estimated coordinates of  $j^{th}$  subject node and  $\hat{d}_{ij}$  is estimated distance between anchor and subject node. Substituting Eq. (4.33) in Eq. (4.32) yields Eq. (4.34):

$$\mathbf{G}_M = \begin{bmatrix} \frac{\hat{x}_j - x_1}{\hat{d}_{1j}} & \frac{\hat{y}_j - y_1}{\hat{d}_{1j}} \\ \frac{\hat{x}_j - x_2}{\hat{d}_{2j}} & \frac{\hat{y}_j - y_2}{\hat{d}_{2j}} \\ \frac{\hat{x}_j - x_3}{\hat{d}_{3j}} & \frac{\hat{y}_j - y_3}{\hat{d}_{3j}} \end{bmatrix} \quad (4.34)$$

Here LS can be used by multiplying both sides of Eq. (4.30) by matrix transpose of  $\mathbf{G}_M$ .

$$\Delta d = (\mathbf{G}_M^T \mathbf{G}_M)^{-1} \mathbf{G}_M^T \Delta \rho \quad (4.35)$$

where  $\mathbf{G}_M^T$  is the transpose of  $\mathbf{G}_M$ . Since  $\mathbf{G}_M^T$  has full rank (provided anchors are not collinear),  $\mathbf{G}_M^T \mathbf{G}_M$  will be invertible, then Eq. (4.35) can be given as:

$$\Delta \rho = (\mathbf{G}_M^T \mathbf{G}_M)^{-1} \mathbf{G}_M^T \Delta d \quad (4.36)$$

Let  $\xi_p$  and  $\xi_r$  is the positioning and ranging error respectively. Due to the random nature of  $\xi_p$  and  $\xi_r$  Eq. (4.36) can be given as Eq. (4.37), which shows the functional relationship between ranging errors and location error [53].

## 4.5 Geometric Dilution of Precision (GDOP)

---

$$\xi_p = (\mathbf{G}_M^T \mathbf{G}_M)^{-1} \mathbf{G}_M^T \xi_r \quad (4.37)$$

$$= \mathbf{K} \xi_r \quad (4.38)$$

where  $\mathbf{K}$  is considered equal to  $(\mathbf{G}_M^T \mathbf{G}_M)^{-1} \mathbf{G}_M^T$ . It can be evaluated by the covariance of the measurement  $\text{cov}(\cdot)$  [31, 53].

$$\text{cov}(\xi_p) = E [\xi_p \xi_p^T] \quad (4.39)$$

$$= E [\mathbf{K} \xi_r \mathbf{K}^T \xi_r^T] \quad (4.40)$$

$$= E [((\mathbf{G}_M^T \mathbf{G}_M)^{-1} \mathbf{G}_M^T) (\xi_r d_x^T) ((\mathbf{G}_M^T \mathbf{G}_M)^{-1} \mathbf{G}_M)] \quad (4.41)$$

$$= \mathbf{K} \text{cov}(\xi_r) \mathbf{K}^T \quad (4.42)$$

Here  $\text{cov}(\xi_r)$  represents the ranging errors. In LOS environments, all the measurement errors can be considered to be zero-mean independent and identically distributed Gaussian variables. So the covariance matrix  $\text{cov}(E_r)$  can be expressed as  $\text{cov}(\xi_r) = \mathbf{I} \sigma^2$ , where  $\mathbf{I}$  is  $N \times N$  identity matrix. Now, Eq. (4.42) can be given as:

$$\text{cov}(\xi_p) = \sigma^2 (\mathbf{G}_M^T \mathbf{G}_M)^{-1} \quad (4.43)$$

where in 2-D  $\text{cov}(\xi_p)$  is a  $2 \times 2$  matrix. As  $\text{cov}(\xi_p)$  is statistically independent, it will result in a diagonal covariance matrix. Assume,  $(\mathbf{G}_M^T \mathbf{G}_M)^{-1}$  is equivalent to  $\mathbf{G}$  and in component form can be given by Eq. (4.44):

$$\mathbf{G} = (\mathbf{G}_M^T \times \mathbf{G}_M)^{-1} = \begin{bmatrix} \mathbf{G}_{11} & \mathbf{G}_{12} \\ \mathbf{G}_{21} & \mathbf{G}_{22} \end{bmatrix} \quad (4.44)$$

The elements of  $\mathbf{G}$  matrix quantify how ranging errors translate into elements of  $\text{cov}(\xi_r)$ . From Eq. (4.44), GDOP is equivalent to taking the square root of the

## 4.5 Geometric Dilution of Precision (GDOP)

---

sum of the diagonal elements of  $G$  as given by Eq. (4.45):

$$\text{GDOP} = \sqrt{\text{tr}(G)} = \sqrt{G_{11} + G_{22}} \quad (4.45)$$

where  $T$  and  $tr$  indicate the transpose and trace of matrix, respectively. Now, Eq. (4.43) can be rearranged as:

$$\begin{bmatrix} \sigma_{x_j}^2 & \sigma_{x_j}^2 \sigma_{y_j}^2 \\ \sigma_{x_j}^2 \sigma_{y_j}^2 & \sigma_{y_j}^2 \end{bmatrix} = \sigma^2 \text{GDOP} \quad (4.46)$$

where left hand side of Eq. (4.46) is  $\text{cov}(\xi_p)$ . Eq. (4.46) can be related to Eq. (4.23) as below:

$$E_{\text{RMS}}^{\text{loc}} = E_{\text{RMS}}^r \text{GDOP} \quad (4.47)$$

It can be observed that, Eq. (4.47) is equivalent to Eq. (4.23), where  $E_{\text{RMS}}^{\text{loc}}$  (square root of the sum of the diagonal elements of left hand side of Eq. (4.46)) and  $E_{\text{RMS}}^r$  is given by Eq. (4.24) and Eq. (4.25) respectively.

In the context of Cartesian coordinate system,  $G_M$  matrix (from Eq. (4.43)) defines the three DOP mechanism [31, 32, 53], vertical dilution of precision (VDOP-altitude) for 1-D, horizontal dilution of precision (HDOP-latitude and longitude) for 2-D plane, and position dilution of precision (PDOP) for 3-D sphere. The accuracies of these three mechanisms in terms of  $\frac{E_{\text{RMS}}^{\text{loc}}}{E_{\text{RMS}}^r}$  and geometry matrix can be given by Eq. (4.48), Eq. (4.49) and Eq. (4.50) respectively:

$$\text{PDOP} = \sqrt{G_{11} + G_{22} + G_{33}} = \frac{\sqrt{E_{\text{RMSx}}^2 + E_{\text{RMSy}}^2 + E_{\text{RMSz}}^2}}{E_{\text{RMS}}^r} \quad (4.48)$$

## 4.5 Geometric Dilution of Precision (GDOP)

---

$$\text{HDOP} = \sqrt{G_{11} + G_{22}} = \frac{\sqrt{E_{\text{RMSx}}^2 + E_{\text{RMSy}}^2}}{E_{\text{RMS}}^r} \quad (4.49)$$

$$\text{VDOP} = \sqrt{G_{33}} = \frac{\sqrt{E_{\text{RMSz}}^2}}{E_{\text{RMS}}^r} \quad (4.50)$$

In the context of GPS, GDOP elements are 4x4, where the 3<sup>rd</sup> and 4<sup>th</sup> term correspond to  $z$ -axis and clock corrections [29, 53].

### 4.5.1 Simulation Results and Analysis

Since the GDOP illustrates the functions of geometric configuration of the anchor and subject nodes, it is obvious that certain anchor locations would offer better accuracy than others. Fig. 4.6 shows a subject nodes with 24 in-range anchors/pseudo-anchors. In this case,  $A_1$  and  $A_2$  are considered fixed to location  $[0, 5]$ m and  $[10, 5]$ m, whereas  $A_3$  is changed from  $A_3$  to  $A_{24}$  in anti-clockwise to get 22 different combinations (i.e.  $[A_1, A_2, A_3]$ ,  $[A_1, A_2, A_4]$ ,  $[A_1, A_2, A_5]$ ,  $\dots$ ,  $[A_1, A_2, A_{24}]$ ). For each combination as shown in Fig. 4.6, the corresponding HDOP and  $E_{\text{RMS}}$  is calculated at noise variance of 4 and for each combination 1000 samples are collected. It can be observed that as the angle between the anchors decreases, HDOP increases. This is because a small angle (angles are not spread) between the anchors will results in large uncertainty region. It can be observed that as the HDOP increases,  $E_{\text{RMS}}$  also increases. As shown, the minimum HDOP is observed when  $[A_1, A_2, A_n]$  are deployed as shown in Fig. 4.6. It suggests that a combination of anchors/pseudo-anchors with minimum HDOP can help to enhance the localization accuracy. In next section, the location refinement process based on the HDOP is discussed to enhance the estimated location.

Fig. 4.8 shows a scenario, where anchor nodes are considered as fixed and subject node location is changed from  $s_1$  to  $s_{10}$ . The corresponding HDOP and  $E_{\text{RMS}}$  is illustrated in Fig. 4.8. It can be observed that, in addition to anchor nodes

## 4.5 Geometric Dilution of Precision (GDOP)

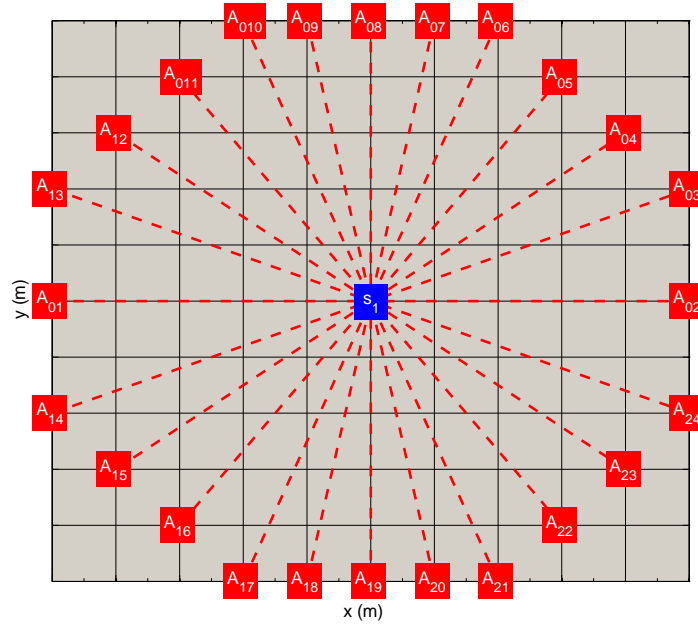


Figure 4.6: Subject node with 24 in-range anchors/pseudo-anchors, where  $A_1$ ,  $A_2$  are fixed and  $A_3$  is changed from  $A_3$  to  $A_{24}$

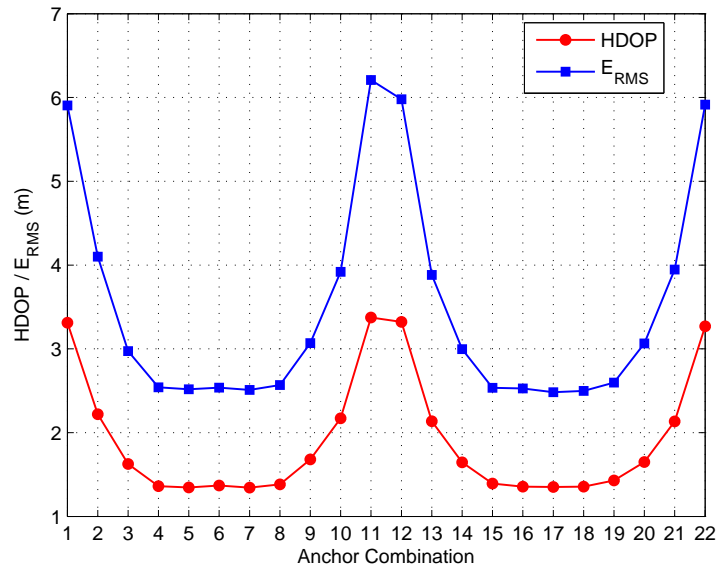


Figure 4.7: Comparison of GDOP and  $E_{RMS}$  for 24 in-range anchor nodes, where  $A_1$ ,  $A_2$  are fixed and  $A_3$  is changed from  $A_3$  to  $A_{24}$  as shown in Fig. 4.6.

## 4.5 Geometric Dilution of Precision (GDOP)

geometry, subject node placement is very crucial. As the subject node moves towards the anchor nodes, HDOP hence  $E_{RMS}$  increases. The lowest  $E_{RMS}$  is observed at location [5, 4], which also reflects the minimum HDOP hence optimal subject node placement. In many WSN applications, subjects are often considered as randomly deployed nodes or their location is not fixed due to the mobility. It suggests subject nodes an infeasible option to enhance the location accuracy on the basis of geometry. Hence, it makes optimal anchor nodes geometry an important criteria to enhance the localization accuracy.

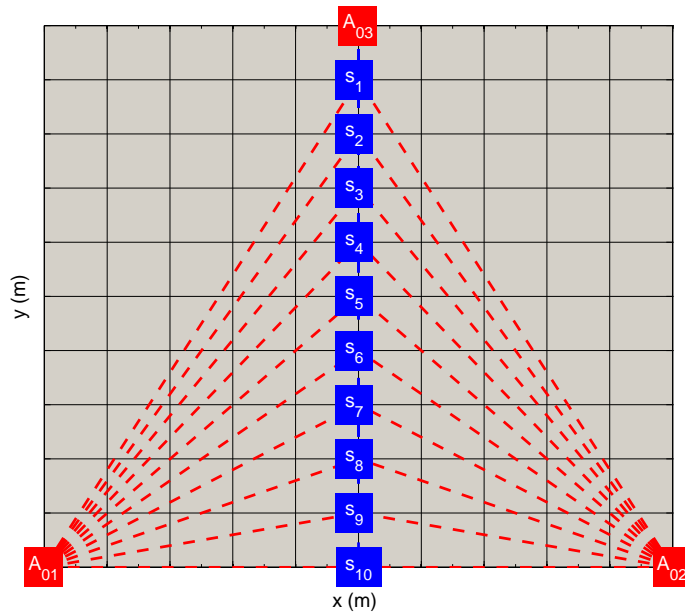


Figure 4.8: Subject node with 3 in-range anchors/pseudo-anchors, where  $A_1$ ,  $A_2$ ,  $A_3$  are fixed and  $s_j$  is changed from  $s_1$  to  $s_{10}$ .

Fig. 4.10 shows a scenario, where anchor nodes are considered as fixed and subject node location is changed from  $s_1$  to  $s_{21}$ . In this case,  $s_1$ - $s_5$  and  $s_{17}$ - $s_{21}$  are deployed outside of the triangle formed by the anchor nodes. The associated HDOP and  $E_{RMS}$  are illustrated in Fig. 4.11. It can be observed that when a subject node is outside of the anchor's triangle and away from  $A_1$  and  $A_2$  (i.e.  $s_1$ ), it results in poor HDOP. This poor HDOP is the effect of poor subject node placement. As the subject node enters into the anchor's triangle and moves towards the  $A_1$  and  $A_2$ , it decreases the HDOP. The minimum HDOP is observed

## 4.6 Modified Sub-Optimal Blind Trilateration (MSBT)

---

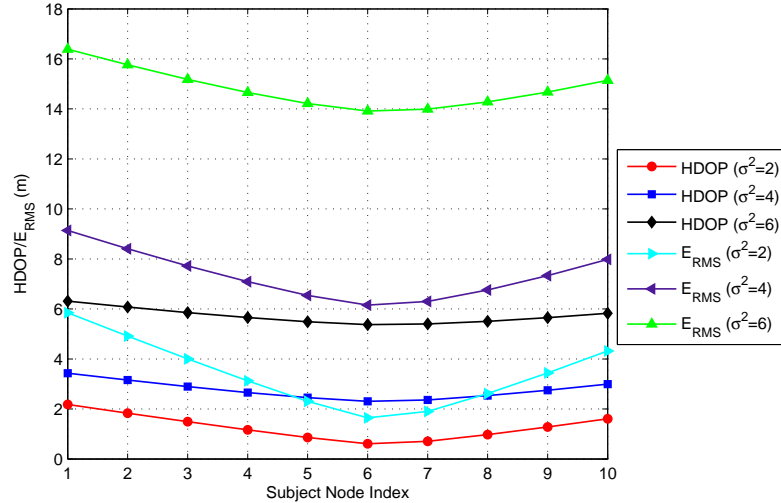


Figure 4.9: Comparison of HDOP and  $E_{RMS}$  for 3 in-range anchor nodes, where  $A_1, A_2, A_3$  are fixed and  $s_j$  is changed from  $s_1$  to  $s_{10}$  as shown in Fig. 4.8.

when subject node ( $s_{16}$ ) along with  $A_1$  and  $A_2$  are collinear, where  $s_{16}$  is almost at equal distance from  $A_1, A_2$  and  $A_3$ ). Beyond  $s_{16}$ , HDOP starts increasing as subject nodes move away from the anchor nodes. It can be observed from Fig. 4.9 and Fig. 4.11 that a minimum HDOP is obtained, when a subject node is almost at equal distance within anchor's triangle.

## 4.6 Modified Sub-Optimal Blind Trilateration (MSBT)

In WSNs, nodes are often deployed in a random fashion with a distributed nature of localization. In such an environment, many nodes can be densely packed and localization sequence of the subject nodes cannot be guaranteed. Thus we cannot expect all node being localized with strong geometry. But, as the localization phase is processed, localized subject nodes turned into pseudo-anchor nodes and a subject node may have choices on the selection of anchor/pseudo-anchor nodes with strong geometry to perform the localization. Here, the location can be refined on the basis of strong geometry to enhance the location

#### 4.6 Modified Sub-Optimal Blind Trilateration (MSBT)

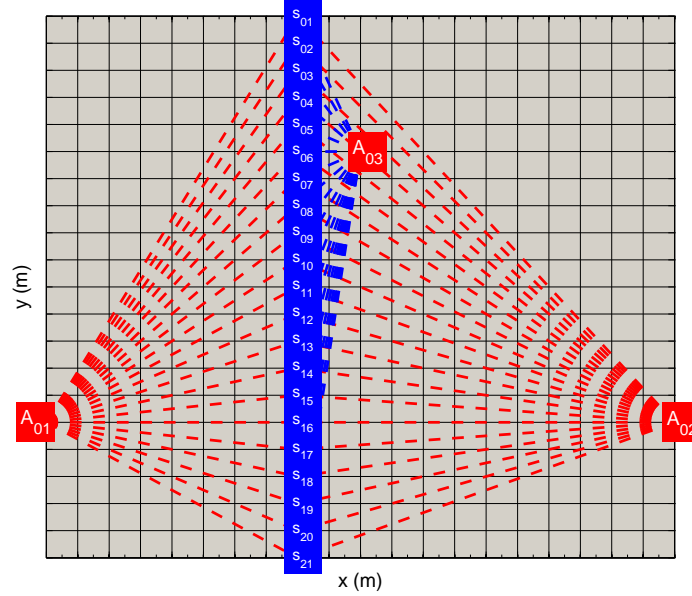


Figure 4.10: Subject node with 3 in-range anchor nodes, where  $A_1, A_2, A_3$  are fixed and  $s_j$  is changed from  $s_1$  to  $s_{21}$ .

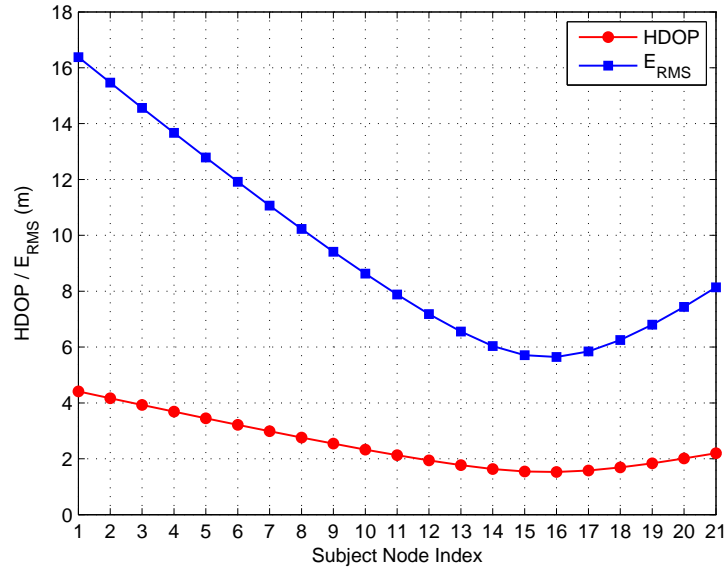


Figure 4.11: Comparison of GDOP and  $E_{RMS}$  for 3 in-range anchor nodes, where  $A_1, A_2, A_3$  are fixed and  $s_j$  is changed from  $s_1$  to  $s_{21}$  as shown in Fig. 4.10.

## 4.6 Modified Sub-Optimal Blind Trilateration (MSBT)

---

estimates and to alleviate error propagation by pseudo-anchor nodes. Consider Fig. 4.12, where a subject node ( $s_j$ ) has five in-range neighbours which can act as anchors/pseudo-anchors ( $A_1, A_2, A_3, A_4,$  and  $A_5$ ). A subject node can use any 3 anchors to perform SBT (i.e. without considering anchor geometry) and may result in poor localization performance. To overcome poor blind selection, hence poor localization performance, a subject node can select 3 out of 5 in-range anchor/pseudo-anchors based on the strong geometry between anchors. To achieve this, 5 in-range anchors/pseudo-anchors can be exploited in to 10 different possible combinations as a set of 3 using Eq. (4.51), where each combination will exhibit a individual HDOP and  $E_{\text{RMS}}$ .

$$A_c = \frac{A_{ir} !}{A_N ! (A_{ir} - A_N) !} \quad (4.51)$$

where  $A_N$  is the number of anchor/pseudo-anchors to use sub-optimal trilateration (i.e. 3) and  $A_{ir}$  is equal to the number of in-range anchor/pseudo-anchors.

Fig. 4.13(a)-4.13(j) shows the 10 different possible combinations for Fig. 4.12. Once sub-optimal trilateration is performed with all combinations, HDOP is calculated for each individual combination. Based on minimum optimized HDOP an anchor/pseudo-anchor node combination set is selected for location estimate of the subject node ( $s_j$ ). Algorithm 1 shows the different stages of the MSBT for location refinement and Fig. 4.14 shows the simulation flow chart for MSBT.

Fig. 4.15 shows the comparison between HDOP and  $E_{\text{RMS}}$  for all 10 anchor combinations (Fig. 4.13). The averaged HDOP and  $E_{\text{RMS}}$  are obtained for a noise variance of 4 and 1,000 iterations. It can be observed that an increase in HDOP also increases the  $E_{\text{RMS}}$ . The minimum GDOP of 1.19 is observed for anchor combination 2 (Fig. 4.13(b)), which also reflects the highest accuracy in the estimated location. The maximum HDOP of 2.34 and 2.3 is observed for anchor combination 6 and 7 with  $E_{\text{RMS}}$  of 4.28m and 4.26m (Fig. 4.13(f) and Fig. 4.13(g)) respectively.

It is evident from the results that using location refinement by exploiting HDOP allow us to select the anchor combination with minimum HDOP, hence

## 4.6 Modified Sub-Optimal Blind Trilateration (MSBT)

---



---

### Algorithm 1 Stages of MSBT Algorithm for Location Refinement

---

```

1: %  $A_N$  is total number of Anchor and Pseudo-Anchor
2: %  $A_{ir}$  is in-range anchor/pseudo-anchor nodes
3: %  $A_c$  is total number of anchor/pseudo-anchor combinations
4: %  $\hat{A}_c$  is the selected anchor/pseudo-anchor combination from  $A_c$  based on
   minimum HDOP
5: %  $E_{\text{RMS}}^{\text{loc}}$  is root-mean-square error of estimated location
6: %  $E_{\text{RMS}}^r$  is root-mean-square error of ranging error
7: %  $\text{Est}_{\text{loc}}$  is estimated location
8: while  $s_{j=1,\dots,N} \neq 0$  do
9:   for  $j = 1$  to  $s_j$  do
10:    for  $i = 1$  to  $\text{size}(A_N)$  do
11:      if  $(s_j(j), A_N(i))$  Adjacent then
12:         $A_{ir} \leftarrow \text{In-range } A_N(i)$ 
13:      end if
14:    end for
15:    % Get all possible  $A_N$  combinations from  $A_{ir}$  as a set of 3
16:     $A_c = \frac{A_{ir}!}{3! \times (A_{ir}-3)!}$ 
17:    for  $k = 1$  to  $\text{size}(A_c)$  do
18:      Perform sub-optimal trilateration for each  $k$ 
19:      Calculate  $E_{\text{RMS}}^{\text{loc}}$  of estimated location for each  $k$ 
20:      Calculate  $E_{\text{RMS}}^r$  of ranging error for each  $k$ 
21:      Calculate HDOP for each  $k$ 
22:       $\hat{s}_j = \text{Est}_{\text{loc}}(k), \text{RMSE}_{\text{loc}}(k), \text{HDOP}(k)$ 
23:    end for
24:    % Get best  $A_c$  based on the minimum HDOP
     $\hat{A}_c \leftarrow \min(\text{HDOP})$ 
25:     $\hat{s}_j \leftarrow$  associated with  $\hat{A}_c$  combination
26:  end for
27: end while

```

---

## 4.7 Optimal Multi-lateration (OML)

---

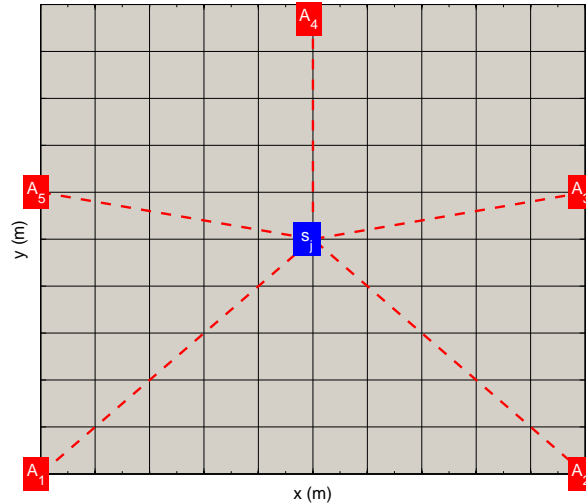


Figure 4.12: Subject node with 5 in-range anchor/pseudo-anchor nodes.

highest accuracy in an estimated location. It also helps to reduce the error propagation due to pseudo-anchors in subsequent phases of localization.

## 4.7 Optimal Multi-lateration (OML)

Optimal multi-lateration is a technique for determining the location of a node using the distance from all in-range anchors i.e. optimally using all available information [109]. In OML, location estimation for a subject node is calculated by using (4.21) for a set of  $N - 1$  linear equations, where  $N$  is the number of the in-range anchors/pseudo-anchors. Fig. 4.16 shows an example where a subject node  $s_j$  is surrounded by 8 in-range anchors/pseudo-anchors. In this case, the function of the coordinates of the anchor nodes  $A$  and matrix  $b$  which is a function of the distance between the anchor nodes to the subject nodes and the coordinates of the anchor nodes is given by Eq. (4.52) and Eq. (4.53) respectively.

## 4.7 Optimal Multi-lateration (OML)

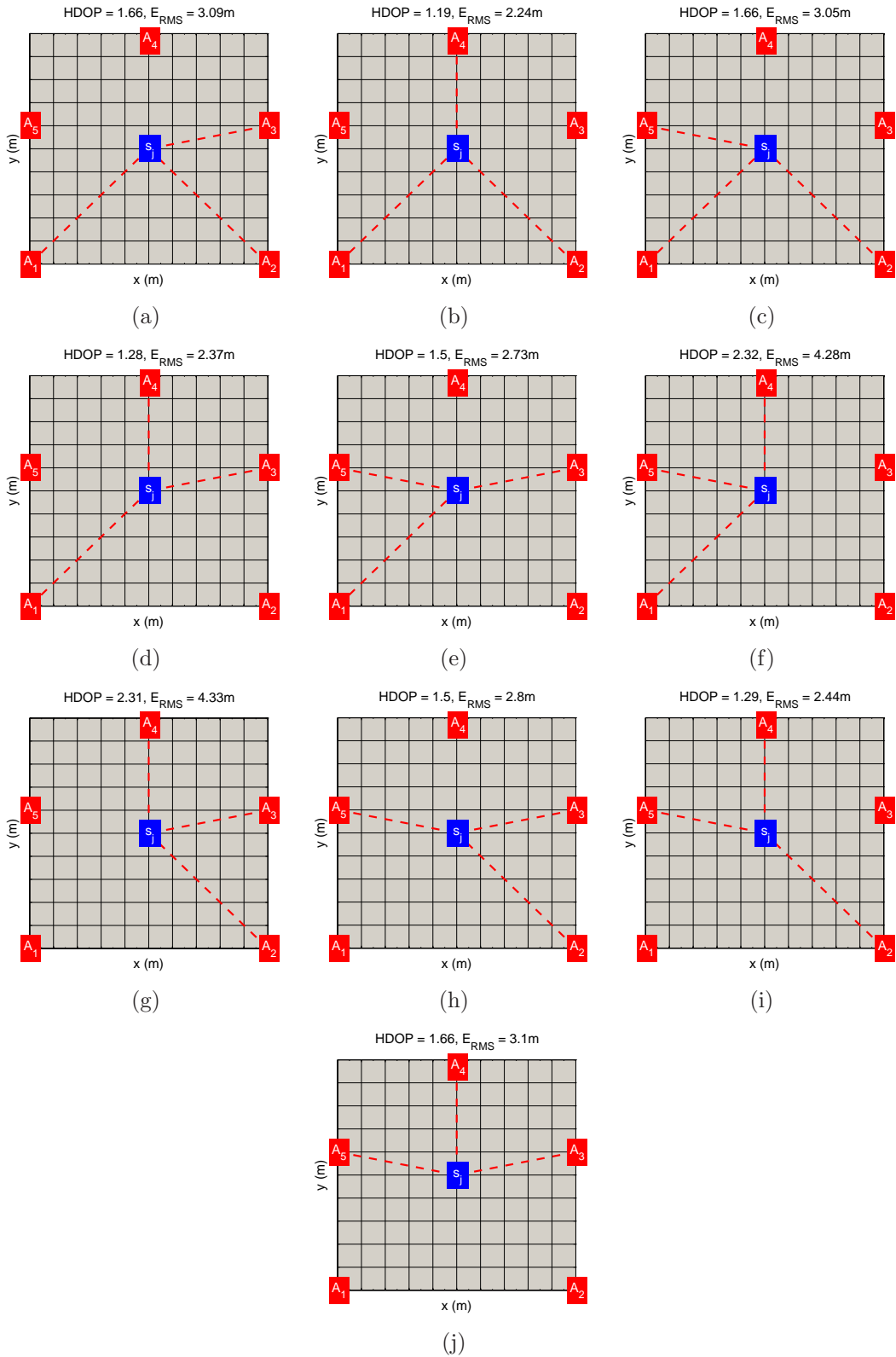


Figure 4.13: Possible anchor/pseudo-anchor node combinations.

## 4.7 Optimal Multi-iteration (OML)

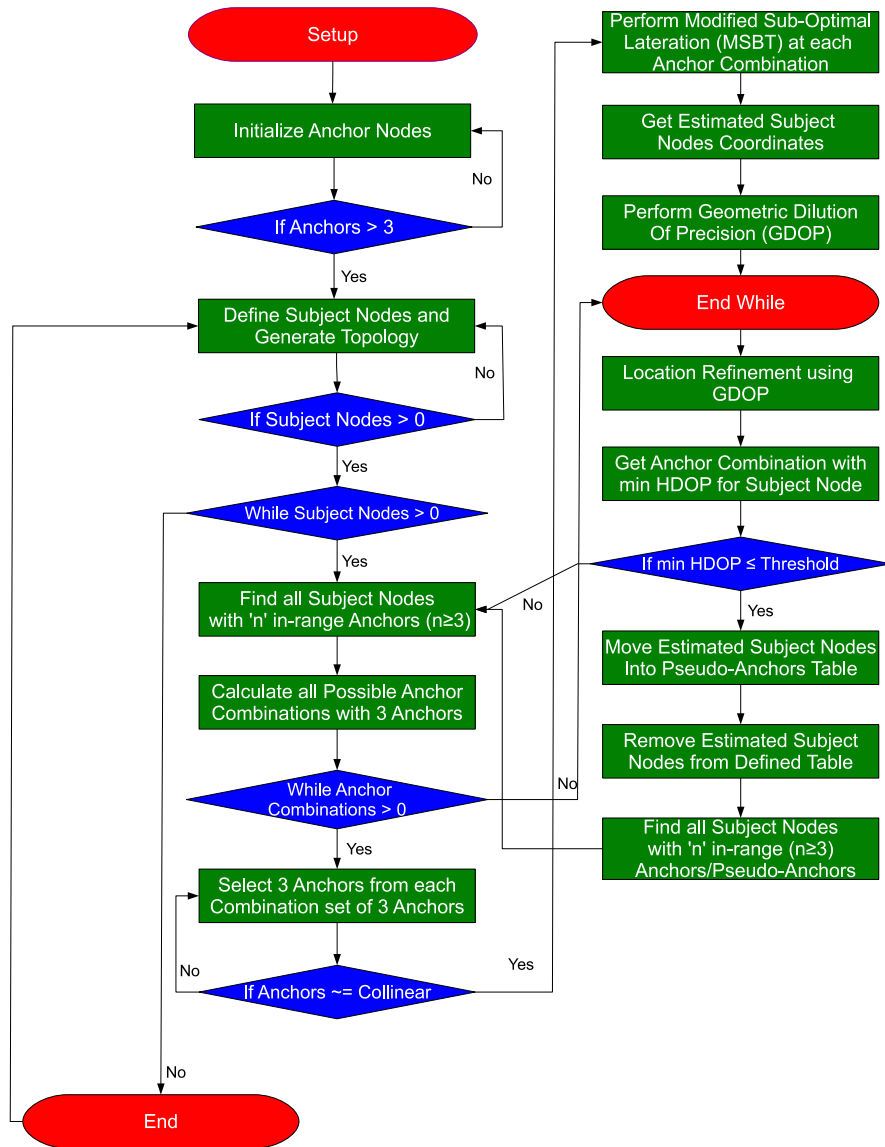


Figure 4.14: Simulation Flow chart for MSBT.

## 4.7 Optimal Multi-lateration (OML)

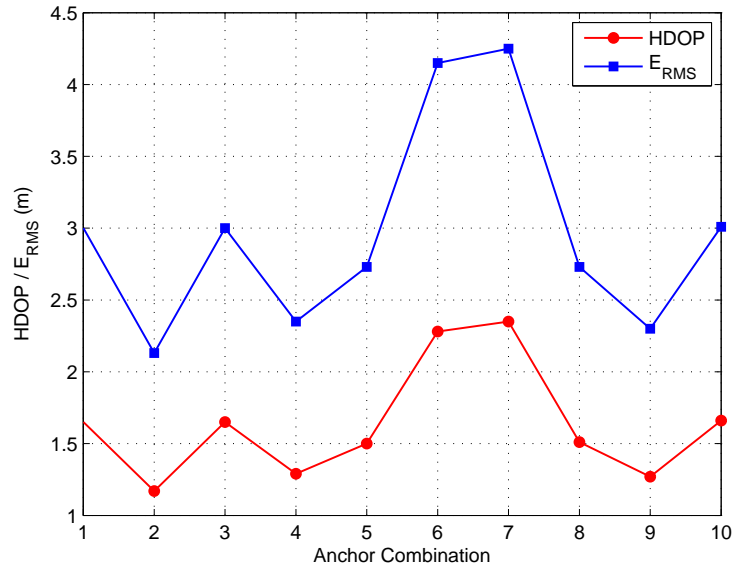


Figure 4.15: Comparison of HDOP and  $E_{RMS}$  for all anchor combinations as shown in Fig. 4.13.

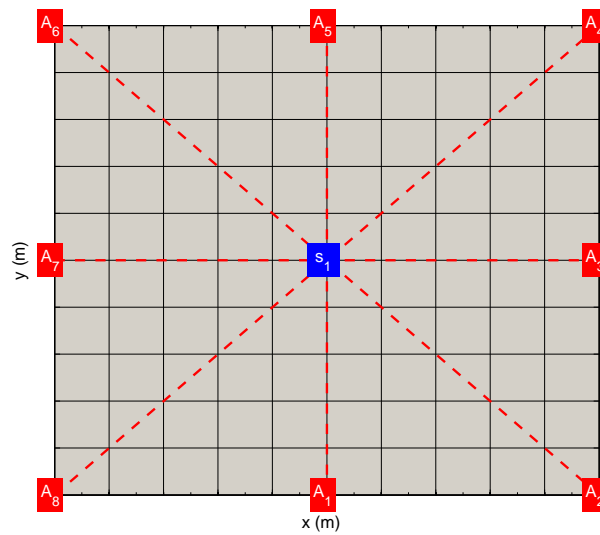


Figure 4.16: Optimal multi-lateration, where 8 anchor/pseudo-anchor nodes are in-range of a subject node.

## 4.7 Optimal Multi-lateration (OML)

---

$$A = \begin{bmatrix} x_2 - x_1 & y_2 - y_1 \\ x_3 - x_1 & y_3 - y_1 \\ x_4 - x_1 & y_4 - y_1 \\ \dots & \dots \\ \dots & \dots \\ x_n - x_1 & y_n - y_1 \end{bmatrix} \quad (4.52)$$

$$b = \frac{1}{2} \begin{bmatrix} (d_1^2 - d_2^2) + (x_2^2 - x_1^2) + (y_2^2 - y_1^2) \\ (d_1^2 - d_3^2) + (x_3^2 - x_1^2) + (y_3^2 - y_1^2) \\ (d_1^2 - d_4^2) + (x_4^2 - x_1^2) + (y_4^2 - y_1^2) \\ \dots \quad \dots \quad \dots \\ (d_1^2 - d_n^2) + (x_n^2 - x_1^2) + (y_n^2 - y_1^2) \end{bmatrix} \quad (4.53)$$

The algebraic manipulations lead to a system of linear equations which can be expressed in matrix form as given by Eq. (4.13) and can be solved by the LS method to provide an estimated location, as given by Eq. (4.21).

Fig. 4.17 displays the HDOP and  $E_{\text{RMS}}$  as a function of number of anchor nodes. It is noted that as the number of anchors increases the effect of noise on the location error becomes smaller. In this case, HDOP is calculated for 3 to 8 in-range anchor nodes. A considerable improvement is observed by increasing the number of anchors from 3-8. It can be observed that, using only three anchors (i.e.  $A_1$ ,  $A_2$  and  $A_3$ ), results in a high HDOP value, hence poor localization accuracy. This is because of the poor geometry of anchors (i.e.  $A_1$ ,  $A_2$  and  $A_3$ ), which are very close to each other. With all in-range anchor nodes, minimum  $E_{\text{RMS}}$  value obtained is 3.45m compared to  $E_{\text{RMS}}$  obtained with only 3 anchors is 21.3m.

Once a subject node localized its position using all in-range anchors/pseudo-anchors, it becomes a pseudo-anchor node in subsequent iterations to locate remaining nodes. The process repeats until all the nodes in the network are localized. Fig. 4.18 shows the flow chart for OML. In a dense network, a solution based on optimal multi-lateration (i.e. selecting all in range information) requires more processing time, hence more processing power is required to perform localization, which is undesirable for resource constrained WSNs. Here, reducing the number of anchors/pseudo-anchors to limit calculation complexity and to preserving power resources can improve the network life time at the cost of

## 4.8 Performance Analysis and Results

---

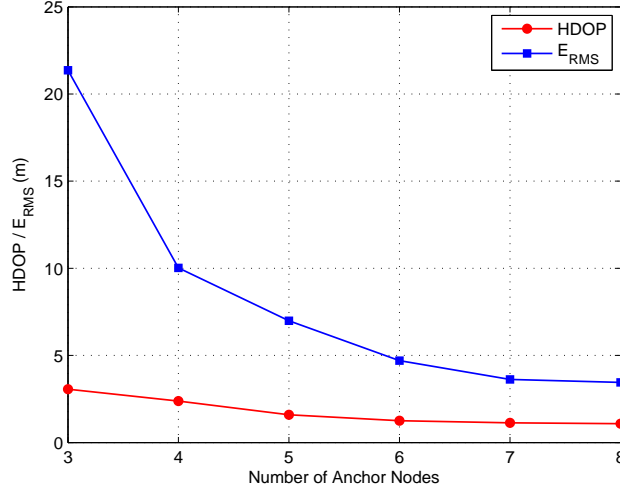


Figure 4.17: HDOP and  $E_{RMS}$  for OML, where 8 anchor/pseudo-anchor nodes are in-range of a subject node as shown in Fig. 4.16.

additional location error.

## 4.8 Performance Analysis and Results

In this section, a simulation tool is developed to evaluate the performance of the optimal and sub-optimal schemes. A number of static nodes (*i.e.* 100, 200,  $\dots$ , 600) are randomly distributed in 2-D. To vary the number of in-range anchors/pseudo-anchors, transmission range of 40m, 80m and 100m is used within 100m by 100m, 200m by 200m and 400m by 400m networks respectively, as shown in Table 4.2. Here, all three approaches (SBT, MSBT and OML) are distributed approaches and each subject nodes can run it individually to be localized. Fig. 4.5, Fig. 4.14 and Fig. 4.18 shows the simulation flowchart for SBT, MSBT and OML respectively.

To simulate the analysis, the estimated distance ( $\hat{d}_{ij}$ ) as given by Eq. (4.4) is considered. Since anchor nodes are considered pre-surveyed, their location is assumed to be error free. A static and stable sensor network (*i.e.* no mobility and no node failures) without obstacles and with nodes having accurate and symmetric radio ranges is assumed. A subject node ( $s_j$ ) is adjacent to anchor

## 4.8 Performance Analysis and Results

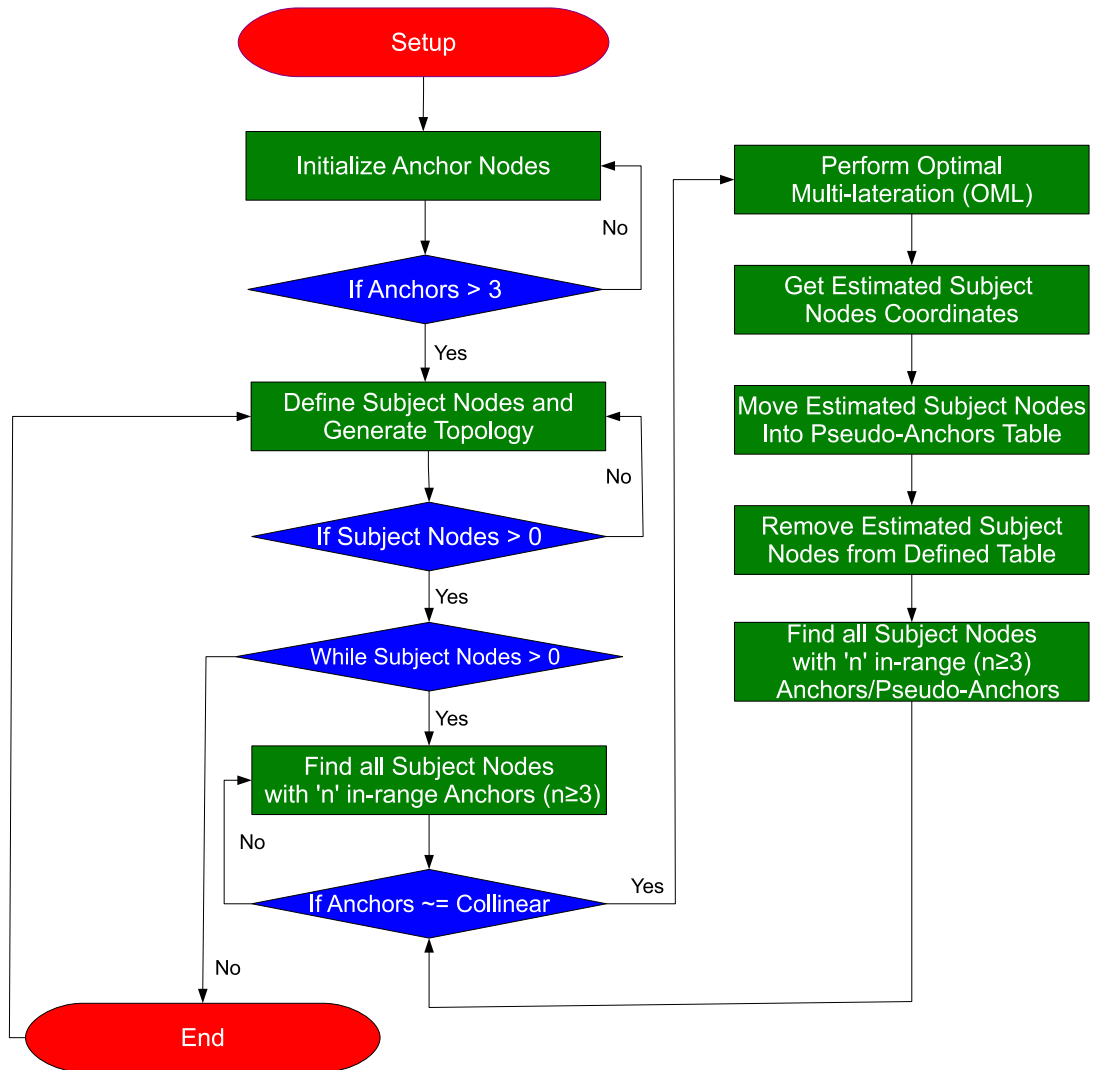


Figure 4.18: Simulation Flow chart for OML.

## 4.8 Performance Analysis and Results

---

Table 4.2: Network Simulation Parameters for SBT, MSBT and OML

Parameters	Value
Area(m)	100 × 100, 200 × 200, 400 × 400
Transmission Range(m)	40m, 80m, 100m
Subject Nodes	100, 200, 300, 400, 500, 600
Anchor Nodes	3, 4, 5, 6, 7, 8, all in-range

( $A_i$ ), if and only if  $\hat{d}_{ij} \leq$  transmission range. All simulations are averaged over 100 random network topologies. In all simulations to keep the processing time within tolerable limits, the threshold of GDOP to enhance accuracy is set as below 4. As a metric to evaluate the lateration schemes, the root-mean-square error  $E_{RMS}$  of the location estimate obtained from  $N$  anchors as given by Eq. (4.22) is considered.

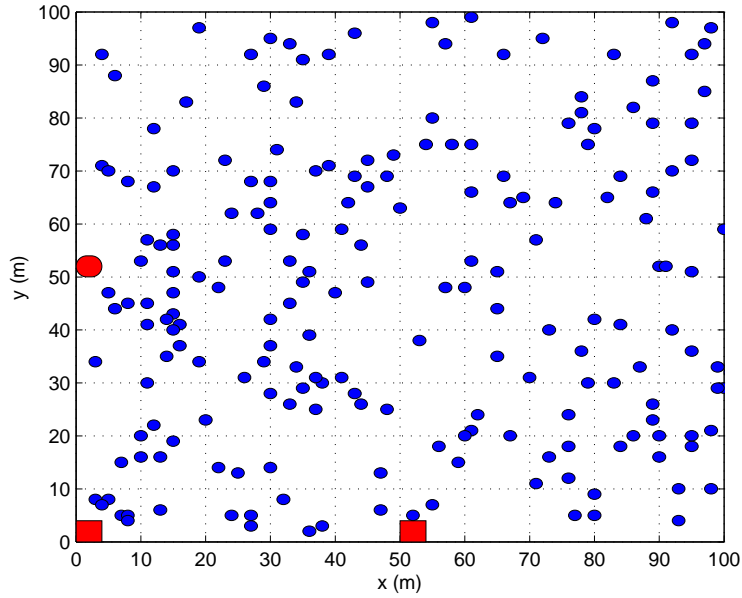
Fig. 4.19(a) shows an example of simulation setup with 3 anchors nodes (red squares) and 200 randomly deployed subject nodes (blue circles). Fig. 4.19(b) shows the result of different phases of OML lateration scheme at noise variance of 2. In first phase of the simulation, all subject nodes in-range of 3 anchor nodes are localized and turned into pseudo anchor nodes as shown by yellow squares in Fig. 4.19(b). In this case, 3 subject nodes are localized; hence number of anchor nodes is increased from 3 to 6. The next subsequent phase considered the pseudo anchor nodes along with anchor nodes in order to locate the remaining subject nodes. In phase two, subject nodes are localized (pink squares) using 6 anchor/pseudo-anchor nodes. This process continues until all the nodes in the network have been localized and turn into pseudo-anchors as shown by (cyan and green squares). As shown, after 4 simulation phases, subject nodes are progressively changed to pseudo-anchors within the field. In the case of SBT, a subject node will use blindly 3 from  $N$  in-range anchor/pseudo-anchor, whereas MSBT will make all possible combinations as a set of 3 anchors/pseudo-anchors by exploiting all in-range anchor/pseudo-anchors.

### 4.8.1 Impact of Ranging Error

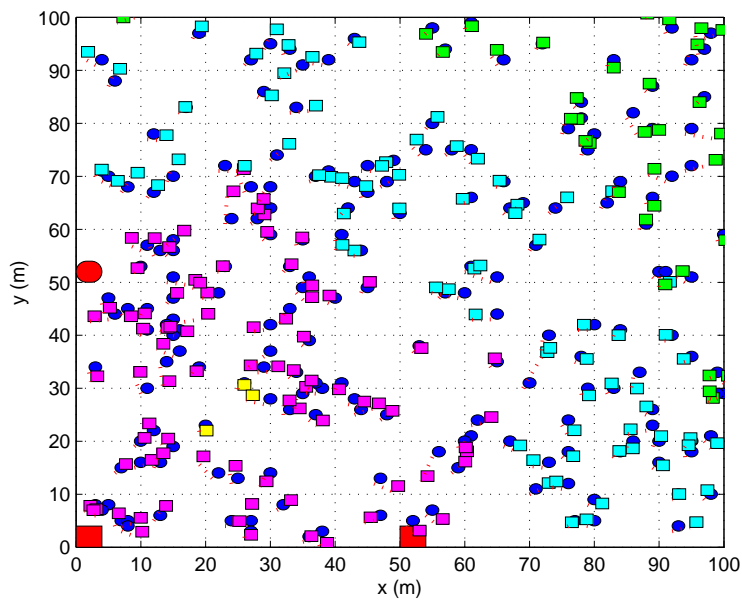
Fig. 4.20 compares the average  $E_{RMS}$  of the location estimate for OML, SBT and MSBT by increasing the ranging error ( $\sigma^2$ ). As expected, increasing the rang-

## 4.8 Performance Analysis and Results

---



(a)



(b)

Figure 4.19: Fig. 4.19(a). Example of simulation setup for 3 anchors (red squares), subject nodes (blue circles). Fig. 4.19(b). Example of simulation setup for 3 anchors (red squares), subject nodes (blue circles), and estimated subject nodes (yellow, pink, cyan and green squares) from each localization phase.

## 4.8 Performance Analysis and Results

---

ing error for each node from 0.1 to 0.5 along with bad geometry associated with anchors/pseudo-anchors increases the average RMS location error. As expected, OML and MSBT outperforms SBT (due to the blind selection). MSBT, which considers the maximum of **56** (8 in-range anchors/pseudo-anchors) different combinations in this case to avoid poor topographic arrangement, therefore reduces the average RMS location error compared with the SBT. The extra processing cost helps MSBT to outperform OML (with an average number of anchors/pseudo-anchors equal to 21), by average location error of **0.1140m**. At noise variance of 0.3, Fig. 4.20 shows that, It is better to have few good anchor nodes than few good ones and lots of poor ones. Here, a confidence level can be used to utilize the information more appropriately. As the cost of processing continues to fall this approach which trades continuous processing for reliance on a reduced number of anchors becomes increasingly attractive.

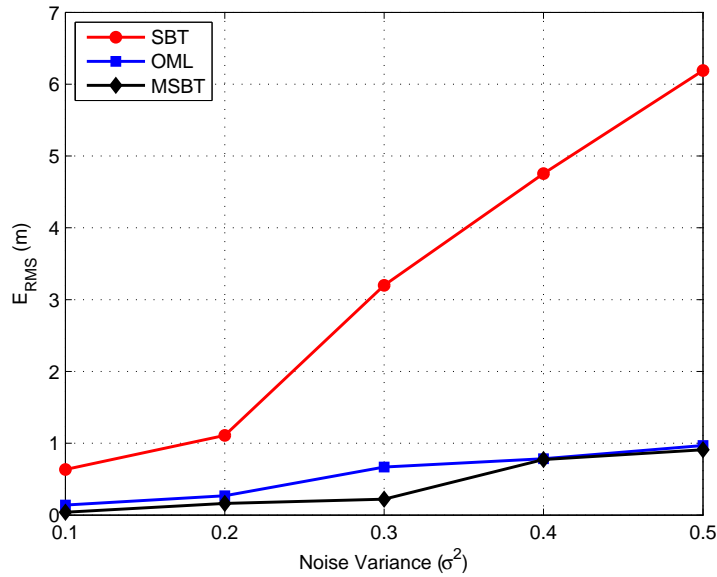


Figure 4.20: Impact of ranging error on average  $E_{RMS}$  for 400 randomly deployed nodes.

### 4.8.2 Impact of Node Density

Fig. 4.21 illustrates the average RMS error comparison by increasing the number of deployed nodes, which makes the sensing field more complex. Compared with the SBT, the MSBT scheme achieves better location accuracy as the network density increases. This is because a dense network provides a large number of combinations and makes the MSBT scheme more likely to select the anchors/pseudo-anchors which are topographically strong which achieves minimum average RMS location error. Compared with the OML, a proper selection of anchors/pseudo-anchors based on GDOP helps MSBT to stay very close to OML when the network density increases.

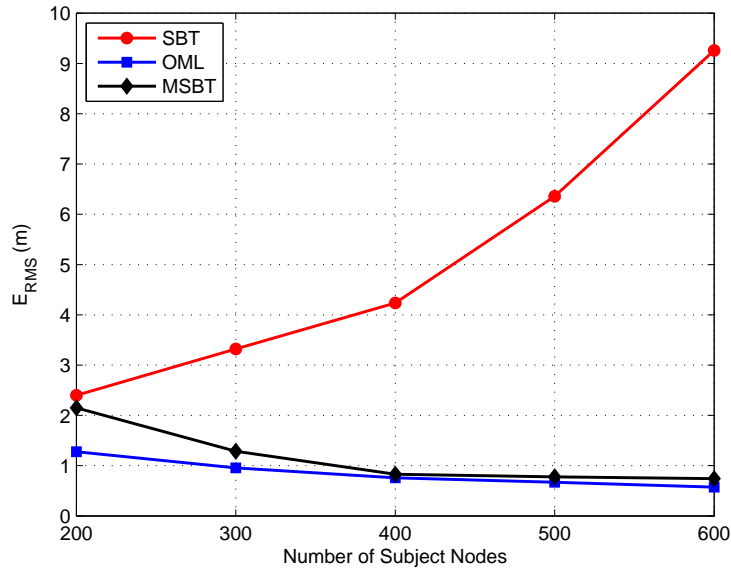


Figure 4.21: Impact of node density on average  $E_{RMS}$  at  $\sigma^2 = 0.5\text{m}$ .

Fig. 4.22 illustrates the average number of anchors/pseudo-anchors used by each subject node for localization with reference to Fig. 4.21. As shown, for SBT, the number of required anchor nodes is fixed to three. In order to keep the processing time within tolerable limits for MSBT, the maximum number of anchors/pseudo-anchors (possible combinations) are set to **8** which shows average processing of **56** different combinations for each node, even though combinations may be higher in a dense environment. However, in case of OML there is no

## 4.8 Performance Analysis and Results

---

defined tolerable limit and it reflects the change in number of anchors/pseudo-anchors as the node density increases. It helps OML to reduce the estimated location error.

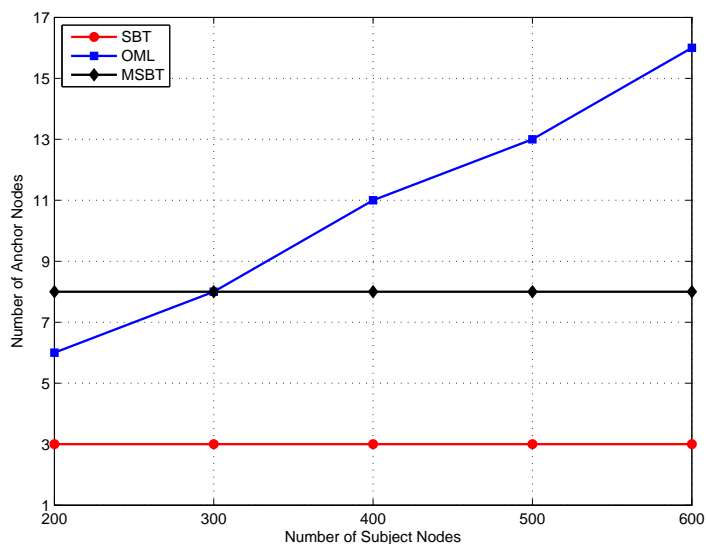


Figure 4.22: Average number of Anchors/Pseudo-Anchors with respect to Node Density ( $\sigma^2 = 0.5\text{m}$ ).

### 4.8.3 Impact of Anchor Nodes on Localization Accuracy

Fig. 4.23 and Fig. 4.24 illustrates the average RMS error comparison by varying the minimum number of the anchor nodes required to perform the localization. An increase in the number of deployed and required anchor nodes to perform localization has a positive impact on estimated location error. As expected, increasing the required anchors/pseudo-anchors to perform localization improves the location accuracy.

Fig. 4.25 illustrates the average root mean square error ( $E_{\text{RMS}}$ ) comparison for MSBT on the basis of the number of possible anchor/pseudo-anchor combinations. The increasing number of combinations (e.g. in-range anchors/pseudo-anchors) suggests different topographic layouts with different GDOP and helps to avoid bad geometry, hence an estimated location error. As shown in Fig. 4.25,

## 4.8 Performance Analysis and Results

---

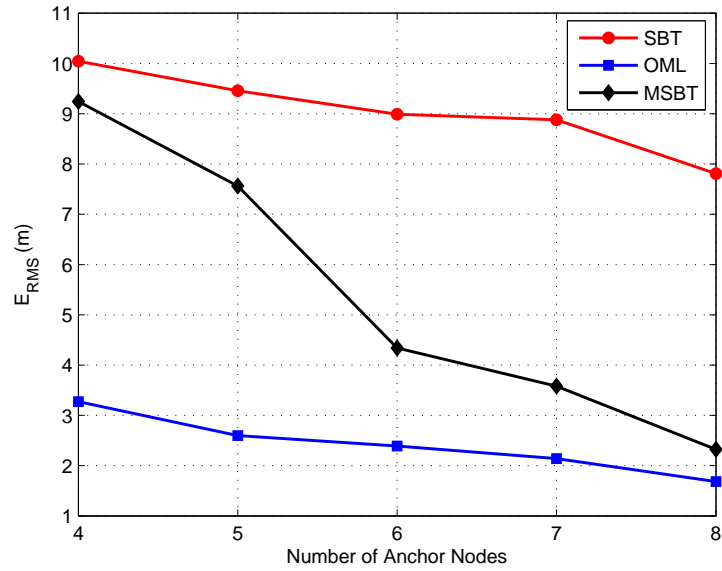


Figure 4.23: Impact of the number of Anchors/Pseudo-Anchors on average  $E_{RMS}$  ( $\sigma^2 = 5\text{m}$ ) in 200m by 200m network.

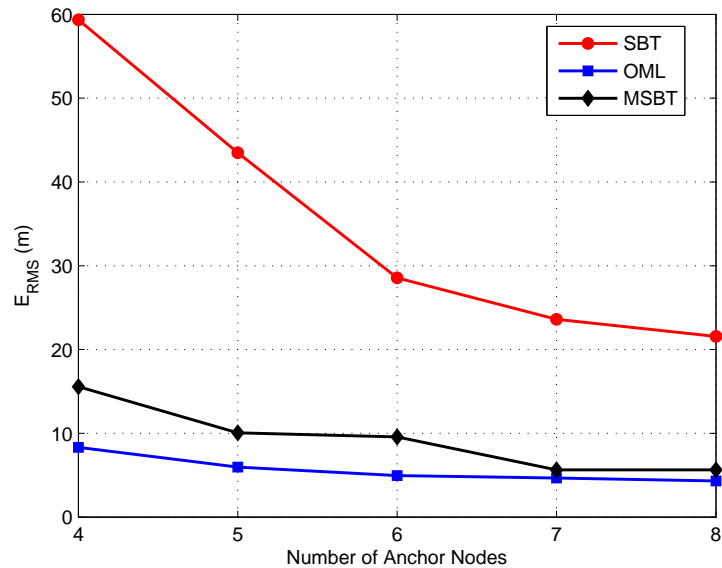


Figure 4.24: Impact of the number of Anchors/Pseudo-Anchors on average  $E_{RMS}$  ( $\sigma^2 = 10\text{m}$ ) in 200m by 200m network.

## 4.8 Performance Analysis and Results

---

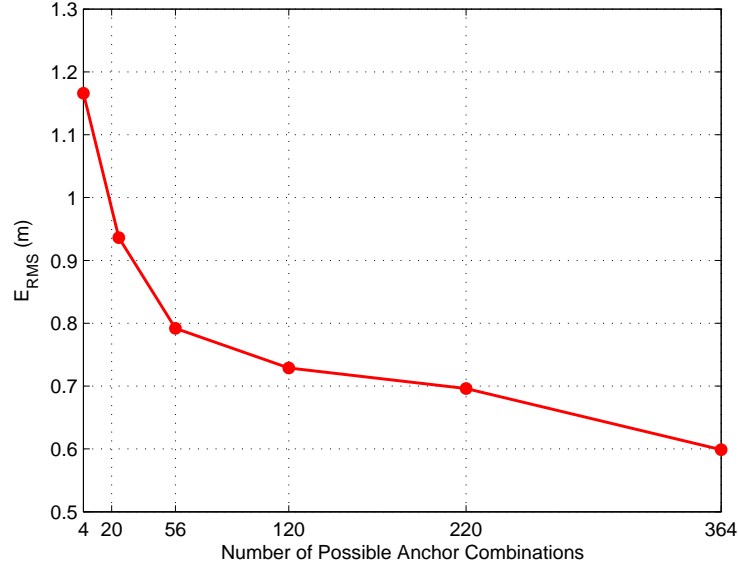


Figure 4.25: Impact of possible combinations of anchors/pseudo-anchors on average RMS location error for 100 randomly deployed nodes (transmission range = 40m,  $\sigma^2 = 0.5\text{m}$ ) for MSBT.

average RMS location error is inversely proportional to the number of different combinations. This is because a large number of combinations make the MSBT scheme more likely to select the anchors/pseudo-anchors which are topographically strong which achieves minimum average RMS location error. This also explains the reason that the processing time (power consumption) increases as the number of combinations increases for a subject node.

### 4.8.4 Analysis of Computational Complexity

Fig. 4.26 illustrates the comparison on average processing time required to perform optimal and sub-optimal iteration. As the number of deployed sensor node increases (i.e. 200 to 600), the processing time also increases for all approaches. Fig. 4.26 shows the average processing time where MSBT takes a long time to perform complex and iterative computations due to choosing a practical combination of three from maximum of **56** anchors/pseudo-anchors combinations. As shown, for **600** sensor nodes, the average time for SBT is **14.3s** and at

## 4.8 Performance Analysis and Results

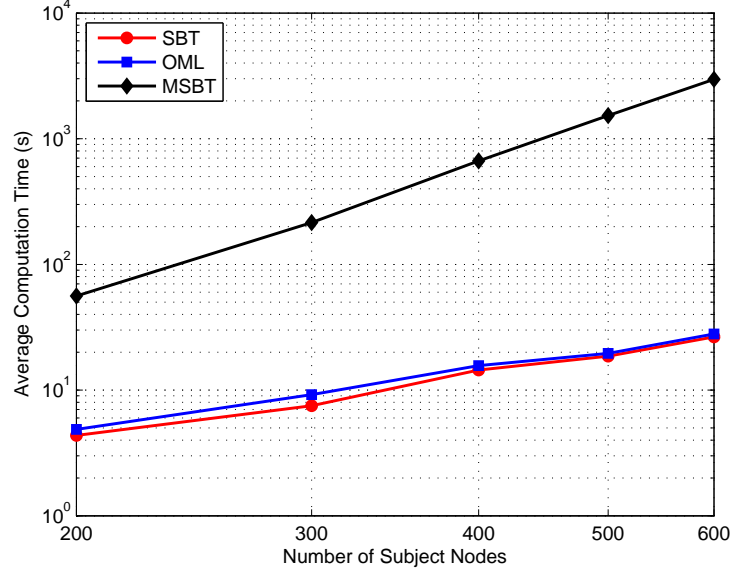


Figure 4.26: Average simulation time for single iteration of computation in 400m by 400m network with transmission range of 100m

the same time MSBT with maximum of **56** different combinations shows more than **75** times of SBT. Compared with the OML, the average processing time of MSBT increases to **70** times of OML as the network density increases. The process of choosing three anchor/pseudo-anchor nodes increases the computation complexity from  $O(1 \text{ combination of anchors/pseudo-anchors})$  to  $O(\text{combination of choosing 3 anchors/pseudo-anchors from } N \text{ anchors/pseudo-anchors combinations})$  and thus more energy consumption. Compared with the SBT, OML achieves about **1.173s** of extra computation when the network density is high. This is because a high density network makes the OML more likely to select the more in-range anchors/pseudo-anchors (with an average of 25) to perform the localization which achieves the extra power consumption. This also explains the reason that the power consumption increases as the connectivity of a subject node with anchors/pseudo-anchors increases. As shown, small average computation time and RMS error of OML compared with SBT and GDOP based MSBT makes optimal multi-lateration the best option for dense and multi-hop sensor network localization where primary power and accuracy are major con-

## 4.8 Performance Analysis and Results

cerns. GDOP based MSBT outperforms SBT in a dense sensor network, where primary power is not a major concern (e.g. tracking of freight containers in a port where primary power can be used perhaps through lighting supplies, which can help anchors / sensors to work on more complex environment [118]).

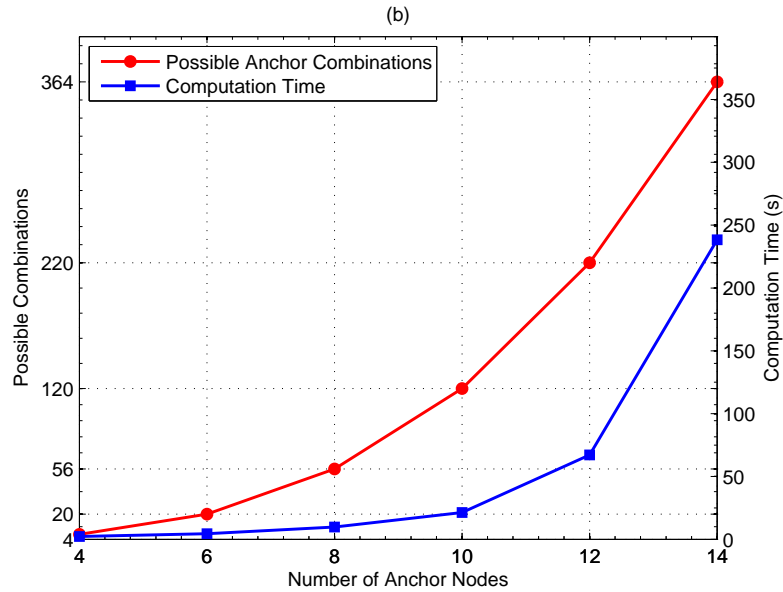


Figure 4.27: Impact of possible combinations of anchors/pseudo-anchors on average computation time for 100 randomly deployed nodes (transmission range = 40m,  $\sigma^2 = 0.5\text{m}$ ) for MSBT.

Fig. 4.27 shows such a relationship, where increasing the number of anchors/pseudo-anchors increases the combinations to perform MSBT. Considering all the possible combinations requires more processing, as Fig. 4.27 shows the average processing time of **250s** for **100** randomly deployed nodes with maximum of **364** possible combinations (14 in-range anchors/pseudo-anchors). The processing time increases with the increase in number of possible combinations and deployed nodes and considering all possible combinations (not considering any threshold) makes it attractive in terms of localization performance at the cost of huge computational overhead.

## 4.9 Discussion

In this chapter, optimization of localization accuracy is analysed using SBT, OML and GDOP based MSBT that quantifies the topographic effects in the presence of independent range error. In the light of simulation analysis the following are the main observations. The scheme to combine GDOP with SBT incurs huge computation overhead and contradicts the benefit we want to achieve from using sub-optimal lateration and is not affordable where battery power is a major problem. The excess computation is particularly acute when the number of anchors/pseudo-anchors is large; it is in fact larger than using all anchors in an OML algorithm!

As compared to SBT where selection of anchors/pseudo-anchors depends on a first-come first-served scheme. It shows first three in-range anchors/pseudo-anchors will be selected without considering an associated quality figure (to describe the error probability). In this case, there is no iterative test to validate the topological layout of anchors/pseudo-anchors to perform localization, thus blind selection reduces the computation complexity and hence power consumption. However it dramatically increases the location estimation error, especially in an environment where there are many nodes and they are densely packed. Performance of these lateration based approaches presents a trade-off for complex computation, thus energy consumption and accuracy.

## 4.10 Summary

This chapter presents a comprehensive analysis concerning the performance of lateration based localization techniques in the context of WSNs. As expected, the simulation results show that OML, considering ranging information from all in-range anchors/pseudo-anchors to calculate the subjects position performs better in terms of accuracy than SBT and stays very closed to MSBT based on GDOP. The average processing time (close to SBT) and average location error (close to MSBT) of OML provides the best performance in the context of WSNs. SBT reduces the computational complexity and processing but increases the location errors due to potentially poor selection of anchors/pseudo-anchors and

## 4.10 Summary

---

ranging error. GDOP has been shown to avoid poor topographic layout during the selection of anchor/pseudo-anchor nodes in a dense environment at the cost of very high computation from  $O(1)$  combination of anchors) to  $O(\text{combination of choosing 3 anchors from } n \text{ anchors combinations})$ . A combination of SBT and GDOP provides the minimum estimated location error but leads to a substantial performance degradation in terms of power consumption (processing) as compared with the SBT and OML. It makes GDOP less attractive approach in the context of resource constrained WSNs (i.e. where adding extra battery power is not possible).

This comparative performance analysis of localization using optimal and sub-optimal lateration provided the needed motivation to optimize the anchor placement in order to enhance the performance of range aware localization. In addition to that, to model reality most clearly, it certainly makes sense to step beyond the easy and secure reach of unrealistic 2-D representations to the pragmatic world in 3-D visualization. This motivation lead to the next chapter, which discusses the optimization of range aware localization in 2-D (circle representation) and 3-D (sphere representation).

# Chapter 5

## The Optimization of Range Derived Localization in 2D and 3D WSNs

### 5.1 Overview

One of the key factors involved in the accurate and power efficient localization of nodes in low power networks such as wireless sensor networks (WSNs) is the geometric placement of the anchor nodes. This chapter, investigates the problem of optimal placement of anchor nodes to optimize the range derived localization. The objective is to minimize the estimate of location uncertainty by exploiting the geometric placement of the minimum number of anchor nodes required to perform the localization in 2-dimensional (2-D) and 3-dimensional (3-D) scenarios. The localization Cramér-Rao lower bound (CRLB) is derived for a 3-D case, which in previous work has only been limited to a 2-D plane. Conventionally, deploying a large number anchor nodes reduces localization inaccuracy; however this holds true only if the anchors are sub-optimally placed. The optimal and worst anchor positions are determined through extended simulation by comparing their mean Cramér-Rao lower bounds (m-CRLBs). In many applications the subject node can be situated anywhere within the localization field. Since the accuracy of the localization depends on the geometry of the anchor nodes, it is preferred to choose the anchor placement such that it would minimize the inaccuracy at all

## 5.2 Introduction

---

points within the localization field. Therefore, the m-CRLB is to be minimized. Furthermore, the ramification of additive and multiplicative noise models on the minimum m-CRLB is explored.

## 5.2 Introduction

As discussed in chapter 3, ranging accuracy is an important aspect to consider because a localization system obtains position estimates using range estimates. Inaccurate range estimation may lead to unacceptable localization errors. In addition to the ranging accuracy, the majority of the previous work suggests that increasing the number of the anchor nodes yield an enhanced location estimation (see [67, 117, 119–121]). Therefore, in the context of WSNs, it is desirable to have many anchor nodes. On the other hand WSNs are energy limited, taking measurements from many anchors and transmitting these measurements reduce the life time of the network [121]. In [120], different localization techniques (i.e. DV-Hop, DV-Distance, N-Hop and Terrain) were investigated and showed that by varying the average connectivity and the number of anchor nodes with an additional anchor in the centre can help to decrease the estimated location error. The authors did not consider the optimal placement of the anchor nodes (i.e. placed in a circular sequence). In [117], the proposed localization algorithm is based on connectivity information for relative position using sub-optimal trilateration, where each sensor can perform as an anchor node. For better accuracy, distance and angle parameters among anchors are considered to avoid poor geometry. However, the authors did not consider the burden of computational complexity required for trying out all possible combinations. In [67], the proposed localization is based on relative position, where to avoid symmetry ambiguity, line segment and angle information (additional computation) are used to form a robust quadrilateral as the starting point and then trilateration is used if two quadrilaterals have three nodes in common. Geometric dilution of precision (GDOP) has been shown to avoid poor topographic layout by choosing the best selection of anchor/pseudo-anchor nodes in a dense environment at the cost of very high computation from  $O(1 \times \text{combination of anchors/pseudo-anchors})$  to  $O(\text{combination of choosing 3 anchors/pseudo-anchors from } N \text{ anchors/pseudo-anchors combinations})$  [119]. In

### 5.3 Signal Models

---

[122], four, six and seven anchor nodes were placed and deployed in a 2-D square to evaluate the performance of the localization. In addition to anchor node placement, previous work has shown a great interest in subject node deployment due to its impact on the quality of location accuracy. Considering the fact that deployment of the subject nodes in WSNs may change over time (i.e. due to the node mobility), and replacing subject nodes due to depleted batteries in remote locations. Under these conditions, relocating a large number of the subject nodes would be a complex and power consuming process. Various techniques have been developed to solve the trilateration distance equations. These include the LS methods [37], the weighted LS method [38] and the maximum likelihood (ML) approach [39]. The performance of these algorithms is bounded by the CRLB which is dependant on the geometry of the anchors and the target node. The limit on performance calculated in [40] is based on the additive noise model while a modified CRLB based on the multiplicative noise model is proposed in [41]. In this chapter, optimal anchor placement in 2-D and 3-D is investigated for both models.

A review of the two noise models is discussed in section 5.3. Section 5.4 presents the derivation of CRLB for localization in 2-D and 3-D. In section 5.6, the optimal and worst anchor placements in 2-D and 3-D is determined through extensive simulation for both noise models based on the m-CRLB. Section 5.7 provides the discussion, which is followed by the conclusion in section 5.8.

### 5.3 Signal Models

Consider a field of dimensions (length (l)× width (w)× height (h)) for a 3-D and (l × w) for a 2D network, consisting of  $N$  anchor nodes whose locations  $\theta_i = [x_i, y_i, z_i]^T$  for  $i = 1, \dots, N$  are known. This can be achieved by placing these anchors at predefined spots or their position can be determined via GPS. Considering the  $M$  number of unknown subject nodes whose true locations are denoted as  $s_j = [x_j, y_j, z_j]^T$  for  $j = 1, \dots, M$ , where  $\{.\}^T$  is the matrix transpose operation. It is desired to determine the location of a target node  $s_j$ . Two nodes, node  $i$  and node  $j$  are considered as adjacent, if and only if the actual range  $d_{ij}$  between them is less than the transmission range. In practice,  $d_{ij}$  between each

### 5.3 Signal Models

---

anchor and subject node is corrupted by the various factors discussed in Chapter 2. Then the estimated distance between each anchor and the subject node can be modelled either by an additive noise model or multiplicative noise model. The additive noise model is a widely accepted signal model, however the multiplicative noise model is suitable for multipath propagation channels. The additive noise model is discussed in section 4.3 of chapter 4 and therefore not included in this chapter. However, the Eq. (5.1) for additive noise model is given below:

$$\hat{d}_{ij} = d_{ij} + n_{ij} \quad (5.1)$$

where  $d_{ij}$  is the actual distance between node  $i$  and  $j$ ,  $n_{ij} \sim \mathcal{N}(0, \sigma_{ij}^2)$  is the additive white Gaussian noise with constant standard deviation  $\sigma$ , that is independent of  $d_{ij}$ .

Fig. 5.1(a) and Fig. 5.1(b) show how the additive noise model affects the estimated range at difference noise variances.

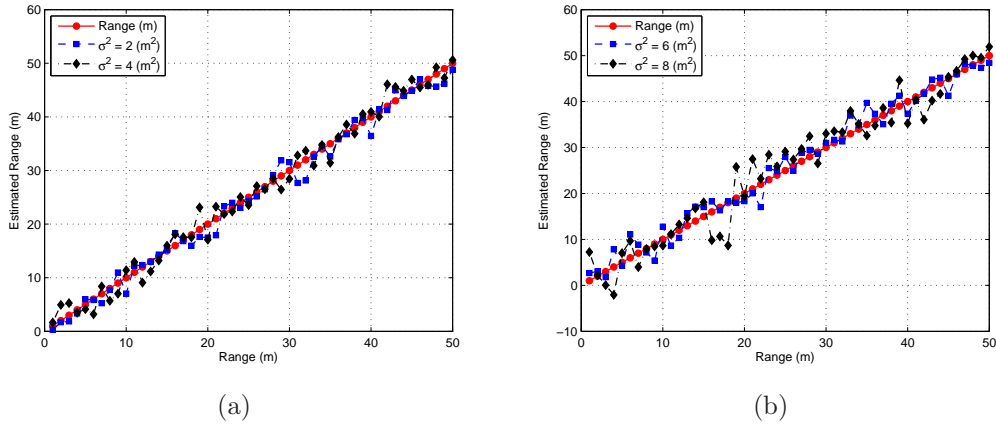


Figure 5.1: Fig. 5.1(a). Effects of additive noise model on the estimated range at noise variance of 2 and 4. Fig. 5.1(b). Effects of additive noise model on the estimated range at noise variance of 6 and 8.

## 5.3 Signal Models

---

### 5.3.1 Multiplicative Noise Model

In contrast to distance independent additive noise model (Eq. (5.1)), multiplicative noise model is dependent on the distance between a subject and anchor node. The noise variance increases together with the distance between a subject and anchor node. For the multiplicative noise model, Eq. (5.1) can be given as:

$$c\hat{\tau}_{ij} = c\tau_{ij} + cn_{ij} \quad (5.2)$$

Then the CRLB on the variance of ToF estimation can be given by Eq. (5.3) [92].

$$\sigma^2(\hat{\tau}) \geq \frac{1}{8\pi^2\text{SNR}\beta^2} \quad (5.3)$$

where SNR is the signal-to-noise-ratio and  $\beta$  is the effective bandwidth of the signal. The received power at  $i^{\text{th}}$  anchor is given as Eq. (5.4) [123]:

$$P_i = P_t \frac{v}{d_i^\eta} \quad (5.4)$$

where  $v$  is the frequency related reference loss at 1m. It is also dependent on antenna heights and other physical layer effects.  $P_t$  is the transmit power and  $\eta$  is the path loss exponent, its value is generally taken between 2 and 6 depending on the environment [123]. The SNR at  $i^{\text{th}}$  anchor is hence given by Eq. (5.5):

$$\text{SNR} = P_i/N_p \quad (5.5)$$

where  $N_p$  is the noise power. Putting the value of  $P_i$  from Eq. (5.4) in Eq. (5.5) and then SNR back in Eq. (5.3), the standard deviation on the estimated distance is given by:

## 5.4 Lower Bounds On Localization Error

---

$$\hat{\sigma}_{ij} = \kappa d_{ij}^\eta \quad (5.6)$$

where  $\kappa$  as given by Eq. (5.7) is constant.

$$\kappa = c \sqrt{\frac{N}{8\pi^2 \beta^2 P_t \vartheta}} \quad (5.7)$$

Following the multiplicative noise model, Eq. (5.1) can be given as:

$$\hat{d}_{ij} = d_{ij} + \kappa d_{ij}^{\frac{\eta}{2}} \epsilon \quad (5.8)$$

where  $\epsilon$  is random variable with zero mean and unit variance. Eq. (5.8) shows that the noise is modelled multiplicative due to the term  $d_{ij}^{\frac{\eta}{2}} \epsilon$ . Fig. 5.2 shows the variation in the estimated range for the model in Eq. (5.8).

Fig. 5.2 shows the estimated range where each range is the mean of 100 ranging samples. Fig. 5.2(a) shows the estimated range when  $\eta$  is 2 and 2.4. Looking at the error function in Eq. 5.8, it can be observed that when the  $\eta$  is 2, then the estimated error is equivalent to the  $d_{ij} \times \kappa$ . The estimated ranging error with respect to distance will increase according to the  $\eta$  and  $\kappa$ . As shown in Fig. 5.2(d), the variation in the estimated range increases when  $\kappa$  is 0.8.

## 5.4 Lower Bounds On Localization Error

The CRLB sets a lower bound on the mean square error (MSE) variance of unbiased estimates of an unknown estimated parameters [124]. It can be used as a practical performance benchmark in order to evaluate the performance of any unbiased estimator. Let  $\mathbf{s} = [s_1, s_2, \dots, s_M]^T$  be the unbiased, position vector of subject nodes, whereas the estimated position vector can be given as  $\hat{\mathbf{s}} = [\hat{s}_1, \hat{s}_2, \dots, \hat{s}_M]^T$ . Then the CRLB inequality can be given by Eq. (5.9) [125]:

## 5.4 Lower Bounds On Localization Error

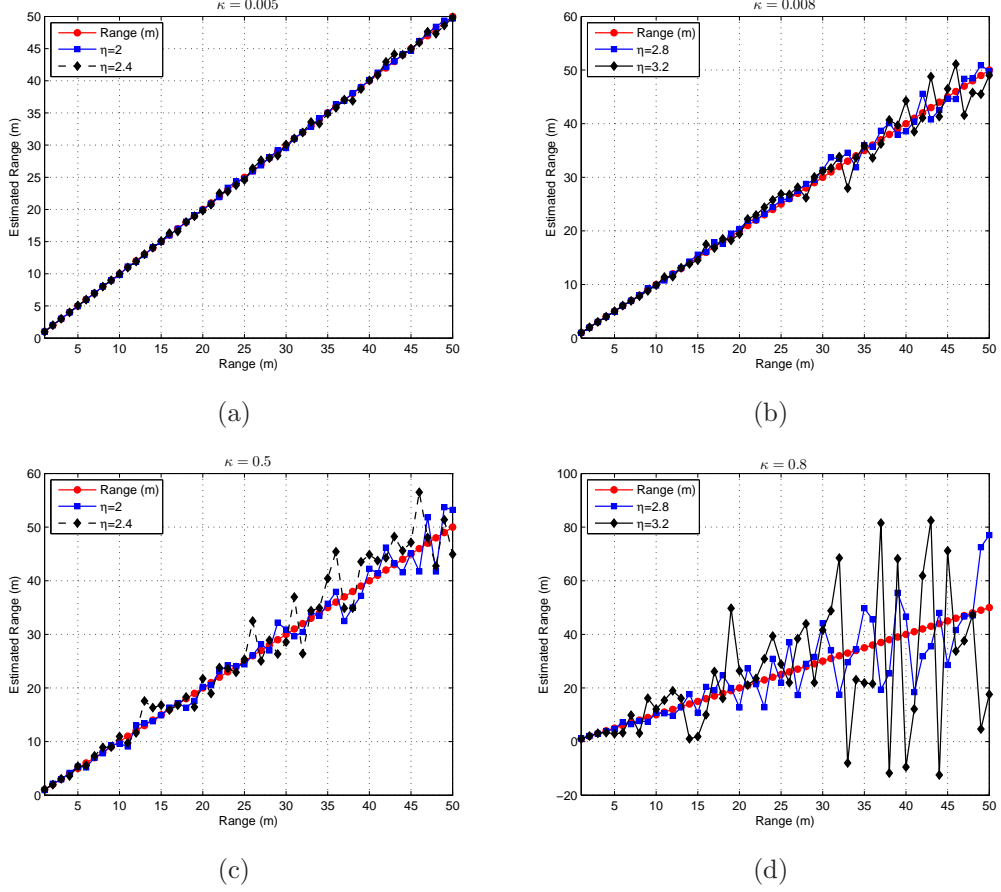


Figure 5.2: Effects of Multiplicative noise model on the estimated range. Fig. 5.2(a). For  $\kappa=0.005$ ,  $\eta=2$  and 2.4. Fig. 5.2(b). For  $\kappa=0.005$ ,  $\eta=2.8$  and 3.2. Fig. 5.2(c). For  $\kappa=0.5$ ,  $\eta=2$  and 2.4. Fig. 5.2(d). For  $\kappa=0.8$ ,  $\eta=2.8$  and 3.2.

$$\sigma^2(\hat{s}) \geq [\mathbf{I}(s)]_{jj}^{-1} \quad (5.9)$$

where  $\sigma^2(\hat{s})$  can be given as  $\sigma^2(\hat{s}) = E \{(\hat{s}_j - s_j)(\hat{s}_j - s_j)^T\}$ ,  $(\mathbf{I}(s)^{-1})_{ij}$  is the lower bound on the variance of  $(\hat{s})$  and  $\mathbf{I}$  is the Fisher Information Matrix (FIM) and is defined as [125]:

$$[\mathbf{I}(s)]_{ij} = -E \left[ \frac{\partial^2 \ln p(\hat{d}; s)}{\partial \theta_i \partial \theta_j} \right] \quad (5.10)$$

## 5.5 Optimal Anchor Placement for Minimum CRLB

---

where  $E\{\cdot\}$  refers to the expected value and is taken w.r.t  $p(\hat{\mathbf{d}};s)$  and the derivatives are taken at the true value of  $s$ .

## 5.5 Optimal Anchor Placement for Minimum CRLB

### 5.5.1 Two-Dimensional (2-D Case)

Consider Fig. 5.3, where an anchor node  $A_i$  with coordinates  $(x_i, y_i)$  and a subject node  $s_j$  with  $(x_j, y_j)$  lie in a 2-D plane, then the following relations hold

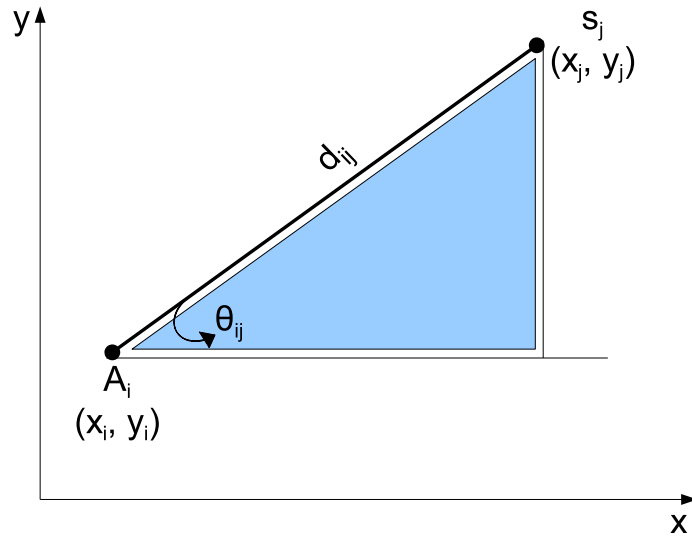


Figure 5.3: Geometric relationship between two nodes in 2-D space.

$$\cos(\theta_{ij}) = \frac{x_i - x_j}{\sqrt{(x_i - x_j)^2 + (y_i - y_j)^2}} \quad (5.11)$$

$$\sin(\theta_{ij}) = \frac{y_i - y_j}{\sqrt{(x_i - x_j)^2 + (y_i - y_j)^2}}$$

if  $\mathbf{d} = [d_{(i_1, \dots, N)(j_1, \dots, M)}]^T$  is the vector of the actual distance between the target node and the anchors, while  $\hat{\mathbf{d}} = [\hat{d}_{(i_1, \dots, N)(j_1, \dots, M)}]^T$  defines the vector of the observed (estimated) distances. Then the conditional PDF of  $\hat{\mathbf{d}}$  is given as [40]:

## 5.5 Optimal Anchor Placement for Minimum CRLB

---

$$p(\hat{\mathbf{d}}; \mathbf{d}) = \prod_{i=1}^N \frac{1}{\sqrt{2\pi\sigma_{ij}^2}} \exp \left\{ -\frac{1}{2\sigma_{ij}^2} (\hat{d}_{ij} - d_{ij})^2 \right\} \quad (5.12)$$

where  $d_{ij} = \sqrt{(x_i - x_j)^2 + (y_i - y_j)^2}$ ,  $i = 1, 2, \dots, N$  and  $N$  is the total number of anchor nodes and the log likelihood function of Eq. (5.12) is given as:

$$\ln p(\hat{\mathbf{d}}; \mathbf{d}) = -\frac{N}{2} \ln 2\pi - \frac{N}{2} \ln \sigma_{ij}^2 - \frac{1}{2\sigma_{ij}^2} \sum_{i=1}^N (\hat{d}_{ij} - d_{ij})^2 \quad (5.13)$$

now Eq. (5.11) takes Eq. (5.14) form by taking derivatives with respect to the actual value of  $x_j$  and  $y_j$  and then taking the expected values:

$$\mathbf{I}(s) = \begin{bmatrix} \sum_{i=1}^N \frac{(x_j - x_i)^2}{\sigma_{ij}^2 d_{ij}^2} & \sum_{i=1}^N \frac{(x_j - x_i)(y_j - y_i)}{\sigma_{ij}^2 d_{ij}^2} \\ \sum_{i=1}^N \frac{(x_j - x_i)(y_j - y_i)}{\sigma_{ij}^2 d_{ij}^2} & \sum_{i=1}^N \frac{(y_j - y_i)^2}{\sigma_{ij}^2 d_{ij}^2} \end{bmatrix} \quad (5.14)$$

and using Eq. (5.11) we get (5.15) for 2D [40]:

$$\mathbf{I}(s) = \begin{bmatrix} \sum_{i=1}^N \frac{\cos^2(\alpha_{ij})}{\sigma_{ij}^2} & \sum_{i=1}^N \frac{\cos(\alpha_{ij}) \sin(\alpha_{ij})}{\sigma_{ij}^2} \\ \sum_{i=1}^N \frac{\cos(\alpha_{ij}) \sin(\alpha_{ij})}{\sigma_{ij}^2} & \sum_{i=1}^N \frac{\sin^2(\alpha_{ij})}{\sigma_{ij}^2} \end{bmatrix} \quad (5.15)$$

The FIM in Eq. (5.14) and (5.15) is given for the additive noise model (Eq. (5.1)), where  $\alpha_{ij}$  being the angle of the  $j^{th}$  subject node with  $i^{th}$  anchor node. Similarly, for multiplicative noise model (Eq. (5.8)), 2-D FIM takes the form as [41]:

## 5.5 Optimal Anchor Placement for Minimum CRLB

---

$$\mathbf{I}(s) = \begin{bmatrix} \sum_{i=1}^N \frac{v_{ij} \cos^2(\alpha_{ij})}{\hat{\sigma}_{ij}^2} & \sum_{i=1}^N \frac{v_{ij} \cos(\alpha_{ij}) \sin(\alpha_{ij})}{\hat{\sigma}_{ij}^2} \\ \sum_{i=1}^N \frac{v_{ij} \cos(\alpha_{ij}) \sin(\alpha_{ij})}{\hat{\sigma}_{ij}^2} & \sum_{i=1}^N \frac{v_{ij} \sin^2(\alpha_{ij})}{\hat{\sigma}_{ij}^2} \end{bmatrix} \quad (5.16)$$

where  $v_{ij} = 1 + \frac{\eta^2 \kappa}{2} d_{ij}^{\eta-2}$ , which is distance dependent.

### 5.5.2 Three-Dimensional (3-D Case)

Consider Fig. 5.4, where an anchor node  $A_i$  with coordinates  $(x_i, y_i, z_i)$  and a subject node  $s_j$  with  $(x_j, y_j, z_j)$  lie in a 3-D space. Similar to 2-D space, FIM for additive and multiplicative noise models in 3-D space can be given as below.

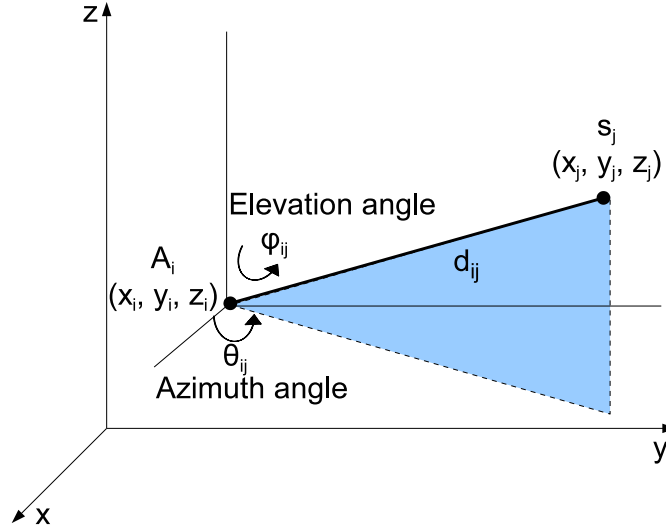


Figure 5.4: Geometric relationship between two nodes in 3-D space.

Let an anchor node with coordinates  $(x_i, y_i, z_i)$  and a target node at  $(x_j, y_j, z_j)$  lie in a three-dimensional plane (as shown in Fig. 5.4), then the following relations hold:

$$\cos(\theta_{ij}) \sin(\phi_{ij}) = \frac{x_i - x_j}{\sqrt{(x_i - x_j)^2 + (y_i - y_j)^2 + (z_i - z_j)^2}} \quad (5.17)$$

## 5.5 Optimal Anchor Placement for Minimum CRLB

---

$$\sin(\theta_{ij}) \sin(\phi_{ij}) = \frac{y_i - y_j}{\sqrt{(x_i - x_j)^2 + (y_i - y_j)^2 + (z_i - z_j)^2}}$$

$$\cos(\phi_{ij}) = \frac{z_i - z_j}{\sqrt{(x_i - x_j)^2 + (y_i - y_j)^2 + (z_i - z_j)^2}}$$

where  $0 \leq \theta_{ij} < 2\pi$  is the azimuthal angle in the  $xy$  plane and  $0 \leq \phi_{ij} \leq \pi$  is the elevation angle from the positive  $z$ -axis.

Let  $\mathbf{d}_{ij} = [d_{ij}, d_{ij}, \dots, d_N]^T$  be the vector of actual distances, where  $i = 1, \dots, N$ , and  $j \neq i$ , while  $\hat{\mathbf{d}}_{ij} = [\hat{d}_{ij}, \hat{d}_{ij}, \dots, \hat{d}_N]^T$  defines the vector of the observed (estimated) distances. Then the conditional pdf of  $\hat{\mathbf{d}}_{ij}$  is given as [40]:

$$p(\hat{\mathbf{d}}_{ij}; \mathbf{d}_{ij}) = \prod_{i=1}^N \frac{1}{\sqrt{2\pi\sigma_{ij}^2}} \exp\left\{-\frac{1}{2\sigma_{ij}^2}(\hat{d}_{ij} - d_{ij})^2\right\} \quad (5.18)$$

where  $d_{ij} = \sqrt{(x_i - x_j)^2 + (y_i - y_j)^2 + (z_i - z_j)^2}$ ,  $i = 1, 2, \dots, N$  and  $N$  is the total number of anchor nodes and the log likelihood function of Eq. (5.18) is given as:

$$\ln p(\hat{\mathbf{d}}_{ij}; \mathbf{d}_{ij}) = -\frac{N}{2} \ln 2\pi - \frac{N}{2} \ln \sigma_{ij}^2 - \frac{1}{2\sigma_{ij}^2} \sum_{i=1}^N (\hat{d}_{ij} - d_{ij})^2 \quad (5.19)$$

finally taking derivatives with respect to the actual value of  $x$  and  $y$  and then taking the expected values yields

$$-E \left[ \frac{\partial^2 \ln p(\hat{\mathbf{d}}_{ij}; \mathbf{d}_{ij})}{\partial x^2} \right] = \sum_{i=1}^N \frac{1}{\sigma_{ij}^2} \left( \frac{x_i - x_j}{\sqrt{(x_i - x_j)^2 + (y_i - y_j)^2 + (z_i - z_j)^2}} \right)^2 \quad (5.20)$$

and

$$-E \left[ \frac{\partial^2 \ln p(\hat{\mathbf{d}}; \mathbf{d})}{\partial y^2} \right] = \sum_{i=1}^N \frac{1}{\sigma_{ij}^2} \left( \frac{y_i - y_j}{\sqrt{(x_i - x_j)^2 + (y_i - y_j)^2 + (z_i - z_j)^2}} \right)^2 \quad (5.21)$$

## 5.5 Optimal Anchor Placement for Minimum CRLB

---

$$-E \left[ \frac{\partial^2 \ln p(\hat{\mathbf{d}}; \mathbf{d})}{\partial z^2} \right] = \sum_{i=1}^N \frac{1}{\sigma_{ij}^2} \left( \frac{z_i - z_j}{\sqrt{(x_i - x_j)^2 + (y_i - y_j)^2 + (z_i - z_j)^2}} \right)^2$$

also

$$-E \left[ \frac{\partial^2 \ln p(\hat{\mathbf{d}}; \mathbf{d})}{\partial x \partial y} \right] = \sum_{i=1}^N \frac{1}{\sigma_{ij}^2} \frac{(y_i - y_j)(x_i - x_j)}{(x_i - x_j)^2 + (y_i - y_j)^2 + (z_i - z_j)^2} \quad (5.22)$$

$$-E \left[ \frac{\partial^2 \ln p(\hat{\mathbf{d}}; \mathbf{d})}{\partial x \partial z} \right] = \sum_{i=1}^N \frac{1}{\sigma_{ij}^2} \frac{(x_i - x_j)(z_i - z_j)}{(x_i - x_j)^2 + (y_i - y_j)^2 + (z_i - z_j)^2}$$

$$-E \left[ \frac{\partial^2 \ln p(\hat{\mathbf{d}}; \mathbf{d})}{\partial y \partial z} \right] = \sum_{i=1}^N \frac{1}{\sigma_{ij}^2} \frac{(y_i - y_j)(z_i - z_j)}{(x_i - x_j)^2 + (y_i - y_j)^2 + (z_i - z_j)^2}$$

then the FIM in Eq. (5.23) takes the form as Eq. (5.24)

$$[\mathbf{I}(s)]_{ij} = -E \left[ \frac{\partial^2 \ln p(\hat{\mathbf{d}}; \theta)}{\partial \theta_i \partial \theta_j} \right] \quad (5.23)$$

$$\mathbf{I}(s) = \begin{bmatrix} \sum_{i=1}^N \frac{(x_i - x_j)^2}{\sigma_{ij}^2 d_{ij}^2} & \sum_{i=1}^N \frac{(y_i - y_j)(x_i - x_j)}{\sigma_{ij}^2 d_{ij}^2} & \sum_{i=1}^N \frac{(x_i - x_j)(z_i - z_j)}{\sigma_{ij}^2 d_{ij}^2} \\ \sum_{i=1}^N \frac{(y_i - y_j)(x_i - x_j)}{\sigma_{ij}^2 d_{ij}^2} & \sum_{i=1}^N \frac{(y_i - y_j)^2}{\sigma_{ij}^2 d_{ij}^2} & \sum_{i=1}^N \frac{(y_i - y_j)(z_i - z_j)}{\sigma_{ij}^2 d_{ij}^2} \\ \sum_{i=1}^N \frac{(x_i - x_j)(z_i - z_j)}{\sigma_{ij}^2 d_{ij}^2} & \sum_{i=1}^N \frac{(y_i - y_j)(z_i - z_j)}{\sigma_{ij}^2 d_{ij}^2} & \sum_{i=1}^N \frac{(z_i - z_j)^2}{\sigma_{ij}^2 d_{ij}^2} \end{bmatrix} \quad (5.24)$$

using Eq. (5.17), we get:

$$\mathbf{I}(s) = \begin{bmatrix} \frac{\cos^2(\theta_{ij}) \sin^2(\phi_{ij})}{\sigma_{ij}^2} & \frac{\cos(\theta_{ij}) \sin^2(\phi_{ij}) \sin(\theta_{ij})}{\sigma_{ij}^2} & \frac{\cos(\theta_{ij}) \sin(\phi_{ij}) \cos(\phi_{ij})}{\sigma_{ij}^2} \\ \frac{\cos(\theta_{ij}) \sin^2(\phi_{ij}) \sin(\theta_{ij})}{\sigma_{ij}^2} & \frac{\sin^2(\theta_{ij}) \sin^2(\phi_{ij})}{\sigma_{ij}^2} & \frac{\sin(\theta_{ij}) \sin(\phi_{ij}) \cos(\phi_{ij})}{\sigma_{ij}^2} \\ \frac{\cos(\theta_{ij}) \sin(\phi_{ij}) \cos(\phi_{ij})}{\sigma_{ij}^2} & \frac{\sin(\theta_{ij}) \sin(\phi_{ij}) \cos(\phi_{ij})}{\sigma_{ij}^2} & \frac{\cos^2(\phi_{ij})}{\sigma_{ij}^2} \end{bmatrix} \quad (5.25)$$

Now the CRLB for the  $x$ ,  $y$  and  $z$  coordinates of the target node can be

## 5.6 Optimal Anchor Placements

---

estimated by an unbiased estimator from the FIM

$$E((\hat{x} - x)^2) \geq [\mathbf{I}(s)]_{11}^{-1}$$

$$E((\hat{y} - y)^2) \geq [\mathbf{I}(s)]_{22}^{-1} \quad (5.26)$$

$$E((\hat{z} - z)^2) \geq [\mathbf{I}(s)]_{33}^{-1}$$

and CRLB for the localization of the target node can be estimated by an unbiased estimator from the FIM

$$\sigma^2(\hat{s}) = E \{(\hat{x}_j - x_j)(\hat{y}_j - y_j)(\hat{z}_j - z_j)\}^T \geq Tr([\mathbf{I}(s)]^{-1}) \quad (5.27)$$

Similar to Eq. (5.25), FIM for multiplicative noise model in 3-D space can be given by Eq. (5.28):

$$\mathbf{I}(s) = \begin{bmatrix} \sum_{i=1}^N v_{ij} \frac{(x_j - x_i)^2}{\hat{\sigma}_{ij}^2 d_{ij}^2} & \sum_{i=1}^N v_{ij} \frac{(x_j - x_i)(y_j - y_i)}{\hat{\sigma}_{ij}^2 d_{ij}^2} & \sum_{i=1}^N v_{ij} \frac{(x_j - x_i)(z_j - z_i)}{\hat{\sigma}_{ij}^2 d_{ij}^2} \\ \sum_{i=1}^N v_{ij} \frac{(x_j - x_i)(y_j - y_i)}{\hat{\sigma}_{ij}^2 d_{ij}^2} & \sum_{i=1}^N v_{ij} \frac{(y_j - y_i)^2}{\hat{\sigma}_{ij}^2 d_{ij}^2} & \sum_{i=1}^N v_{ij} \frac{(y_j - y_i)(z_j - z_i)}{\hat{\sigma}_{ij}^2 d_{ij}^2} \\ \sum_{i=1}^N v_{ij} \frac{(x_j - x_i)(z_j - z_i)}{\hat{\sigma}_{ij}^2 d_{ij}^2} & \sum_{i=1}^N v_{ij} \frac{(y_j - y_i)(z_j - z_i)}{\hat{\sigma}_{ij}^2 d_{ij}^2} & \sum_{i=1}^N v_{ij} \frac{(z_j - z_i)^2}{\hat{\sigma}_{ij}^2 d_{ij}^2} \end{bmatrix} \quad (5.28)$$

Since the lower bounds in both noise models are functions of the geometry of the anchors and the target node, it is clear that certain anchor locations offer better accuracy than others. In the next section, we analyse the optimal anchor placement for both additive and multiplicative noise models and the impact on the m-CRLB in 2-D and 3-D space.

## 5.6 Optimal Anchor Placements

The estimation of different subject node positions are subject to different accuracies. The objective is to find anchor locations that would provide an overall best accuracy for all target positions. Thus the anchors that offer the minimum

## 5.6 Optimal Anchor Placements

---

of the mean CRB are selected. In the following subsection, the optimal and worst anchor placement are discussed based on the m-CRLB for both additive and multiplicative error models as explained above in section 5.3.

### 5.6.1 Two-Dimensional (2-D) Case

Trilateration in a 2-D case requires a minimum of three anchor nodes. Individual distances between each anchor and the subject node is represented by a circle or line of position (LoP). The point of intersection of these circles is the subject node location. In order to get an insight on how the lower bound is affected by the relative angle of between the subject and the anchor node, the CRLB for every point in a 2-D plane is calculated for fixed anchor position. Furthermore, in order to observe the optimal anchor placement that gives the minimum m-CRLB and optimizes the range derived localization, a detailed and extensive set of simulations is executed, where all the combinations of anchors are taken.

Consider a field of  $11 \times 11$ , where a single anchor node can have 121 possible placements, and so a set of 3 anchors can have 287,980 different possible anchor placements in 2-D using Eq. (5.29):

$$A_P = \frac{M_{PL}!}{A_N! (M_{PL} - A_N)!} \quad (5.29)$$

where  $A_N$  is the number of anchors used and  $M_{PL}$  is maximum possible locations equivalent to the product of the field dimensions. Fig. 5.5 shows the relationship between possible combinations for anchors placement and field dimensions. It can be observed from Fig. 5.5(a) and Fig. 5.5(b) that as the number of anchors increase the possible anchor placements also increases. However, as the number of anchors cross half of the field dimension or maximum possible locations (i.e. 4.5 for  $3\text{m} \times 3\text{m}$  and 8 for  $4\text{m} \times 4\text{m}$ ), the possible anchor placements start decreasing.

It is well known that when all anchors are placed along the same axis (i.e. when all anchors lie on the same line) then the variance of the CRLB rises to infinity and in such cases positioning algorithms such as the LS fail to estimate

## 5.6 Optimal Anchor Placements

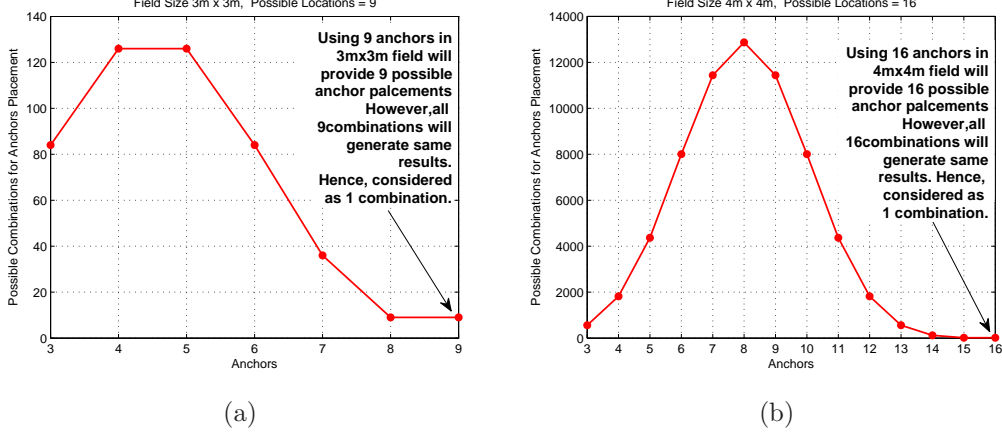


Figure 5.5: Fig. 5.5(a) Relationship between possible combinations of anchor placements and  $3 \times 3$  field dimensions. Fig. 5.5(b). Relationship between possible combinations of anchor placements and  $4 \times 4$  field dimensions.

the subject node coordinates. Thus in order to avoid this problem and to reduce the computational cost, all the collinear anchor placements are considered invalid in our simulations. The number of invalid collinear anchor placements ( $C_{AP}$ ) depends on the field dimensions and the number of anchor nodes used and can be calculated using generalized relation as given by Eq. (5.30). For a  $11 \times 11$  square field, 3,630 collinear anchor placements are avoided.

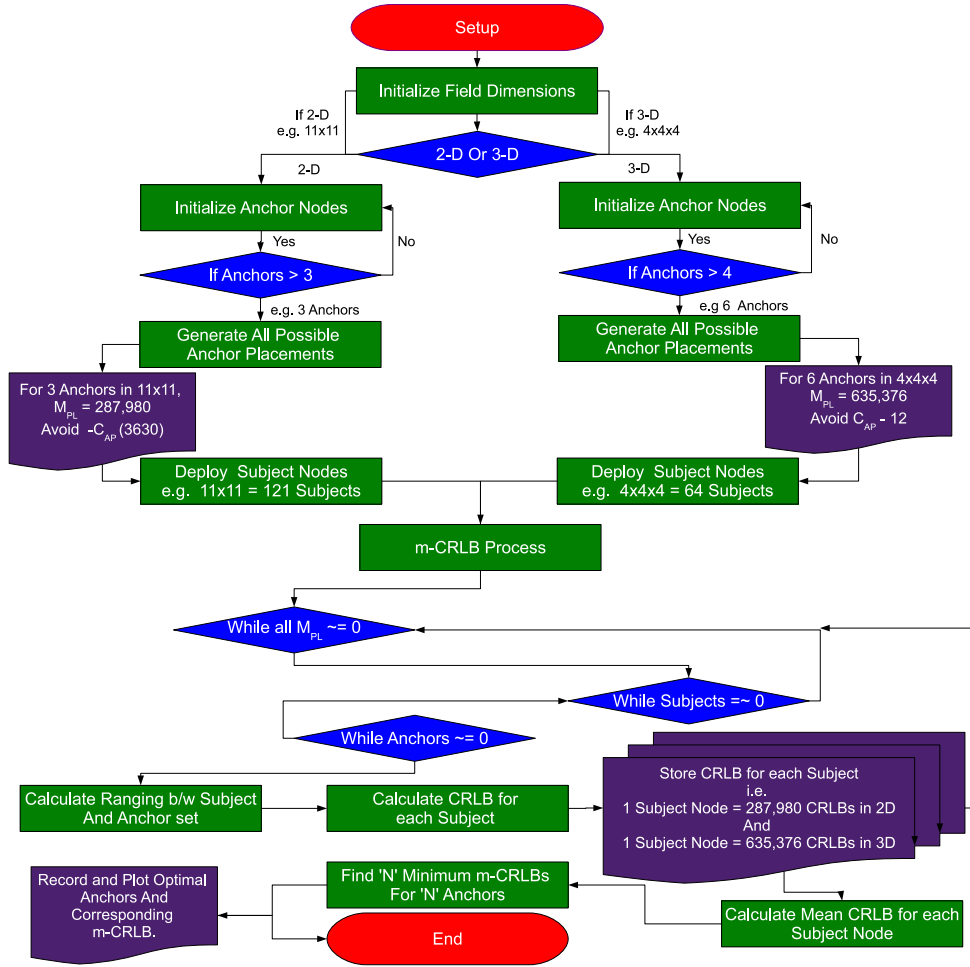
$$C_{AP} = l \frac{l!}{A_N (l - A_N)!} + w \frac{w!}{A_N (w - A_N)!} + h \frac{h!}{A_N (h - A_N)!} \quad (5.30)$$

where  $l$ ,  $w$  and  $h$  are the field dimensions.

All 287,980 placements for 3 anchors in 2-D will have a different impact on the location estimates. In order to optimize the location estimates, it is required to select the best combination for anchors placement. To select the optimal placement for 3 to 8 anchor nodes, the m-CRLB is calculated for each combination. The best optimal placement for each anchor node combination (i.e. from 3 to 8 anchors) is selected on the basis of minimum m-CRLB, whereas worst anchor placement is selected on the maximum m-CRLB. Fig. 5.6 illustrates the m-CRLB process flowchart, whereas Fig. 5.7 shows the CRLB value for each set of anchor

## 5.6 Optimal Anchor Placements

placement and the mean CRLB for all anchor placements for a single node  $s$ . In a similar fashion, each subject location corresponds a mean CRLB. Once all the subject locations are covered with mean CRLB,  $N$  optimal and worst anchor placements are determined by selecting the  $N$  minimum mean and maximum mean CRLB respectively. The spikes in the Fig 5.7 indicate the poor anchor placement (i.e. anchors are very close to each other).

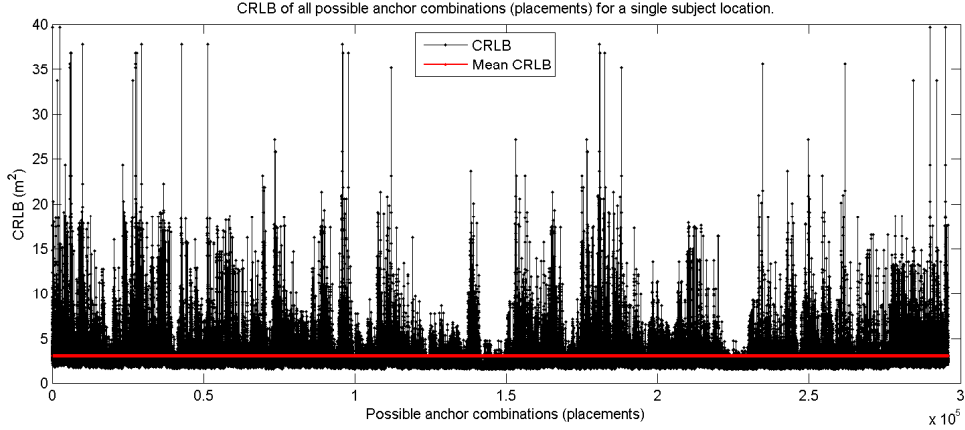


(a)

Figure 5.6: m-CRLB Flow Chart.

The average time to determine the optimal anchor placement for 8 anchors in a  $5 \times 5$  2-D plane is  $\sim 7$  days. This processing time is observed on three different brands (i.e. Dell, Sony and Toshiba laptops) with 2.4GHz processor and 1GB

## 5.6 Optimal Anchor Placements



(a)

Figure 5.7: CRLB of all possible anchor combinations (placements) for a single subject location.

random access memory (RAM). As the dimension of the 2-D plane increases, the possible locations (grid points) also increase. It results in huge number of combination for anchors placement. Furthermore, it is observed that, due to the lack of high performance computing systems, MATLAB even failed to generate the possible combinations for 6 anchors in  $10 \times 10$  2-D plane. This computational burden is increased more, when 2-D plane is extended to 3-D space.

### 5.6.1.1 Optimal Anchor Placement for Additive Noise Model

Fig. 5.8(a) - Fig. 5.8(f) shows the best placement for 3 to 8 anchors in 2-D space for additive noise model, whereas Fig. 5.9 shows the contour plots for the optimal anchors placement as shown in Fig. 5.8.

Fig. 5.9(b)-Fig. 5.9(g) obtained for a constant  $\sigma^2$  for all cases (i.e.  $\sigma_{ij}^2 = \sigma^2 = 2$ ). It is observed that when only 3 anchors are placed in a square area, the highest accuracy in the estimated location is achieved when the trio is placed at the corners of an equilateral triangle. This triangle is of maximum size as 2 anchors are placed at the corners of one side of the square area while the 3<sup>rd</sup> anchor is placed at the centre of the opposite side. It is also noted that the bound increases as the subject node goes near any of the anchor nodes. The best location for 4 anchors is at the corners of the square area while the best location

## 5.6 Optimal Anchor Placements

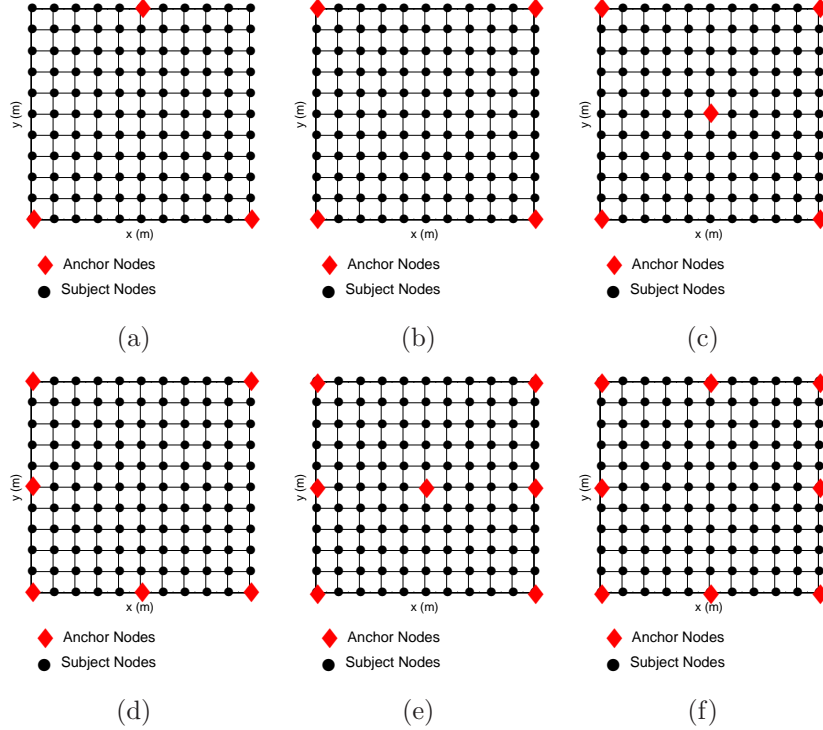


Figure 5.8: Optimal anchor placement for additive noise model in a  $11 \times 11$  2-D plane for 3 to 8 anchors.

for an additional  $5^{th}$  anchor is the centre of the area. Similarly such symmetrical anchor locations are exhibited in Fig. 5.9 (Fig. 5.9(e)-Fig.5.9(g)), where 6, 7 and 8 anchors are used. The white points in the figures show the anchor locations and subject node placement is not considered valid. It should be noted that these configurations are independent of rotation i.e. same results are obtained if the entire set of anchors are simultaneously rotated clockwise or counter-clock wise by  $90^\circ$  or  $180^\circ$ . Fig. 5.9(a) displays the m-CRLB as a function of variance and number of anchor nodes. It is noted that as the number of anchors increases the effect of noise on the m-CRLB becomes smaller.

Furthermore, it is observed that, optimal anchor placement for additive noise model for any scale remains the same. To illustrate this, simulations are executed for 8 anchor nodes where different field dimensions are considered for a constant  $\sigma^2$ . Fig. 5.10(a), Fig. 5.10(b) and Fig. 5.10(c) show the contours plot for 8 anchor nodes for  $20 \times 20$ ,  $30 \times 30$ , and  $40 \times 40$  at  $\sigma^2 = 2$  respectively. It can

## 5.6 Optimal Anchor Placements

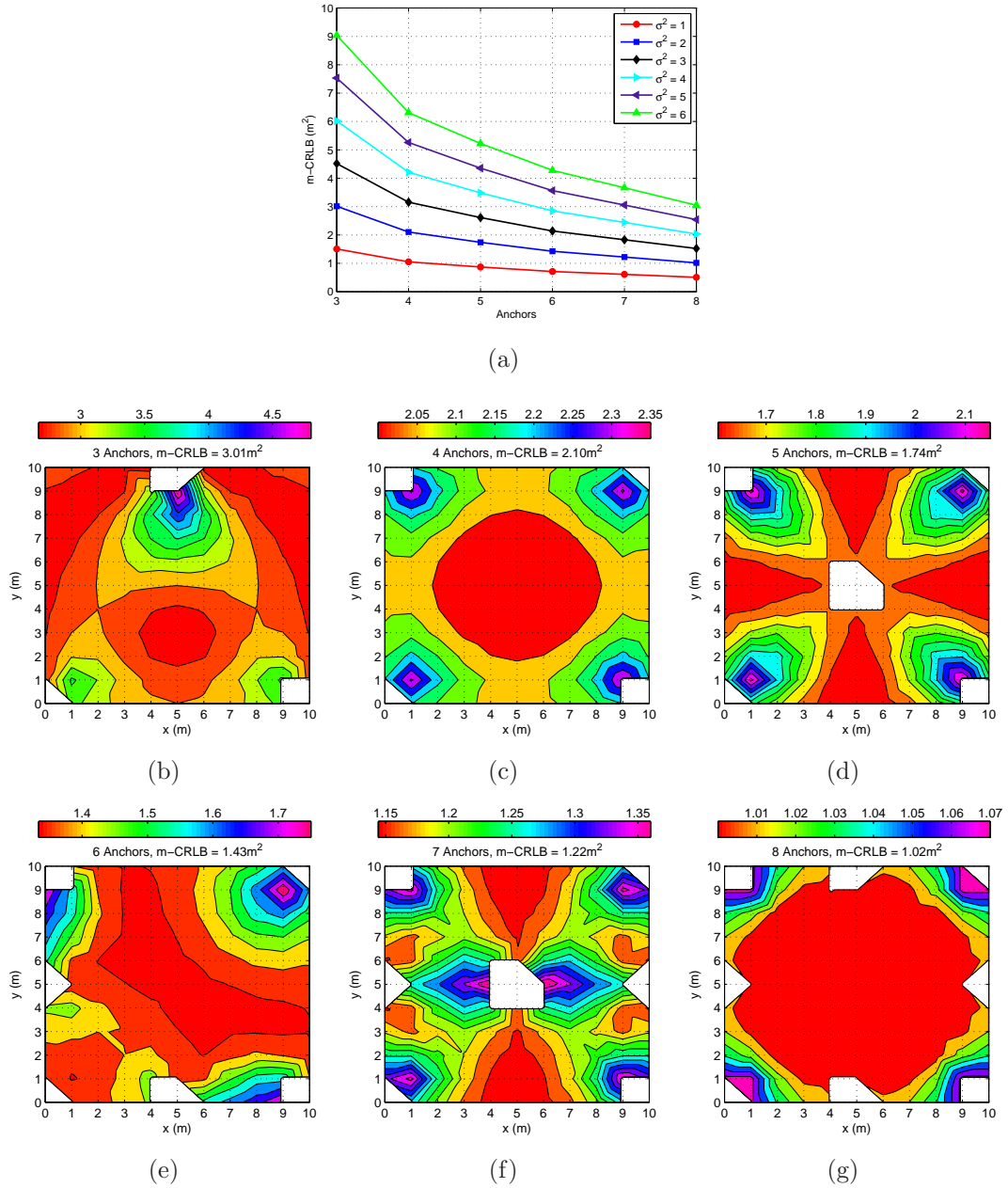


Figure 5.9: Optimal anchor placement and corresponding m-CRLB for additive noise model using 3 to 8 anchor nodes as shown in Fig. 5.8(a) - Fig. 5.8(f) for deployed subject nodes on a 11×11 2-D plane. Fig. 5.9(a). Impact of anchor nodes on m-CRLB. Fig. 5.9(b) - Fig. 5.9(g). contour plots for 3 to 8 anchors in 2-D for  $\sigma^2 = 2$ .

## 5.6 Optimal Anchor Placements

be observed that m-CRLB ( $1.02\text{m}^2$ ) remains the same for each scale. This is because the  $\sigma^2$  is constant for each distance. Unlike multiplicative noise model, m-CRLB in additive noise model does not vary with distance and therefore Fig. 5.10 shows constant m-CRLB for 8 anchors at each scale. As explored that these optimal anchor placements are same at any  $\sigma^2$  value, however, the m-CRLB value increases with the increase of  $\sigma^2$ .

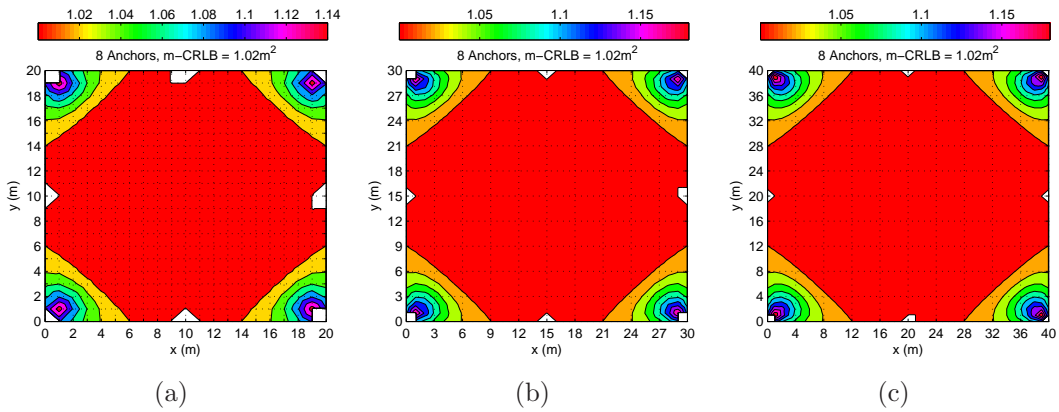


Figure 5.10: Optimal anchor placement for 8 anchor nodes for three different scales. Fig. 5.10(a). For  $21 \times 21$ . Fig. 5.10(b). For  $31 \times 31$ . Fig. 5.10(c). For  $41 \times 41$ .

Fig. 5.11(a) - Fig. 5.11(f) shows the worst placement for 3 to 8 anchors in 2-D space for additive noise model. Fig. 5.12 illustrates the anchor locations which exhibit the worst localization accuracy and give the maximum m-CRLB for the additive noise model using 3 - 8 anchors. It is observed that the variance of the estimator is the highest if all the anchors are placed at the corner of a square area. It is also seen in Fig. 5.12(a) that the improvement in performance is negligible if the number of anchors is increased from 5 - 8 for a poor network geometry. Furthermore, it is evident from both Fig. 5.9 and Fig. 5.12 that even if the minimum 3 anchors are placed optimally (m-CRLB = 1.50 and 9.03 for  $\sigma^2 = 1$  and 6 respectively), it outperforms a poor deployment of 8 anchors (m-CRLB = 13.5 and 81.7 for  $\sigma^2 = 1$  and 6 respectively).

## 5.6 Optimal Anchor Placements

---

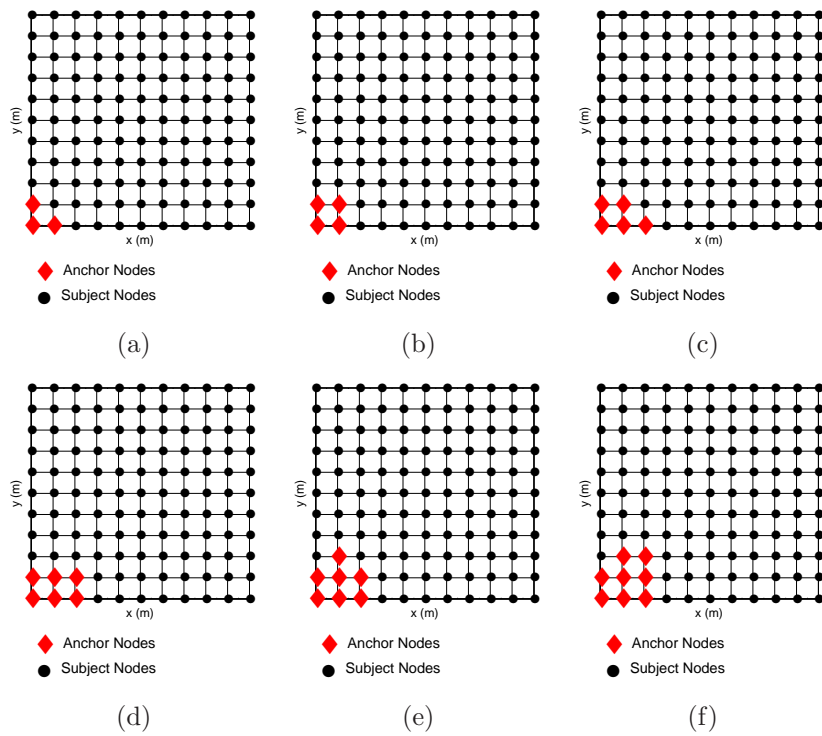


Figure 5.11: Worst anchor placement for additive noise model in a  $11 \times 11$  2-D plane for 3 to 8 anchors.

## 5.6 Optimal Anchor Placements

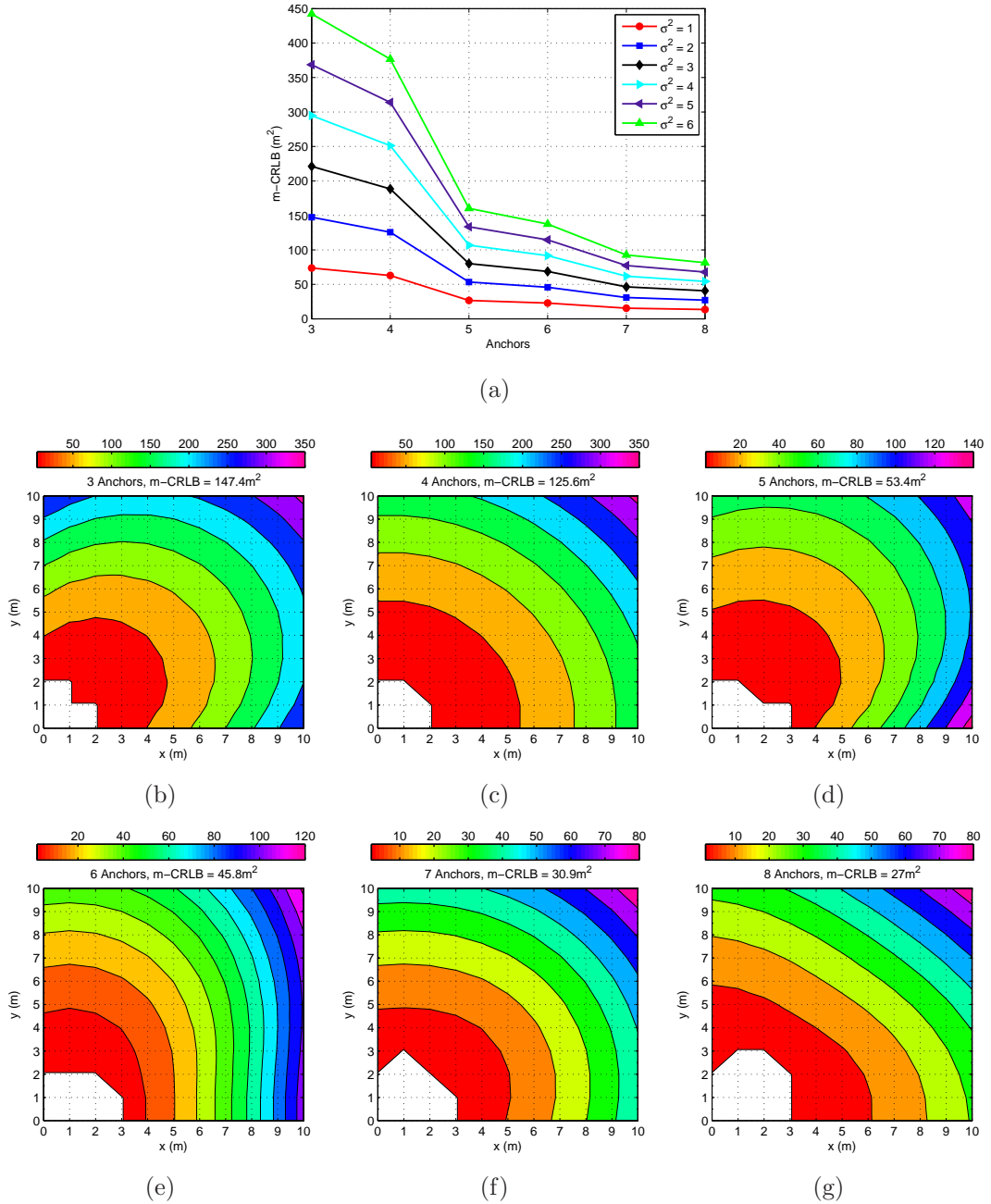


Figure 5.12: Contour plot of worst anchor placement and corresponding m-CRLB for additive noise model for 3 to 8 anchor nodes.

## 5.6 Optimal Anchor Placements

### 5.6.1.2 Optimal Anchor Placement for Multiplicative Noise Model

Fig. 5.13 illustrates the m-CRLB contour plots for multiplicative noise model as a function of the number of anchor nodes placed at the optimal positions for the additive noise model. The contour plots given in Fig. 5.13(a)-Fig. 5.13(f) are for  $\kappa = 0.001$  and  $\eta = 2$ . When compared Fig. 5.13 with Fig. 5.9(b)-Fig. 5.9(g) (additive noise model), it is observed that the m-CRLB for the multiplicative noise model is lower than the additive noise model for anchors 3 and more. However this is not true for all values of  $\kappa$  and  $\eta$ . It is further demonstrated in Fig. 5.14(a)-Fig. 5.14(c) for different values of  $\eta$  (2.0 and 2.8) and  $\kappa$  (0.002, 0.004, ... 0.01 and 0.2, 0.4, ... 1) respectively.

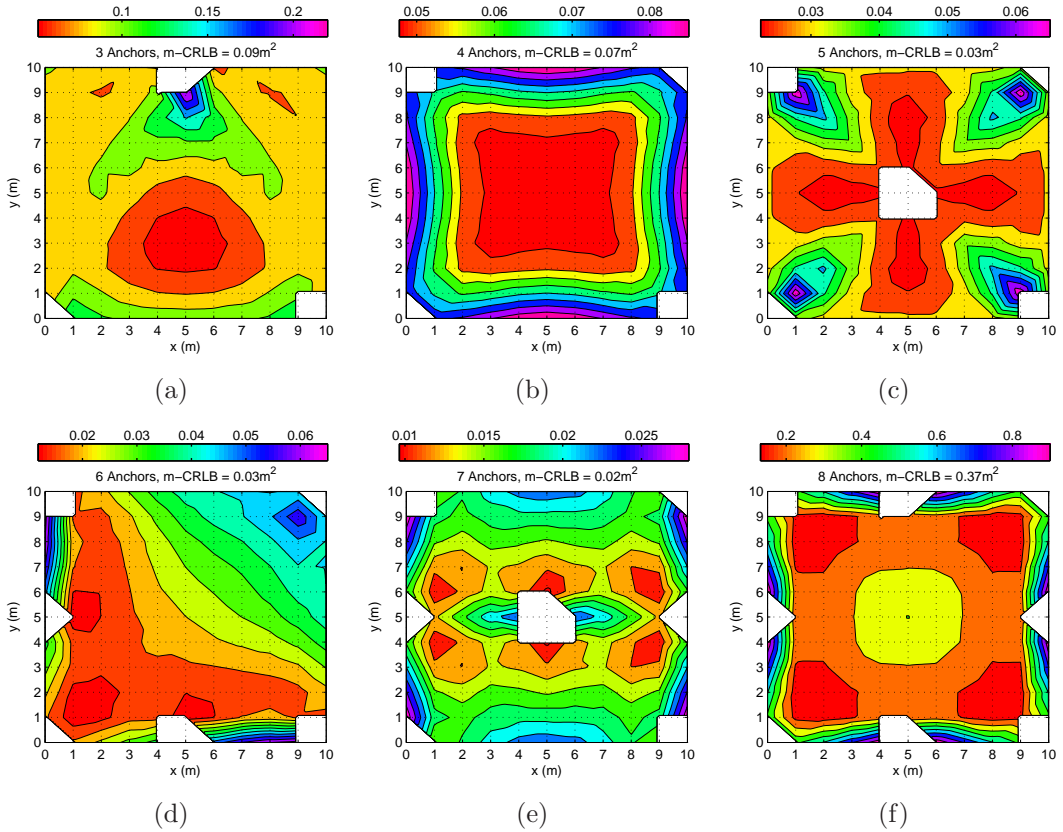


Figure 5.13: Arbitrary anchor placement and corresponding minimum m-CRLB for multiplicative noise model using 3 - 8 Anchor nodes as shown in Fig. 5.8(a) - Fig. 5.8(f) (optimal for additive noise model) for deployed subject nodes on a 11×11 2-D space for  $\eta = 2$  and  $\kappa = 0.001$ .

## 5.6 Optimal Anchor Placements

Fig. 5.14(a) shows that m-CRLB for multiplicative noise model is lower than the additive noise model ( $\sigma^2 = 2$ ) for all values of  $\kappa$  when  $\eta = 2$ . Furthermore, m-CRLB for multiplicative is observed lower even for  $\eta = 2.8$  and  $\kappa$  below 0.006. It proves that the m-CRLB for multiplicative noise model depends on the  $\eta$  and  $\kappa$  in addition to the distance. The m-CRLB becomes higher as values of  $\eta$  and  $\kappa$  are increased. However, it is observed from Fig. 5.14(a)-Fig. 5.14(c) that as  $\kappa$  increases for any value of  $\eta$ , the impact of  $\kappa$  on m-CRLB decreases. Fig. 5.14(d) shows such impact more clearly, where increasing  $\kappa$  shows a very small impact, hence closer values of m-CRLB at each value of  $\kappa$ .

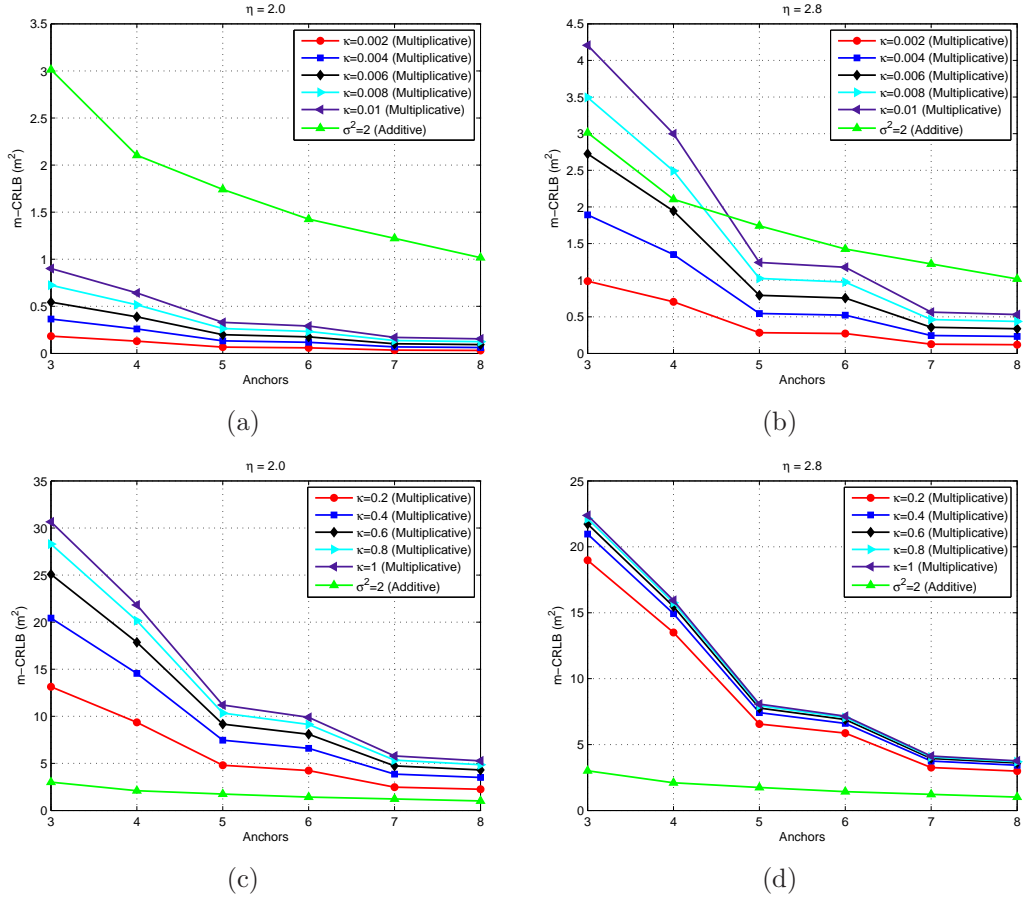


Figure 5.14: m-CRLB for multiplicative noise model as a function of the number of anchor nodes placed at the optimal positions for additive noise model.

The dependency of  $\eta$  and  $\kappa$  on multiplicative noise model distinguishes it from the additive noise model, therefore this the motivation to determine the

## 5.6 Optimal Anchor Placements

optimal anchor placement for multiplicative noise model. To determine the optimal anchors placement for multiplicative noise model, extensive simulations are executed in the previously described 2-D setup. However, due to the limited high computing resources and for general comparison between optimal anchor placements for additive and multiplicative noise models, a smaller scale is considered initially.

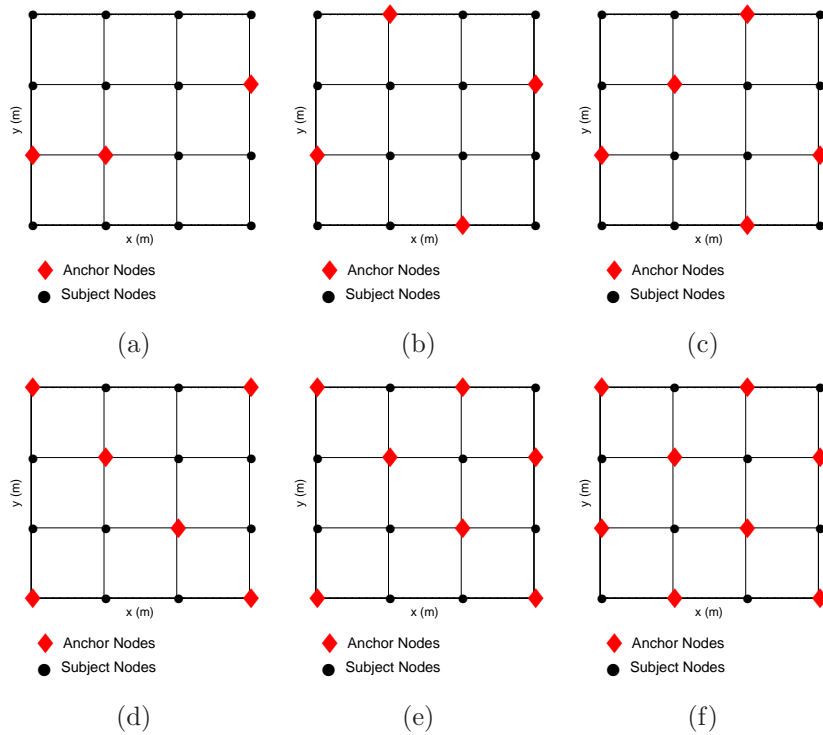


Figure 5.15: Optimal anchor placement for multiplicative noise model in a  $4 \times 4$  2-D plane for 3 to 8 anchors, where  $\kappa = 0.001$  and  $\eta = 4$ .

Fig. 5.15(a) - Fig. 5.15(f) shows the best placement for 3 to 8 anchors in a  $4 \times 4$  2-D plane for multiplicative noise model. Since the optimality of anchor placement for additive noise model is independent of scale and therefore Fig. 5.15 ( $4 \times 4$ ) is compared with the Fig. 5.8 ( $11 \times 11$ ). Comparison of both Fig. 5.15 and Fig. 5.8 illustrates that the optimal anchor placements for multiplicative are different from those for additive. Multiplicative noise model suggests that the m-CRLB of the anchor placement will be minimum, when few of the anchors are placed in the centre of the field (i.e. Fig. 5.15(a), Fig. 5.15(e), Fig. 5.15(f))

## 5.6 Optimal Anchor Placements

---

because measurement on average will be subject to less noise. It is in conflict with additive noise model, which suggest the boundary line of the field as optimal placement for anchors (i.e. when the trio is placed at the corners of an equilateral triangle, or 4 anchors are at the corners of the square area). Like optimal placement in additive, these placements are independent of rotation i.e. same results are obtained if the entire set of anchors are simultaneously rotated clockwise or counter-clock wise by  $90^\circ$  or  $180^\circ$ .

### Impact of $\kappa$ and $\eta$ on Optimal Anchors Placement

It is assumed that the optimal anchor placement in multiplicative noise model will vary with respect to the parameters like  $\kappa$ ,  $\eta$  and the field dimension. Therefore, to analyse and to verify the impact of these parameters, firstly,  $\kappa$  and  $\eta$  are considered by deploying the same  $4 \times 4$  2-D plane but with different  $\kappa$  and  $\eta$ . Fig. 5.16 shows the optimal anchor placement for multiplicative noise model in a  $4 \times 4$  2-D plane for 3 to 8 anchors, where  $\kappa = 0.005$  and  $\eta = 2$ . When Fig. 5.16 is compared with Fig. 5.15, it is noticed that optimal anchor placement in a  $4 \times 4$  2-D plane for 3 to 8 anchors at different  $\kappa$  and  $\eta$  is same for 4 and more anchors. However, the only difference is observed for the 3 anchor's optimal placement.

### Impact of Scale (Field Dimension) on Optimal Anchors Placement

The analysis is further extended by increasing the scale from  $4 \times 4$  2-D plane to  $5 \times 5$  2-D plane. Fig. 5.6.1.2 shows the optimal anchor placement in a  $5 \times 5$  2-D plane for 3 to 5 anchors, where  $\kappa = 0.001$  and  $\eta = 4$ . It is noticeable that, optimal anchor placement is slightly different as the scale is changed from  $4 \times 4$  (Fig. 5.15) to  $5 \times 5$  (Fig. 5.6.1.2). However, this difference is only due to the even and odd dimensions. Further comparisons can be carried out between Fig. 5.17(a) - Fig. 5.17(c) for  $5 \times 5$  2-D plane and Fig. 5.17(d) - Fig. 5.17(f) for  $6 \times 6$  2-D plane, where anchors configuration is observed to be same, when avoiding the even and odd scaling factor. In the case of even scaling factor, field will be divided in to  $l/2$ ,  $l/2 - 1$  grid points, where  $l$  is the length of the field, which slightly deviate the angle for optimal placement.

## 5.6 Optimal Anchor Placements

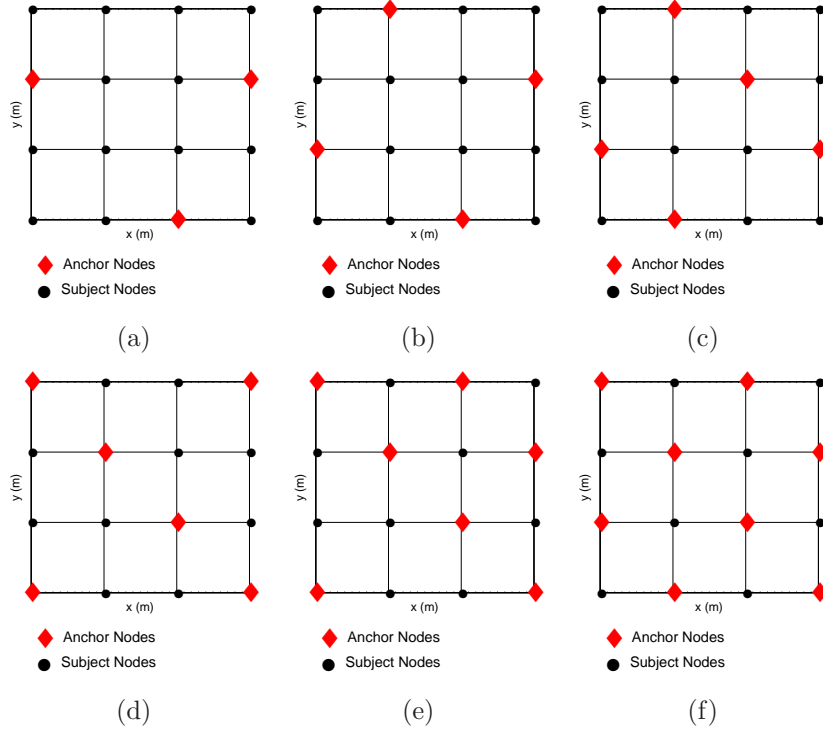


Figure 5.16: Optimal anchor placement for multiplicative noise model in a  $4 \times 4$  2-D plane for 3 to 8 anchors, where  $\kappa = 0.005$  and  $\eta = 2$ .

Fig. 5.18 shows the contour plot  $11 \times 11$  2-D plane for optimal anchor placement and corresponding minimum m-CRLB at  $\kappa = 0.001$  and  $\eta = 4$ . The white points in the contour plot represent the anchor placement, which is very similar to the Fig.5.17(a) - Fig. 5.17(c). When comparing with the optimal placement for additive noise model, it is noticed that when only 3 anchors are placed in a square area, the highest accuracy in the estimated location is achieved when the trio is placed at the centre of the square area. This square is of maximum size as 2 anchors are placed at the centres of one side of the square area while the 3<sup>rd</sup> anchor is placed a little below of the centre of the square. It is also noted that the bound increases as the subject node goes near any of the anchor nodes. The best location for 4 anchors is at the centre of each side of the square area while the best location for an additional 5<sup>th</sup> anchor is also the centre of the area.

Furthermore, to observe the impact of scale on m-CRLB,  $11 \times 11$  optimal placement is considered and compared with the  $21 \times 11$ ,  $31 \times 31$ , and  $41 \times 11$  as

## 5.6 Optimal Anchor Placements

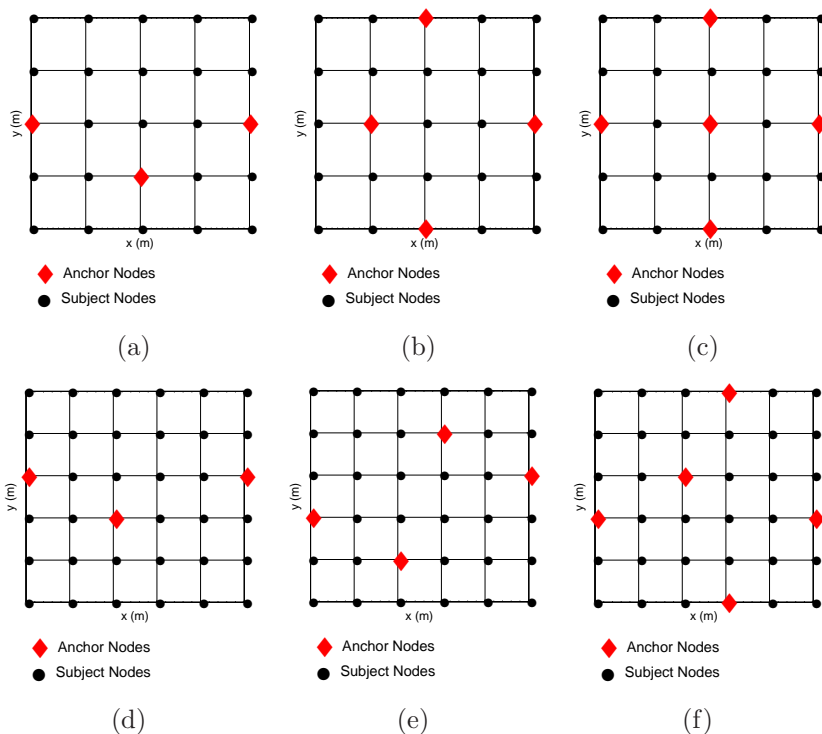


Figure 5.17: Fig. 5.17(a)-Fig. 5.17(c). Optimal anchor placement for multiplicative noise model in a  $5 \times 5$  2-D plane for 3 to 6 anchors, where  $\kappa = 0.001$  and  $\eta = 4$ . Fig. 5.17(d)-Fig. 5.17(f). Optimal anchor placement for multiplicative noise model in a  $6 \times 6$  2-D plane for 3 to 6 anchors, where  $\kappa = 0.001$  and  $\eta = 2$ .

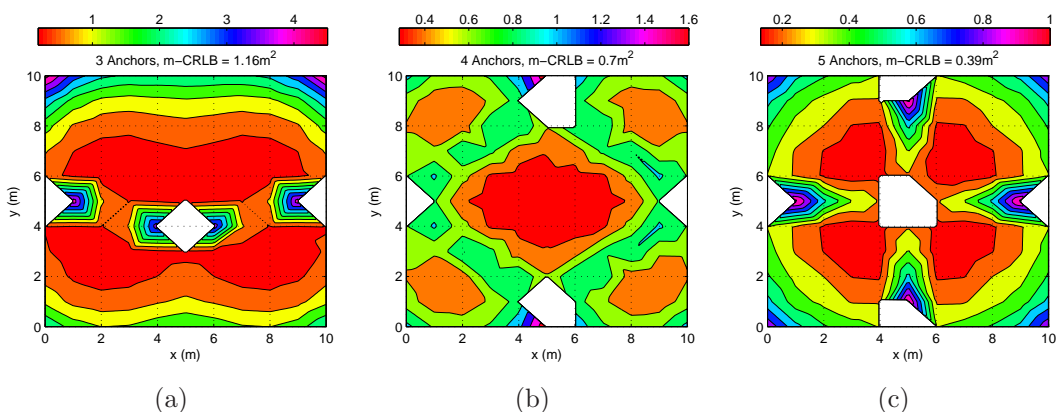


Figure 5.18: Optimal anchor placement and corresponding minimum m-CRLB at  $\kappa = 0.001$  and  $\eta = 4$  for multiplicative noise model using 3-5 anchor nodes for deployed subject nodes on  $11 \times 11$  2-D plane.

## 5.6 Optimal Anchor Placements

shown in Fig. 5.19 respectively. It can be observed that m-CRLB in Fig. 5.19 at each scale is different. This is because the  $\hat{\sigma}^2$  is not constant for each scale. It increases as the distance between the nodes increases (i.e. field dimension). It is therefore, unlike additive noise mode, m-CRLB for multiplicative depends on the scale. It is observable that that an increase in scale increases the m-CRLB however, the optimal anchor placement remains the same for each scale as shown above.

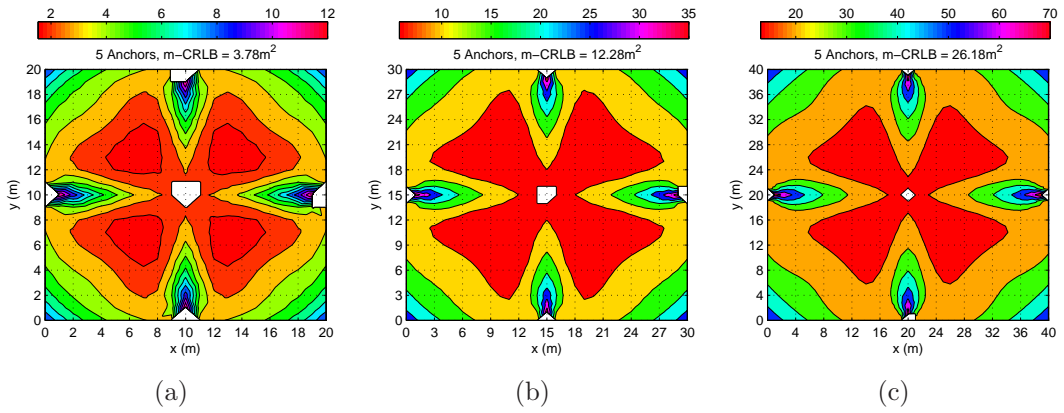


Figure 5.19: Optimal anchor placement and corresponding minimum m-CRLB at  $\kappa = 0.001$  and  $\eta = 4$  for multiplicative noise model using 5 anchor nodes for deployed subject nodes on  $21 \times 21$ ,  $31 \times 31$  and  $41 \times 41$  2-D space.

Fig. 5.20(a) - Fig. 5.20(f) show the worst placement for 3 to 8 anchors in 2-D space for multiplicative noise model. The worst anchor placement for multiplicative noise model is very similar to the additive noise mode, where all the anchor are placed at one side of the square.

### 5.6.1.3 CRLB Analysis of Anchor Node Constraints in 2-D

As discussed in chapter 4, In 2-D trilateration, no unique solution exists under the following two conditions.

1. If all the anchor nodes involved in trilateration are collinear.
2. If two of the anchor nodes involved to perform trilateration are co-incident.

## 5.6 Optimal Anchor Placements

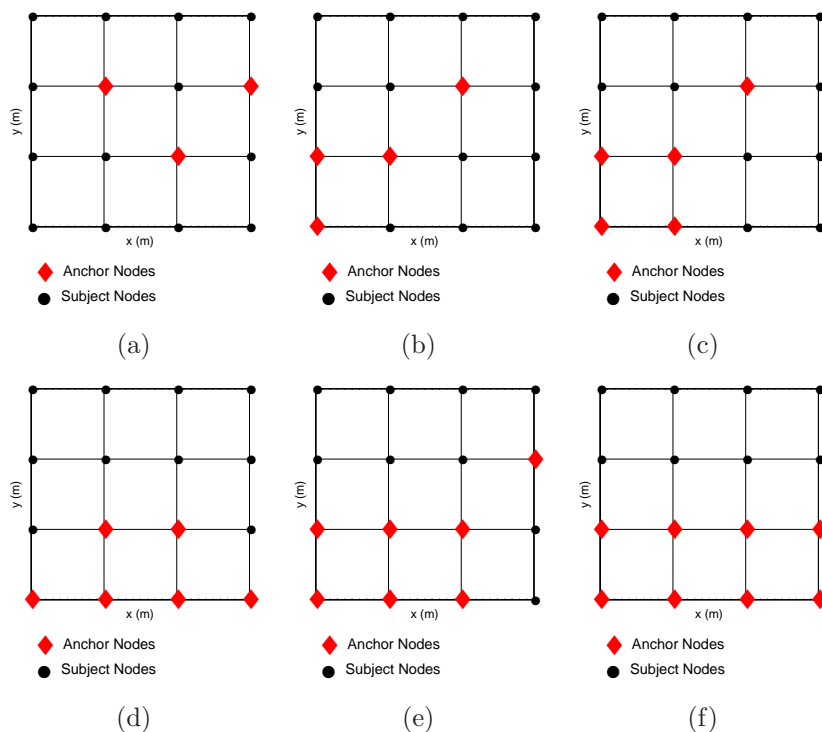
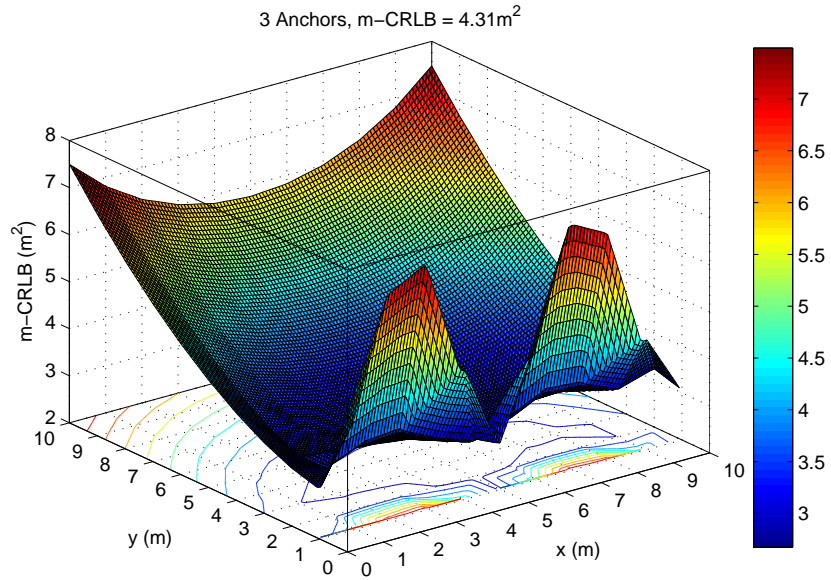


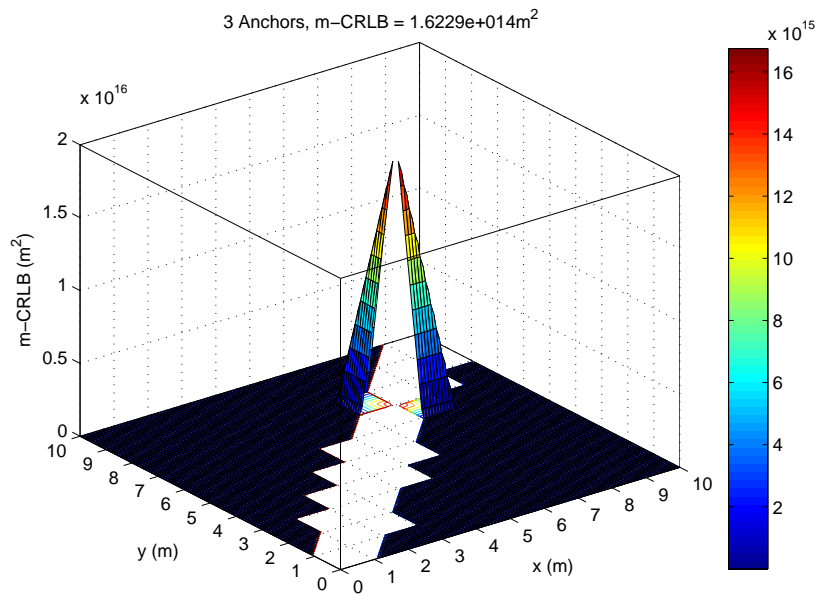
Figure 5.20: Worst anchor placement for multiplicative noise model in a  $4 \times 4$  2-D plane for 3 to 8 anchors, where  $\kappa = 0.001$  and  $\eta = 4$ .

Fig. 5.21(a) shows the CRLB for 3 anchors placed on a straight line as  $[0, 0]$ ,  $[5, 0]$ , and  $[10, 0]$ , whereas subject are place on each point of the  $10 \times 10$  grid in 2-D. There is no CRLB observed on a line where the 3 anchors were placed in a straight line (as shown by bottom row on x-axis in Fig. 5.21(a)). As the subject node moves away from the anchors straight line (i.e. closer to the centre of the field), a lower value of CRLB is observed, which gradually increases on the other side of the centre. Fig. 5.21(b) shows the CRLB for 3 anchors placed as  $[0, 0]$ ,  $[0, 0]$ , and  $[10, 10]$ , where two anchors are co-incident. The white diagonal in Fig. 5.21(b) shows the CRLB which reaches to infinity. In this case, LS algorithm does not bear enough information to decide on which side of the line determined by the anchors the final position lies, so it outputs results in ambiguity on both side.

## 5.6 Optimal Anchor Placements



(a)



(b)

Figure 5.21: Fig. 5.21(a). CRLB for 3 anchor nodes in 2-D, when anchor nodes are in a straight line ( $\sigma^2 = 2$  for all anchors). Fig. 5.21(b). CRLB for 3 anchor nodes in 2-D, when two of the anchor nodes are co-incident ( $\sigma^2 = 2$  for all anchors).

## 5.6 Optimal Anchor Placements

---

### 5.6.2 Three-Dimensional (3-D) Case

To determine the optimal anchor placement in 3-D, the 2-D simulation setup is extended into the 3-D. It is observed from 2-D results that, optimal anchor placement for additive noise model is independent of field dimensions (i.e. same optimal anchor placement is obtained at all scales). Based on this observation, optimal anchor placement for 4-8 anchors in 3-D is obtained in a small scale of  $3 \times 3 \times 3$  and extended to  $11 \times 11 \times 11$  scale.

#### 5.6.2.1 Optimal Anchor Placement for Additive Noise Model

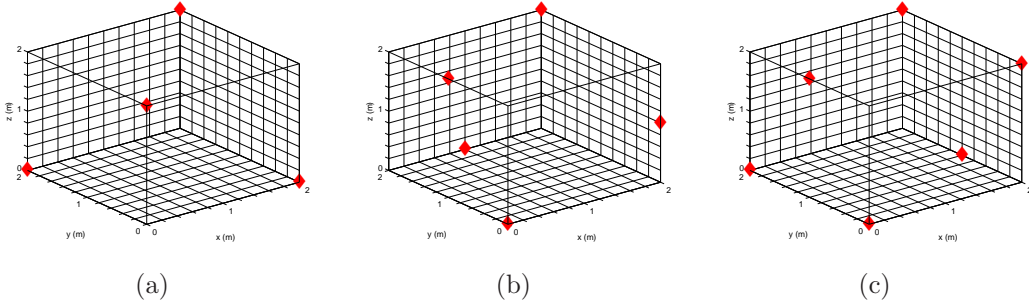


Figure 5.22: Optimal anchor placement for additive noise model in  $3 \times 3 \times 3$  3-D space for 4 to 6 anchors.

Fig. 5.22 shows optimal anchor placement for additive noise model in  $3 \times 3 \times 3$  3-D space for 4 to 6 anchors, which is further extended to  $11 \times 11 \times 11$  as shown in Fig. 5.23 for 4 to 8 anchors. The contour plots Fig. 5.24(a)-Fig. 5.24(e) are obtained for a constant  $\sigma^2$  for all cases (i.e.  $\sigma_i^2 = \sigma^2 = 2$ ). It is observed that when only 4 anchors are placed in a square area, the highest accuracy in the estimated location is achieved when the 4 anchors are placed at the corner of the square with diagonals on the same axis. The best location for 8 anchors is at each corners of the square area as shown in Fig. 5.24(e). Fig. 5.24(f) displays the m-CRLB as a function of the number of anchor nodes. As expected, as the number of anchors increases the variance effect on the m-CRLB becomes smaller and the bound increases as the target node goes near any of the anchor nodes.

## 5.6 Optimal Anchor Placements

---

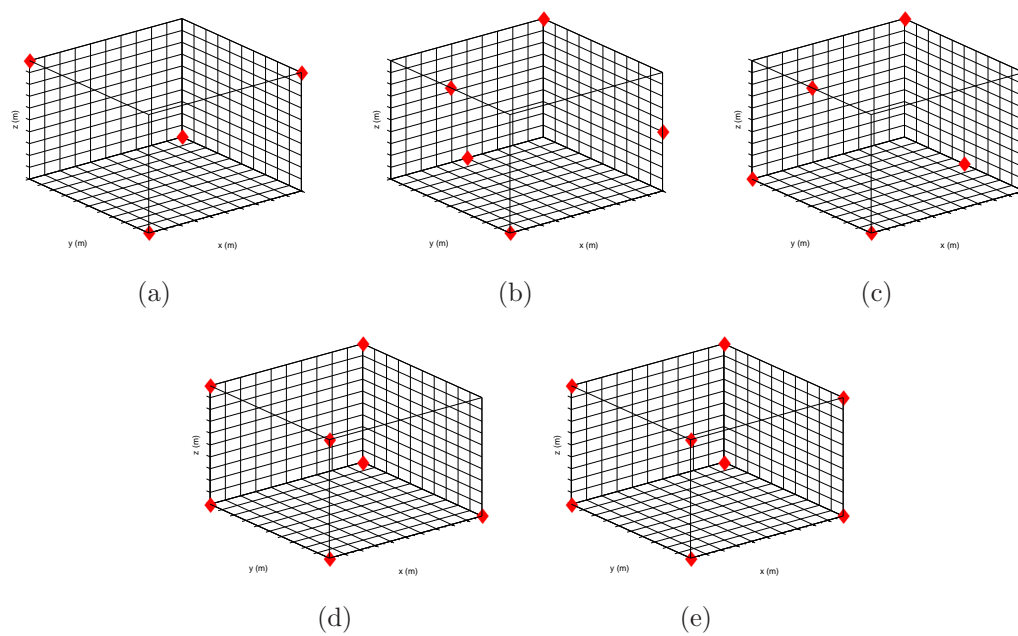


Figure 5.23: Optimal anchor placement for additive noise model in  $11 \times 11 \times 11$  3-D space for 4 to 8 anchors.

## 5.6 Optimal Anchor Placements

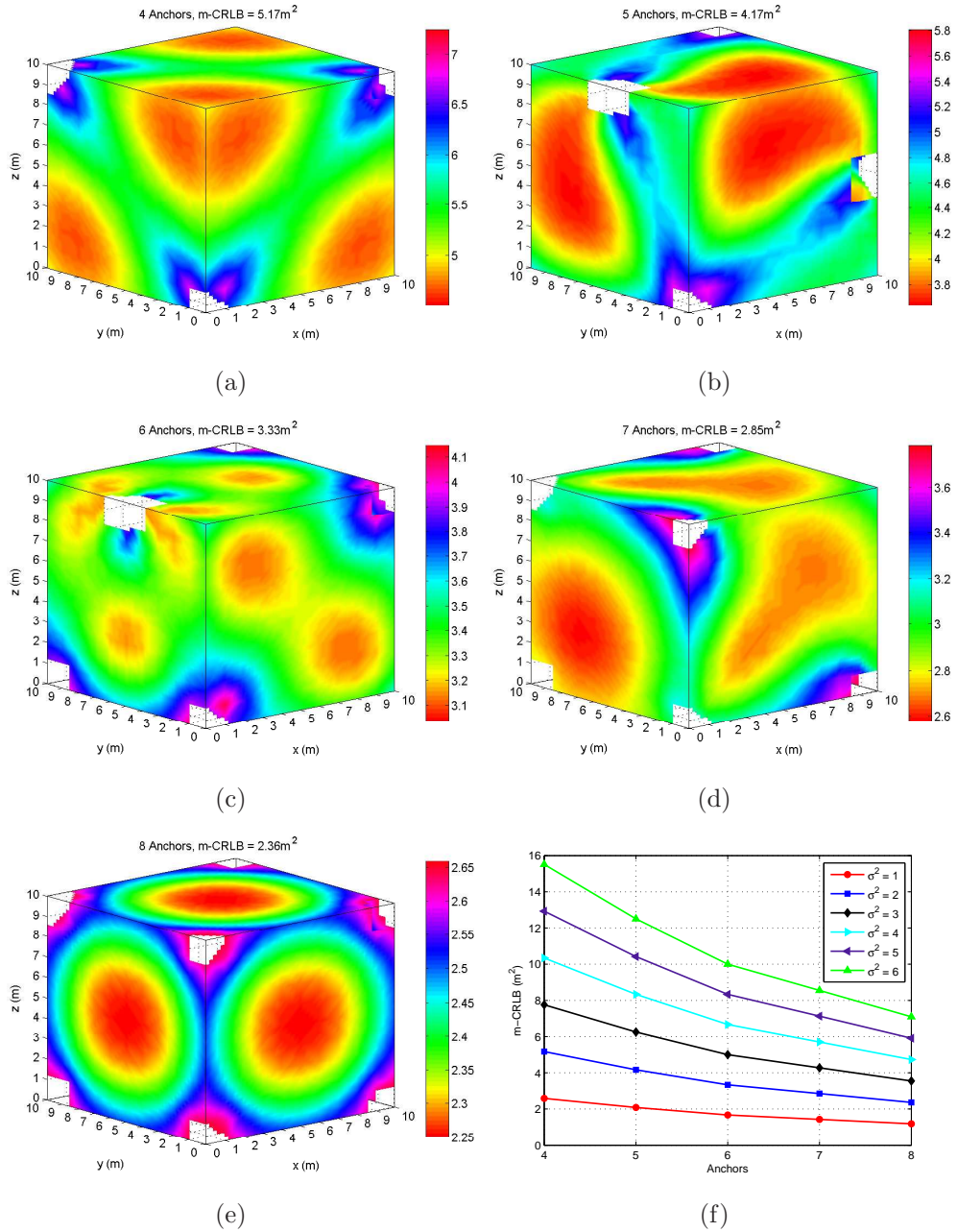


Figure 5.24: Optimal anchor placement and corresponding minimum m-CRLB for additive noise model for 4 to 8 Anchor nodes as shown in Fig. 5.23(a) - Fig. 5.23(e) for deployed subject nodes in  $11 \times 11 \times 11$  3-D space for  $\sigma^2 = 2$ .

## 5.6 Optimal Anchor Placements

---

Similar to 2-D case, optimal anchor placement in 3-D is also independent of the scale. It can be observed from Fig. 5.25, which shows contour plot for 8 anchors in  $5 \times 5 \times 5$  and  $12 \times 12 \times 12$ . The m-CRLB for both scales is found to be the same as for  $10 \times 10 \times 10$  scale in Fig. 5.24(e).

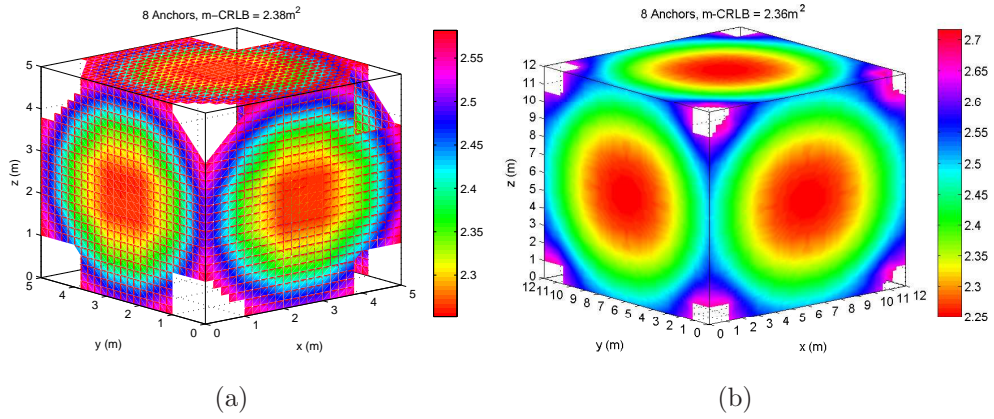


Figure 5.25: Optimal anchor placement for 8 anchor nodes in 3-D for two different scales. Fig. 5.25(a) for  $5 \times 5 \times 5$  scale. Fig. 5.25(b) for  $12 \times 12 \times 12$  scale.

## 5.6 Optimal Anchor Placements

---

### 5.6.2.2 Optimal Anchor Placement for Multiplicative Noise Model

Fig. 5.26(a)-Fig. 5.26(e) illustrate the multiplicative noise model contour plots  $\kappa = 0.001$  and  $\eta = 4$  using the number of anchor nodes placed at the optimal positions for the additive noise model as shown in Fig. 5.23. Similar to 2-D, when comparing the Fig. 5.26 and Fig. 5.24, a higher m-CRLB is observed for the multiplicative noise model than additive noise model for all 4 to 8 anchors. However, as explained above, this is not true for all values of  $\kappa$  and  $\eta$ . Similar to 2-D, it suggests that, the optimal anchor placement for multiplicative noise model is to be achieved in a similar fashion for 3-D as well.

Fig. 5.27 shows the optimal anchor placement for multiplicative noise model. Fig. 5.27(a) - Fig. 5.27(c) show the case 1, where  $\kappa = 0.005$  and  $\eta = 2$ , whereas Fig. 5.27(a) - Fig. 5.27(c) show the case 2, where  $\kappa = 0.001$  and  $\eta = 4$ . It can be observed from the Fig. 5.27(f) that optimal anchor placement is in the centre of the field to minimize the distance to all possible points. Since the noise in multiplicative noise model increases with the distance, It is therefore important to consider the optimal anchor placement in order to minimize the distance between anchor and subject nodes, hence noise. Based on the determined optimal anchor placements, it is observed that case 1 for 4 and 5 anchors is similar to additive noise model. Comparison of both results at small scale suggests that, optimal anchor placement for multiplicative model in 3-D depends on the value of  $\kappa$  and  $\eta$ . It can be observed from Fig. 5.27(a) and Fig. 5.27(d) for 4 anchors, which exhibit the different optimal placement due to the change in  $\eta$  from 2 to 4 and  $\kappa$  from 0.001 to 0.005. The analysis to optimal anchor placement in 3-D for multiplicative model is limited to the small scale at this stage, due to the limited high computing resources. It is further discussed in section 5.7.

## 5.6 Optimal Anchor Placements

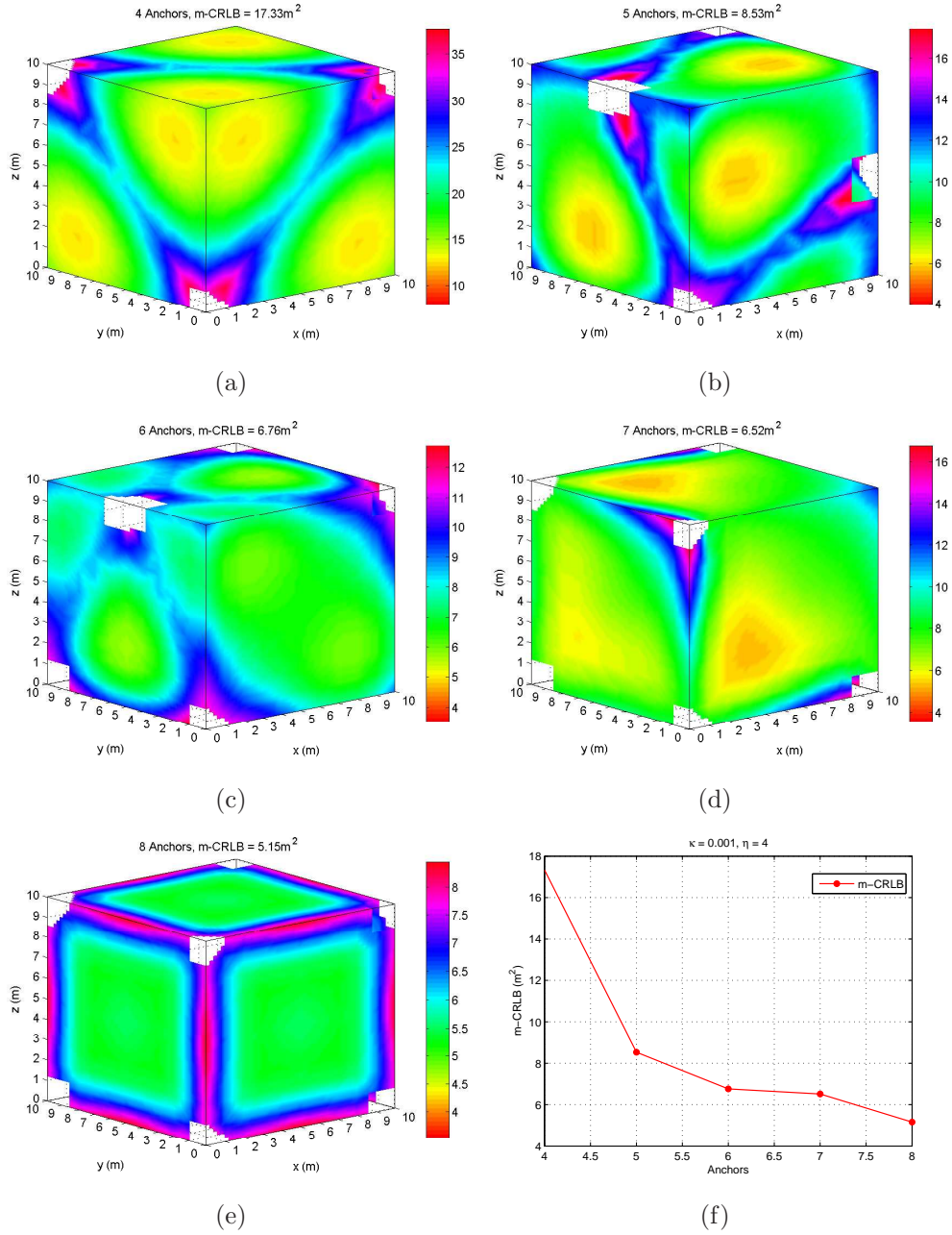


Figure 5.26: Suboptimal anchor placement and corresponding minimum m-CRLB for multiplicative noise model using 4 - 8 Anchor nodes as shown in Fig. 5.23(a) - Fig. 5.23(e) for deployed subject nodes on a  $11 \times 11 \times 11$  3-D space for  $\kappa = 0.001$  and  $\eta = 4$ .

## 5.6 Optimal Anchor Placements

---

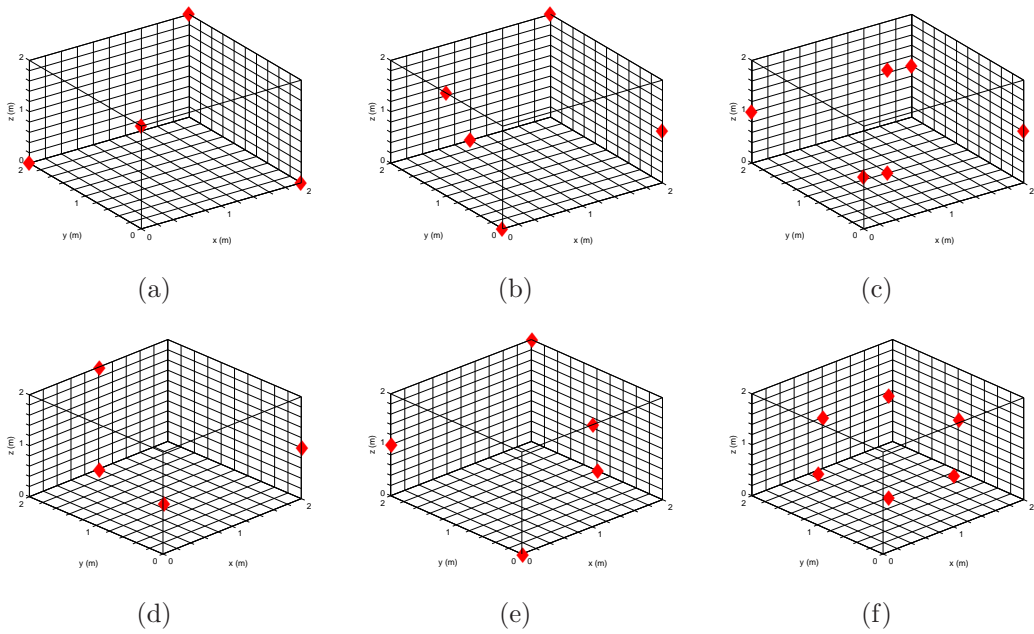


Figure 5.27: Optimal anchor placement for multiplicative noise model in  $3 \times 3 \times 3$  3-D space for 4 to 6 anchors. Fig. 5.27(a) - Fig5.27(c). For  $\kappa = 0.005$  and  $\eta = 2$ . Fig. 5.27(d) - Fig5.27(f). For  $\kappa = 0.001$  and  $\eta = 4$ .

## 5.6 Optimal Anchor Placements

---

### 5.6.2.3 CRLB Analysis of Anchor Node Constraints in 3D

In 3-D, no unique solution exists if all the anchor nodes involved in trilateration are placed on a single plane. Fig. 5.28 shows the CRLB for 4 anchors placed on a single plane as  $[0, 0, 0]$ ,  $[10, 0, 0]$ ,  $[10, 10, 0]$  and  $[0, 10, 0]$  in 3D. There is no CRLB observed at the bottom of field (spotted by white rows and column), where the anchors are placed as a single plane. The 2-D and 3-D mathematical consequence of anchor nodes constraints, which lead to no solution, is that the matrix expression will be singular.

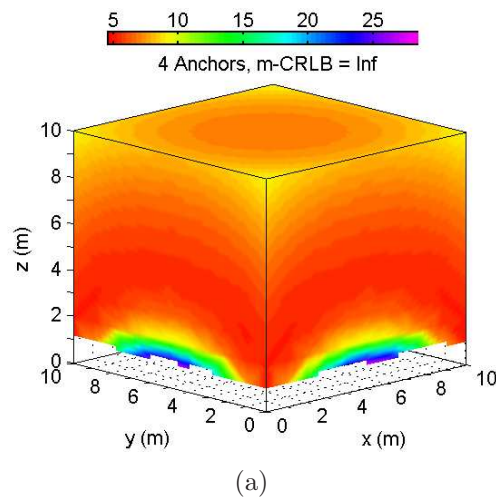


Figure 5.28: CRLB for 4 anchor nodes in 3-D, where anchor nodes are placed on a single plane.

### 5.7 Discussion

In this chapter, optimal anchors placement is determined and analysed by exploiting the additive and multiplicative noise models for both 2-D and 3-D case. In the light of extensive simulation analysis the following are the main observations.

- Optimal anchor placement for both additive and multiplicative noise models is different.
- Optimal anchor placement for additive noise model is independent of field dimensions (scale) and depends only on the relative angle between subject and anchor node.
- m-CRLB of additive noise model for  $N$  number of anchor nodes would be constant regardless of changing the field dimension.
- Similar to additive noise model, optimal anchor placement for multiplicative noise model is also independent of field dimension.
- Unlike additive noise model, m-CRLB of multiplicative noise model for  $N$  number of anchors will increase with the increase of field dimension. In addition to that, increasing the value parameters ( $\kappa$  and  $\eta$ ) will also increase the m-CRLB. However, optimal anchor placement will be the same. However, the only difference in optimal placement can be observed due to the even or odd dimensions (i.e. optimal placement for even dimension can be slightly different from odd dimensions due to the centre point.)

Furthermore, looking at the contour plots, it is observed that:

- There is no CRLB (i.e. a singular matrix), when the  $[x_i, y_i] = [x_j, y_j]$ , as shown by white points in contour plots.
- A lower value of CRLB is observed, when a subject nodes moves away from a single anchor node toward the centre of the 3 anchor nodes.
- An increase in CRLB is observed, when a subject node moves outside of the anchor nodes surrounding.

## 5.7 Discussion

---

- A higher value of CRLB is observed when anchor nodes are placed very close to each other as shown by worst anchor placement.

In addition to that it is observed that the computational complexity increases with the increase of field dimensions, where each grid point is analysed in a sequence so that none of the point misses out, which may turn into the optimal placement. As the number of combinations increases, MATLAB generates the 'Out of Memory' errors, which suggests that system has in fact run out of heap space to hold all of the variables. Hence, there is no unallocated virtual address space on system for MATLAB to use, and therefore no new variables can be created. Apart from this, memory fragmentation is also a cause of 'Out of Memory' errors. It suggest that, there can be free memory available, but there is no contiguous piece of memory that is large enough to hold the specified variables. When virtual memory is used and freed during normal operation of MATLAB, memory becomes fragmented. This means that the amount of total free memory is greater than or equal to the amount of contiguous free memory. Since a matrix in MATLAB must be stored in a contiguous block of virtual memory, the largest matrix that can be created at a particular point in time is limited by the amount of contiguous free virtual address space. However to avoid the memory problem, an effort is made to divide the simulation code into sub-blocks and for each sub-block code, a separate desktop/laptop machine is used, where fragmentation (i.e. clearing unwanted variables, writing existing variables off to disk, and then reloading) is performed before and during each simulation run.

An extension of 3-D from 2-D increased the complexity, where  $z$ -axis is taken into the account. In a scale like  $5 \times 5 \times 5$ , an anchor node can be placed on 125 difference placements. Hence for 4 anchors in 3-D, a total combination of 969,137,5 anchor placements. In order to calculate the m-CRLB, each subject location (125 in total) individually calculates the CRLB at each anchor placement (969,137,5). It means that in total  $125 \times 969,137,5 = 1.2114 \times 10^9$  calculations to determine the m-CRLB. The computational complexity of this simulation requires the high computing resources. Regardless of the computational complexity and limited high computing resource, this chapter presents the optimal anchor placement for

## 5.8 Conclusion

---

3 to 8 anchors for both additive and multiplicative noise models in 2-D and as well as 3-D.

## 5.8 Conclusion

Range aware localization in WSNs has been intensively studied in recent years by assuming: 1) the arbitrary anchor placements; 2) the use  $n$  number of anchor nodes to enhance the localization accuracy; 3) the use of same arbitrary anchor placement regardless of the signal model (i.e. additive and multiplicative); 4) computationally expensive refinement process to extract a set of optimal anchors (i.e. GDOP based or exploiting angular information between nodes); 5) solutions limited to 2-D plane. Unfortunately, in resource constraint WSNs these assumptions are not truly applicable. This chapter presents the optimized anchor placements based on the minimum CRLB. The CRLB for the accuracy on localization in a 3-D environment is derived as a function of the elevation and azimuth angle. The optimality in the anchor placement for both noise models has been achieved by choosing the combination of anchors with the minimum m-CRLB in both 2-D and 3-D environments. The purpose of the determining the optimal anchor placement is to maximize the localization performance by reducing the uncertainty in localization error due to arbitrary anchor placements, which is demonstrated in chapter 4 through geometric dilution of precision (GDOP).

To evaluate the effectiveness, it is required to compare the localization performance at determined optimal placement with arbitrary anchor placement in both 2-D and 3-D environments. The motivation to address performance analysis at optimized anchor placements leads to the next chapter (chapter 6), which presents the localization at optimal and arbitrary anchor placements and their comparison with m-CRLB using least squares (LS) and approximate maximum likelihood (AML) methods.

# Chapter 6

## Localization Performance at Optimized Anchor Placement

### 6.1 Introduction

This chapter presents the performance analysis of optimized anchor placement (as determined and discussed in chapter 5). To analyse localization performance for optimized anchor placement in 2-D and 3-D, a simulation tool is developed with LS and AML method for position estimation in MATLAB. The LS method is explained in chapter 4, whereas AML is discussed in chapter 2 and therefore not included in this chapter. Based on simulation results, It is confirmed that the optimal anchor placement of the minimum number of anchors outperforms the degraded deployment of many nodes. Fig. 6.1(a) shows the screen shot of the 2-D system, whereas 3-D system is illustrated in Fig. 6.1(b). In both cases, subject nodes are placed at each grid point (i.e. for  $11 \times 11$  field, a total of 121 subject nodes are placed, where subject nodes with same anchor positions are avoided). The simulation tool calculates the distance between anchor and subject nodes based on the additive and multiplicative noise model as discussed in chapter 5. It is assumed that network is connected and the optimally placed anchor nodes are aware of their location.

As a performance metric, MSE as given by  $MSE = \text{Tr}(E\{(\hat{s} - s)(\hat{s} - s)^T\})$  is considered. The MSE for all target locations is computed and its mean is compared with the m-CRLB. Table 6.1 lists the network simulation parameters

## 6.1 Introduction

---

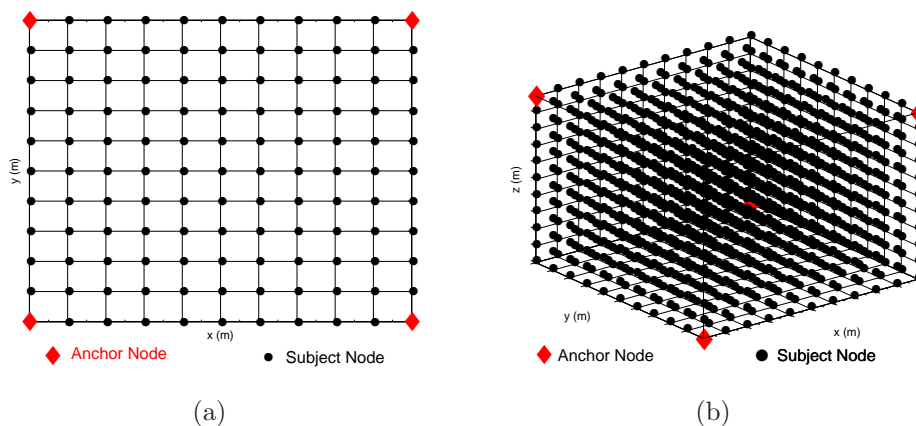


Figure 6.1: Fig. 6.1(a). Simulation setup in 2-D plane. Fig. 6.1(b). Simulation setup in 3-D space.

whereas Fig. 6.2, Fig. 6.3 and Fig. 6.4 shows the arbitrary anchor placement 1, 2 and 3 respectively whose performance is compared with the optimal anchor placement for additive and multiplicative noise models as shown in chapter 4.

Parameters	2-D Case	3-D Case
Area(m)	$11 \times 11, 5 \times 5$	$11 \times 11 \times 11$
Subject Nodes	121, 25	1331
Anchor Nodes	3, 4, 5, 6, 7, 8	4, 5, 6, 7, 8
$\sigma^2$ (m <sup>2</sup> )	1, 3, and 5	1, 3, and 5
$\eta$	2.0, 2.4, 2.8, 3.2, and 3.6	2.0, 2.4, 2.8, 3.2, and 3.6
$\kappa$	0.001, 0.002, 0.003, and 0.004	0.001, 0.002, 0.003, and 0.004
Iterations	300	200
Iterations for AML	5	5

Table 6.1: Network Simulation Parameters to analyse the anchor placement.

## 6.1 Introduction

---

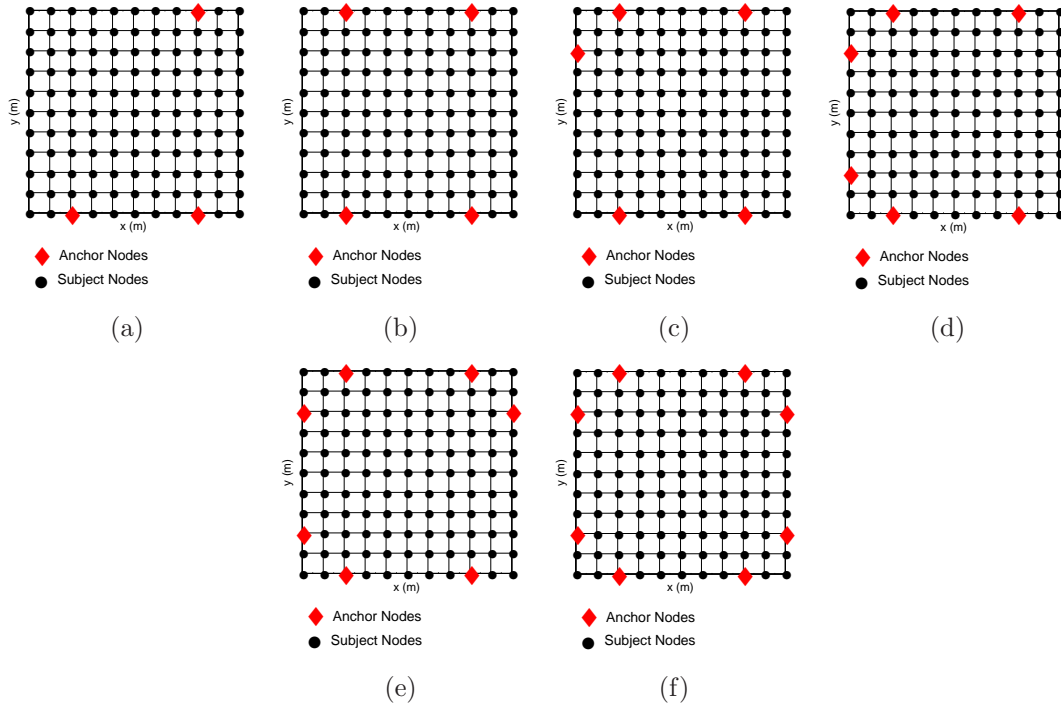


Figure 6.2: Arbitrary anchor placement 1 in  $10 \times 10$  2-D space for 3 to 8 anchors.

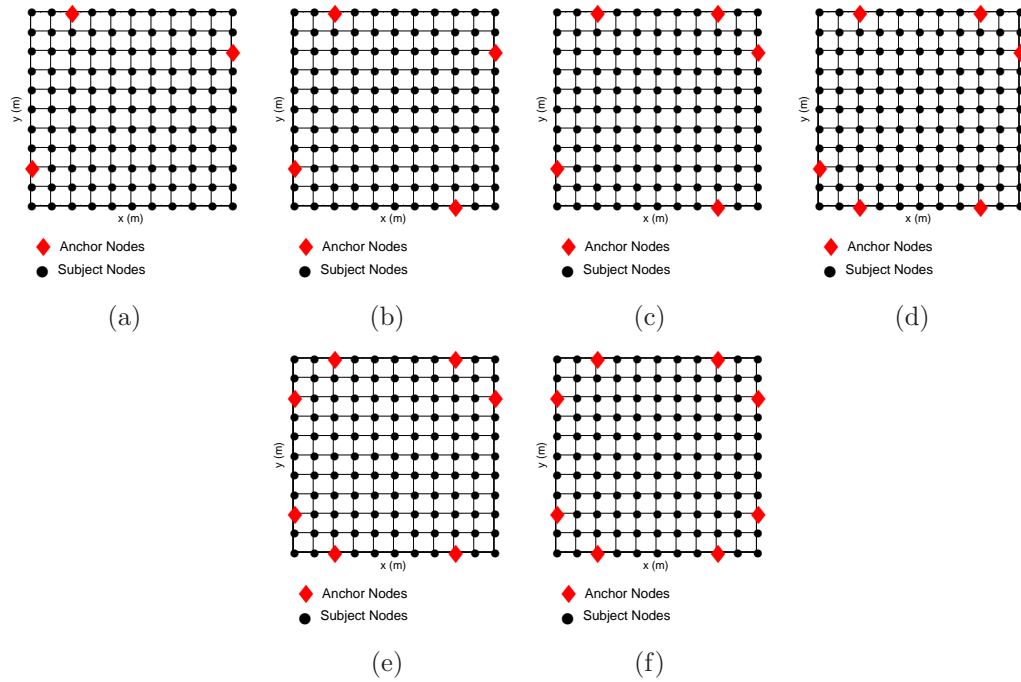


Figure 6.3: Arbitrary anchor placement 2 in  $10 \times 10$  2-D space for 3 to 8 anchors.

## 6.1 Introduction

---

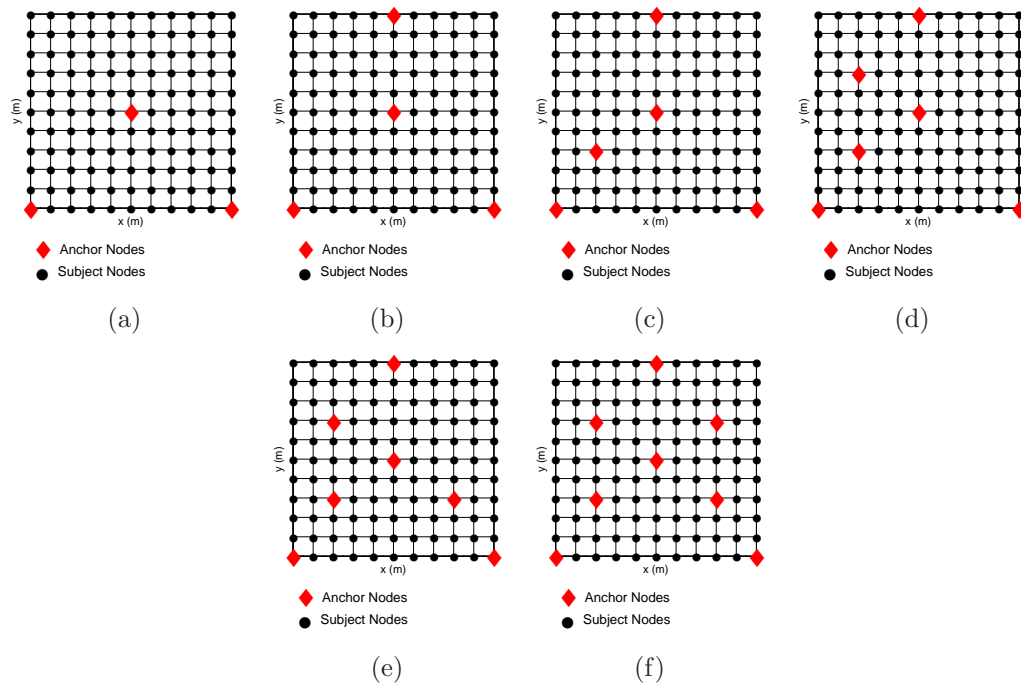


Figure 6.4: Arbitrary anchor placement 3 in  $10 \times 10$  2-D space for 3 to 8 anchors.

## 6.2 2-D Case: Additive and Multiplicative Noise Model

Fig. 6.5(a)-Fig. 6.5(b) compares the MSE of the LS method with the m-CRLB for the additive noise model for optimal (Fig. 5.8) and arbitrary anchor placement as shown in Fig. 6.2, Fig. 6.3 and Fig. 6.4 respectively. The variance is  $\sigma^2 = 1$  and 5 for Fig. 6.5(a) and Fig. 6.5(b) respectively. The plot shows the performance for 3-8 anchors. As expected, increasing the  $\sigma^2$  for a given set of nodes, increases the MSE and also the difference between the bound and MSE. However, it can be observed that the localization performance at determined optimal anchor placement is better than the arbitrary anchor placements. With the increase in  $\sigma^2$ , the MSE difference between optimal and arbitrary anchor placement for 3 anchors increases as compared to 4 and more anchors. For example, the MSE difference for 3 anchors at optimal placement and arbitrary anchor placement 1 for  $\sigma^2 = 1$  is  $2.38\text{m}^2$ . This difference is further increased to  $5.67\text{m}^2$  for  $\sigma^2 = 5$ . Furthermore, it is observed that, as the number of anchor node increased from 6 to 8, LS showed a very close performance for optimal placement and arbitrary placement 1 and 2. This is because many of the anchors are placed on the boundary of the field in a similar fashion as of additive's optimal instead of the centre (arbitrary anchor placement 3). It should be noted that the MSE error for the 8 anchors at arbitrary placement 3 and for 6 anchors at arbitrary placement 1 and 2 is larger than those of 4 optimally placed anchors.

Fig. 6.6(a)-Fig. 6.5(b) compares the MSE of the AML method with the m-CRLB for the additive noise model for optimal (Fig. 5.8) and arbitrary anchor placement as shown in Fig. 6.2, Fig. 6.3 and Fig. 6.4. The variance is  $\sigma^2 = 1$  and 5 for Fig. 6.6(a) and Fig. 6.6(b) respectively. The plot shows the performance for 3-8 anchors. Similar to LS method, MSE for AML method at optimal anchor placement was found to be very close for 4 and more anchors at arbitrary anchor placements 1 and 2, whereas a significant difference is observed for all anchors at arbitrary anchor placement 3. Compared to LS method, it is noted that MSE error for AML approaches closer to the m-CRLB as the number anchors increases for each anchor placement. Further analysis on AML and LS is given below.

## 6.2 2-D Case: Additive and Multiplicative Noise Model

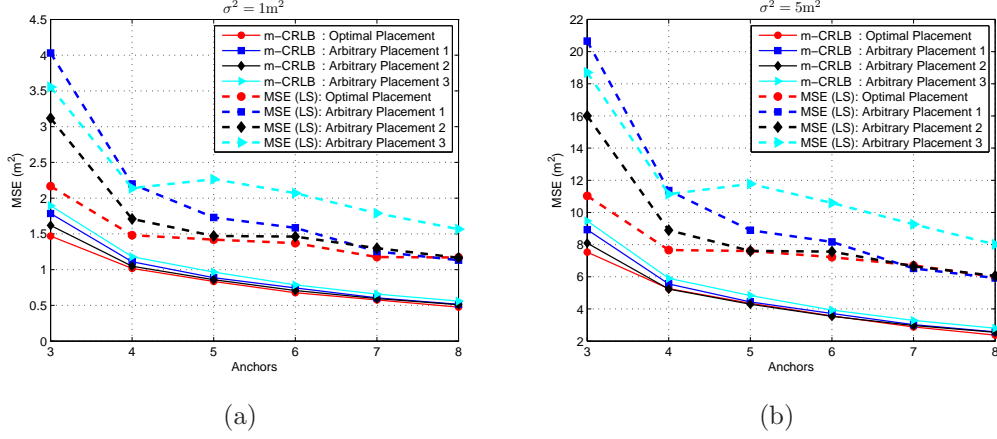


Figure 6.5: Performance of the LS method for additive noise model at optimal and arbitrary anchor placement and comparison with m-CRLB.

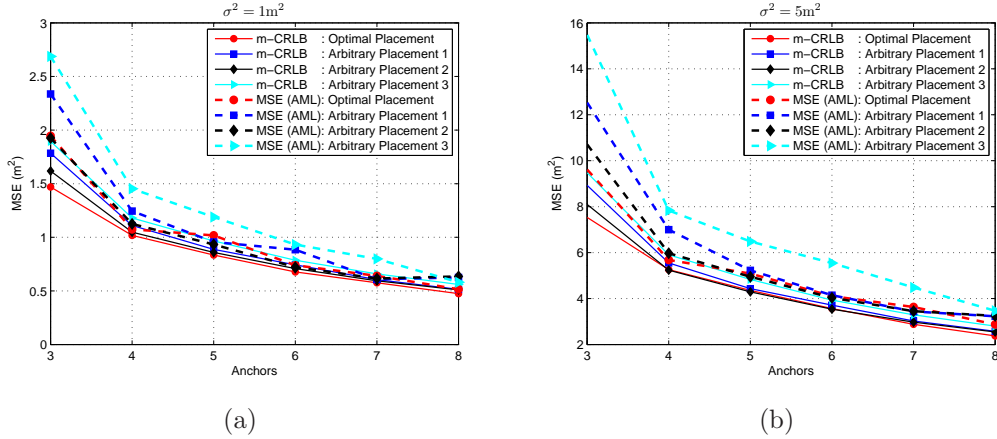


Figure 6.6: Performance of the AML method for additive noise model at optimal and arbitrary anchor placement and comparison with m-CRLB.

Fig. 6.7 shows the performance comparison between LS and AML methods at optimal and arbitrary anchor placements for  $\sigma^2 = 1$  and 5. It can be observed that at optimal anchor placement, AML outperforms LS (optimal and arbitrary anchor placement) for all number of anchors. It is important to note that at arbitrary anchor placement 3, AML outperforms LS at optimal anchor placement for 5 and more anchors. It suggests that AML with 5 arbitrary anchor nodes can outperform LS at optimal placement. Furthermore, Fig. 6.7(c) shows the comparison based on the worst anchor placement. It can be seen that MSE for

## 6.2 2-D Case: Additive and Multiplicative Noise Model

AML at  $\sigma^2 = 5$  is nearly attaining the MSE for LS at  $\sigma^2 = 1$ . The difference increases with the increase of number of anchor nodes. However, it is noticeable from Fig. 6.7(a) and Fig. 6.7(b) that optimal anchor placement for both LS and AML methods illustrate lower MSE compared to arbitrary and worst anchor placement.

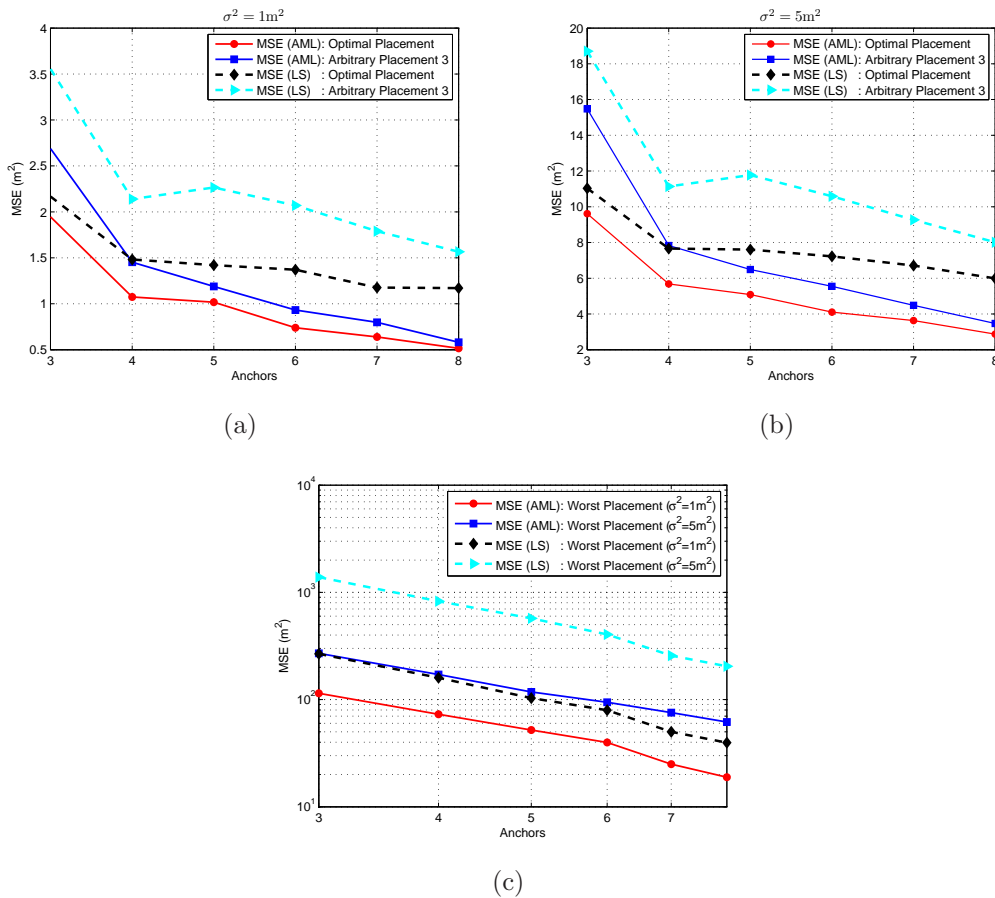


Figure 6.7: Performance comparison of LS and AML method for additive noise model at optimal and arbitrary anchor placement.

For AML method (discussed in chapter 2), one of the major highlighting points is that AML treats the distance equations as non-linear equations. Based on the available anchor positions, it determines a guess value for a subject node. For each guess, it uses  $n$  iterations and for each iteration it estimates a new subject position in order to converge the guess very close to the subject node,

## 6.2 2-D Case: Additive and Multiplicative Noise Model

hence minimizing the cost function. The performance of AML increases as the number of iterations to converge the guess position (minimizing the cost function) increases. After  $n$  iterations, it selects the estimated location that provides the least value of the cost function. Regarding LS, it is a simple algorithm that heavily relies upon the reference node and has only one possible opportunity to estimate the location. Therefore, under any given channel conditions AML will provide better performance. However, the computational complexity of AML is a trade off compared to LS.

Fig.6.8 shows the behaviour of the m-CRLB and MSE when the multiplicative noise model is used while the anchors are optimally placed as derived for the additive noise model and compared with arbitrary placement 2. It can be seen from Fig. 6.8(a) and Fig. 6.8(b) that m-CRLB of arbitrary anchor placement is better than the additive's optimal. In addition, the LS and AML both showed better accuracy compared to the additive's optimal. In other words, arbitrary anchor placement for the additive noise model could perform better for the multiplicative noise models than optimal anchor placement due to the fact that both noise models demonstrate different optimal placements. Therefore, optimal anchor placement specific to signal model is a major factor to enhance localization performance.

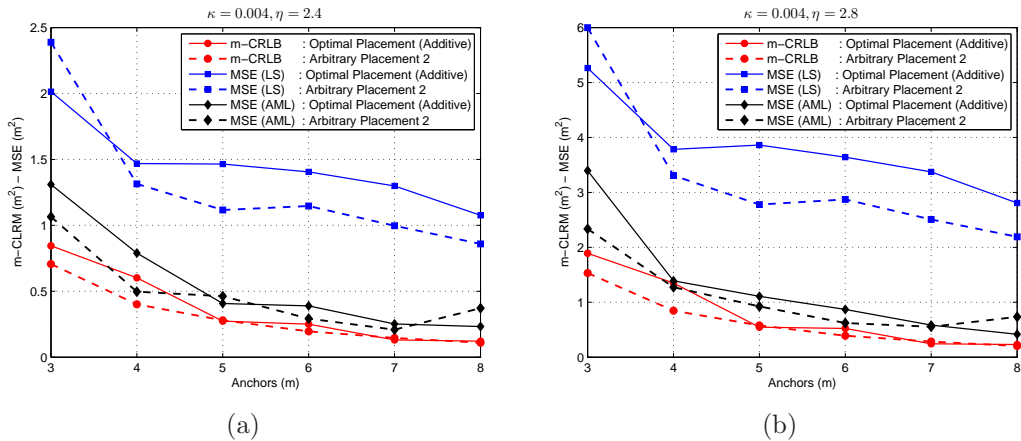


Figure 6.8: Performance comparison of LS and AML method for multiplicative noise model at additive's optimal placement with arbitrary anchor placement.

Fig. 6.9(a) and Fig. 6.9(b) compare the performance analysis of multiplicative

## 6.2 2-D Case: Additive and Multiplicative Noise Model

noise model at optimal and arbitrary anchor placements for  $\kappa = 0.001$  and  $\eta = 4$  in  $5 \times 5$  and  $11 \times 11$  2-D plane. The optimal placement for multiplicative noise model is as shown in Fig. 5.17(a) - Fig. 5.17(c) for  $5 \times 5$  and for  $11 \times 11$  in Fig. 5.18. The arbitrary placement considered for the comparison is the one, which is optimal for the additive noise model as shown in Fig. 5.8. It can be seen from Fig. 6.9(a) and Fig. 6.9(b) that optimal placement for multiplicative noise model show better performance for 4 and more anchors. It is observed due to the fact that, the optimal anchor placement for 3 anchors for multiplicative noise model is closer to the straight line. Thus for LS solution will be closer to singular matrix compared to any arbitrary position. Furthermore, AML with multiplicative's optimal placement outperformed arbitrary placement for 3 and more anchors.

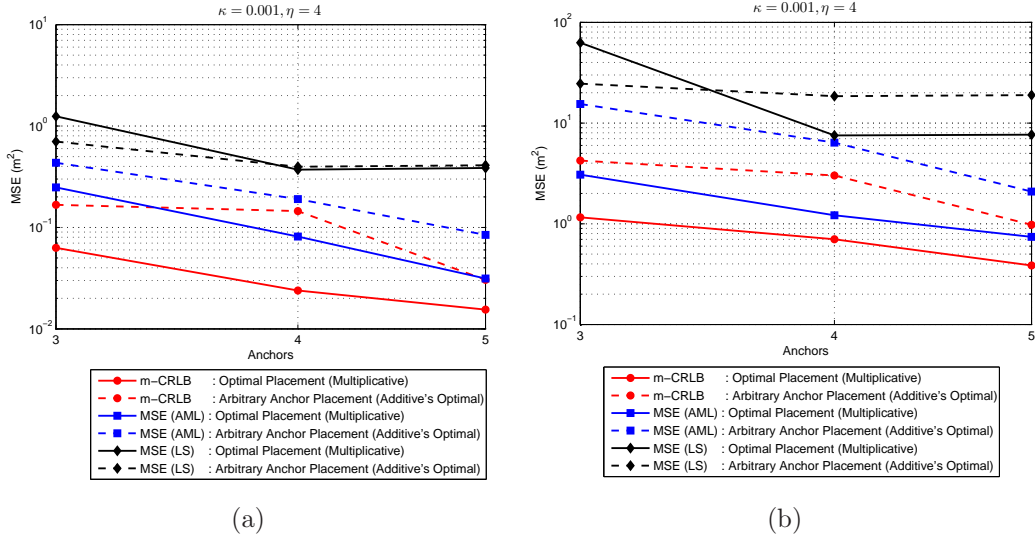


Figure 6.9: Performance of the LS and AML method for multiplicative noise model for  $\kappa = 0.001$  and  $\eta = 4$  at optimal and arbitrary anchor placement and comparison with m-CRLB. Fig. 6.9(b). For  $5 \times 5$ , where optimal placement for multiplicative noise model is as shown in Fig. 5.17(a) - Fig. 5.17(c). Fig. 6.9(a). For  $11 \times 11$ , where optimal placement for multiplicative is as shown in Fig. 5.18.

## 6.3 3-D Case: Additive and Multiplicative Noise Model

Similar to 2-D, this section demonstrates the performance analysis of localization using LS and AML methods at optimal anchor placement in 3-D space. As discussed in chapter 5, an extension from 2-D to 3-D not only adds another dimension but it also increases the complexity in terms of the computation. The complexity to handle the huge amount of data sets require high computing resources. To reduce the computational complexity, number of iterations are reduced to 200 from 300. To analyse the performance of optimal anchor placement for 4 to 8, three arbitrary anchor placements are considered as shown in Fig. 6.10, Fig. 6.11 and Fig. 6.12 respectively.

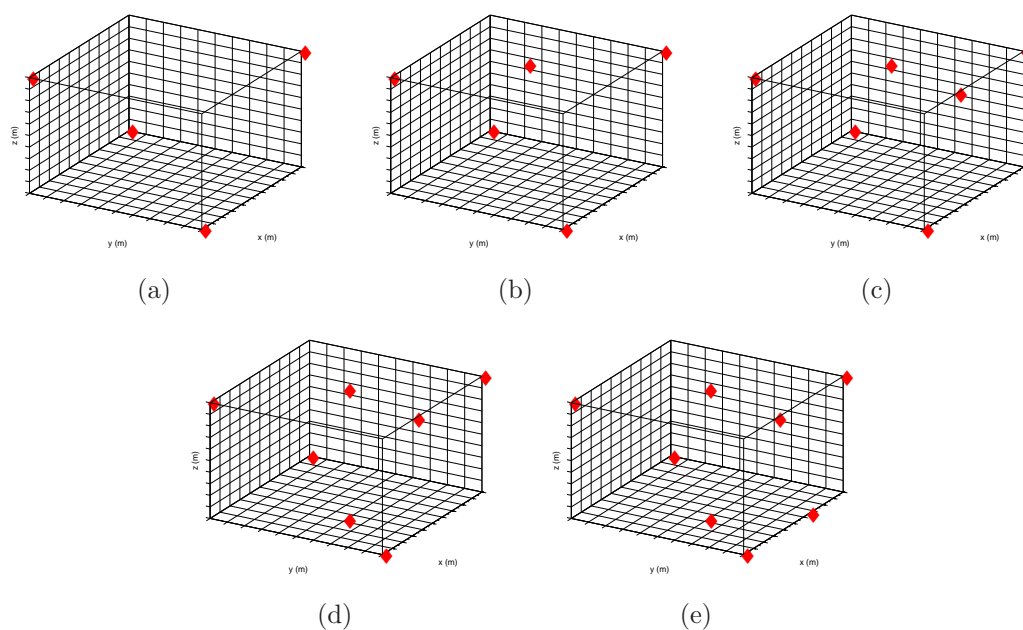


Figure 6.10: Arbitrary anchor placement 1 in  $10 \times 10 \times 10$  3-D space for 4 to 8 anchors.

Fig. 6.13(a)-Fig. 6.13(b) compares the MSE of LS method with m-CRLB for the additive noise model at optimal (Fig. 5.8) and arbitrary anchor placement as shown in Fig. 6.10, Fig. 6.11 and Fig. 6.12. The variance is  $\sigma^2 = 1$  and 5 for Fig. 6.13(a) and Fig. 6.13(b) respectively. The plot shows localization performance

### 6.3 3-D Case: Additive and Multiplicative Noise Model

---

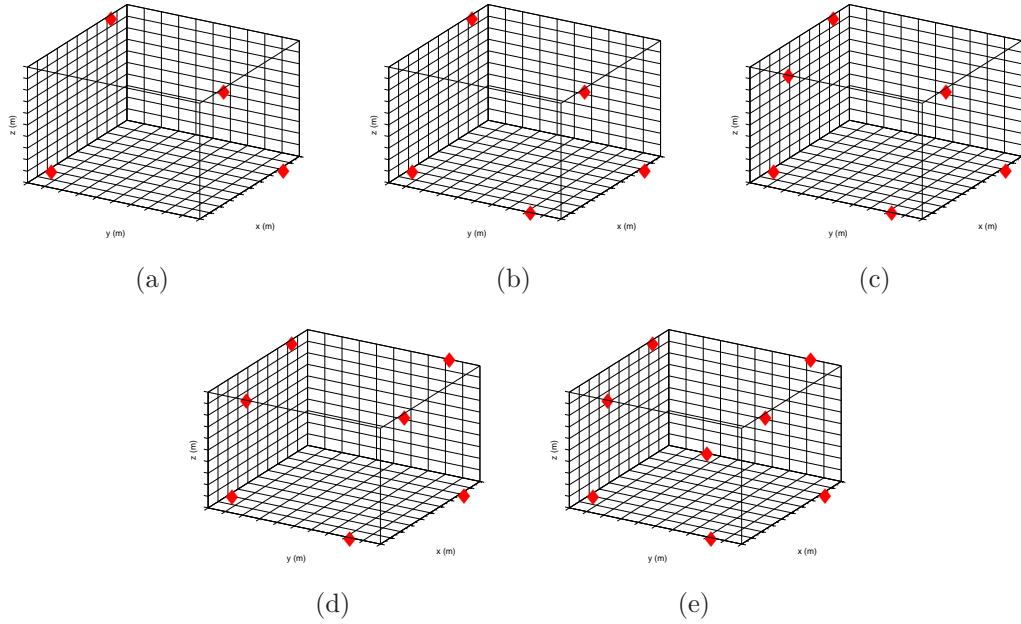


Figure 6.11: Arbitrary anchor placement 2 in  $10 \times 10 \times 10$  3-D space for 4 to 8 anchors.

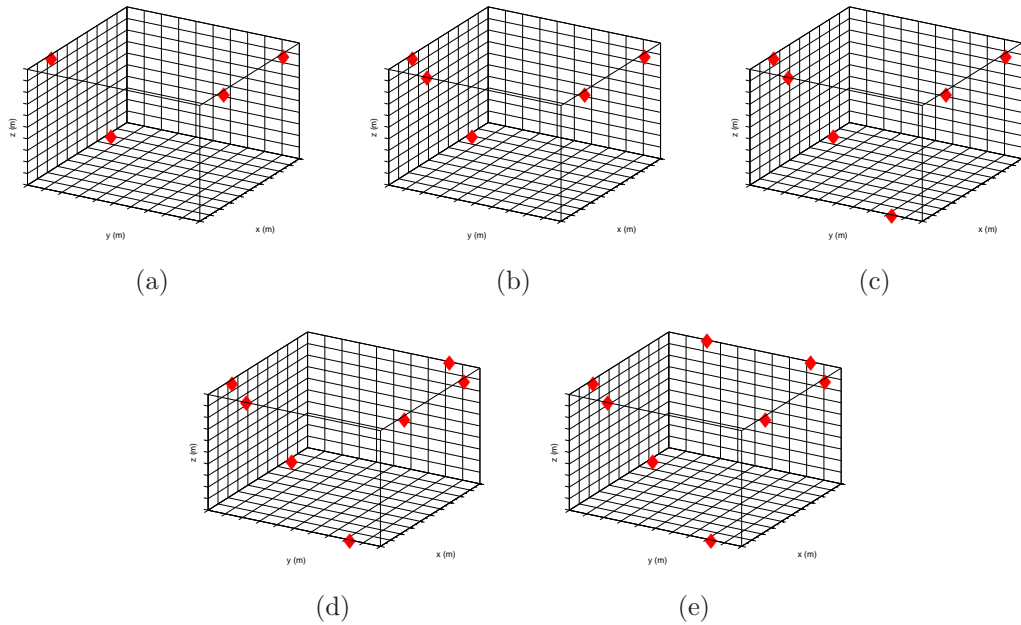


Figure 6.12: Arbitrary anchor placement 3 in  $10 \times 10 \times 10$  3-D space for 4 to 8 anchors.

### 6.3 3-D Case: Additive and Multiplicative Noise Model

for 4-8 anchors. As expected, localization performance at determined optimal anchor placement is better compared to arbitrary anchor placements. However, for 4 anchors, arbitrary anchor placement 2 (Fig. 6.11) showed exactly the same performance, it is due to the fact that optimal and arbitrary anchor placement 2 for 4 anchors are same. However, it can be seen that, for 5 and more anchors, optimal anchor placement outperforms arbitrary anchor placements. Furthermore,

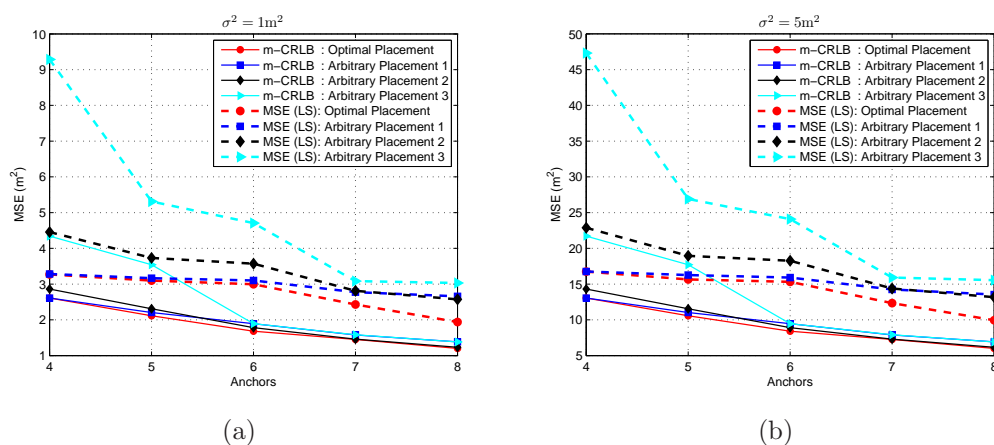


Figure 6.13: Performance of the LS method for additive noise model at optimal and arbitrary anchor placement and comparison with m-CRLB.

Fig. 6.14 and Fig. 6.15 demonstrated the same results as observed in 2-D. However, it is observed that an extension from 2-D to 3-D generated the higher MSE at the same level of variance  $\sigma^2 = 1$  and  $\sigma^2 = 5$ . It is verified that in realistic environment, a system based on the 2-D plane is likely to generate less error compared to 3-D. It is therefore important to observe the real time environment with respect to 3-D localization.

### 6.3 3-D Case: Additive and Multiplicative Noise Model

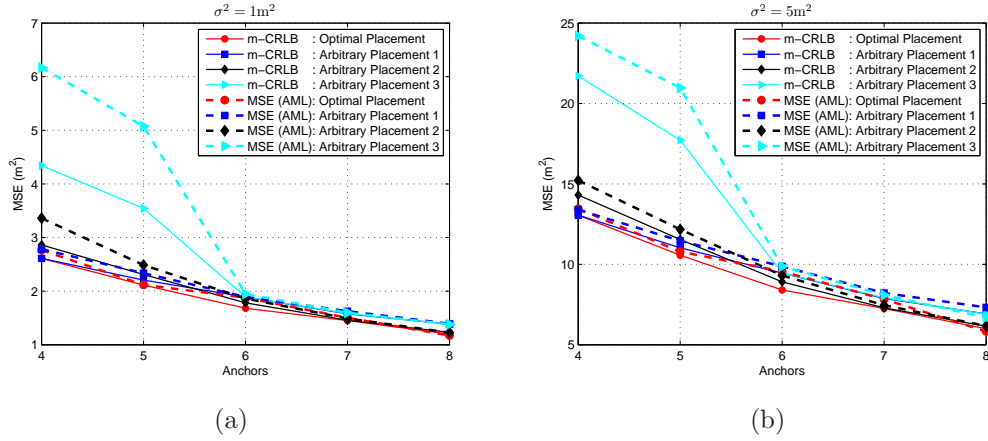


Figure 6.14: Performance of the AML method for additive noise model at optimal and arbitrary anchor placement and comparison with m-CRLB.

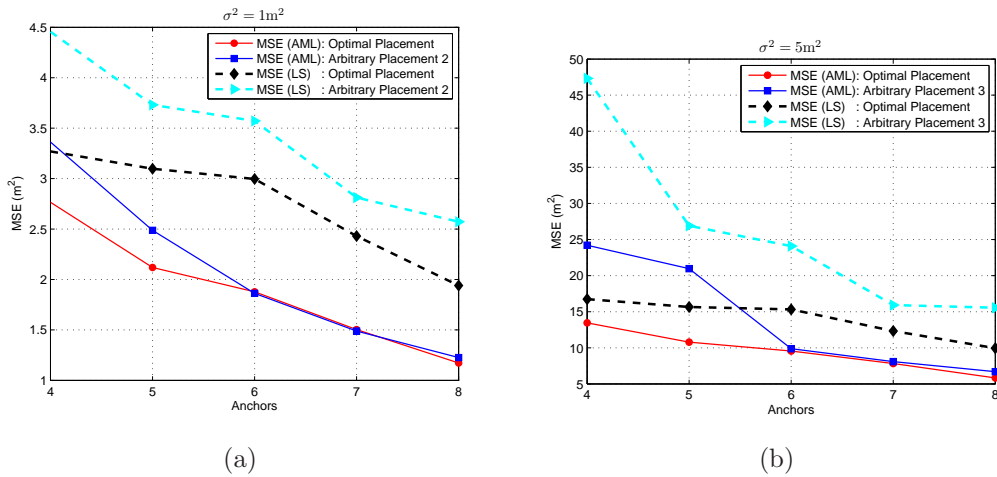


Figure 6.15: Performance comparison of LS and AML method for additive noise model at optimal and arbitrary anchor placement.

## 6.4 Conclusion

In chapter 5, based on the extensive simulation, the optimal positions are determined for both additive and multiplicative noise models. To analyse the impact of optimized anchor placement on localization, this chapter demonstrated the performance comparison between optimal and arbitrary anchor placements using two different methods, linear (LS) and non-linear (AML). Based on the contour mapping and simulation results, It is verified that optimized anchor placements can be used for any range aware localization scheme to get the better localization accuracy as compared to any arbitrary position.

In corroborative terms, the AML shown a better performance than LS across all the channel variance and anchor positions in 2-D and 3-D. The major point to note here is the fact that using 3 anchors AML specifically outperforms the LS method, however as we move from 4 to 8 anchors the difference between the LS and AML becomes less and on many locations for example using 6 anchors the performance of LS and AML in case of 3D becomes the same. This is usually because for both methods, there are enough anchors and information to zero-in on the subject node, however with only 3 nodes and limited resources (i.e. less anchors) the AML gives significantly better performance than LS. Although this accuracy comes with a trade-off, the trade-off is that the computational complexity of AML is significantly higher than LS.

The other major factor is that the optimum positions are different for different noise models and have been computed through m-CRLB and using the combination of given set of anchors that provide minimum m-CRLB. So naturally irrespective of method used (i.e. LS or AML) the optimum anchor positions are going to compute the location of subject nodes with greater accuracy than any other arbitrary position. The other notable point is that AML needs at least 4-5 arbitrary placed anchors to give a performance better than the optimally placed anchors using the LS method. The important thing to note in multiplicative noise model is that the optimal anchor placement for 3 anchors is close to a straight line (i.e. collinear) and therefore, LS/AML will show poor performance as compared to any other arbitrary anchor placement (as long as they are not on a straight line).

## 6.4 Conclusion

---

Lastly, as expected, extension from 2-D to 3-D using 4 optimal anchors showed a significant increase in MSE. For example, In 2-D at  $\sigma^2 = 1$ , the MSE is 3.5m whereas in 3-D it is increased to 9.5m. The error significantly increased as  $\sigma^2$  increased to 5. For example, In 2-D, 3 optimally placed anchor show MSE of 18.5m, where in 3-D MSE goes up to 45.5m. The reason is that error increases with the increase in dimension of the space.

The simulation based interesting results provided the needed motivation to develop a real time location system. This motivation leads to the next chapter, which discuss the implementation of Range Aware Localization System (RALS) in 2-D.

# Chapter 7

## Experiencing RALS

### 7.1 Introduction

In order to analyze the impact of anchor and subject node placement in real time, a Range Aware Localization System (RALS) is developed on the Jennic JN5148 IEEE 802.15.4 compliant devices on top of the Jennic's ToF application programming interface (API) [24]. The RALS testbed for localization uses the devices with 3 different functionalities. The three device types for each functionality are listed below:

- PAN Coordinator
- Anchor Nodes
- Subject Nodes

IEEE 802.15.4/Zigbee network exhibit three types of devices [18]: 1) Coordinator, 2) Router and 3) End Devices. The design of RALS consider the Coordinator node with JN5148-0010-M03 module as a PAN coordinator, router devices are replaced as the anchor nodes with same JN5148-0010-M03 modules, whereas end device used as a subject node with JN5148-0010-M03 module whose position is to be determined. The *eclipse* integrated development environment (IDE) is used on the top of the ToF API to programme the RALS. The corresponding binary file is downloaded on each of the device using Flash Programmer provided by Jennic. Before conducting the experiment, channel activity test is conducted

## 7.2 Principle of Operation

---

to determine the less noisy channel to avoid the interference and packet drop ratio. Based on the activity, channel 26 is selected with the maximum transmission power of 0dBm (1mW).

The localization system as illustrated through flow charts is distributed in nature where each subject node is capable of performing the on-device localization based on the LS method using the anchors position and the measured RT-ToF. It takes less than 2s to produce the results using 100 ranging samples. An important advantage of on-device location engine is that the algorithm is decentralized, allowing processing of the localization to be performed at each node. In addition, unlike centralized systems, it reduces the network traffic and the communication delay. All these nodes can perform localization standalone, without connecting it to laptop via UART for post processing. However, the PAN coordinator can be used to log the estimated data received from the subject nodes to be displayed on the laptop screen via UART or on the Web, where it can be analyzed from any location.

## 7.2 Principle of Operation

A PAN coordinator node (*centralized*) device is setup to start-up the network and is responsible for associating anchor and subject nodes, logging ranging and estimated positions via UART on a mobile laptop. After a successful channel scan, the association process and obtaining the short address as per IEEE 802.15.4 *Media Access Control (MAC) Sublayer Management Entity (MLME)* takes place and then wireless nodes (coordinator, anchor and subject nodes) may communicate as required. Subject node search for the required number of anchor nodes by sending a *request* packet to all anchor nodes. As soon as a subject node finds an in-range anchor node, it requests for the coordinates  $A_i = [x_i \ y_i]^T$  and starts RT-ToF ranging measurements as discussed in section (3.5.1) of chapter 3. On successful ranging operation, subject node stores the relevant ranging data (ToF packet) for further process. The subject node continues the process until it successfully stores ranging packet from at least 3 anchors (2-D case). After a successful reception of 3 anchor positions and the corresponding ToF packet, the subject node performs the localization using the LS method as explained in

## 7.3 Experimental Infrastructure and Setup

chapter 4. The actual coordinates of the subject node are programmed in the node to calculate the root-mean-square-error  $E_{RMS}$ . On the completion of the localization, subject node enters into sleep mode. When the sleep timer stops, the subject node wake ups and performs localization again.

The general principle of operation for PAN, anchors and subject nodes is given in 7.1, 7.2 and 7.3 respectively.

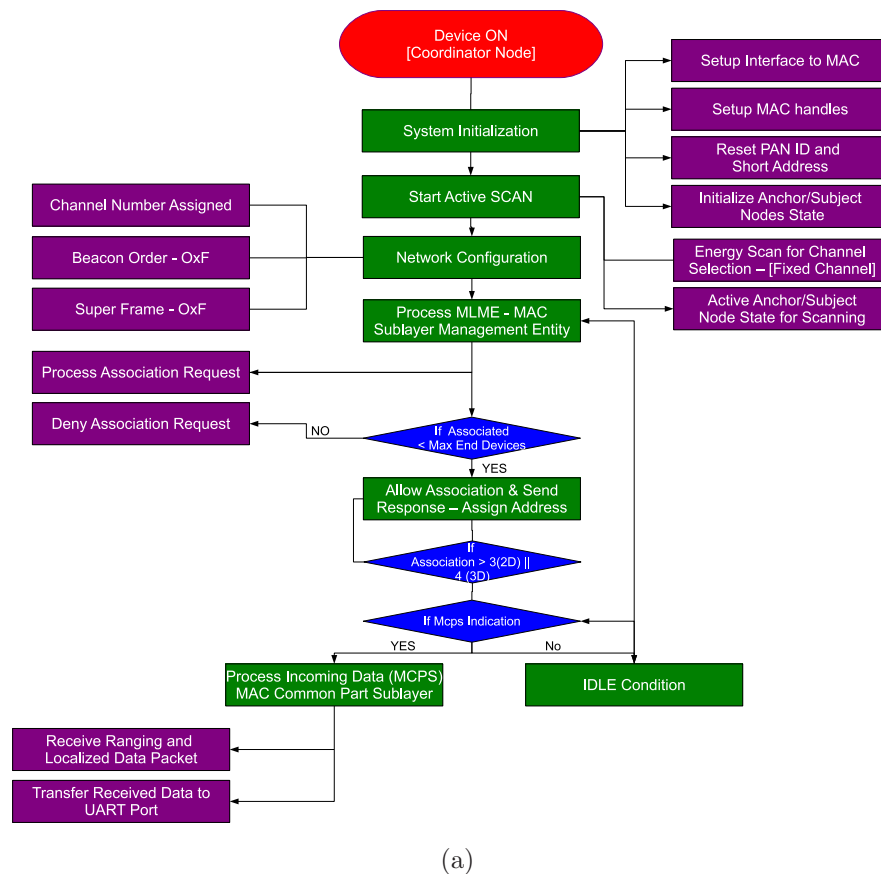


Figure 7.1: Flow Chart for PAN Coordinator node.

## 7.3 Experimental Infrastructure and Setup

The RALS system is developed using the JN5148 – EK010 evaluation kit, which provides a complete environment for the development of 2.4GHz IEEE 802.15.4, JenNet and ZigBee PRO applications based on the JN5148 wireless micro-controller

## 7.3 Experimental Infrastructure and Setup

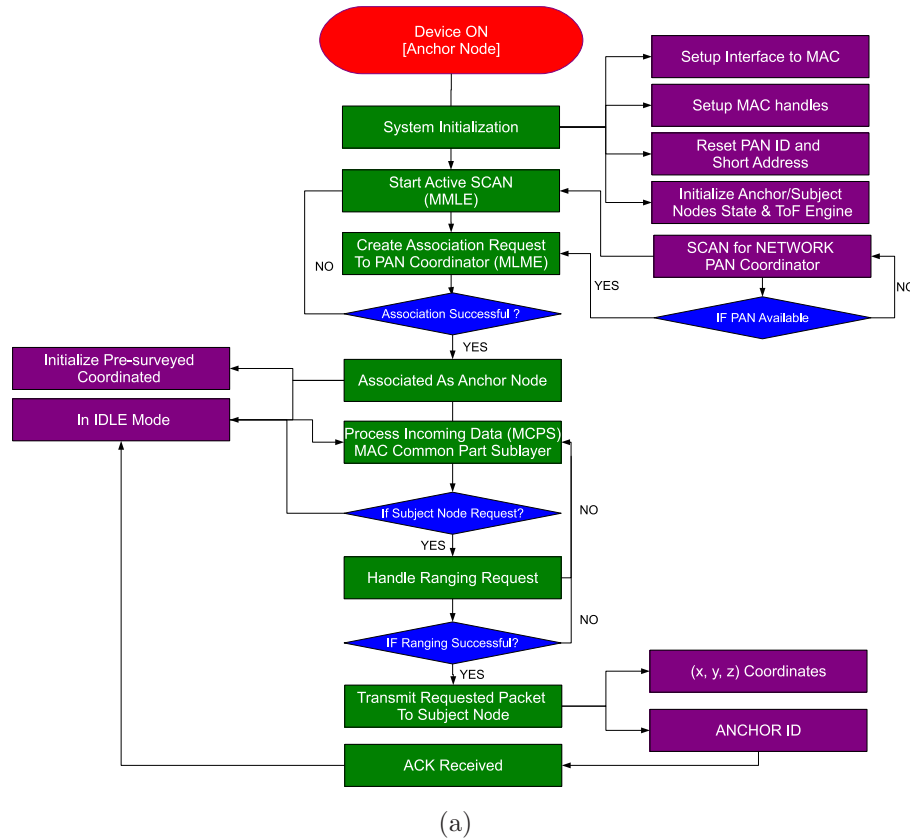


Figure 7.2: Flow Chart for Anchor nodes.

[1]. All five module used in the experimental setup are considered with standard power modules (JN5148-0010-M03) with uFl miniature coaxial RF connectors for external antenna (Nearson S131CL-L-PX-2450S [126]). The JN5148s transceiver provides a RT-ToF engine which is employed for range estimation between each anchor and the subject nodes. The power supply for the devices was provided by two 1.5V AAA batteries.

### 7.3.1 Indoor Setup

The network was deployed in the lecture theatre. The network layout is depicted by Fig. 7.4(a), where three anchors and a subject node are shown. The lecture theatre in which the the localization testbed is tested was a 10m×10m. The initial tested used 5 nodes (1 PAN coordinator, 3 anchor nodes, 1 subject node).

### 7.3 Experimental Infrastructure and Setup

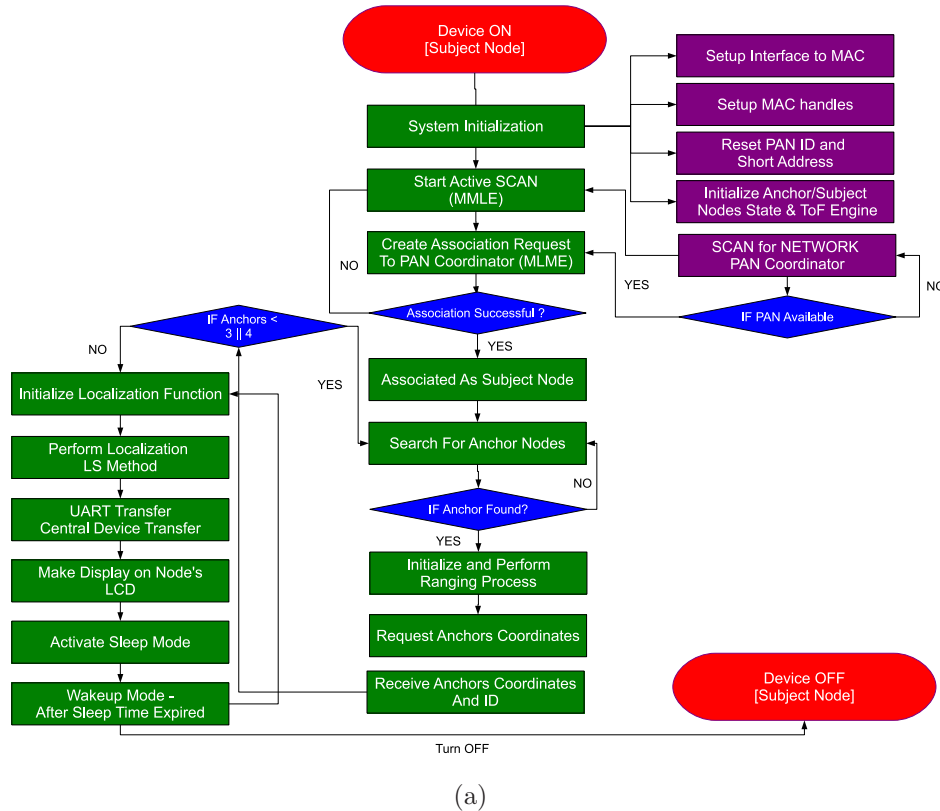


Figure 7.3: Flow Chart for Subject nodes.

A  $6\text{m} \times 6\text{m}$  area is used to deploy 3 anchor nodes. Based on the results from chapter 5 for additive noise model, the trio is placed at the optimal placement i.e. corners of an isosceles triangle. This triangle is of maximum size as 2 anchors are placed at the corners of one side of the square area while the 3<sup>rd</sup> anchor is placed at the centre of the opposite side, as shown in Fig. 7.4(a). Each anchor node is programmed with their coordinates as (i.e. anchor 1 with  $[0\text{m}, 0\text{m}]$ , anchor 2 with  $[6\text{m}, 0\text{m}]$  and anchor 3 with  $[3\text{m}, 6\text{m}]$ ,. Initially, the subject node is placed at the centre of the triangle ( $[3\text{m}, 3\text{m}]$ ), which is later moved at different placement to observe the location error. On setup, PAN coordinator, anchors and subject node perform localization as explained above and shown through flowcharts. Fig. 7.4(b) shows the splash screen on the LCD, when a subject node starts up.

## 7.4 Localization Performance Analysis

---

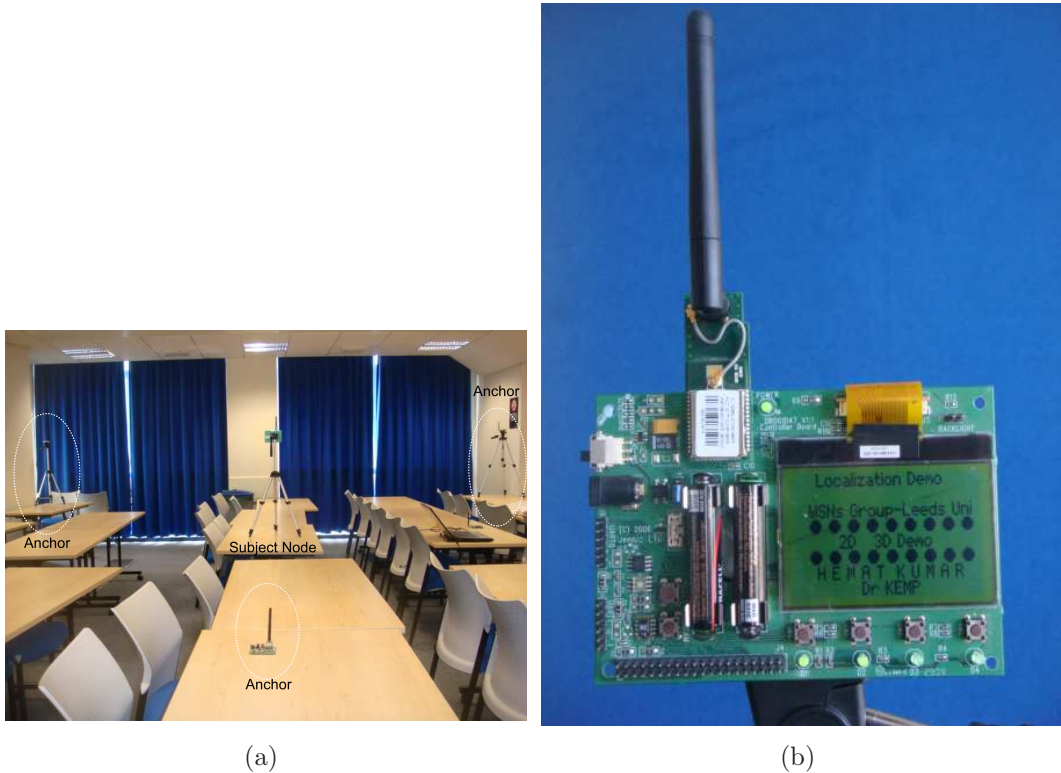


Figure 7.4: Fig. 7.4(a). Localization testbed in a Lecture Theatre, where three anchors are optimally placed, whereas subject node is placed in the centre. Fig. 7.4(b). Jennic JN5148 controller board and LCD splash screen on the subject node.

## 7.4 Localization Performance Analysis

Fig. 7.5(a) and 7.5(b) show the estimated coordinates and the root-mean-square-error ( $E_{\text{RMS}}$ ) in centimetres (cm) on the LCD display, when a subject node is placed at centre of the field along with the optimally placed anchor nodes. The reason to perform the calculation in smaller unit (i.e. cm) is to avoid the floating point routines as they increase code size significantly. It can be seen that when anchors and subject nodes are optimally placed,  $E_{\text{RMS}}$  of 0.86m and 0.48m is observed. A number of readings collected with same setup, and for 90% of the readings an average  $E_{\text{RMS}}$  of below 1m is observed. With 100 ranging iterations, an average time of less than 2 seconds is observed for localization.

Fig. 7.6(a) shows the estimated coordinates and  $E_{\text{RMS}}$  in centimetres (cm)

## 7.4 Localization Performance Analysis



(a)  $A_1=[0m, 0m]$ ,  $A_2=[6m, 0m]$ ,  $A_3=[0m, 6m]$ ,  
 $s_j=[3m, 3m]$ ,  $\hat{s}_j=[3.46m, 3.73m]$   
 $E_{RMS}=[0.86m]$

(b)  $A_1=[0m, 0m]$ ,  $A_2=[6m, 0m]$ ,  $A_3=[0m, 6m]$ ,  
 $s_j=[3m, 3m]$ ,  $\hat{s}_j=[2.65m, 2.65m]$   
 $E_{RMS}=[0.48m]$

Figure 7.5: Estimated subject coordinates and  $E_{RMS}$  in cm, when anchors are optimally placed and subject node is placed at  $[3m,3m]$  as shown in Fig. 7.4(a).

when a subject node is placed on the boundary line between two anchor nodes ( $[3m,0m]$ ). It can be seen that as subject node moved from the optimally placed location (i.e. centre of the triangle),  $E_{RMS}$  is increased to 1.61m. Furthermore, when the subject node is placed at  $[0m,3m]$ ,  $E_{RMS}$  is increased to 2.82m. In addition, when subject node is placed outside of the triangle at ( $[3m,9m]$ ) as shown in the Fig. 7.7(a),  $E_{RMS}$  is increased to 5.52m as shown in Fig. 7.7(b).

All these results are in accord with a MATLAB designed simulator and optimized anchor placement that has been done and established that centre position of the triangle is the optimal position to locate with minimum error. However Outside the field dimensions, performance of localization is effected as discussed below for Fig. 7.7. As observed through contour plots in chapter 5 that, each

## 7.4 Localization Performance Analysis



(a)  $A_1=[0\text{m}, 0\text{m}]$ ,  $A_2=[6\text{m}, 0\text{m}]$ ,  $A_3=[0\text{m}, 6\text{m}]$ ,  $s_j=[3\text{m}, 0\text{m}]$ ,  $\hat{s}_j=[3.19\text{m}, 1.60\text{m}]$ ,  $E_{\text{RMS}}=[1.61\text{m}]$

(b)  $A_1=[0\text{m}, 0\text{m}]$ ,  $A_2=[6\text{m}, 0\text{m}]$ ,  $A_3=[0\text{m}, 6\text{m}]$ ,  $s_j=[3\text{m}, 3\text{m}]$ ,  $\hat{s}_j=[2.39\text{m}, 4.50\text{m}]$ ,  $E_{\text{RMS}}=[2.82\text{m}]$

Figure 7.6: Fig. 7.6(a). Estimated subject coordinates and  $E_{\text{RMS}}$  in cm, when anchors are optimally placed and subject node is placed at  $[3\text{m}, 0\text{m}]$ . Fig. 7.6(b). Estimated subject coordinates and  $E_{\text{RMS}}$  in cm, when anchors are optimally placed and subject node is placed at  $[0\text{m}, 3\text{m}]$ .

subject location represent a different m-CRLB, hence MSE. The m-CRLB, hence MSE increases as a subject node moves away from the centre towards the third anchor, placed opposite to the two anchors. The same relationship is observed here, as a subject node is placed outside the field towards the third anchor node, where RMS is increased to 5.52m. In practice, subject nodes can be placed anywhere within or outside the field and therefore subject nodes cannot be considered from the optimal placement point of view. Therefore, it is important to consider the optimal anchor placement which can reduce localization error due to the geometric placement.

## 7.4 Localization Performance Analysis

---

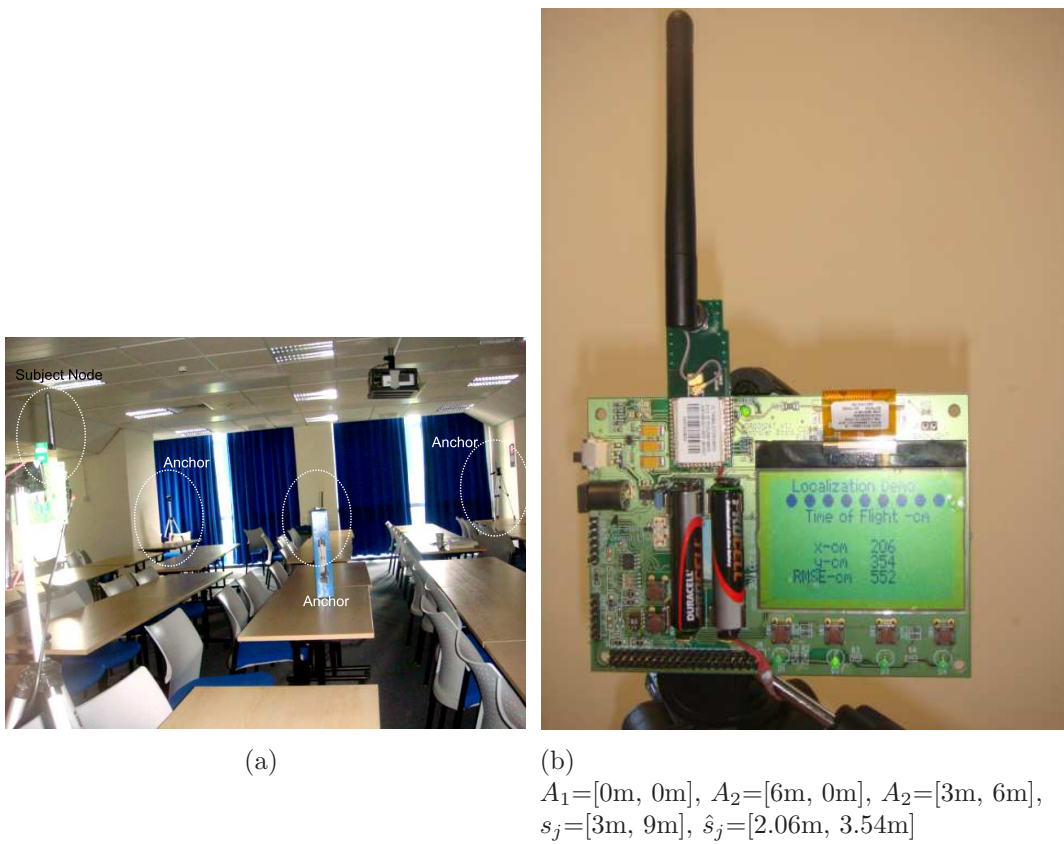


Figure 7.7: Fig. 7.7(a). Three anchors are optimally placed, whereas subject node is placed at  $[3\text{m}, 9\text{m}]$  outside of the triangle. Fig. 7.7(b). Corresponding  $E_{\text{RMS}}(\text{cm})$ .

## 7.4 Localization Performance Analysis

---

### 7.4.1 Arbitrary Anchor Placement

Fig. 7.8 shows the results, when anchor nodes are placed at the arbitrary placement, whereas subject node is placed at  $[3\text{m},3\text{m}]$ . It can be observed that, arbitrary anchor placement increase the  $E_{\text{RMS}}$  compared to the optimal anchor placement with  $0.79\text{m}$  and  $0.56\text{m}$  error. As observed in chapter 5 that, when using the arbitrary anchor placement, more anchors are required to be placed otherwise the performance of the localization system would be affected.



(a)  
 $A_1=[0\text{m},0\text{m}]$ ,  $A_2=[6\text{m},0\text{m}]$ ,  $A_3=[6\text{m},3\text{m}]$ ,  
 $s_j=[3\text{m},3\text{m}]$ ,  $\hat{s}_j=[0.24\text{m},4.55\text{m}]$   
 $E_{\text{RMS}}=[3.23\text{m}]$

Figure 7.8: Fig. 7.8(a). Subject node estimated coordinates and  $E_{\text{RMS}}$  when three anchors are placed at arbitrary placement, whereas subject node is placed in the centre of the field ( $[3\text{m},3\text{m}]$ ).

### 7.5 Summary

This chapter explains a real time RALS with the help of the flowcharts, that is capable of performing the localization in 2-D. The RALS is used to analyse the localization performance in real time by using the optimal anchor placement for 3 anchors as derived for the additive noise model. Its distributed nature allows a subject to localize itself without any centralized calculation of ranging and localization phase. It takes less than 2 seconds to produce and transfer localization results using 100 ranging samples. Moreover, this time can be reduced by avoiding the packet transfer to UART display. For all experimental, same antenna orientation is considered. Through real time experiments, it is concluded that anchor placement as well as subject placement is an important parameter to enhance localization accuracy. In addition to optimal anchor placement, antenna orientation is an important factor to be considered for reliable localization in realistic environments.

# Chapter 8

## Range Aware 3-D Localization in Indoor WSNs

### 8.1 Introduction

In recent years, there has been a great interest in research towards positioning of wireless devices in confined areas. The Global Positioning System (GPS) [29] provides an excellent worldwide lateration framework for determining geographic position. The GPS solution is famous for outdoor applications. However this solution has several limitations, the major is of course the dependency on line-of-sight (LOS) reception, together with relatively high power requirement and hardware complexity from satellites. With such limitations GPS typically fails in harsh environments (i.e. inside homes, offices, shopping malls, underground and between heavy vegetative cover) and exhibits suboptimal performance for WSN applications. To overcome these limitations and to enhance localization accuracy, indoor positioning system, based on the use of Global Navigation Satellite System (GNSS) repeaters [46], CarpetLAN [47], infrared based active-badge system [66], or ultrasounds [49], have been developed. However, their complexity, their power consumption, and their deployment cost are enduring problems [51]. Wireless sensor networks (WSNs) have found their way into a wide range of applications including indoor localization. Indoor localization has been a great interest in research because a reliable, and accurate localization in harsh environments is

## 8.1 Introduction

---

an integral part of many emerging application including logistics, medical services (i.e. neonatal monitoring, patient tracking), enclosed rescue operations (i.e. tunnels, caves, buildings), home automation, and others. In addition, efficient localization in confined areas helps to enhance geographic routing and data dissemination for rescue operations.

Localization performance is highly dependent on the quality of range estimates, which in-turn highly depend on propagation conditions of wireless channels. In practice ranging errors inevitably exist, no matter what ranging method is used. In ideal conditions (i.e. line-of-sight (LOS) case), quality reliable localization performance can be achieved but as propagation criteria change from ideal LOS to non-line-of-sight (NLOS), localization performance also changes. The localization performance degrades significantly in an indoor environment, where range measurements include NLOS errors due to the excess path length caused by signal reflect off objects because of reflection or diffraction [52]. The estimated error in such harsh environments is assumed to have a large positive bias that causes range estimates to be greater than the actual range. Such indoor environments fail a localization system to mark the required accuracy and therefore highlight the indoor localization as a challenging problem.

This chapter presents an attempt along this direction by proposing a new 3-D scheme named *Range Estimate Threshold* (RET). The proposed scheme defines a RET based on the 3-D field dimensions and the signal noise model to mitigate the poor range estimates ( $\hat{d}_{ij}^p$ ) from *Measured Estimation* (ME) to improve localization performance. The ramification of RET on ME for indoor localization is explored through three signal models:

- Additive noise model for time-of-flight (ToF)
- Multiplicative noise model for time-of-flight (ToF)
- Log-Normal shadowing model for received signal strength (RSS)

The additive noise model is a widely accepted signal model; however the multiplicative noise model is more suitable for practical propagation channels. These two noise models are explained in section 4.3 of chapter 4 and section 5.3.1

## 8.1 Introduction

---

of chapter 5 respectively, therefore not included in this chapter. However, the Eq. (8.1) for additive noise model and Eq. (8.2) [41] for multiplicative noise are given below:

$$\hat{d}_{ij} = d_{ij} + n_{ij} \quad (8.1)$$

where  $d_{ij}$  is the actual distance between node  $i$  and  $j$ ,  $n_{ij} \sim \mathcal{N}(0, \sigma_{ij}^2)$  is a Gaussian distributed random variable with zero mean and standard deviation  $\sigma$ , that is independent of  $d_{ij}$ .

$$\hat{d}_{ij} = d_{ij} + \kappa d_{ij}^{\frac{\eta}{2}} \epsilon \quad (8.2)$$

where  $\kappa$  is a proportionality constant to capture the combined physical layer effect on the range estimate [41] and for simplicity, it is assumed to be a constant,  $\eta$  is the path loss exponent and  $\epsilon$  is random variable with zero mean and unit variance.

Furthermore, the multiplicative noise model and log-normal shadowing model are categorized into two different variants based on calibrated channel parameters through *Calibrated Estimation* (CE). In CE, RSS based ranging information between anchor and subject nodes is exploited to calibrate channel parameters such as path loss exponent ( $\eta$ ) and shadowing variance ( $\sigma_{sh}^2$ ). The calibrated  $\eta$  is integrated with multiplicative noise model and RSS model to characterize wireless channel in two different methods [12]:

1. Using an individual calibrated  $\eta$  for each optimally placed anchor node ( $\eta_{Ai}$  for  $i = 1, \dots, N$ , where  $N$  is the number of anchor nodes).
2. Using an average of all individual calibrated  $\eta$  for each optimally placed anchor node ( $\eta_{\mu}$ ).

To evaluate, the least squares (LS) method for localization (as explained in section 4.4.1 of chapter 4) is used, where localization performance of ME and

## 8.2 Geometric Dilution of Precision Test for 3-D Setup

---

CE is compared with RET. Two different 3-D setups are considered in an indoor environment (research lab and computer cluster lab), where IEEE 802.15.4 compliant devices are used to characterize wireless channel parameters. Based on derived channel parameters, and extensive simulations in MATLAB, the performance of these three variants is compared in terms of accuracy. The analysis and comparison validate that localization based on RET provides improved performance compared to ME. This chapter begins with section 8.2, where a GDOP test for additive noise model from chapter 4 is extended into 3 for optimal anchor placement. Section 8.3 explains the RSS propagation model and calibration process (training and estimation phase) to characterize wireless channel model is explained in section 8.4, where based on the results from chapter 3, a less noisy channel is considered. Section 8.5 explains the RET scheme in detail. In section 8.6, simulation results using LS method for ME, CE and RET are presented, which is followed by summary in section 8.7.

## 8.2 Geometric Dilution of Precision Test for 3-D Setup

Before commencing a series of experiments, 2-D GDOP analysis from chapter 4 is extended in the 3-D context. Fig. 8.1 shows the 7 arbitrary anchor placements, where  $(x, y, z)^T$  coordinates of anchor nodes are selected based on the lab dimensions (12m (l)  $\times$  4m (w)  $\times$  3m (h)). To evaluate the 3-D anchor placement, GDOP metric is applied on each anchor placement using Eq. (8.3) for 3-D, which is discussed in section 4.5 of chapter 4 for 2-D.

$$\mathbf{G} = (\mathbf{G}_M^T \times \mathbf{G}_M)^{-1} = \begin{bmatrix} \mathbf{G}_{11} & \mathbf{G}_{12} & \mathbf{G}_{12} \\ \mathbf{G}_{21} & \mathbf{G}_{22} & \mathbf{G}_{12} \\ \mathbf{G}_{31} & \mathbf{G}_{32} & \mathbf{G}_{33} \end{bmatrix} \quad (8.3)$$

## 8.2 Geometric Dilution of Precision Test for 3-D Setup

---

where  $G_M$  is the geometry matrix and its 2-D form from Eq. (4.34) (chapter 4) can be extended into 3-D as Eq. (8.4) [30]:

$$G_M = \begin{bmatrix} \frac{\hat{x}_j - x_1}{\hat{d}_{1j}} & \frac{\hat{y}_j - y_1}{\hat{d}_{1j}} & \frac{\hat{z}_j - z_1}{\hat{d}_{1j}} \\ \frac{\hat{x}_j - x_2}{\hat{d}_{2j}} & \frac{\hat{y}_j - y_2}{\hat{d}_{2j}} & \frac{\hat{z}_j - z_2}{\hat{d}_{2j}} \\ \frac{\hat{x}_j - x_3}{\hat{d}_{3j}} & \frac{\hat{y}_j - y_3}{\hat{d}_{3j}} & \frac{\hat{z}_j - z_3}{\hat{d}_{3j}} \\ \frac{\hat{x}_j - x_4}{\hat{d}_{4j}} & \frac{\hat{y}_j - y_4}{\hat{d}_{4j}} & \frac{\hat{z}_j - z_4}{\hat{d}_{4j}} \end{bmatrix} \quad (8.4)$$

where,  $\hat{x}_j$  and  $\hat{y}_j$  are the estimated coordinates of  $j^{th}$  subject node and  $\hat{d}_{ij}$  is estimated distance between anchor and subject node. The elements of  $G_M$  defines the direction cosines for subject to  $i^{th}$  anchor nodes. From Eq. (8.3), PDOP can be given by Eq. 8.5:

$$PDOP = \sqrt{tr(G)} \quad (8.5)$$

Fig. 8.1 shows the 7 arbitrary anchor placements, whereas Fig. 8.2 shows the simulation setup with anchor placement 1 and 80 randomly deployed subject nodes. For each anchor placement 80 subject nodes were deployed and 1000 samples were collected at noise variance (i.e.  $\sigma^2 = 1, \dots, 10$ ). Fig. 8.3 and Fig. 8.4 compares the impact of anchor placement and  $\sigma^2$  on position DOP (PDOP) and root-mean-square error ( $E_{RMS}$ ) (as given by Eq. (4.22) in chapter 4) respectively. Fig. 8.3 shows that anchor arrangement 1 results in lowest PDOP and  $E_{RMS}$  value as compared to other anchor placements. It can be observed that arrangement 7 shows the worst topology hence high PDOP and  $E_{RMS}$ . Based on this analysis, anchor placement 1 is selected for all three models (additive, multiplicative and RSS), whose coordinates are shown in Fig. 8.1.

## 8.2 Geometric Dilution of Precision Test for 3-D Setup

---

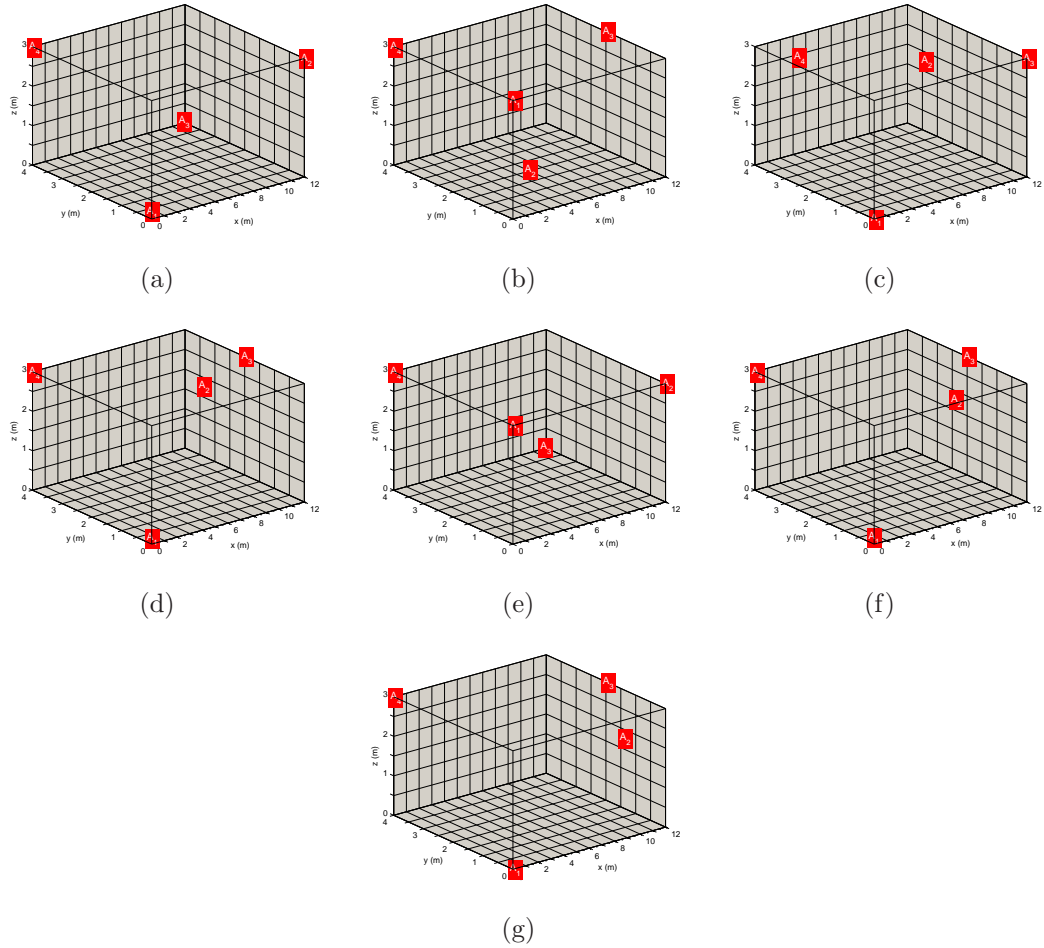


Figure 8.1: 7 different 3-D anchor placements according to the dimensions of Wireless Sensor Networks Research Group lab (262b) at University of Leeds.

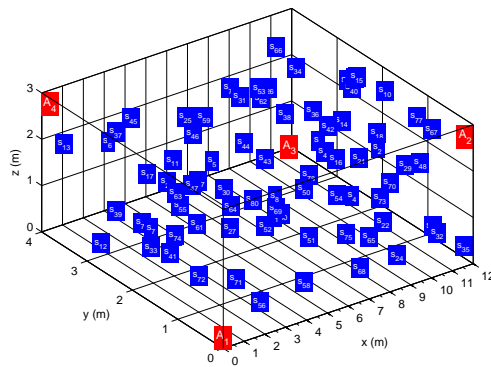


Figure 8.2: Simulation setup for anchor placement 1 as shown in Fig. 8.1.

## 8.2 Geometric Dilution of Precision Test for 3-D Setup

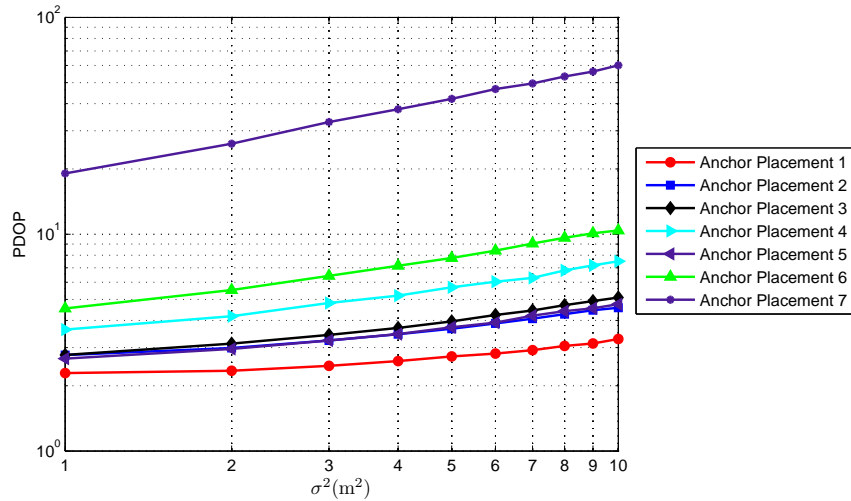


Figure 8.3: Impact of noise variance and anchor node placements on PDOP in 3-D context.

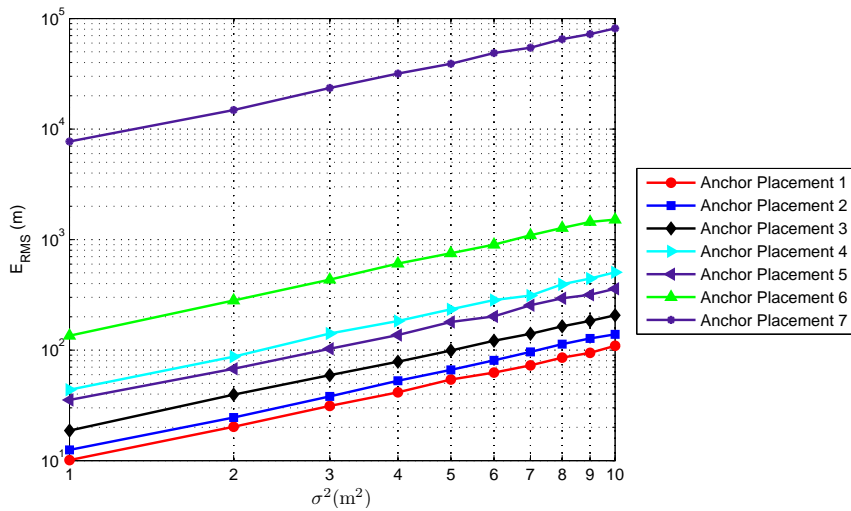


Figure 8.4: Impact of noise variance and anchor node arrangements on  $E_{RMS}$  in 3-D context (based on 3-D trilateration using LS method for 7 different anchor combinations and 50 randomly deployed subject nodes.)

## 8.3 Received Signal Strength

As explained in Chapter 3, In practice, distance dependent, deterministic path loss model (Eq. (8.6)) [94, 98] do not correctly predict the received power strength due to the complex nature of real propagation.

$$P_r(d_{ij})[dBm] = \Psi[dBm] - 10\eta \log_{10} \frac{d}{d_0} \quad (8.6)$$

where  $P_r(d_{ij})[dBm]$  is the received power at node  $i$  from a transmitting node  $j$   $\Psi$  is received power at a reference distance  $d_0$ ,  $\eta$  is the path loss exponent based on the propagation environment (normally taken between 2 and 6) [94, 98]. The relationship between distance and path loss exponent in Eq. (8.6) does not consider the harsh environment that may experience different propagation at two different positions with same distance between transmitter and receiver. To overcome this, a *log-normal shadowing model* (Eq. (8.7)) is considered, which states that with a specific value of  $d_{ij}$ , the  $\eta$  at particular location is random and distributed as lognormally (normal in dB) about the mean distance-dependent value [94, 98].

$$P_r(d_{ij})[dBm] = \Psi[dBm] - 10\eta \log_{10} \frac{d}{d_0} + \sigma_{sh} \quad (8.7)$$

where  $\sigma_{sh}$  is the shadowing variance (zero mean Gaussian distributed random variable in dB with standard deviation  $\sigma$ ). In practice, the  $\eta$  will be different in each environment. Therefore, it is important to approximate this unit-less constant analytically or experimentally.

In an indoor environment, RSS becomes a poor function of ranging, where the multipath components are common and presents severe limitations. Therefore an accurate and environment dependent channel model is crucial to alleviate the limitation due to the multipath components. To alleviate these limitations, location systems use a *priori* calibration process to fingerprint (aka profiling) the area of interest [11, 12]. Most of the previous work is limited to 2-D where

### 8.3 Received Signal Strength

---

optimal anchor placement is not considered to calibrate channel parameters [12, 61–63]. Therefore, to profile an area of interest, the link information between each optimally placed anchor and the subject node can be exploited through different variants such as:

- Profiling an area of interest by exploiting the link information between pair of anchors [61, 62] and using the average propagation parameters (i.e.  $\eta$  and  $\sigma_{sh}$ ) for each anchor node to characterize a channel model [12, 62]
- Profiling an area of interest by exploiting the link information between pair of anchor and subject nodes [12] and using the same propagation parameters (i.e.  $\eta$  and  $\sigma_{sh}$ ) for each anchor node to characterize a channel model [12]
- Profiling an area of interest by exploiting the link information between pair of anchors [61, 62] and using the individual set of propagation parameters (i.e.  $\eta$  and  $\sigma_{sh}$ ) for each anchor node to characterize a channel model [61]
- Profiling an area of interest by exploiting the link information between pair of anchor and subject nodes [12] and using the individual set of propagation parameters (i.e.  $\eta$  and  $\sigma_{sh}$ ) for each anchor node to characterize a channel model [12]

As mentioned above, a  $\eta$  can be calibrated by exploiting the link between anchor nodes but calibrating the path loss exponent in 3-D environment by only using the link between optimal placed anchor nodes has limited physical justification. Consider Fig. 8.5, where 4 anchors are optimally placed in 3-D. Assume,  $\eta_{A_4A_2}$  (face diagonal) is the  $\eta$  between  $A_4$  and  $A_2$  and  $\eta_{A_4A_3}$  is the  $\eta$  between  $A_4$  and  $A_3$ . It can be observed that  $\eta$  between anchor 4 and anchor 2 ( $\eta_{A_4A_2}$ ) or between anchor 4 and 3 ( $\eta_{A_4A_3}$ ) has limited channel information. For example, looking at the optimal placement of the ceiling anchor nodes  $A_4$  and  $A_2$ , they are most likely in a path with no moving objects in between. Therefore, the relation between the path loss exponent corresponding to this link, and the one corresponding to the link between  $A_4$  and a randomly placed sensor node (that may experience link obstruction) has limited justification. The same remark holds for the other link between anchor nodes  $A_4$  and  $A_3$  or  $A_4$  and  $A_1$ , which shows the

## 8.4 Calibration of Path loss Exponent

---

face diagonal right through the wall without counting the centre. These paths may experience independent attenuation and fading that are unrelated to the ones experienced by the link between  $A_4$  and a randomly placed sensor node, that may have close-by objects obstructing the link. It is therefore, path loss exponent for each deployed anchor node is profiled by exploiting the link information between anchor and subject nodes instead of exploiting only the link between pairs of anchors. The calibration of  $\eta$  is explained in section 8.4.1.

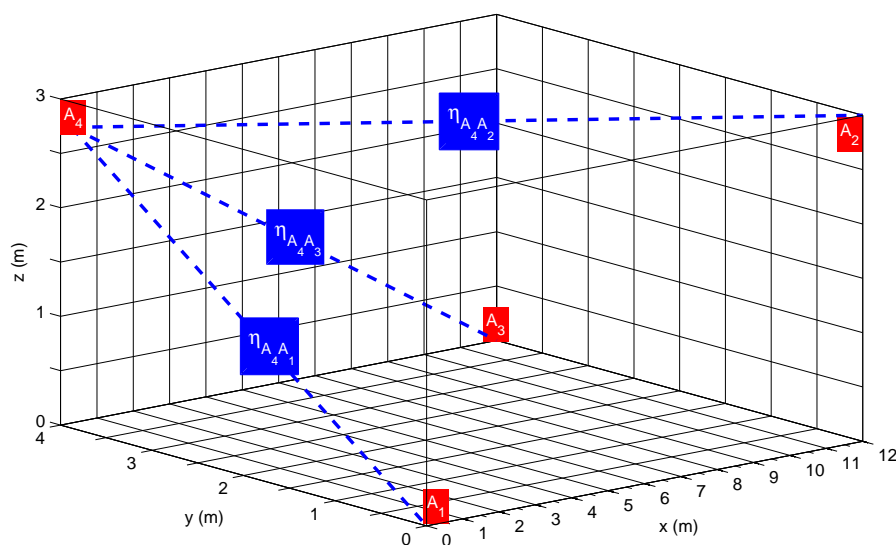


Figure 8.5: Profiling an area of interest by exploiting the link information (face diagonal) between pair of anchors in 3-D, where 4 anchors are optimally placed.

## 8.4 Calibration of Path loss Exponent

The path loss calibration process has two phases:

1. Training Phase: In the training phase, a number of RSS measurements between optimally placed anchor and the subject nodes are logged within an area of interest for post processing to formulate the lookup tables. The training phase is discussed in section 8.4.1.
2. Estimation Phase: In the estimation phase, formulated lookup tables are used to map RSSI in to estimated distance for localization phase.

## 8.4 Calibration of Path loss Exponent

---

### 8.4.1 Training Phase

The experiments for training phase have been performed in two different lab environments (Wireless Sensor Networks Research Group Lab (Lab-262b) and Computer Cluster Lab (Lab160)) in the School of Electronic and Electrical Engineering, at the University of Leeds as shown in Fig. 8.6(a) and Fig. 8.6(b). The dimensions of lab-262b are 12m×4m×3m whereas the dimensions of lab-160 are 16m×9m×3m. Experimental results are based on the Jennic's IEEE 802.15.4 compliant modules with an integrated antenna. The integrated antenna are based on a folded-monopole, omni-directional characteristic [1]. To place the anchor nodes optimally, tripods and multi-purpose tac are used to mount the anchors at specified height. The highest transmit power of 0dBm is used for all ranging measurements. Both labs have furniture, computers, and cabinets.

#### 8.4.1.1 Experimental Infrastructure and setup

To model wireless channel, parameters  $\eta$  and  $\sigma_{sh}$  are calibrated for above mentioned lab environments. The experimental setup for both labs is comprised of 4 optimally placed anchors ( $A_i$  for  $i = 1, \dots, 4$ ), 8 subject nodes ( $s_j$  for  $j = 1, \dots, 8$ ) and a laptop to log RSSI. For each optimal placed anchor and a subject node link ( $A_i s_j$ ),  $\sim 750$  RSSI samples were logged via universal asynchronous receiver/transmitter (UART) port to laptop as shown in Fig. 8.6(c). The LOS in experimental setup is blocked by the presence of furniture, computers and cabinets. Due to the multipath environment, it is possible to have non-symmetric, therefore, the obtained RSSI is the average of RSSI measurements from anchor to subject and subject to anchor node for the same radio link.

Fig. 8.7 and Fig. 8.8 shows the node placement for calibration in lab-262b and lab-160 respectively, where for simplicity only 8 subject nodes are considered and placed in a circular shape at the height of 1.5m. Fig. 8.9 shows the calibration process for anchor  $A_i$  (for  $i = 1, \dots, 4$ ), where RSSI between  $A_i$  and  $s_j$  is shown by  $\text{RSS-}A_i s_1$ ,  $\text{RSS-}A_i s_2$ ,  $\text{RSS-}A_i s_3$ ,  $\text{RSS-}A_i s_4$ ,  $\text{RSS-}A_i s_5$ ,  $\text{RSS-}A_i s_6$ ,  $\text{RSS-}A_i s_7$ , and  $\text{RSS-}A_i s_8$  links. Once RSSI samples between and anchor and the subject nodes are logged via UART port to laptop, path loss exponent is calculated for each

## 8.4 Calibration of Path loss Exponent

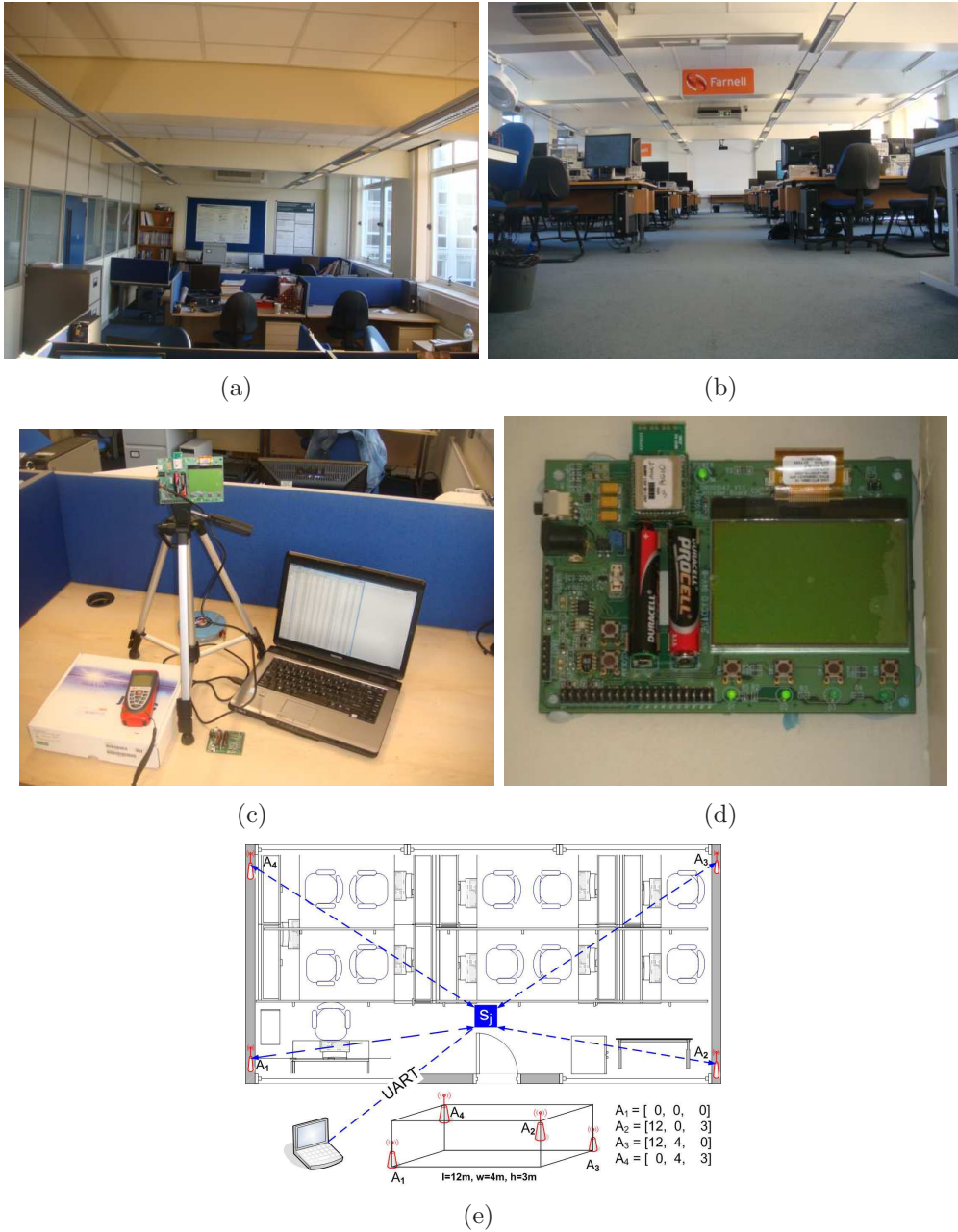


Figure 8.6: Fig. 8.6(a). Wireless Sensor Networks Research Group Lab (Lab-262b) in the School of Electronic and Electrical Engineering at the University of Leeds. Fig. 8.6(b). Computer Cluster Lab (Lab-160 in the School of Electronic and Electrical Engineering at the University of Leeds. Fig. 8.6(c). Node mounted on a tripod and connected to laptop via UART. Fig. 8.6(d). Node mounted with multi-purpose tac around the corner of the wall. Fig. 8.6(e). Experimental setup along with anchor nodes arrangement 1.

## 8.4 Calibration of Path loss Exponent

anchor node by using a minimum mean-square error (MMSE) fit to empirical measurements, in a similar manner as discussed in chapter 3.

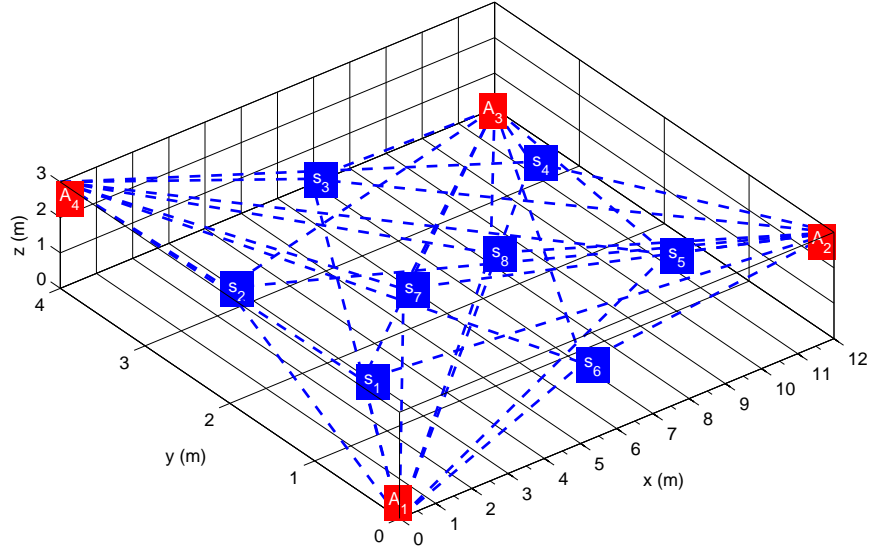


Figure 8.7: Node placement for calibration of path loss exponent in Lab-262b.

Table 8.1 contains the calibrated parameters for four anchor nodes, where  $\eta_{A_i}$  and  $\sigma_{sh}$  are approximated separately for each anchor using experimental data. An averaged calibrated path loss exponent ( $\eta_\mu$ ) for each anchor node  $\eta_{A_i}$  (for  $i = 1, \dots, N$  number of anchors) can be given by Eq. (8.8):

$$\eta_\mu = \frac{\sum_{i=1}^N \eta_{A_i}}{N} \quad (8.8)$$

where  $N$  is the total number of anchor nodes (i.e. 4 in 3-D case) and  $\eta_\mu$  is the average of all path loss exponents.

It is observed that,  $\eta$  for all four anchors is very similar despite their different physical arrangement and surrounding. However, for analysis and comparison, both variants are considered. In a centralized network, the advantage of using an averaged  $\eta$  is that it avoids the need for individual lookup table of each anchor [12].

## 8.4 Calibration of Path loss Exponent

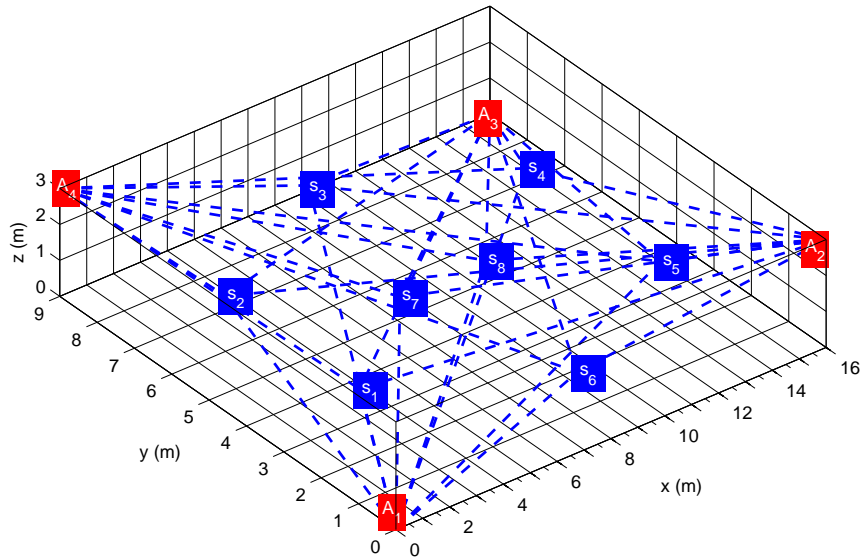


Figure 8.8: Node placement for calibration of path loss exponent in Lab-160.

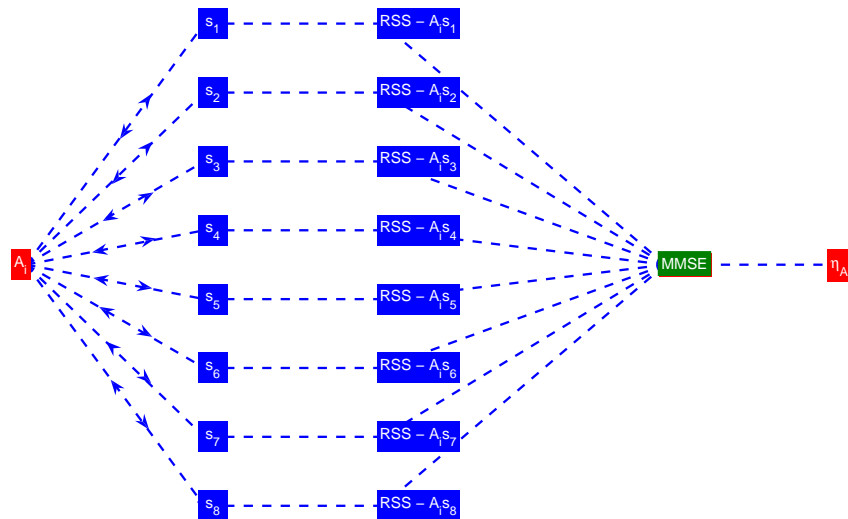


Figure 8.9: Path loss exponent calibration process for  $A_i$  where  $i = 1, \dots, N$ .

## 8.4 Calibration of Path loss Exponent

---

Table 8.1: Calibrated Propagation Parameters

<i>Anchors</i>	<b>Lab-262b</b>			<b>Lab-160</b>		
	$\Psi$ dBm	$\eta$	$\sigma_{sh}$ dB	$\Psi$ dBm	$\eta$	$\sigma_{sh}$ dB
$A_1=\eta_{A1}$		2.36			2.43	
$A_2=\eta_{A2}$	-39.12	2.1	3.75~3.85	-39.12	1.94	3.75~3.85
$A_3=\eta_{A3}$		2.27			2.29	
$A_4=\eta_{A4}$		1.87			2.2	
$\eta_\mu$		2.15			2.21	

However, in a distributed network, where each anchor can have their own lookup table, using a separate  $\eta$  for each anchor can improve localization performance.

Fig. 8.10(a) - Fig. 8.10(d) illustrate the experimental RSSI ranging samples between  $A_{i=1, 2, 3, \text{ and } 4}$  and subject node ( $s_1$ ) respectively for lab-262b, where dotted points (red) represent the RSSI samples, dotted line represent the averaged RSSI and solid line (blue) shows the ideal RSSI with parameters  $\eta_{A_i} = 2.36$ ,  $\sigma_{sh} = 3.85$ , received power ( $\Psi_{\text{dBm}}$ ) of  $-39.18\text{dBm}$  at reference distance ( $d_0$ ) of 1m.

### 8.4.1.2 Formulation of Lookup Table

The calibrated channel parameters from training phase (as shown in table 8.1) are post processed in MATLAB and transformed into lookup tables using Eq. (8.9) for each anchor node (refer section 3.6 of chapter 3 for detailed explanation on RSS principle of operation for Jennic IEEE 802.15.4 transceiver). Fig. 8.11(a) and Fig. 8.11(b) illustrate the lookup table graph based on  $\eta_{A_i}$  and  $\eta_\mu$  to map RSSI samples into estimated distance for each anchor node placed in lab-262b and lab-160 respectively.

$$d_{A_i} = e^{1/10 \frac{\ln(10)(-P_r(\text{dBm}) + \Psi_{\text{dBm}} + \sigma_{sh}(\text{dB}))}{\eta}} d_0 \quad (8.9)$$

where  $d_{A_i}$  is the mapped distance for anchor  $A_i$ ,  $P_r(\text{dBm})$  is the received power at distance  $d_{ij}$ ,  $\Psi_{\text{dBm}}$  is the received power at reference distance ( $d_0$ ) of 1m,  $\eta$  is

## 8.4 Calibration of Path loss Exponent

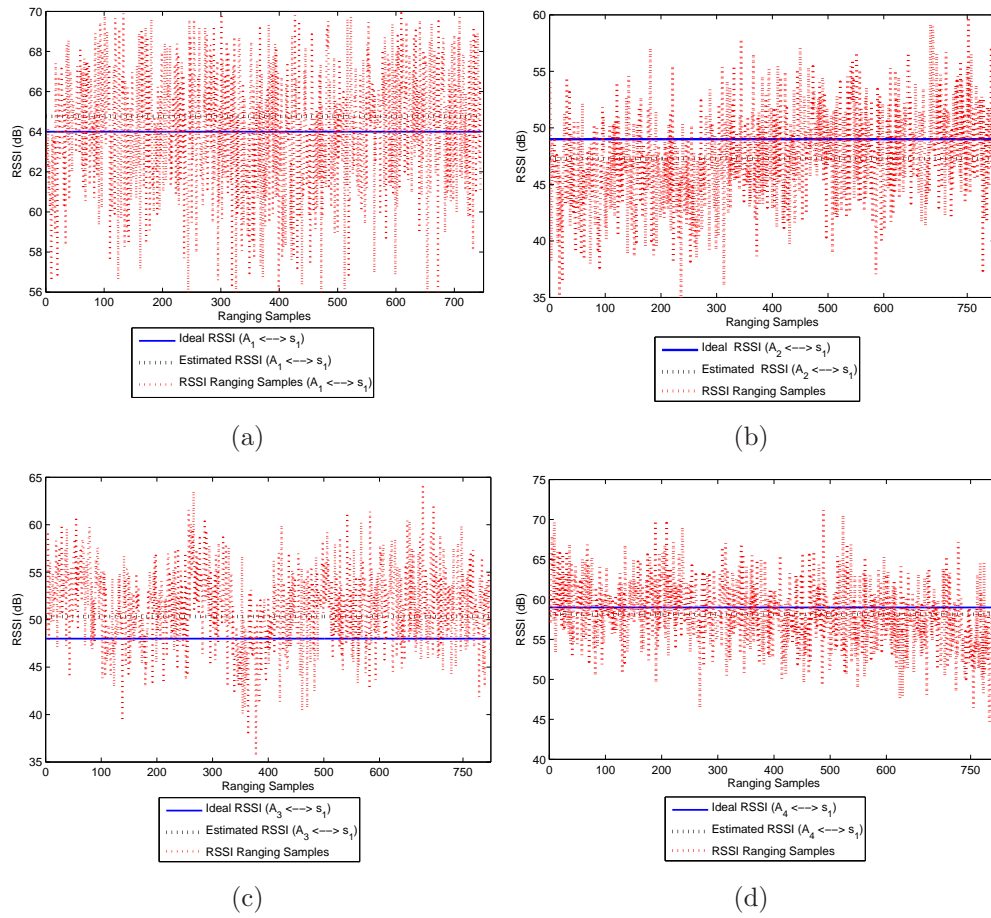


Figure 8.10: RSSI ranging samples between each anchor and subject node 1 as shown in Fig. 8.7 (lab-262b).

## 8.5 Range Estimate Threshold (RET)

the path loss exponent and  $\sigma_{sh}$ (dB) is the shadow fading (zero mean Gaussian distributed random variable in dB with standard deviation  $\sigma$ ).

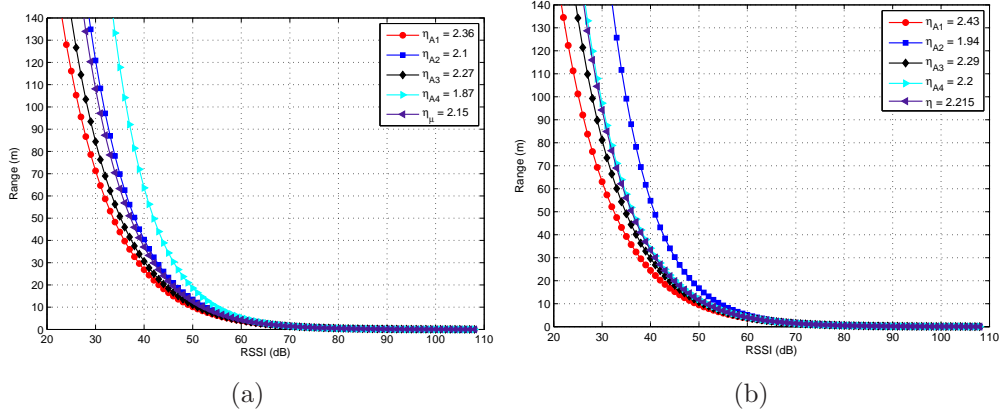


Figure 8.11: Fig. 8.11(a). Lab-262b lookup table mapping using  $\eta_{A_i}$  and  $\eta_{\mu}$  as shown in table 8.1 for each anchor node. Fig. 8.11(b). Lab-160 lookup table mapping using  $\eta_{A_i}$  and  $\eta_{\mu}$  as shown in table 8.1 for each anchor node.

### 8.4.2 Estimation Phase

The estimation phase is based on a MATLAB designed simulation tool, where each lookup table based on calibrated path  $\eta$  is mapped with the corresponding anchor. Two different variants are implemented for both lab environments, (1). Using  $\eta_{A_i}$  for each corresponding anchor node, (2). Using  $\eta_{\mu}$  for each anchor node. During range estimation process, RSSI between an anchor and a subject node for the same radio link is mapped into the estimated distance using the corresponding lookup table. Fig. 8.12 shows the subject node estimation process, where a subject node  $s_j$  obtains range estimates based on channel model corresponding to each anchor node. Once range estimates ( $\hat{d}_{ij}$ ) are obtained, LS method is performed to estimate subject position.

## 8.5 Range Estimate Threshold (RET)

Research in the field of localization suggest that, providing a prior information (i.e. finger prints) of an environment is one way to enhance range estimate, hence

## 8.5 Range Estimate Threshold (RET)

---

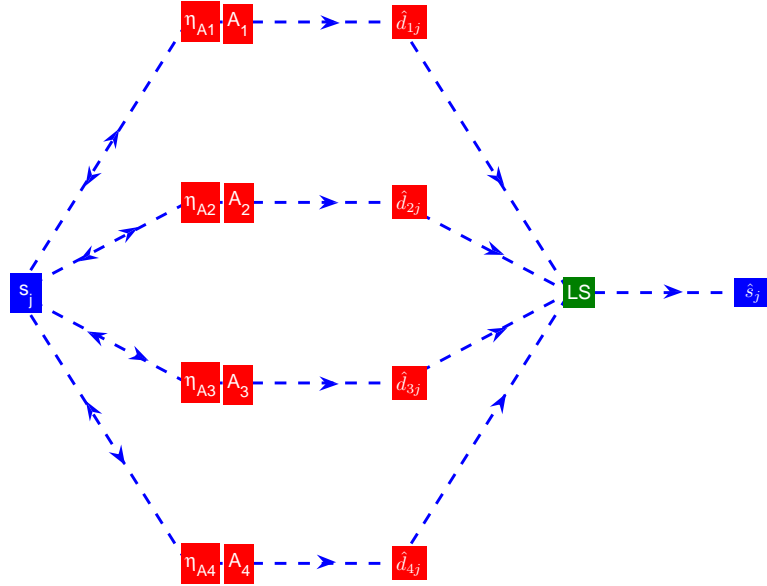


Figure 8.12: Subject node estimation using calibrated path loss exponent with respect to each anchor node  $A_i$  for  $i = 1, \dots, N$ .

localization performance [12]. As discussed above, for RSS the prior knowledge of environment is crucial to model a path loss exponent. Similarly, a prior knowledge of dimensions of an indoor environment can be used to define a RET. Consider Fig. 8.6(e), where a subject node acquires the time based or RSS based range measurement from all 4 in-range anchors to perform localization. Considering the fact that, in practice ranging errors inevitably exist to make localization inaccurate therefore it is important to make the best use of known information (i.e. field dimensions) along with the noise model to mitigate poor range estimates.

Consider Fig. 8.13, where dimensions are fixed, known and equivalent to lab-262b dimensions. Fig. 8.13 shows the space diagonal (blue dashed line) and face diagonal (green dashed line) between an anchor and a subject node. A rectangular cuboid has twelve face diagonals and four space diagonals. The cuboid's face diagonals can have up to three different lengths whereas all the space diagonals have the same and maximum length as given by Eq (8.10).

## 8.5 Range Estimate Threshold (RET)

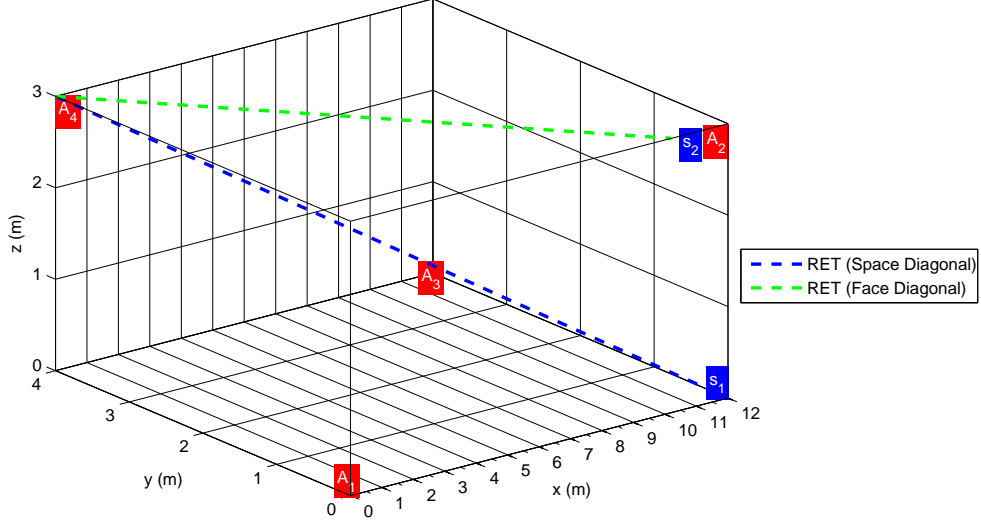


Figure 8.13: Space and face diagonal between anchor  $A_i$  and subject  $s_j$  nodes in 3-D for RET.

$$\text{RET} = \sqrt{l^2 + w^2 + h^2} \quad (8.10)$$

Based on the known field dimensions and signal model, a possible maximum range (space diagonal) between an anchor and a subject node can be defined as a threshold for the range measurement phase using Eq. (8.11):

$$\text{RET} = \sqrt{l^2 + w^2 + h^2} + \chi \quad (8.11)$$

where  $\chi$  is the signal model dependant parameter and can be given as Eq. (8.12) for additive noise model ( $\chi_{aNm}$ ), Eq. (8.13) for multiplicative noise model using  $\eta_\mu$  ( $\chi_{mNm}^{\eta_\mu}$ ), Eq. (8.14) for multiplicative noise model using  $\eta_{Ai}$  ( $\chi_{mNm}^{\eta_{Ai}}$ ) and Eq. (8.15) for log-normal shadowing model respectively.

$$\chi_{aNm} = n_{ij} \quad (8.12)$$

## 8.5 Range Estimate Threshold (RET)

---

where  $n_{ij} \sim \mathcal{N}(0, \sigma_{ij}^2)$  is a Gaussian distributed random variable with zero mean and standard deviation  $\sigma$  that is independent of distance between node  $i$  and node  $j$ .

$$\chi_{mNm}^\mu = \kappa d_{ij}^{\frac{\eta_\mu}{2}} \epsilon \quad (8.13)$$

where  $\kappa$  is constant [41],  $d_{ij}$  is distance between node  $i$  and node  $j$ ,  $\eta_\mu$  is the path loss exponent for each anchor node,  $\epsilon$  is a Gaussian distributed random variable with zero mean and standard deviation  $\sigma$  that is dependent on distance between node  $i$  and node  $j$ .

$$\chi_{mNm}^{Ai} = \kappa d_{ij}^{\frac{\eta_{Ai}}{2}} \epsilon \quad (8.14)$$

where  $\eta_{Ai}$  is the path loss exponent for anchor  $i$ .

$$\chi_{\sigma_{sh}} = \sigma_{sh}^2 \quad (8.15)$$

where  $\sigma_{sh}$  is the shadowing variance with zero mean Gaussian distributed random variable in dB with standard deviation  $\sigma$ .

Fig. 8.14(a) shows RET for additive noise model whereas Fig. 8.14(b) shows RET for multiplicative noise model using  $\eta_\mu$  and  $\eta_{Ai}$  according to lab-262b dimensions. It can be observed from Fig. 8.14(a) that RET for additive noise model increases as the noise variance increases. Similarly, Fig. 8.14(b) shows an increase in RET with respect to  $\kappa$ . In addition, due to different  $\eta$  for each anchor node Fig. 8.14(b) shows different RET to eliminate poor range estimates.

Similarly, Fig 8.15(a) shows space and face diagonal between anchor and subject nodes in 3-D for lab-160. Based on lab-160 dimensions, RET using space diagonal for additive and multiplicative noise models is defined as shown in Fig. 8.15(b) and Fig. 8.15(c) respectively.

## 8.5 Range Estimate Threshold (RET)

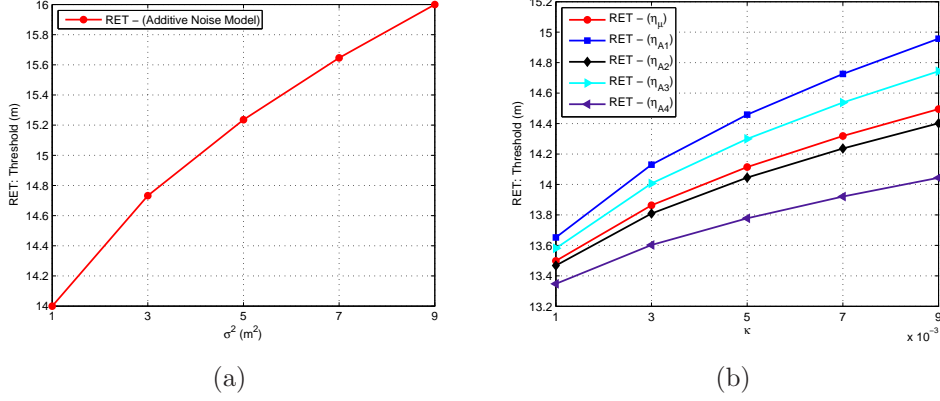


Figure 8.14: Fig. 8.14(a). RET for additive noise model where  $\sigma^2 = 1, 3, 5, 7,$  and  $9$ . Fig. 8.14(b). RET for multiplicative noise model where  $\kappa = 0.001, 0.003, 0.005, 0.007,$  and  $0.009$ .

### 8.5.1 RET Algorithm Description

Algorithm 2 shows the algorithm steps for RET, where RET is space diagonal of an indoor environment (i.e. Fig. 8.14 for lab-262b and Fig. 8.15 for lab-160). When a subject node finds 4 in-range anchor nodes, it starts ranging process to each anchor node. During the ranging process between an anchor and the subject node ( $A_i s_j$ ),  $s_j$  keeps the record of all ranging samples with corresponding  $A_i$ . Then a check is imposed for preferred range estimates based on the defined RET. Range estimates ( $\hat{d}_{ij}$ ) greater than RET are considered as *poor range estimate* ( $\hat{d}_{ij}^p$ ) and can be defined by Eq.

(8.16):

$$\hat{d}_{ij}^p : \left\{ \hat{d}_{ij}^p \mid \hat{d}_{ij}^p \notin \hat{d}_{ij}, \hat{d}_{ij}^p > \text{RET} \right\} \quad (8.16)$$

where RET is range estimate threshold based on field dimensions and signal model. The imposed check mitigates all of the poor range estimates after the completion of  $n$  number of ranging iterations. Similarly, range estimate smaller than RET are considered as *preferred range estimate* ( $\hat{d}_{ij}^o$ ) as defined by Eq. (8.17):

## 8.5 Range Estimate Threshold (RET)

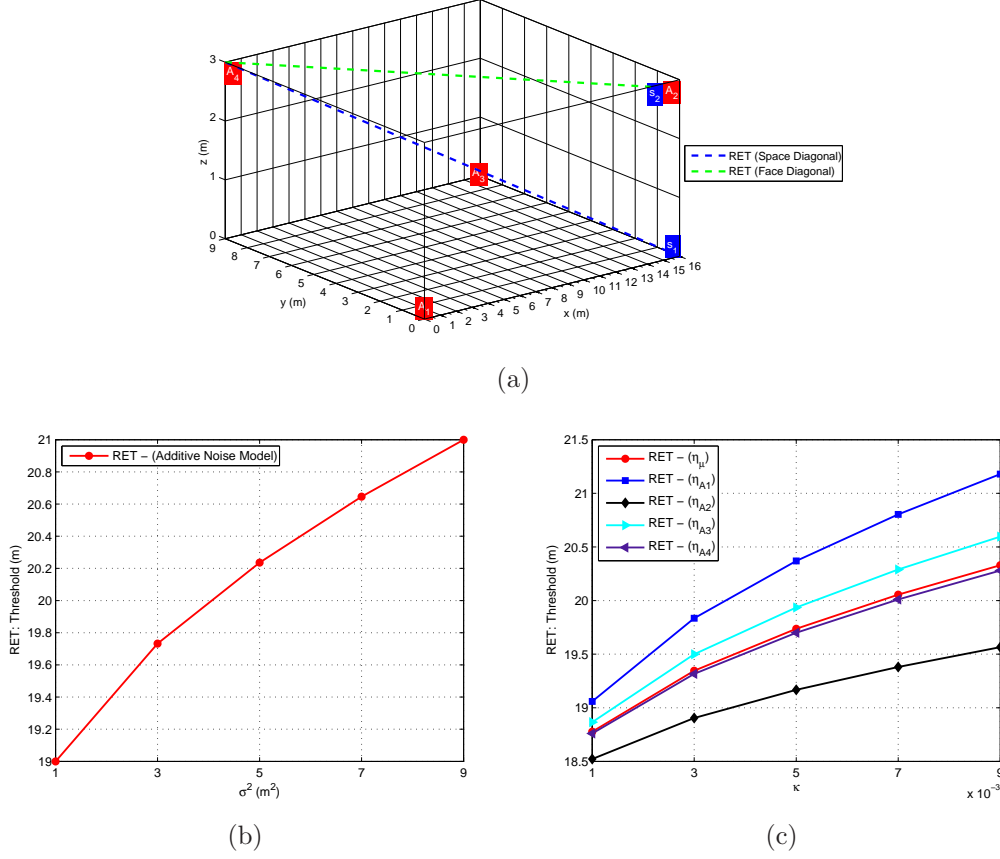


Figure 8.15: Fig. 8.15(a). Space and face diagonals between anchors and subject nodes in 3-D for RET of Lab-160. Fig. 8.15(b). RET for additive noise model where  $\sigma^2 = 1, 3, 5, 7,$  and  $9$ . Fig. 8.15(c). RET for multiplicative noise model where  $\kappa = 0.001, 0.003, 0.005, 0.007,$  and  $0.009$ .

$$\hat{d}_{ij}^{\circ} : \left\{ \hat{d}_{ij}^{\circ} \mid \hat{d}_{ij}^{\circ} \notin \hat{d}_{ij}, \hat{d}_{ij}^{\circ} \leq \text{RET} \right\} \quad (8.17)$$

Once a subject node performs range estimates with all in-range anchor nodes (i.e. 4), algorithm impose another check on successful ranging iterations. In iteration check, it finds out the number of successful ranging iterations (i.e. range estimates smaller than RET) with respect to each anchor node. The purpose of this iteration check is to make sure that a subject node uses the same number of iterations with all in-range anchor nodes. If successful range estimates between

## 8.5 Range Estimate Threshold (RET)

---

an anchor and the subject node are equal to 0, then ranging process starts again for  $n$  number of iteration. When a iteration check stops, subject node determines the location estimate using lateration scheme as discussed in chapter 4.

## 8.5 Range Estimate Threshold (RET)

---



---

### Algorithm 2 Stages of RET Algorithm

---

```

1: %  $A_N$  is total number of Anchor and Pseudo-Anchor
2: %  $A_{ir}$  is in-range anchor/pseudo-anchor nodes
3: %  $\hat{d}_{ij}^p$  is poor range estimate (i.e. greater than RET)
4: %  $\hat{d}_{ij}^o$  is preferred range estimate (i.e. smaller than RET)
5: %  $E_{RS}$  is equal number of range estimates
6: %  $Est_{loc}$  is estimated location
7: %  $E_{RMS}^{loc}$  is root-mean-square error of estimated location
8: while  $s_{j=1,\dots,N} \neq 0$  do
9:   for  $j = 1$  to  $s_j$  do
10:    for  $i = 1$  to  $size(A_N)$  do
11:      if  $(s_j(j), A_N(i))$  Adjacent then
12:         $A_{ir} \leftarrow$  In-range  $A_N(i)$ 
13:      end if
14:    end for
15:    for  $k = 1$  to  $size(A_{ir})$  do
16:      for  $l = 1$  to iterations do
17:        %  $\hat{d}_{ij}$  based on RT-ToF and RSS
18:         $\hat{d}_{ij} = d_{ij} + n_{ij}$ 
19:        if  $\hat{d}_{ij} \geq$  Range Estimate Threshold (RET) then
20:           $\hat{d}_{ij}^p \leftarrow \hat{d}_{ij}$ 
21:        else
22:           $\hat{d}_{ij}^o \leftarrow \hat{d}_{ij}$ 
23:        end if
24:      end for
25:      if  $size(\hat{d}_{ij}^o) \geq 1$  then
26:         $\hat{d}_{ij}^o \leftarrow \hat{d}_{ij}^o$ 
27:         $\hat{d}_{ij}^o \rightarrow []$ 
28:         $\hat{d}_{ij}^p \rightarrow []$ 
29:      else
30:        Go to Step 16 to perform range estimates with same anchor node
31:      end if
32:    end for
33:     $E_{RS} =$  Get equal number of ranging samples for a  $s_j$  to all  $A_i$  nodes
34:    if  $size(E_{RS}) \geq 1$  then
35:      for  $k = 1$  to  $length(E_{RS})$  do
36:        Perform lateration for each  $k$ 
37:        Calculate  $Est_{loc}$  for each  $k$ 
38:        Calculate  $E_{RMS}^{loc}$  of estimated location for each  $k$ 
39:      end for
40:    end if
41:  end for
42: end while

```

---

## 8.6 Results and Analysis

In this section, a 3-D simulation tool is developed in MATLAB to evaluate the performance of ME, CE and RET variants as listed below:

- ME Vs RET for additive noise model
- ME Vs RET for multiplicative noise model using  $\eta_{Ai}$
- ME Vs RET for multiplicative noise model using  $\eta_\mu$
- CE Vs RET for RSS path loss model using  $\eta_{Ai}$
- CE Vs RET for RSS path loss model using  $\eta_\mu$

Table 8.2: Simulation Parameters for indoor scenario

Parameter	Simulation Case 1	Simulation Case 2
Simulation scenario	Lab-262b	Lab-160b
Field dimensions (m)	12 (l) $\times$ 4 (w) $\times$ 3 (h)	12 (l) $\times$ 9 (w) $\times$ 3 (h)
RET Value	Fig.8.14	Fig. 8.15
Anchor nodes	4	4
Anchors position	$A_1 = [0 \ 0 \ 0]$ $A_2 = [12 \ 0 \ 3]$ $A_3 = [12 \ 4 \ 0]$ $A_4 = [0 \ 4 \ 3]$	$A_1 = [0 \ 0 \ 0]$ $A_2 = [16 \ 0 \ 3]$ $A_3 = [16 \ 9 \ 3]$ $A_4 = [0 \ 9 \ 3]$
Number of subject nodes	100	100
Number of iterations	100	100
Reference distance ( $d_0$ )(m)	1	1
Reference $P_r$ at $d_0$ ( $\Psi$ ) (dBm)	-39.12	-39.12
Wavelength ( $\lambda$ ) (m)	0.12	0.12
Path loss exponent ( $\eta_{Ai}$ )	$\eta_{A1} = 2.36$ $\eta_{A2} = 2.1$ $\eta_{A3} = 2.27$ $\eta_{A4} = 1.87$	$\eta_{A1} = 2.43$ $\eta_{A2} = 1.94$ $\eta_{A3} = 2.29$ $\eta_{A4} = 2.2$
Path loss exponent ( $\eta_\mu$ )	2.15	2.21
Shadowing variance ( $\sigma_{sh}^2$ )(dB)	$3.75^2 \sim 3.85^2$	$3.75^2 \sim 3.85^2$
Noise variance ( $\sigma_{RT-ToF}^2$ )(m)	1, 3, 5, 7, 9	1, 3, 5, 7, 9
$\kappa$ [41]	0.001, 0.003, 0.005 0.007, and 0.009	0.001, 0.003, 0.005, 0.007, and 0.009

## 8.6 Results and Analysis

---

To evaluate the performance, 100 randomly generated topologies are considered for 100 subject nodes. Table 8.2 shows the network simulation parameters. Since anchor nodes are considered pre-surveyed, their location is assumed to be error free. A static and stable sensor network (i.e. no mobility and no node failures) without obstacles and with nodes having accurate and symmetric radio ranges is assumed. As a metric to evaluate performance, the cumulative distribution function (CDF) plot and root-mean-square error ( $E_{\text{RMS}}$ ) of the location estimate are considered.

### 8.6.1 Simulation Case 1 : Lab-262b

Fig. 8.16 illustrates the extraction of poor range estimates ( $\hat{d}_{ij}^p$ ) which are greater than the defined RET. Fig. 8.16(a) shows range estimates for additive noise model at different values of  $\sigma^2$ . For each value of  $\sigma^2$ , RET changes for preferred range estimates by excluding  $\hat{d}_{ij}^p$ . In addition, when  $\sigma^2$  increases, the number of  $\hat{d}_{ij}^p$  also increases. Fig. 8.16 shows  $\sim 200$  more ranging samples at  $\sigma^2 = 9$  as compared to ranging samples at  $\sigma^2 = 1$ , which greater than the corresponding RET.

Fig. 8.16(b) shows poor range estimates ( $\hat{d}_{ij}^p$ ) for multiplicative noise model based on  $\eta_\mu$  and different values of  $\kappa$ . Similar to additive noise model, RET for multiplicative noise model increases with an increase in  $\kappa$ . Fig. 8.16(b) is based on  $\eta_\mu$ , therefore it shows a flat RET for each anchor node. When compared with the Fig. 8.16,  $\sim 70\%$  less  $\hat{d}_{ij}^p$  (i.e. above RET threshold) are observed for multiplicative noise model, where noise variance depends on the  $\hat{d}_{ij}$ ,  $\eta_\mu$  and  $\kappa$ .

Fig. 8.16(c) shows the poor range estimates ( $\hat{d}_{ij}^p$ ) for multiplicative noise model based on  $\eta_{Ai}$  and different values of  $\kappa$ . It can be observed that for each value of  $\kappa$ , RET varies. It is because that each anchor estimates distance with respect to its corresponding  $\eta$ . It allows each anchor to optimize range estimates by excluding the  $\hat{d}_{ij}^p$  according to individual defined RET. When compared to Fig. 8.16(b), where RET is based on  $\eta_\mu$ , and therefore same number of  $\hat{d}_{ij}^p$  are observed, but  $\hat{d}_{ij}^p$  eliminated based on individual RET. Fig. 8.16(d) shows the extraction of poor range estimates ( $\hat{d}_{ij}^p$ ) for RSS path loss model based on the defined  $\sigma_{sh}$ . Compared to additive and multiplicative noise models, RSS path loss model exclude the  $\hat{d}_{ij}^p$  based on flat RET.

## 8.6 Results and Analysis

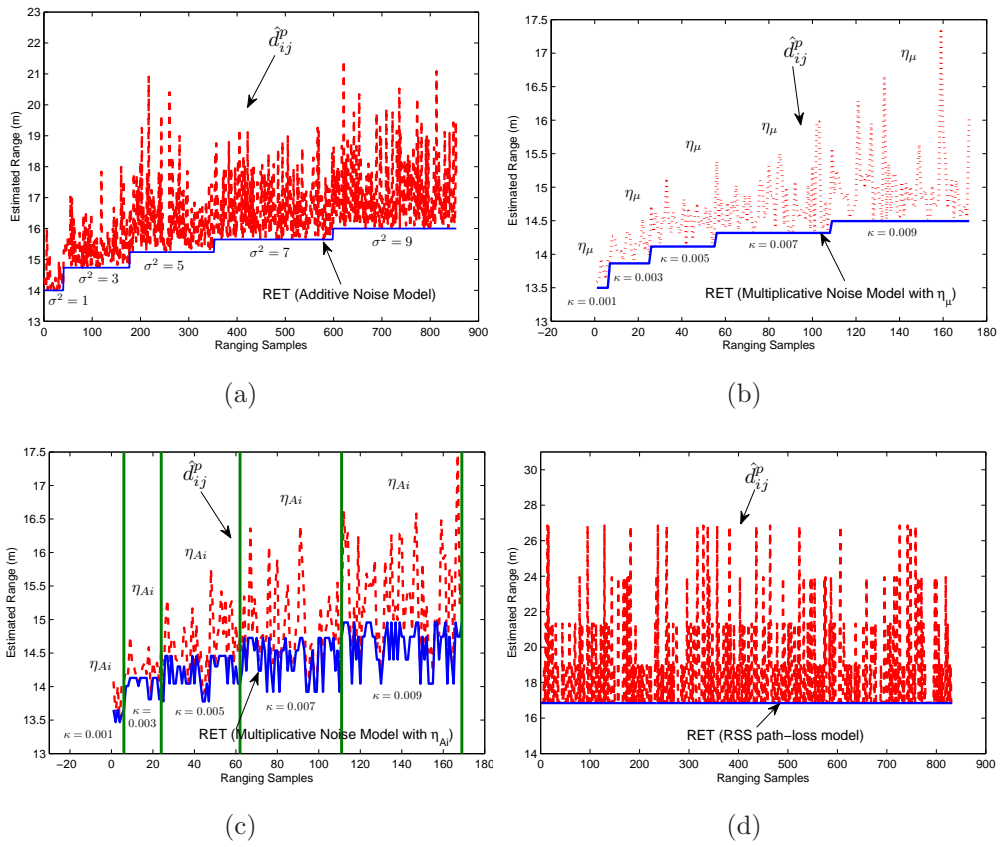


Figure 8.16: Extraction of poor range estimates ( $\hat{d}_{ij}^p$ ) based on RET defined by using lab262b field dimensions and signal models. Fig. 8.16(a). Additive noise model. Fig. 8.16(b). Multiplicative noise model using  $\eta_\mu$ . Fig. 8.16(c). Multiplicative noise model using  $\eta_{A_i}$ . Fig. 8.16(d). RSS path loss model.

## 8.6 Results and Analysis

---

Fig. 8.17 compares the CDF of  $E_{\text{RMS}}$  for additive and multiplicative noise model based on  $\eta_\mu$  and  $\eta_{A_i}$ . For this case, the simulation parameters are shown in simulation case 1 column of table 8.2. Fig. 8.17(a) shows localization performance at  $\sigma^2 = 1$  and  $\kappa = 0.001$ . As can be seen for localization based on ME (additive noise model) that only  $\sim 10\%$  of the results are accurate to within 2.5m. When compared with the localization based on ME, localization based on RET (additive noise model) seen to be more accurate and achieved up to  $\sim 40\%$  more accurate results within 2.5m. Similarly, localization based on ME (multiplicative noise model) using  $\eta_\mu$  and  $\eta_{A_i}$  shown a very close performance, where  $\sim 60\% - 75\%$  are accurate to within 1m respectively. A slightly improved performance of 10% is observed, when  $\eta_\mu$  is used. However, the performance of both variants is improved by  $\sim 10\%$ , when  $\hat{d}_{ij}^p$  are excluded based on the defined RET. This is because ME accounts all of the ranging errors, without the consideration of RET, which excludes all of the  $\hat{d}_{ij}^p$  greater than the defined RET (as plotted in Fig.8.14).

Furthermore, It is observed from Fig. 8.17(a) - Fig. 8.17(e), as  $\sigma^2$  for additive noise model and  $\kappa$  for multiplicative noise model increases, localization performance based on RET also increases. It is because as the noise variance increases,  $\hat{d}_{ij}^p$  also increases. Hence excluding  $\hat{d}_{ij}^p$  using RET enhance localization performance. It is further illustrated in Fig. 8.18(a) and Fig. 8.18(b) for additive and multiplicative noise model, where a significant improvement is observed for additive noise model. Fig. 8.18(c) illustrates the average of all samples from Fig. 8.17(a) - Fig. 8.17(e) for both additive and multiplicative noise models. It can be observed from the CDF plot that eliminating poor range estimates helps to reduce the median error from 8.5m to 4.7m for additive noise model. For multiplicative noise mode, median error is approximately reduced by 0.7m.

## 8.6 Results and Analysis

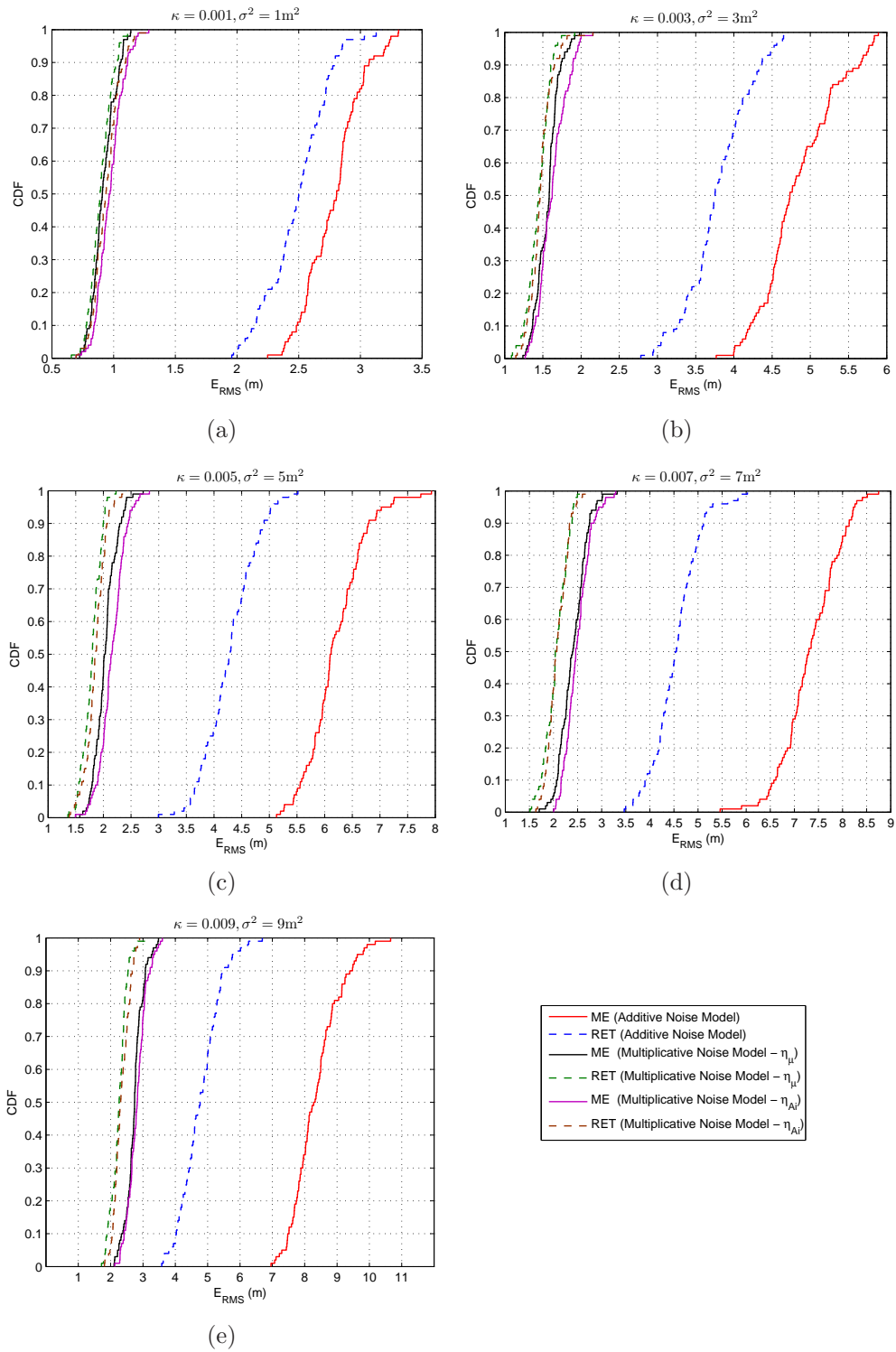


Figure 8.17: CDF comparison of ME and RET for additive and multiplicative noise models.

## 8.6 Results and Analysis

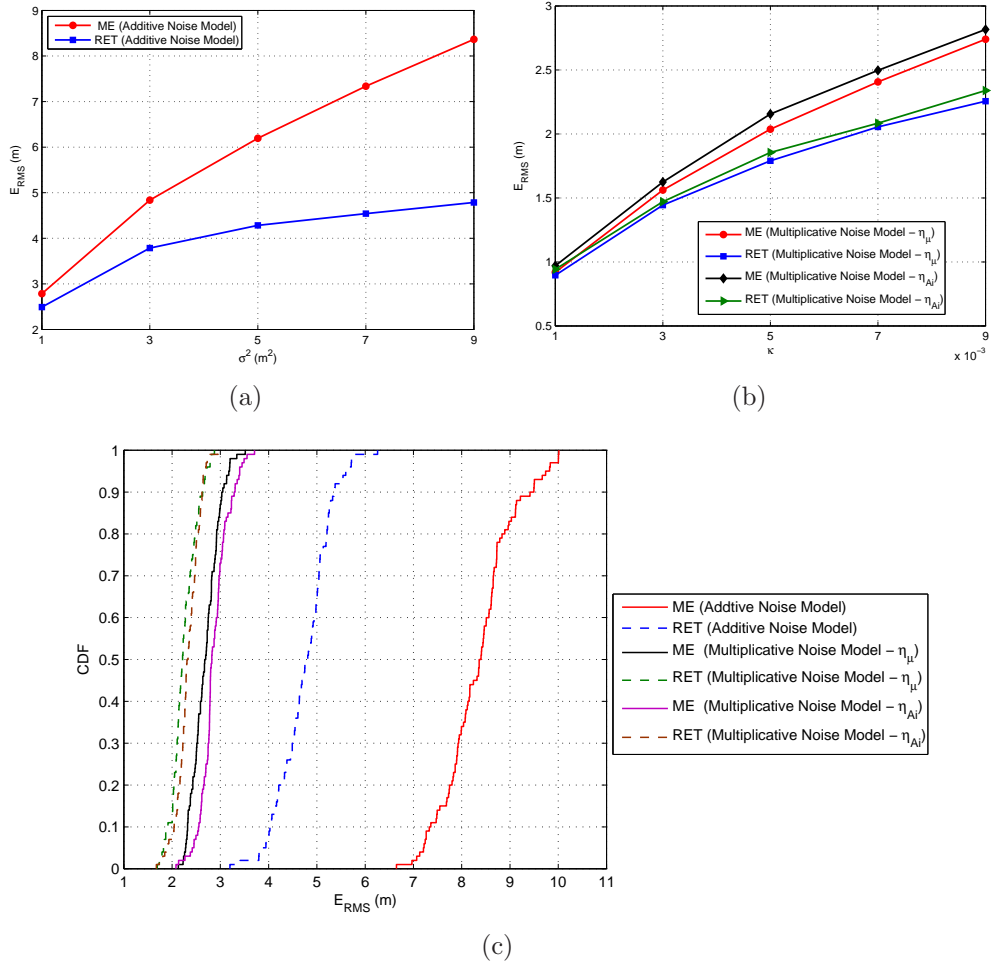


Figure 8.18: Comparison of ME and RET for additive and multiplicative noise models. Fig. 8.18(a). Additive noise model. Fig. 8.18(b). Multiplicative noise model. Fig. 8.18(c). CDF comparison of ME and RET based on all samples at  $\sigma^2 = 1, 3, 5, 7, \text{ and } 9$  for additive and  $\kappa = 0.001, 0.003, 0.005, 0.007, \text{ and } 0.009$  for multiplicative noise model from Fig. 8.17(a) - Fig. 8.17(e) for both additive and multiplicative noise models.

## 8.6 Results and Analysis

Fig. 8.19 illustrates the comparison of  $E_{\text{RMS}}$  for 100 randomly generated subject nodes for additive noise model at  $\sigma^2 = 1$  and 7. It can be seen from Fig. 8.19(a) that impact of RET compared to ME is not significant for each subject node, however the performance becomes significant as  $\sigma^2$  changes from 1 to 7, as shown in Fig. 8.19(b). Furthermore, it is observed that  $E_{\text{RMS}}$  based on RET is always smaller than ME and performance becomes significant as  $\sigma^2$  increases.

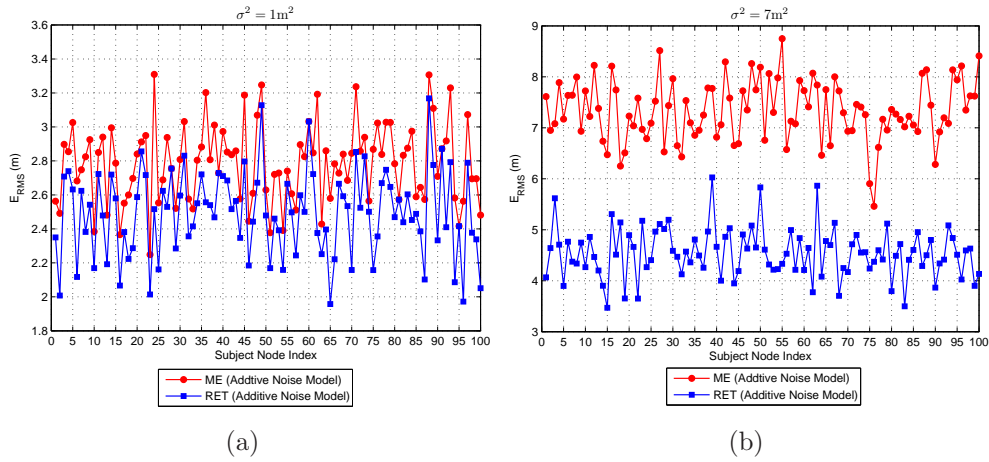


Figure 8.19:  $E_{\text{RMS}}$  comparison for each node index for additive noise model. Fig. 8.19(a) and Fig. 8.19(b) at  $\sigma^2 = 1$  and 7 respectively.

Fig. 8.20 illustrates the comparison of  $E_{\text{RMS}}$  for 100 randomly generated subject nodes for multiplicative noise model at  $\kappa = 0.001$  and 0.007. Fig. 8.20(a) and Fig. 8.20(b) present the  $E_{\text{RMS}}$  for each subject node with respect to different  $\kappa$ . It can be seen from Fig. 8.20(a) that impact of RET compared to ME is not significant for each subject node, however the difference becomes significant as  $\kappa$  changes from 0.001 to 0.007, as shown in Fig. 8.20(b). Furthermore, it is observed that  $E_{\text{RMS}}$  based on RET is always smaller than ME and the difference increases with an increase in  $\kappa$ . A very similar trend is observed for Fig. 8.20(c) and Fig. 8.20(d), where different  $\eta$  is used for each anchor node.

## 8.6 Results and Analysis

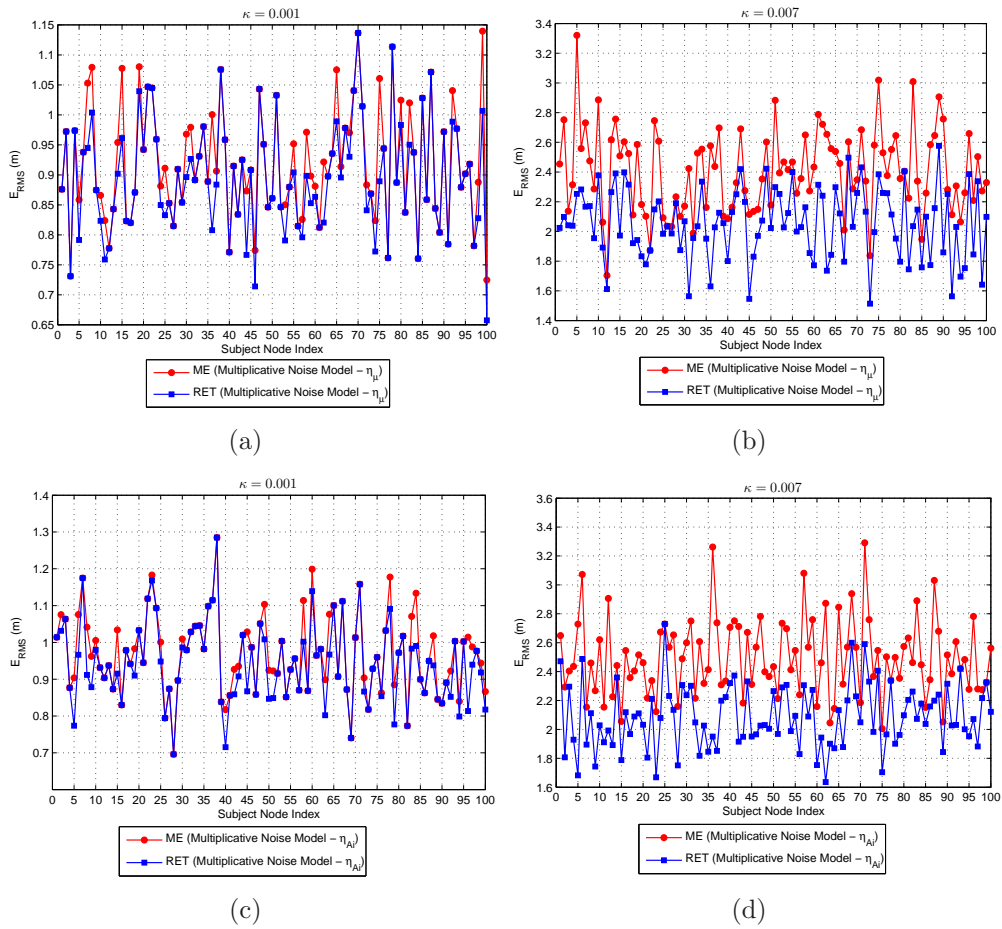


Figure 8.20:  $E_{\text{RMS}}$  comparison for each node index for multiplicative noise model. Fig. 8.20(a) and Fig. 8.20(b). Using  $\eta_{\mu}$  at  $\kappa = 0.001$  and  $0.007$  respectively. Fig. 8.20(c) and Fig. 8.20(d). Using  $\eta_{A_i}$  at  $\kappa = 0.001$  and  $0.007$  respectively.

## 8.6 Results and Analysis

Fig. 8.21 compares the CDF of  $E_{\text{RMS}}$  using CE with both variants of path loss exponents ( $\eta_{A_i}$  and  $\eta_\mu$ ). Fig. 8.21 shows the localization based on ME for (CE -  $\eta_{A_i}$ ) where 60% of the results are accurate to within 5m, however this percentage is reduced to 50% for  $\eta_{A_\mu}$ , where the average of  $\eta_{A_i}=2.15$  is used by each anchor nodes (as shown in table 8.2). It is observed that using a different but environment based  $\eta$  for each anchor node enhance localization accuracy as compared to averaged  $\eta$ . This accuracy for CE is further enhanced by using a defined RET to eliminate the  $\hat{d}_{ij}^p$  from ME. Fig. 8.21 shows that RET achieved up to  $\sim 65\%$  results more accurate to within 2m for ME (CE -  $\eta_{A_i}$ ) and  $\sim 60\%$  for ME (CE -  $\eta_\mu$ ) within 2m. This is because ME accounts all of the ranging errors, without the consideration of RET.

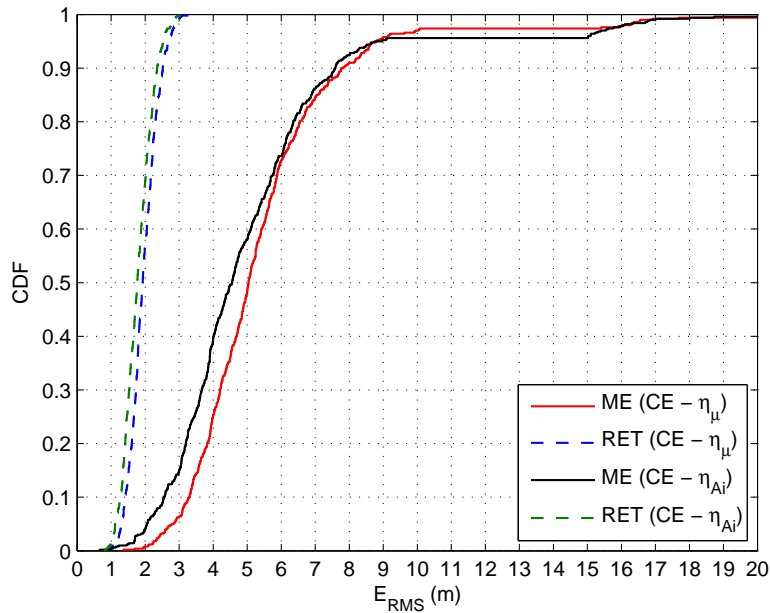


Figure 8.21: CDF comparison of ME and RET for CE based RSS localization using  $\eta_{A_i}$  and  $\eta_\mu$  in lab-262-b.

Fig. 8.22 illustrates the comparison of  $E_{\text{RMS}}$  for 100 randomly generated subject nodes for RSS based on CE. Similar to additive noise model, RET improved localization performance for each subject node by excluding  $\hat{d}_{ij}^p$  using Eq. (8.11) and Eq. (8.15). A very similar trend is observed for Fig. 8.22(b), where different

## 8.6 Results and Analysis

$\eta$  is used for each anchor node. Further, improved localization performance is observed for ME and RET based on  $CE-\eta A_i$  compared to RET based on  $CE-\eta\mu$ .

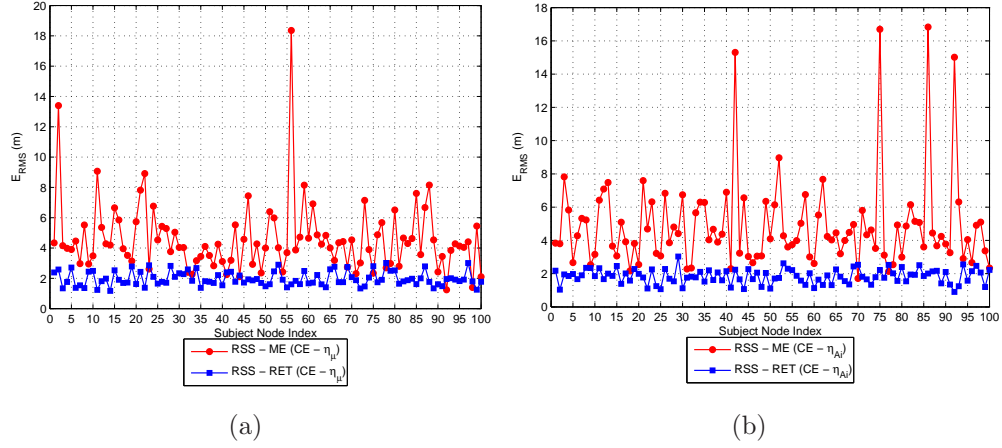


Figure 8.22:  $E_{RMS}$  comparison for each node index for RSS path loss model based on CE. Fig. 8.22(a) and Fig. 8.22(b). Using  $\eta\mu$  and  $\eta A_i$  respectively.

## 8.6 Results and Analysis

### 8.6.2 Simulation Case 2: Lab-160

Similar to Fig. 8.16 for lab-262b, Fig. 8.23 illustrates the extraction of  $\hat{d}_{ij}^p$  according to lab-160 dimensions and signal model. Fig. 8.23(a) illustrates the RET for additive noise model at different  $\sigma^2$  values. When compared to Fig. 8.16(a), a similar trend is observed, where  $\hat{d}_{ij}^p$  increases as noise variance increases. It can be seen that, at  $\sigma^2 = 7$ , RET is changed to 20.6m from 19m at  $\sigma^2 = 1$ .

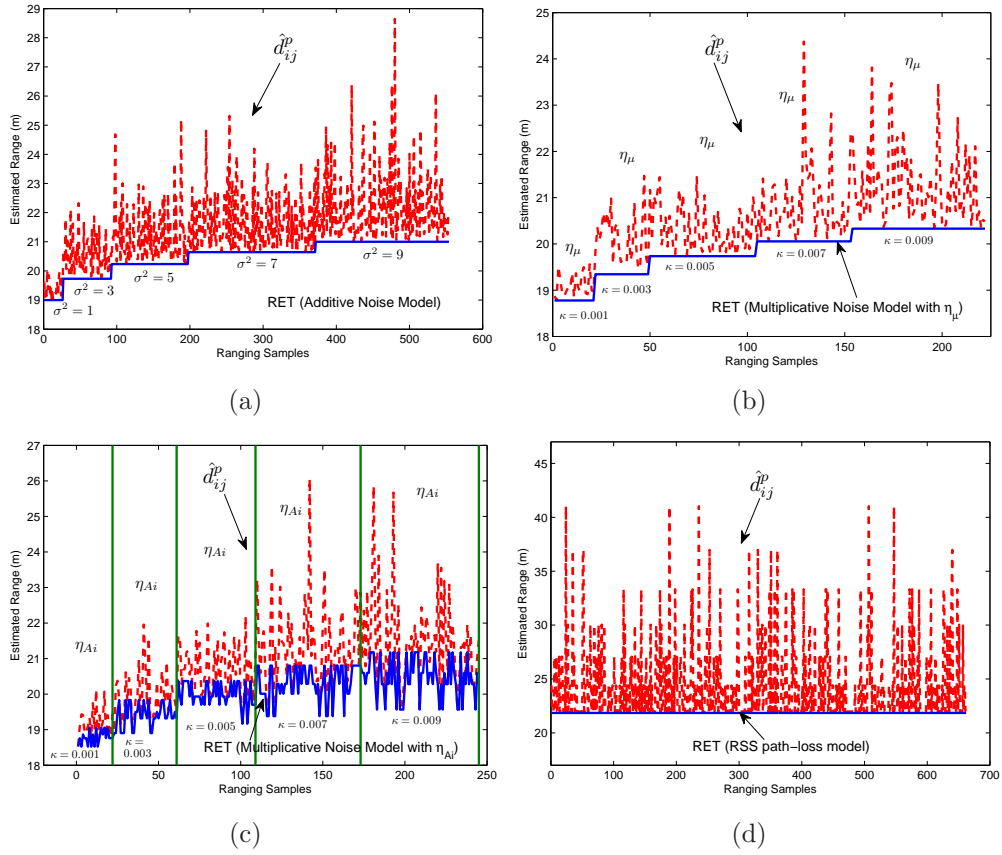


Figure 8.23: Extraction of poor range estimates ( $\hat{d}_{ij}^p$ ) based on RET defined by using lab169 field dimensions and signal models. Fig. 8.16(a). Additive noise model. Fig. 8.16(b). Multiplicative noise model using  $\eta_\mu$ . Fig. 8.16(c). Multiplicative noise model using  $\eta_{Ai}$ . Fig. 8.16(d). RSS path loss model.

Fig. 8.23(b) illustrates the RET and  $\hat{d}_{ij}^p$  for multiplicative noise model with different  $\kappa$ , where  $\eta_\mu$  is averaged  $\eta$  for each anchor. Due to the  $\eta_\mu$  for each anchor node, RET is flat at each value of  $\kappa$ . Fig. 8.23(c) shows the variation in RET,

## 8.6 Results and Analysis

where  $\eta A_i$  is used for anchor  $i$ . Fig. 8.23(d) illustrates the RET and  $\hat{d}_{ij}^p$  for RSS path loss model, where RET is flat based on the  $\sigma_{sh}^2$ .

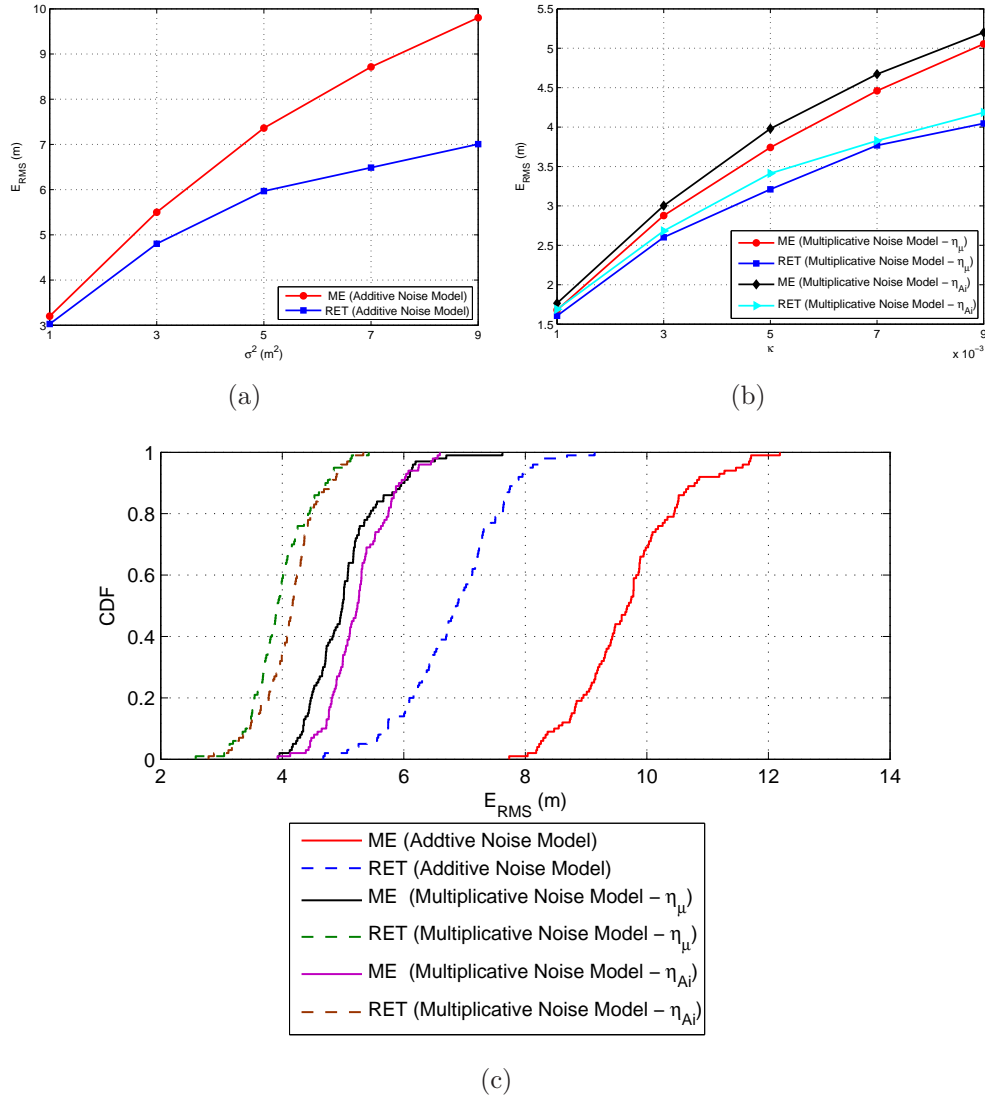


Figure 8.24: Comparison of ME and RET using additive and multiplicative noise models for lab-160 dimensions. Fig. 8.24(a). Additive noise model. Fig. 8.24(b). Multiplicative noise model. Fig. 8.24(c). CDF comparison of ME and RET based on all samples at  $\sigma^2 = 1, 3, 5, 7,$  and  $9$  for additive and  $\kappa = 0.001, 0.003, 0.005, 0.007,$  and  $0.009$  for multiplicative noise model.

Fig. 8.24(a) illustrates the comparison of ME and RET for additive noise model. As shown, RET outperformed ME for each value of  $\sigma^2$ . At  $\sigma^2 = 9$ ,

## 8.6 Results and Analysis

---

$E_{\text{RMS}}$  of  $\sim 10\text{m}$  for ME is reduced to  $7\text{m}$  for RET, which is  $\sim 1.4\text{m}$  higher than the difference observed at  $\sigma^2 = 5$ . It suggests that, performance of localization based on RET increases as  $\hat{d}_{ij}^p$  increases. A very close trend is observed, when compared with Fig. 8.24(a) (lab-262b). Fig. 8.24(b) illustrates the comparison of ME and RET for multiplicative noise model using  $\eta_\mu$  and  $\eta_{A_i}$ . Similar to additive noise model, RET based on multiplicative model also outperformed ME for each  $\kappa$ . When compared with ME and RET using  $\eta_{A_i}$ ,  $\eta_\mu$  shows slightly improved performance. Fig. 8.24(c) shows the CDF comparison of ME and RET for both additive and multiplicative noise models, where each curve represent all samples (i.e. at  $\sigma^2 = 1, 3, 5, 7$  and  $9$  for additive and at  $\kappa = 0.001, 0.003, 0.005, 0.007$  and  $0.009$  for multiplicative) from Fig. 8.24(a) and Fig. 8.24(b) respectively. For combined samples, ME for additive noise model shows that only 35% of the results are accurate to within  $6\text{m}$ , which are  $\sim 25$  greater than results for RET (additive noise model). For multiplicative, RET based on  $\eta_\mu$  shows better performance, where  $\sim 82\%$  of the results are accurate to within  $4\text{m}$ , which reflects an improvement of  $\sim 22\%$  compared to ME based on  $\eta_{mu}$ . Similar to Fig. 8.18(c), Fig. 8.24(c) illustrates the average  $E_{\text{RMS}}$  of all samples (i.e.  $\sigma^2 = 1, 3, 5, 7,$  and  $9$ ) for both additive and multiplicative noise models. It can be observed from the CDF plot that throwing away range estimates greater than the defined RET helps to reduce the median error from  $9.7\text{m}$  to  $6.5\text{m}$  for additive noise model. For multiplicative noise mode, median error is approximately reduced by  $0.7\text{m}$ .

Fig. 8.25 compares the CDF of  $E_{\text{RMS}}$  for ME and RET using CE with both variants of path loss exponents ( $\eta_{A_i}$  and  $\eta_\mu$ ). Localization based on ME for (CE -  $\eta_{A_i}$ ) in Fig. 8.25 shows 70% of the results are accurate to within  $6\text{m}$ , whereas this percentage is reduced to 60% for  $\eta_{A_\mu}$ , where the average of  $\eta_{A_i}=2.21$  is used by each anchor (as shown in table 8.2). It is observed that using a different and environment based  $\eta$  for each anchor node enhance localization accuracy compared to averaged  $\eta_\mu$ . This accuracy for CE is further enhanced by using a defined RET to eliminate  $\hat{d}_{ij}^p$  from ME. Fig. 8.25 shows that RET is more accurate and achieved upto  $\sim 85\%$  results more accurate to within  $3\text{m}$  for ME (CE -  $\eta_{A_i}$ ) and  $\sim 40\%$  for ME (CE -  $\eta_\mu$ ) within  $3\text{m}$ .

Fig. 8.26 illustrates the comparison of  $E_{\text{RMS}}$  for 100 randomly generated subject nodes for RSS path loss model based on CE. Similar to additive noise

## 8.6 Results and Analysis

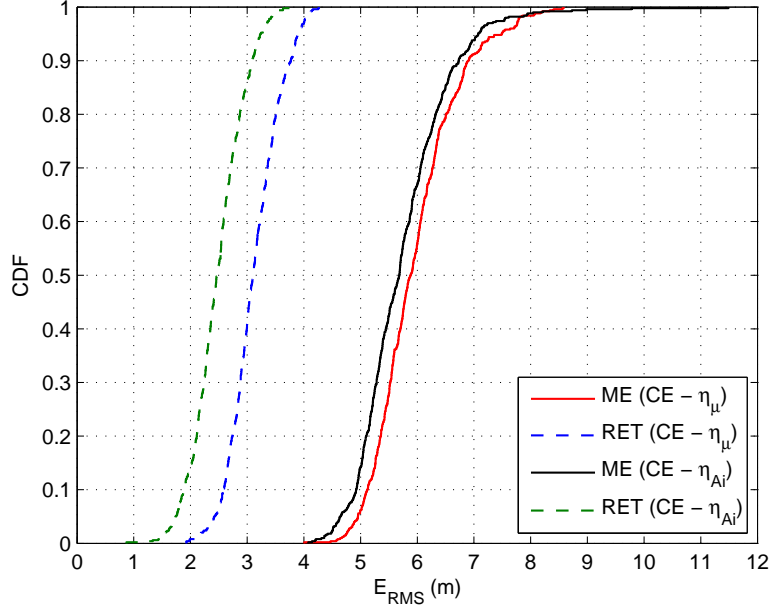


Figure 8.25: CDF comparison of ME and RET for CE based RSS localization using  $\eta_{A_i}$  and  $\eta_\mu$  in lab-160.

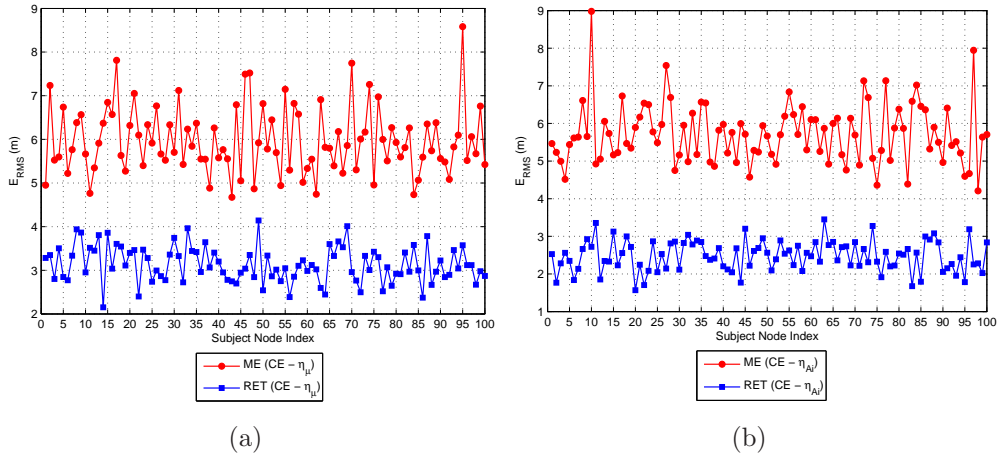


Figure 8.26:  $E_{RMS}$  comparison for each node index for RSS path loss model based on CE. Fig. 8.26(a) and Fig. 8.26(b). Using  $\eta_\mu$  and  $\eta_{A_i}$  respectively.

model, RET improved localization accuracy of each subject node by excluding  $\hat{d}_{ij}^p$  using Eq. (8.11) and Eq. (8.15). A very similar trend is observed for Fig. 8.26(b), where different  $\eta$  is used for each anchor node. Furthermore, Fig. 8.25

## 8.7 Conclusion

---

shows improved localization performance for ME and RET based on CE -  $\eta_{A_i}$  as compared to CE -  $\eta_\mu$ .

## 8.7 Conclusion

This paper presents an indoor 3-D localization based on three signal models named additive, multiplicative noise models for time based ranging and log-normal shadowing model for RSS. Furthermore, the multiplicative noise model and shadowing model are categorized into two different variants according to the calibration process of environment dependent channel parameter named CE. For CE, IEEE 802.15.4 compliant devices are used in two different lab environments (lab-262b and lab-160) to log RSSI for each anchor node. The logged RSSI between each anchor and the subject node is exploited to calibrate the  $\eta_{A_i}$ ,  $\eta_\mu$  and  $\sigma_{sh}$  in order to characterize channel model. Based on the field dimensions and signal model, a new scheme named RET is proposed for improved localization performance. Finally to evaluate, the LS method for localization is used and performance is compared. Observations based on extensive simulations in a MATLAB designed tool highlight the following points:

- For additive noise model, the advantage of RET compared to ME depends on  $\sigma^2$ . A smaller value of  $\sigma^2$  indicates the presence of less ranging error, hence it reduces the occurrence of the poor range estimates (i.e. greater than the defined RET). As  $\sigma^2$  increases, the advantage of RET compared to ME also increases, due to the fact that, a larger value indicates the presence of more poor range estimates. Hence, RET enhance localization performance by mitigating ( $\hat{d}_{ij}^p$ ) from ME according to the defined RET.
- For multiplicative noise model, the advantage of RET compared to ME depends on the  $\eta$  and  $\kappa$ . It is observed that the difference of range optimization through RET compared to ME becomes larger as the value of  $\kappa$  increases.
- A very close localization performance is observed for multiplicative noise model based on  $\eta_\mu$  and  $\eta_{A_i}$ . However,  $\eta_\mu$  showed slightly improved localization accuracy.

## 8.7 Conclusion

---

- For RSS, it is observed that the actual knowledge of the  $\eta$  plays a vital role in the performance of the system. Due to the environment dependent nature of  $\eta$ , the knowledge of exact  $\eta$  is unattainable. Hence, a priori calibration may become impractical. To overcome,  $\eta$  should be considered as random variable instead of a deterministic value.

On the whole, localization based on RET compared to ME showed improved accuracy for additive, multiplicative and RSS path loss model.

# Chapter 9

## Conclusions and Future Research

### 9.1 Conclusions

This thesis presents a research into optimization of range aware localization in wireless sensor networks. In general, localization error in the sensor networks context is a result of several mechanisms such as inaccurate range estimates, error propagation due to pseudo-anchors, and bad geometric placement of anchor nodes. This dissertation deals with these location error mechanisms to optimize the range aware localization. The contribution of this dissertation involve analysis of round-trip time-of-flight (RT-ToF) and received signal strength (RSS) based ranging using Jennic's JN5148, performance analysis of lateration based schemes incorporating geometric dilution of precision (GDOP) and pseudo-anchors, potential of optimal anchor placement in 2-D and 3-D, implementation of Range Aware Localization System (RALS) on IEEE 802.15.4 compliant devices and indoor localization based on range estimate threshold (RET). This chapter summarizes the contribution for each of the focused area as follows:

- **Chapter 3:** This chapter analyse the performance limits of round-trip time-of-flight (RT-ToF) and received signal strength (RSS) based ranging using Jennic's JN5148, IEEE 802.15.4 compliant WSNs. The fundamental CRLB on ToF and RSS ranging performance is compared with the performance limits of JN5148 series ranging modules. The results indicate that the measured performance limits of ToF and RSS based range measurement

## 9.1 Conclusions

---

approaches the theoretical CRLB. Using a site survey tool prior to measuring ToF and RSS over different lower noise channels helped not only to improve the confidence in a burst of readings but also improved accuracy. The results over a short range demonstrate that RSS is a good candidate for range estimation at ranges less than  $\sim 7\text{m}$  for outdoor and indoor unobstructed paths. Uncertainty in RSS based range estimation increases with distance and beyond  $7\text{m}$ , presents severe limitations in using RSS. Further investigating NLOS path, RSS ranging is found to be too erratic to be used in realistic location systems as compared to ToF at any range. Comparing ToF on LOS paths for different antenna heights in outdoor and indoor environment, ToF measurements are seen to be largely independent of antenna height. However, at antenna height of  $1.5\text{m}$  the MMRE is found to be lowest. As compared to ToF, RSS is found to be more dependent on antenna heights as range increases. However, antenna height of  $1.5\text{m}$  showed better ranging accuracy at range less than  $\sim 7\text{m}$ .

- **Chapter 4:** When using a lateration scheme, the localization accuracy is highly influenced by poor anchor placement. Comparative performance analysis of localization using sub-optimal lateration (SBT), optimal-multi-lateration (OML), and modified sub-optimal blind trilateration (MSBT) based on knowledge of geometric dilution of precision (GDOP) is explored. OML, considering ranging information from all in-range anchors/pseudo-anchors to calculate the subject position performs better in terms of accuracy than SBT and stays very close to MSBT based on GDOP. The average processing time (close to SBT) and average location error (close to MSBT) of OML provides the best performance in the context of WSNs. SBT reduces the computational complexity and processing but increases the location errors due to potentially poor selection of anchors/pseudo-anchors and ranging error. GDOP has been shown to avoid poor topographic layout during the selection of anchor/pseudo-anchor nodes in a dense environment at the cost of very high computation from  $O(1)$  combination of anchors) to  $O(\text{combination of choosing } 3 \text{ anchors from } n \text{ anchors combinations})$ . A combination of SBT and GDOP provides the minimum estimated

## 9.1 Conclusions

---

location error but leads to substantial performance degradation in terms of power consumption (processing) as compared with the SBT and OML. It makes GDOP less attractive approach in the context of resource constrained WSNs (i.e. where adding extra battery power is not possible). Performance of these lateration based approaches (SBT, OML and MSBT) presents a trade-off for complex computation, thus energy consumption and accuracy. It leads to investigate the problem of optimal placement of anchor nodes to optimize the range aware localization.

- **Chapter 5:** Conventionally, deploying large number anchor nodes reduces localization inaccuracy; however this holds true only if the anchors are in alternative arbitrary placement. The optimality in the anchor placement for both additive and multiplicative noise models has been achieved by choosing the combination of anchors with the minimum m-CRLB in 2-D and 3-D environments. It is concluded through extensive simulations, that optimal anchor placement for the additive noise and multiplicative noise model are different. This chapter further extends the understanding of optimal anchor placement and its impact on range aware localization error. The anchor placement findings for both noise models are the exploited to analyse the performance comparison between optimal and arbitrary anchor placement.
- **Chapter 6:** The least-squares (LS) and approximate maximum likelihood (AML) methods are used for localization performance analysis in 2-D and 3-D and their performance is compared with the lower bound for optimal, worst and arbitrary anchor placements. In corroborative terms, the AML has shown better performance than LS across all the channel variance and anchor positions in 2-D and 3-D. It is observed that using 3 anchors AML specifically outperforms the LS method, however as anchors increase from 4 to 8 the difference between the LS and AML becomes lesser and on many locations for example using 6 anchors the performance of LS and AML in case of 3D becomes same. This is usually because for both methods, there are enough anchors and information to zero-in on the subject node. However with only 3 anchors, the AML gives significantly better performance than

## 9.1 Conclusions

---

LS. Although this accuracy comes with a trade-off, the trade-off is that the computational complexity of AML is significantly higher than LS. In addition, it is observed that AML needs at least 4-5 arbitrary placed anchors to give a performance better than the optimally placed anchors using the LS method. For multiplicative noise model, It is noticed that the optimal anchor placement for 3 anchors is close to a straight line (i.e. collinear) and therefore, LS/AML will show poor performance as compared to any other arbitrary anchor placement (as long as they are not on a straight line). It is concluded that the geometry of anchors and subject node has a serious impact on the localization process.

- **Chapter 7:** This chapter extends the understanding and importance of optimal anchor placement through the development of distributed Range Aware Localization System (RALS). RALS is implemented on IEEE 802.15.4 compliant devices, where a device (i.e. subject node) takes less than 2 seconds to perform localization using LS method. RALS is exploited on a 6m×6m testbed to compare localization performance using different anchor and subject node placements. It is verified through RALS that, the optimized anchor placement is an important factor to enhance localization accuracy.
- **Chapter 8:** A new 3-D scheme named *Range Estimate Threshold* (RET) is proposed. The proposed scheme defines a RET based on the 3-D field dimensions and the signal noise model to mitigate the poor range estimates ( $\hat{d}_{ij}^p$ ) from *Measured Estimation* (ME) to optimize range estimates. The ramification of RET on ME for indoor localization is explored through additive, multiplicative and log-normal shadowing models. Furthermore, the multiplicative noise model and shadowing model are categorized into two different variants according to the calibration process of environment dependant channel parameter named calibrated estimation (CE). Performance comparison based on the extensive simulations in MATLAB designed tool highlight the following points:

## 9.2 Future Research and Improvements

---

- For additive noise model, the advantage of RET compared to ME depends on  $\sigma^2$ . A smaller value of  $\sigma^2$  indicates the presence of less ranging error, hence it reduces the occurrence of the poor range estimates (i.e. greater than the defined RET). As  $\sigma^2$  increases, the advantage of RET compared to ME also increases, due to the fact that, a larger value indicates the presence of more poor range estimates. Hence, RET enhance localization performance by optimizing the ME (i.e. mitigates the  $\hat{d}_{ij}^p$ ) according to the defined RET.
- For multiplicative noise model, the advantage of RET compared to ME depends on the  $\eta$  and  $\kappa$ . It is observed that the difference of range mitigation through RET compared to ME becomes larger as the value of  $\kappa$  or  $\eta$  increases.
- For RSS, it is observed that the actual knowledge of the  $\eta$  plays a vital role in the performance of the system. Due to the environment dependent nature of  $\eta$ , the knowledge of exact  $\eta$  is unattainable. Hence, a priori calibration may become impractical. To overcome,  $\eta$  should be considered as random variable instead of a deterministic value based on the calibration.

On the whole, localization performance based on the RET scheme over ME showed better localization performance for additive, multiplicative and RSS path loss model.

## 9.2 Future Research and Improvements

The following are some promising directions.

### 9.2.1 Cooperative Localization (Extension to chapter 4)

In many scenarios a number of subject nodes have to be localized, in such cases, not all nodes are in radio range of the minimum number of anchor nodes. However, this problem can be overcome by cooperation of nodes with each other. Thus a subject node, when located can act as a pseudo anchor and then in turn

## 9.2 Future Research and Improvements

---

locate the unknown subject locations (as explained and simulated in chapter 4). Furthermore, even if all subject nodes are in radio range of all the anchors, cooperation between devices can enhance system performance with a trade-off for complex computation, thus energy consumption. In many cases, the anchor nodes are to be located via GPS. Positioning with GPS has an inherent location error associated with it. When these anchors are used in locating subject nodes in a cooperative environment, the error propagates through the network and the end subject node location can have unacceptable errors. Thus the distance equation between the anchors and subject node can now be given as:  $\hat{d}_{ij} = d_{ij} + n_{ij} + e_{ij}$ , where  $n_{ij}$  is Gaussian error associated with distance measurement and  $e_i$  is error in the anchor location. Furthermore,  $e_i$  can also be assumed as a Gaussianly distributed error. Thus there is a need for a comprehensive error analysis for cooperative localization with the anchors position in error.

### 9.2.2 Additive/Multiplicative noise model

The additive noise model has been predominantly accepted by researchers. However, theoretically the accuracy depends on the received signal to noise ratio (SNR) which in turn depends on the distance. In order to have conclusive evidence to see which noise model best fits the observed distance, further experimentations are to be carried out with real time systems. This requires range measurement at incrementing distances and analyse the variance of the distribution of error.

### 9.2.3 Gaussianity assumption

Gaussianity assumption is prevalent and fundamental to many statistical theories and engineering applications. Range measurement errors are generally assumed to reveal Gaussian distribution. We analysed the  $X_i = \mathcal{N}(\mu, \sigma^2)$  for  $i = 0, 1, \dots, n$ , where  $n$  is total number of range measurements  $X$ . To scrutinize this hypothesis, instead of relying on artificially generated random variables, real time ranging data was obtained from experiments using IEEE 802.15.4 compliant devices, covering outdoor/indoor environment with both line-of-sight (LOS) and non-line-of-sight (NLOS) conditions [127]. Distribution of range measurements were analysed using four goodness-of-fit (GOF) tests i.e. Graphical

## 9.2 Future Research and Improvements

---

technique, Linear correlation coefficient, Anderson-Darling, and Chi-squared. It was observed that majority of the outcomes are same in all the tests with a high percentage disagreement with the assumption. However further experiments are to be conducted as future work to conclusively reach a distribution that best describes the distance error.

### 9.2.4 Path loss Exponent ( $\eta$ )

In the RSS case and hybrid signal (RSS+TOA) the actual knowledge of the  $\eta$  plays an important role in system performance. The  $\eta$  in general is considered to be known and its value lies between 2-6. This is achieved by off-line measurements. However, in real time systems the  $\eta$  is environment dependant and such prior measurements may become impractical. Hence knowledge of its exact true value is unattainable. Thus the value of the  $\eta$  has to be estimated instead of assuming any prior value. In this regard, a joint estimator has been proposed in [128], which jointly estimates the  $\eta$  alongside the unknown coordinates of the subject node for the RSS case. For a hybrid signal model case, [129] provides an error analysis when the  $\eta$  is considered to be in error. However, the  $\eta$  can be considered as a random variable instead of a deterministic quantity. This calls for the derivation of Bayesian type estimators where we could use the prior distribution of the  $\eta$  (obtained through experimentations). This approach promises better performances and is to be investigated in future work.

### 9.2.5 Optimal anchor placement

In chapter 5, the optimal anchor placements for anchor nodes were achieved on the basis of the minimum m-CRLB for additive and multiplicative noise model. As an alternative, the optimal anchor placement can be based on rejecting all anchor positions that offer higher than a threshold m-CRLB. This is helpful when a specific area is chosen and it is desired to obtain higher accuracy within that area, disregarding other points (such as near the anchors). Thus we might expect different anchor positions than as shown in chapter 5. Furthermore, optimal anchor placement for more complex area shapes other than a simple square area is to be investigated. In addition, the anchor placement as shown in chapter 5 are

### 9.3 Sectorization Using Optimal Anchor Placement

---

achieved for a uniform (grid) subject node deployment. As a future work, optimal anchor placement for more distribution such a Gaussian and Poisson subject node distribution are to be investigated.

#### 9.2.6 Experiencing RALS

Future work will target to enhance the capability of RALS in following areas:

- In this work, RALS is limited to the 3 anchors for localization in 2-D. As seen in chapter 5 and chapter 6 that increasing the number of anchor nodes increases the localization accuracy. To analyse the impact on localization accuracy, future work will target more number of anchor nodes in 2-D and 3-D.
- In addition to RT-ToF, RALS development will be extend by integrating RSS based localization.
- Implementation of the 3-D proposed scheme RET in different environment for potential applications in indoor environment.
- Analyses the impact of antenna orientation and height on localization performance using RALS.

### 9.3 Sectorization Using Optimal Anchor Placement

It is verified in chapter 5 and 6, that for multiplicative noise model that as the field dimensions increase, the m-CRLB increases at constant  $\kappa$  and  $\eta$  (as shown in Fig. 5.19(a), Fig. 5.19(b) and Fig. 5.19(c) for  $21 \times 21$ ,  $31 \times 31$  and  $41 \times 41$  respectively, hence MSE increases. Thus one of the approaches to reduce the MSE could be dividing a large dimension of area into small sectors, such that each sector has a smaller dimension to handle. As the anchors would be near to the subject nodes, the estimated distance, hence noise variance would be fairly small as compared to un-sectored case

### 9.3 Sectorization Using Optimal Anchor Placement

---

As it is observed from results in section 6.2 that optimal placement for 3 anchors (Fig. 5.18(a)) in multiplicative noise model does not exhibit better accuracy compared to arbitrary placement (additive's optimal), it is therefore, additive's optimal placement for 3 anchors can be used as optimal anchor placement for multiplicative. Fig. 9.1(a) - Fig. 9.1(c) show the sectorization of localization field for 3, 4 and 5 anchors. Fig. 9.1(a) shows that a  $100 \times 100$  is divided into the 4 sub-sectors using 4 optimally placed anchor nodes. It can be seen from sectorized scenario Fig. 9.1(d), that it will consume more number of anchors. However, as observed in chapter 4 that, optimal multi-lateration (OML) needs extra computation as the number of anchors to perform localization increases, whereas sub-optimal trilateration (SBT), which limits to the 3 anchors exhibit lower processing. Thus, it would help to reduce the processing as each sector would be limited to use minimum 3 or 4 anchors. A further in-depth analysis of sectorization compared to un-sectorized localization field will be carried out in future work.

### 9.3 Sectorization Using Optimal Anchor Placement

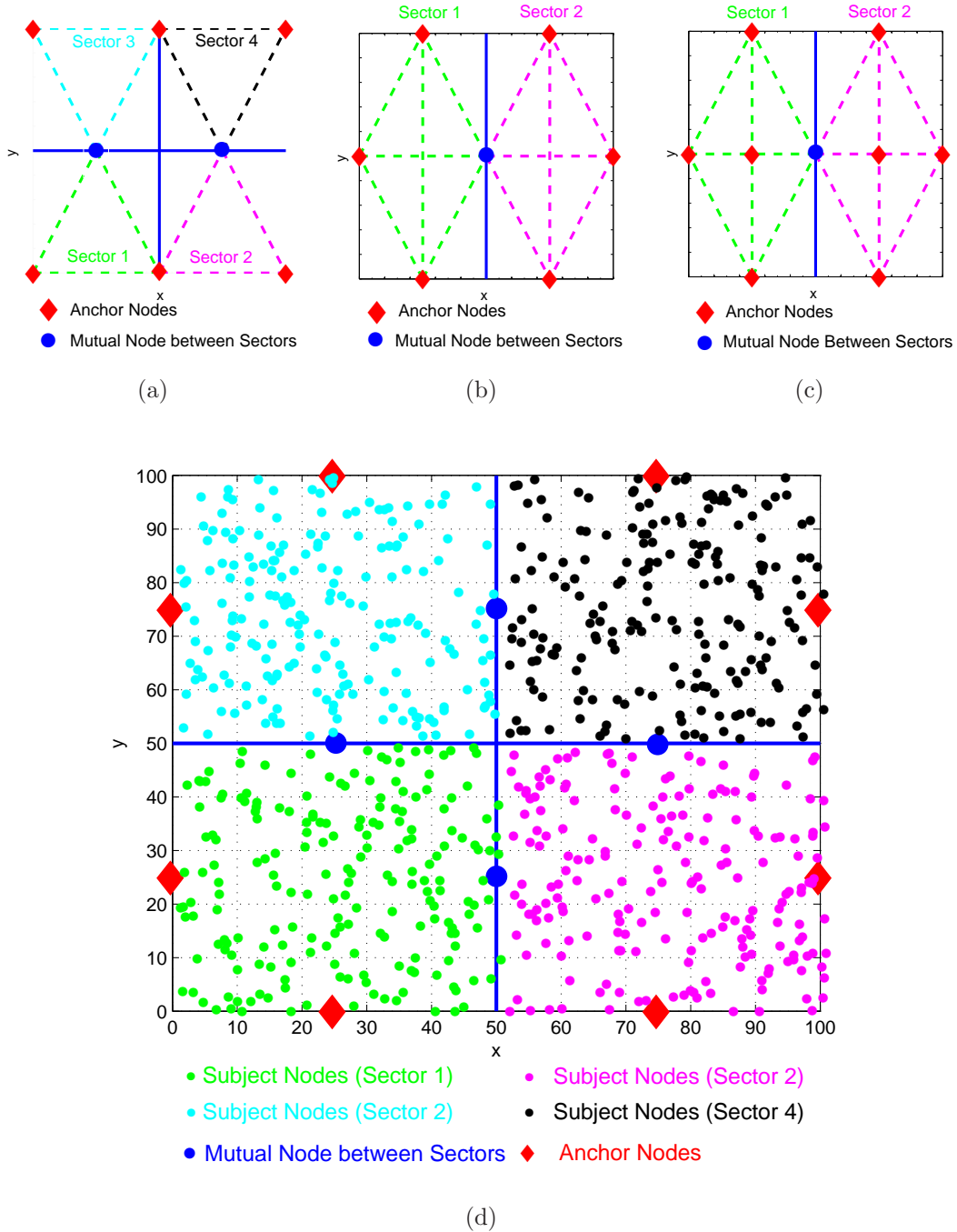


Figure 9.1: Fig. 9.1(a) - Fig. 9.1(c). Sectorization of localization field with respect to 3, 4 and 5 optimally placed anchor nodes for multiplicative noise model. Fig. 9.1(d). Simulation setup for sectorization with respect to 4 optimal placed anchors for multiplicative noise model.

# References

- [1] “Data Sheet: JN5148-001, IEEE802.15.4 Wireless Microcontroller,” 2011. [Online]. Available: [http://www.jennic.com/files/product\\_briefs/JN-DS-JN5148-1v6.pdf](http://www.jennic.com/files/product_briefs/JN-DS-JN5148-1v6.pdf) xi, 1, 2, 47, 48, 49, 184, 202
- [2] J. Hightower, B. Brumitt, and G. Borriello, “The location stack: a layered model for location in ubiquitous computing,” in *Mobile Computing Systems and Applications, 2002. Proceedings Fourth IEEE Workshop on*, 2002, pp. 22 – 28. xi, 16, 17
- [3] “Jennic NXP: Single-Ended PCB Antenna Module, Reference Manual,” 2008. [Online]. Available: [http://www.jennic.com/files/support\\_files/JN-RM-2040-Single-Ended-PCB-Antenna-Module-1v1.pdf](http://www.jennic.com/files/support_files/JN-RM-2040-Single-Ended-PCB-Antenna-Module-1v1.pdf) xi, 49, 50
- [4] “10 Technologies That Will Change the World,” February 2004, Online accessed: June 2011. [Online]. Available: <http://www.technologyreview.com/Infotech/13438/> 1, 3, 17
- [5] I. F. Akyildiz, W. Su, Y. Sankarasubramaniam, and E. Cayirci, “Wireless sensor networks: a survey,” *Computer Networks (Amsterdam, Netherlands: 1999)*, vol. 38, no. 4, pp. 393–422, 2002. 2
- [6] B. Peng, A. Kemp, and H. Maheshwari, “Impact of location errors on energy-efficient geographic routing in wireless sensor networks,” in *15th Asia-Pacific Conference on Communications, 2009. APCC 2009.*, oct 2009, pp. 830 –833. 3

## REFERENCES

---

- [7] A. Srinivasan and J. Wu, “A Survey on Secure Localization in Wireless Sensor Networks,” in *International Conference on Wireless and Mobile Communications*, 2007. [3](#)
- [8] N. Bulusu, J. Heidemann, and D. Estrin, “GPS-less low-cost outdoor localization for very small devices,” *Personal Communications, IEEE*, vol. 7, no. 5, pp. 28–34, oct 2000. [3](#), [8](#)
- [9] T. He, C. Huang, B. M. Blum, J. A. Stankovic, and T. Abdelzaher, “Range-free localization schemes for large scale sensor networks,” in *Proceedings of the 9th annual international conference on Mobile computing and networking*, ser. MobiCom ’03. New York, NY, USA: ACM, 2003, pp. 81–95.
- [10] E. Garci anda, A. Bermu anddez, and R. Casado, “Range-free localization for air-dropped WSNs by filtering node estimation improvements,” in *Wireless and Mobile Computing, Networking and Communications (WiMob), 2010 IEEE 6th International Conference on*, oct. 2010, pp. 471–478. [3](#), [25](#), [40](#)
- [11] A. Smith, H. Balakrishnan, M. Goraczko, and N. Priyantha, “Tracking moving devices with the cricket location system,” in *Proceedings of the 2nd international conference on Mobile systems, applications, and services*, ser. MobiSys ’04. New York, NY, USA: ACM, 2004, pp. 190–202. [3](#), [20](#), [199](#)
- [12] P. Bahl and V. Padmanabhan, “RADAR: an in-building RF-based user location and tracking system,” in *INFOCOM 2000. Nineteenth Annual Joint Conference of the IEEE Computer and Communications Societies. Proceedings. IEEE*, vol. 2, 2000, pp. 775–784 vol.2. [20](#), [22](#), [35](#), [41](#), [194](#), [199](#), [200](#), [204](#), [209](#)
- [13] Z. Yang and Y. Liu, “Quality of Trilateration: Confidence Based Iterative Localization,” in *Distributed Computing Systems, 2008. ICDCS ’08. The 28th International Conference on*, june 2008, pp. 446–453. [3](#)
- [14] G. Mao, B. Fidan, and B. D. O. Anderson, “Wireless sensor network localization techniques,” *Computer. Networks.*, vol. 51, pp. 2529–2553, July 2007. [3](#), [4](#), [16](#), [18](#), [21](#), [40](#), [41](#), [80](#)

## REFERENCES

---

- [15] J. Kolodziej, K.W. ; Hjelm, *Local Positioning Systems: LBS Applications and Services*. CRC Press, 2006. [3](#), [18](#)
- [16] R. Mautz, W. Ochieng, G. Brodin, A. Kemp, and B. Peng, “iPLOT - An intelligent pervasive location tracking system,” in *Crime and Security, 2006. The Institution of Engineering and Technology Conference on*, june 2006, pp. 408 –413. [3](#), [19](#), [40](#), [41](#)
- [17] N. Patwari, I. Hero, A.O., M. Perkins, N. Correal, and R. O’Dea, “Relative location estimation in Wireless Sensor Networks,” *Signal Processing, IEEE Transactions on*, vol. 51, no. 8, pp. 2137 – 2148, aug. 2003. [3](#), [19](#), [40](#), [41](#), [81](#)
- [18] IEEE, “IEEE Standard for Information Technology- Telecommunications and Information Exchange Between Systems- Local and Metropolitan Area Networks- Specific Requirements Part 15.4: Wireless Medium Access Control (MAC) and Physical Layer (PHY) Specifications for Low-Rate Wireless Personal Area Networks (WPANs),” *IEEE Std 802.15.4-2006 - Revision of IEEE Std 802.15.4-2003*, pp. 1–305, 2006. [4](#), [181](#)
- [19] A. F. Molisch, K. Balakrishnan, D. Cassioli, C. Chong, S. Emami, A. Fort, J. Karedal, J. Kunisch, H. Schantz, U. Schuster, and K. Siwiak, “IEEE802.15.4a channel model final report,,” in *IEEE 802.15.4a, Technical Report*, 2005. [4](#), [48](#), [54](#), [58](#)
- [20] B. Thorbjornsen, N. White, A. Brown, and J. Reeve, “Radio Frequency (RF) Time-of-Flight Ranging for Wireless Sensor Networks,” *Measurement Science and Technology*, vol. 21, no. 3, pp. 1–12, 2010. [4](#)
- [21] A. C. H. Arslan and M. Benedetto, *Ultra-Wideband Wireless Communication*. New Jersey, USA: Wiley Interscience, 2006. [5](#), [59](#)
- [22] N. He and C. Tepedelenlioglu, “Performance analysis of non-coherent UWB receivers at different synchronization levels,” *Wireless Communications, IEEE Transactions on*, vol. 5, no. 6, pp. 1266 –1273, june 2006. [5](#)

## REFERENCES

---

- [23] M.-K. Oh and J.-Y. Kim, "Ranging Implementation for IEEE 802.15.4a IR-UWB Systems," in *Vehicular Technology Conference, 2008. VTC Spring 2008. IEEE*, may 2008, pp. 1077–1081. 5
- [24] "Jennic NXP: IEEE 802.15.4 Wireless Networks, User Guide," 2006. [Online]. Available: [www.jennic.com/files/support\\_files/JN-UG-3024-IEEE802.15.4-1v1.pdf](http://www.jennic.com/files/support_files/JN-UG-3024-IEEE802.15.4-1v1.pdf) 5, 48, 54, 181
- [25] "IDTechEx Energy Harvesting and WSN Awards," Munich, Germany, 2011. [Online]. Available: <http://www.idtechex.com/energy-harvesting-and-storage-europe-11/> 5
- [26] "CC2531: System-on-Chip Solution for IEEE 802.15.4 and ZigBee Applications," 2010. [Online]. Available: <http://focus.ti.com/lit/ds/symlink/cc2531.pdf> 5
- [27] "MC1323x Low Cost SoC Remote Control Platform for the 2.4 GHz IEEE 802.15.4 Standard," 2011. [Online]. Available: <http://www.freescale.com> 5
- [28] "ATmega128RFA1: 8-bit Microcontroller with Low Power 2.4GHz Transceiver for ZigBee and IEEE 802.15.4," 2011. [Online]. Available: [http://www.atmel.com/dyn/resources/prod\\_documents/8266S.pdf](http://www.atmel.com/dyn/resources/prod_documents/8266S.pdf) 5
- [29] M. Kennedy, *The Global Positioning Systems and GIS (Second Edition)*. Traylor and Francis, 2002. 6, 8, 90, 93, 99, 192
- [30] R. Yarlagadda, I. Ali, N. Al-Dhahir, and J. Hershey, "GPS GDOP metric," *Radar, Sonar and Navigation, IEE Proceedings -*, vol. 147, no. 5, pp. 259–264, oct 2000. 23, 81, 93, 196
- [31] R. Nielsen, "Relationship between dilution of precision for point positioning and for relative positioning with GPS," *Aerospace and Electronic Systems, IEEE Transactions on*, vol. 33, no. 1, pp. 333–338, jan. 1997. 94, 97, 98
- [32] N. Blanco-Delgado and F. Nunes, "Satellite Selection Method for Multi-Constellation GNSS Using Convex Geometry," *Vehicular Technology, IEEE Transactions on*, vol. 59, no. 9, pp. 4289–4297, nov. 2010. 23, 81, 94, 98

## REFERENCES

---

- [33] N. Levanon, “Lowest GDOP in 2-D scenarios,” *Radar, Sonar and Navigation, IEE Proceedings -*, vol. 147, no. 3, pp. 149–155, jun 2000.
- [34] H. Sairo, D. Akopian, and J. Takala, “Weighted dilution of precision as quality measure in satellite positioning,” *Radar, Sonar and Navigation, IEE Proceedings -*, vol. 150, no. 6, pp. 430–436, dec. 2003.
- [35] D. Torrieri, “Statistical Theory of Passive Location Systems,” *Aerospace and Electronic Systems, IEEE Transactions on*, vol. AES-20, no. 2, pp. 183–198, march 1984. [23](#), [81](#)
- [36] H. Lee, “A Novel Procedure for Assessing the Accuracy of Hyperbolic Multilateration Systems,” *Aerospace and Electronic Systems, IEEE Transactions on*, vol. AES-11, no. 1, pp. 2–15, jan. 1975. [6](#), [90](#)
- [37] J. Caffery, J.J., “A new approach to the geometry of TOA location,” in *Vehicular Technology Conference, 2000. IEEE VTS-Fall VTC 2000. 52nd*, vol. 4, 2000, pp. 1943–1949 vol.4. [7](#), [126](#)
- [38] S. Gezici and Z. Sahinoglu, “Uwb geolocation techniques for ieee 802.15.4a personal area networks,” *MERL Technical report*, Aug. 2004. [7](#), [126](#)
- [39] Y.-T. Chan, H. Yau Chin Hang, and P. chung Ching, “Exact and approximate maximum likelihood localization algorithms,” *Vehicular Technology, IEEE Transactions on*, vol. 55, no. 1, pp. 10–16, jan. 2006. [7](#), [126](#)
- [40] C. Chang and A. Sahai, “Estimation bounds for localization,” in *Sensor and Ad Hoc Communications and Networks, 2004. IEEE SECON 2004. 2004 First Annual IEEE Communications Society Conference on*, oct. 2004, pp. 415–424. [7](#), [126](#), [131](#), [132](#), [134](#)
- [41] T. Jia and R. Buehrer, “A new Cramer-Rao lower bound for TOA-based localization,” in *Military Communications Conference, 2008. MILCOM 2008. IEEE*, nov. 2008, pp. 1–5. [7](#), [126](#), [132](#), [194](#), [211](#), [216](#)
- [42] S. Dulman, A. Baggio, P. J. M. Havinga, and K. Langendoen, “A geometrical perspective on localization,” in *Mobile Computing and Networking, 2008*, pp. 85–90. [7](#), [23](#)

## REFERENCES

---

- [43] M. Spirito, “On the accuracy of cellular mobile station location estimation,” *Vehicular Technology, IEEE Transactions on*, vol. 50, no. 3, pp. 674–685, may 2001. 7, 23, 84
- [44] J. Hightower, C. Vakili, G. Borriello, and R. Want, “Design and Calibration of the SpotON Ad-Hoc Location Sensing System,” 2001. 8
- [45] K. Whitehouse and D. Culler, “Macro-calibration in sensor/actuator networks,” *Mob. Netw. Appl.*, vol. 8, pp. 463–472, August 2003. [Online]. Available: <http://dx.doi.org/10.1023/A:1024548100497> 8
- [46] J. Caratori, M. Francois, N. Samama, ervisch Picois, and Alexandre, “UP-GRADE RnS Indoor Positioning System in an Office Building,” in *Proceedings of the 17th International Technical Meeting of the Satellite Division of The Institute of Navigation (ION GNSS 2004)*, ser. IONGNSS 2004. Manassas, VA, USA: ION, 2004, pp. 1959–1969. 8, 192
- [47] M. Fukumoto and M. Shinagawa, “CarpetLAN: A Novel Indoor Wireless(-like) Networking and Positioning System,” in *UbiComp 2005: Ubiquitous Computing*, ser. Lecture Notes in Computer Science, M. Beigl, S. Intille, J. Rekimoto, and H. Tokuda, Eds. Springer Berlin / Heidelberg, 2005, vol. 3660, pp. 903–903. 8, 192
- [48] A. Harter, A. Hopper, P. Steggles, A. Ward, and P. Webster, “The anatomy of a context-aware application,” in *Proceedings of the 5th annual ACM/IEEE international conference on Mobile computing and networking*, ser. MobiCom '99. New York, NY, USA: ACM, 1999, pp. 59–68. [Online]. Available: <http://doi.acm.org/10.1145/313451.313476> 8, 19, 22, 34
- [49] N. B. Priyantha, A. Chakraborty, and H. Balakrishnan, “The Cricket location-support system,” in *MobiCom '00: Proceedings of the 6th annual international conference on Mobile computing and networking*. New York, NY, USA: ACM, 2000, pp. 32–43. 8, 19, 22, 34, 192
- [50] R. Mautz, “Overview of Current Indoor Positioning Systems,” *Geodesy And Cartography*, vol. 35, no. 1, pp. 18–22, 2009. 8, 9, 34

## REFERENCES

---

- [51] S. Zirari, P. Canalda, and F. Spies, “A Very First Geometric Dilution of Precision Proposal for Wireless Access Mobile Networks,” in *Advances in Satellite and Space Communications, 2009. SPACOMM 2009. First International Conference on*, july 2009, pp. 162 –167. [9](#), [192](#)
- [52] C.-D. Wann and H.-C. Chin, “Hybrid TOA/RSSI Wireless Location with Unconstrained Nonlinear Optimization for Indoor UWB Channels,” in *Wireless Communications and Networking Conference, 2007.WCNC 2007. IEEE*, march 2007, pp. 3940 –3945. [9](#), [193](#)
- [53] C. Kaplan, Elliott; Hegarty, *Understanding GPS, Principles and Applications*. Norwood, MA, USA: Artech House Publishers, 2006. [15](#), [80](#), [94](#), [96](#), [97](#), [98](#), [99](#)
- [54] Z. Sahinoglu, S. Gezici, and I. Guvenc, *Ultra-Wideband Positioning Systems: Theoretical Limits, Ranging Algorithms, and Protocols*. Cambridge, UK: Cambridge University Press, 2008. [16](#)
- [55] S. Figueuras, Joao; Frattasi, *Mobile Positioning and Tracking - From Conventional to Cooperative Techniques (1st Edition)*. John Wiley and Sons Ltd, 2010. [16](#), [17](#), [18](#), [21](#), [23](#), [41](#)
- [56] J. Hightower and G. Borriello, “Location systems for ubiquitous computing,” *Computer*, vol. 34, no. 8, pp. 57 –66, aug 2001. [17](#), [25](#), [80](#), [81](#)
- [57] I. Amundson, J. Sallai, X. D. Koutsoukos, and Á. Lédeczi, “Radio Interferometric Angle of Arrival Estimation,” in *European Conference on Wireless Sensor Networks (EWSN)*, 2010, pp. 1–16. [18](#)
- [58] N. B. Priyantha, A. K. Miu, H. Balakrishnan, and S. Teller, “The cricket compass for context-aware mobile applications,” in *Proceedings of the 7th annual international conference on Mobile computing and networking*, ser. MobiCom '01. New York, NY, USA: ACM, 2001, pp. 1–14. [Online]. Available: <http://doi.acm.org/10.1145/381677.381679> [18](#)

## REFERENCES

---

- [59] N. Patwari, J. Ash, S. Kyperountas, I. Hero, A.O., R. Moses, and N. Correal, “Locating the nodes: cooperative localization in wireless sensor networks,” *Signal Processing Magazine, IEEE*, vol. 22, no. 4, pp. 54 – 69, july 2005. 18, 56
- [60] D. Koks, “Numerical Calculations for Passive Geolocation Scenarios,” 2007. [Online]. Available: <http://www.dsto.defence.gov.au/publications/4949/DSTO-RR-0319.pdf> 18
- [61] C. Ladha, B. Sharif, and C. Tsimenidis, “Mitigating propagation errors for indoor positioning in wireless sensor networks,” in *Mobile Adhoc and Sensor Systems, 2007. MASS 2007. IEEE International Conference on*, oct. 2007, pp. 1 –6. 20, 200
- [62] P. Barsocchi, S. Lenzi, S. Chessa, and G. Giunta, “A novel approach to indoor rssi localization by automatic calibration of the wireless propagation model,” in *Vehicular Technology Conference, 2009. VTC Spring 2009. IEEE 69th*, april 2009, pp. 1 –5. 200
- [63] G. Zanca, F. Zorzi, A. Zanella, and M. Zorzi, “Experimental comparison of RSSI-based localization algorithms for indoor wireless sensor networks,” in *Proceedings of the workshop on Real-world wireless sensor networks*, ser. REALWSN '08. New York, NY, USA: ACM, 2008, pp. 1–5. [Online]. Available: <http://doi.acm.org/10.1145/1435473.1435475> 20, 200
- [64] Z. Fang, Z. Zhao, D. Geng, Y. Xuan, L. Du, and X. Cui, “RSSI variability characterization and calibration method in wireless sensor network,” in *Information and Automation (ICIA), 2010 IEEE International Conference on*, june 2010, pp. 1532 –1537. 20
- [65] M. Bal, M. Liu, W. Shen, and H. Ghenniwa, “Localization in cooperative Wireless Sensor Networks: A review,” in *Computer Supported Cooperative Work in Design, 2009. CSCWD 2009. 13th International Conference on*, april 2009, pp. 438 –443. 21, 22, 25, 26

## REFERENCES

---

- [66] R. Want, A. Hopper, V. Falcao, and J. Gibbons, “The active badge location system,” *ACM Trans. Inf. Syst.*, vol. 10, pp. 91–102, January 1992. [22](#), [33](#), [34](#), [192](#)
- [67] D. Moore, J. Leonard, D. Rus, and S. Teller, “Robust distributed network localization with noisy range measurements,” in *Proceedings of the 2nd international conference on Embedded networked sensor systems*, ser. SenSys ’04. New York, NY, USA: ACM, 2004, pp. 50–61. [22](#), [125](#)
- [68] R. Fan, H. Jiang, S. Wu, and N. Zhang, “Robust Localization in Wireless Sensor Networks,” in *Communications, 2008. ICC ’08. IEEE International Conference on*, may 2008, pp. 4209 –4213. [22](#), [81](#)
- [69] L.-C. Chu, P.-H. Tseng, and K.-T. Feng, “GDOP-Assisted Location Estimation Algorithms in Wireless Location Systems,” in *Global Telecommunications Conference, 2008. IEEE GLOBECOM 2008. IEEE*, dec 2008, pp. 1 –5. [23](#), [84](#)
- [70] J. Schroeder, S. Galler, K. Kyamakya, and K. Jobmann, “Practical considerations of optimal three-dimensional indoor localization,” in *Multisensor Fusion and Integration for Intelligent Systems, 2006 IEEE International Conference on*, sept. 2006, pp. 439 –443.
- [71] W.-W. Ji and Z. Liu, “Optimum Geometry Selection in Mobile Sensor Networks,” in *Communication Technology, 2006. ICCT ’06. International Conference on*, nov. 2006, pp. 1 –4. [23](#)
- [72] A. Bishop, B. Fidan, B. Anderson, P. Pathirana, and K. Dogancay, “Optimality Analysis of Sensor-Target Geometries in Passive Localization: Part 2 - Time-of-Arrival Based Localization,” in *Intelligent Sensors, Sensor Networks and Information, 2007. ISSNIP 2007. 3rd International Conference on*, dec. 2007, pp. 13 –18. [23](#), [24](#), [25](#)
- [73] A. N. Bishop, B. Fidan, B. D. O. Anderson, K. Doğançay, and P. N. Pathirana, “Optimality analysis of sensor-target localization geometries,” *Automatica*, vol. 46, pp. 479–492, March 2010. [Online]. Available: <http://dx.doi.org/10.1016/j.automatica.2009.12.003> [23](#), [25](#)

## REFERENCES

---

- [74] A. Bishop and P. Jensfelt, “An optimality analysis of sensor-target geometries for signal strength based localization,” in *Intelligent Sensors, Sensor Networks and Information Processing (ISSNIP), 2009 5th International Conference on*, dec. 2009, pp. 127–132. [25](#)
- [75] T. He, C. Huang, B. M. Blum, J. A. Stankovic, and T. Abdelzaher, “Range-free localization schemes for large scale sensor networks,” in *MobiCom ’03: Proceedings of the 9th annual international conference on Mobile computing and networking*. New York, NY, USA: ACM, 2003, pp. 81–95. [25](#)
- [76] L. Lazos and R. Poovendran, “SeRLoc: secure range-independent localization for wireless sensor networks,” in *WiSe ’04: Proceedings of the 3rd ACM workshop on Wireless security*. New York, NY, USA: ACM, 2004, pp. 21–30. [25](#)
- [77] Y.-T. Chan, H. Yau Chin Hang, and P. chung Ching, “Exact and approximate maximum likelihood localization algorithms,” *Vehicular Technology, IEEE Transactions on*, vol. 55, no. 1, pp. 10–16, jan. 2006. [28](#), [29](#), [30](#), [84](#)
- [78] S. Duggal, *A Surveying*. Tata McGraw-Hill Education, 2004. [30](#)
- [79] D. C. Montgomery, G. C. Runger, and N. F. Hubele, *Engineering Statistics*. John Wiley & Sons; 4th Edition edition, 2007. [31](#)
- [80] M. Youssef and A. Agrawala, “The Horus WLAN location determination system,” in *Proceedings of the 3rd international conference on Mobile systems, applications, and services*, ser. MobiSys ’05. New York, NY, USA: ACM, 2005, pp. 205–218. [Online]. Available: <http://doi.acm.org/10.1145/1067170.1067193> [35](#)
- [81] “KidSpotter,” Dublin, Ireland, 2011. [Online]. Available: <http://kidspotter.com/> [36](#)
- [82] S. Schaefer, “Secure trade lane: a sensor network solution for more predictable and more secure container shipments,” in *Companion to the 21st ACM SIGPLAN symposium on Object-oriented programming systems, languages, and applications*, ser. OOPSLA ’06.

## REFERENCES

---

- New York, NY, USA: ACM, 2006, pp. 839–845. [Online]. Available: <http://doi.acm.org/10.1145/1176617.1176732> 36
- [83] D. Gasca and M. Yarza, “Wireless Sensor Networks to Control Radiation Levels,” Spain, 2011. [Online]. Available: <http://www.libelium.com/libeliumworld/articles/111091091717> 37
- [84] “Xbox 360 World Premier Biggest Blockbuster Games and Entertainment,” Los Angeles, 2011. [Online]. Available: <http://www.xbox.com> 37
- [85] A. Joshi, I. VishnuKanth, N. Samdaria, S. Bagla, and P. Ranjan, “GPS-less animal tracking system,” in *Wireless Communication and Sensor Networks, 2008. WCSN 2008. Fourth International Conference on*, dec. 2008, pp. 120–125. 37
- [86] S. Schultz, “Engineers and biologists design wireless devices to unlock secrets of animal kingdom,” Princeton, 2002.
- [87] J. Li, J. Fang, Y. Fan, and C. Zhang, “Design on the monitoring system of physical characteristics of dairy cattle based on zigbee technology,” in *World Automation Congress (WAC), 2010*, sept. 2010, pp. 63–66. 37
- [88] M. Battelli and S. Basagni, “Localization for Wireless Sensor Networks: Protocols and Perspectives,” in *Electrical and Computer Engineering, 2007. CCECE 2007. Canadian Conference on*, april 2007, pp. 1074–1077. 40, 80
- [89] K. Chintalapudi, A. Dhariwal, R. Govindan, and G. Sukhatme, “Ad-hoc localization using ranging and sectoring,” in *INFOCOM 2004. Twenty-third Annual Joint Conference of the IEEE Computer and Communications Societies*, vol. 4, march 2004, pp. 2662–2672 vol.4. 41
- [90] T. Karalar and J. Rabaey, “An RF ToF Based Ranging Implementation for Sensor Networks,” in *Communications, 2006. ICC '06. IEEE International Conference on*, vol. 7, june 2006, pp. 3347–3352. 41, 55, 56

## REFERENCES

---

- [91] K. Bronk and J. Stefanski, “Bad Geometry Influence on Positioning Accuracy in Wireless Networks,” in *EUROCON, 2007. The International Conference on Computer as a Tool*;, sept. 2007, pp. 1131 –1135. [41](#), [81](#), [93](#)
- [92] S. Lanzisera, D. Lin, and K. Pister, “RF Time of Flight Ranging for Wireless Sensor Network Localization,” in *Intelligent Solutions in Embedded Systems, 2006 International Workshop on*, june 2006, pp. 1 –12. [41](#), [57](#), [128](#)
- [93] P. Barsocchi, S. Lenzi, S. Chessa, and G. Giunta, “Virtual Calibration for RSSI-Based Indoor Localization with IEEE 802.15.4,” in *Communications, 2009. ICC '09. IEEE International Conference on*, june 2009, pp. 1 –5. [41](#)
- [94] T. S. Rappaport, *Wireless Communications: Principles and Practice (2nd Edition)*. New Jersey, USA: Prentice Hall PTR, 2002. [41](#), [43](#), [48](#), [199](#)
- [95] C. Groß, H. Hermanns, and R. Pulungan, “Does clock precision influence ZigBee’s energy consumptions?” in *Proceedings of the 11th international conference on Principles of distributed systems*, ser. OPODIS’07. Berlin, Heidelberg: Springer-Verlag, 2007, pp. 174–188. [42](#)
- [96] D. Dardari, A. Conti, U. Ferner, A. Giorgetti, and M. Win, “Ranging With Ultrawide Bandwidth Signals in Multipath Environments,” *Proceedings of the IEEE*, vol. 97, no. 2, pp. 404 –426, feb. 2009. [42](#)
- [97] T. Stoyanova, F. Kerasiotis, A. Prayati, and G. Papadopoulos, “A Practical RF Propagation Model for Wireless Network Sensors,” in *Sensor Technologies and Applications, 2009. SENSORCOMM '09. Third International Conference on*, june 2009, pp. 194 –199. [44](#)
- [98] A. Goldsmith, *Wireless Communications*. New York, NY, USA: Cambridge University Press, 2005. [44](#), [48](#), [60](#), [199](#)
- [99] B. H. Liu, B. Otis, S. Challa, P. Axon, C. T. Chou, and S. Jha, “On the fading and shadowing effects for wireless sensor networks,” in *Mobile Adhoc and Sensor Systems (MASS), 2006 IEEE International Conference on*, oct. 2006, pp. 51 –60. [44](#)

## REFERENCES

---

- [100] F. S., *Zigbee Wireless Networks and Transceivers*. Burlington, USA: NEWNES, Elsevier Inc, 2008. 46, 61
- [101] M. Ab-Rahman, M. Ibrahim, and A. Rahni, “Thermal Noise Effect in FTTH Communication Systems,” in *Telecommunications, 2008. AICT '08. Fourth Advanced International Conference on*, june 2008, pp. 364 –370. 46
- [102] A. Karl, Holger; Willing, *Protocols and Architecture for Wireless Sensor Networks*. John Wiley and Sons Ltd, 2007. 47, 82, 84, 85, 88
- [103] L. Geosystems, “Leica DISTO A5 The Versatile One For in and outdoor applications,” 2009. [Online]. Available: [http://www.laser-measure.co.uk/downloads/leicadisto\\_a5.pdf](http://www.laser-measure.co.uk/downloads/leicadisto_a5.pdf) 50
- [104] D. Gabor, “Theory of communication. Part 1: The analysis of information,” *Electrical Engineers - Part III: Radio and Communication Engineering, Journal of the Institution of*, vol. 93, no. 26, pp. 429 –441, november 1946. 56
- [105] D. Hill and D. Haworth, “Accurate measurement of low signal-to-noise ratios using a superheterodyne spectrum analyzer,” *Instrumentation and Measurement, IEEE Transactions on*, vol. 39, no. 2, pp. 432 –435, apr 1990. 59
- [106] H. Maheshwari and A. Kemp, “On the Enhanced Ranging Performance for IEEE 802.15.4 Compliant WSN Devices,” in *New Technologies, Mobility and Security (NTMS), 2011 4th IFIP International Conference on*, feb. 2011, pp. 1 –5. 66
- [107] Y. Qi and H. Kobayashi, “On relation among time delay and signal strength based geolocation methods,” in *Global Telecommunications Conference, 2003. GLOBECOM '03. IEEE*, vol. 7, dec. 2003, pp. 4079 – 4083 vol.7. 76
- [108] M. Rahman and L. Kleeman, “Paired Measurement Localization: A Robust Approach for Wireless Localization,” *Mobile Computing, IEEE Transactions on*, vol. 8, no. 8, pp. 1087 –1102, aug. 2009. 80

## REFERENCES

---

- [109] A. Savvides, C.-C. Han, and M. B. Strivastava, “Dynamic fine-grained localization in Ad-Hoc networks of sensors,” in *Proceedings of the 7th annual international conference on Mobile computing and networking*, ser. Mobi-Com '01. New York, NY, USA: ACM, 2001, pp. 166–179. [80](#), [106](#)
- [110] B. Peng, R. Mautz, A. Kemp, W. Ochieng, and Q. Zeng, “On the Effect of Localization Errors on Geographic Routing in Sensor Networks,” in *Communications, 2008. ICC '08. IEEE International Conference on*, may 2008, pp. 3136 –3140. [81](#)
- [111] S. Venkatesh and R. Buehrer, “Multiple-access insights from bounds on sensor localization,” in *World of Wireless, Mobile and Multimedia Networks, 2006. WoWMoM 2006. International Symposium on a*, mar 2006, pp. 10 pp. –12. [81](#)
- [112] W. Foy, “Position-Location Solutions by Taylor-Series Estimation,” *Aerospace and Electronic Systems, IEEE Transactions on*, vol. AES-12, no. 2, pp. 187 –194, march 1976. [84](#)
- [113] Y. Chan and K. Ho, “A simple and efficient estimator for hyperbolic location,” *Signal Processing, IEEE Transactions on*, vol. 42, no. 8, pp. 1905 –1915, aug 1994. [84](#)
- [114] I. Guvenc and C.-C. Chong, “A Survey on TOA Based Wireless Localization and NLOS Mitigation Techniques,” *Communications Surveys Tutorials, IEEE*, vol. 11, no. 3, pp. 107 –124, quarter 2009. [85](#), [93](#)
- [115] K. Cheung, H. So, W.-K. Ma, and Y. Chan, “Least squares algorithms for time-of-arrival-based mobile location,” *Signal Processing, IEEE Transactions on*, vol. 52, no. 4, pp. 1121 – 1130, april 2004. [87](#), [88](#)
- [116] I. Guvenc, S. Gezici, F. Watanabe, and H. Inamura, “Enhancements to Linear Least Squares Localization Through Reference Selection and ML Estimation,” in *Wireless Communications and Networking Conference, 2008. WCNC 2008. IEEE*, april 2008, pp. 284 –289. [88](#)

## REFERENCES

---

- [117] Z. Chaczko, R. Klempos, J. Nikodem, and M. Nikodem, “Methods of Sensors Localization in Wireless Sensor Networks,” in *Engineering of Computer-Based Systems, 2007. ECBS '07. 14th Annual IEEE International Conference and Workshops on the*, march 2007, pp. 145–152. [88](#), [125](#)
- [118] H. K. Maheshwari, A. H. Kemp, and Q. Zeng, “Range Based Real Time Localization in Wireless Sensor Networks,” in *Wireless Networks, Information Processing and Systems*, ser. Communications in Computer and Information Science, D. M. A. Hussain, A. Q. K. Rajput, B. S. Chowdhry, and Q. Gee, Eds. Springer Berlin Heidelberg, 2009, vol. 20, pp. 422–432. [121](#)
- [119] H. Maheshwari and A. Kemp, “Comparative Performance Analysis of Localization Using Optimal and Sub-optimal Lateration in WSNs,” in *Third International Conference on Next Generation Mobile Applications, Services and Technologies, 2009. NGMAST '09.*, sept. 2009, pp. 369–374. [125](#)
- [120] F. Engel and M. Hedley, “A comparison of cooperative localisation techniques for wireless mobile sensor networks,” in *Communications and Information Technologies, 2007. ISCIT '07. International Symposium on*, oct. 2007, pp. 887–892. [125](#)
- [121] V. Isler and R. Bajcsy, “The Sensor Selection Problem for Bounded Uncertainty Sensing Models,” *Automation Science and Engineering, IEEE Transactions on*, vol. 3, no. 4, pp. 372–381, oct. 2006. [125](#)
- [122] C.-H. Chang and W. Liao, “Revisiting Relative Location Estimation in Wireless Sensor Networks,” in *Communications, 2009. ICC '09. IEEE International Conference on*, june 2009, pp. 1–5. [126](#)
- [123] M. S. Haykin, *Modern Wireless Communications*. Pearson Prentice Hall, 2005. [128](#)
- [124] S. Gezici, Z. Tian, G. Giannakis, H. Kobayashi, A. Molisch, H. Poor, and Z. Sahinoglu, “Localization via ultra-wideband radios: a look at positioning aspects for future sensor networks,” *Signal Processing Magazine, IEEE*, vol. 22, no. 4, pp. 70–84, july 2005. [129](#)

## REFERENCES

---

- [125] S. M. Kay, *Fundamentals of Statistical Signal Processing: Estimation Theory*. Upper Saddle River, NJ: Prentice Hall, 1993. 129, 130
- [126] “ S131XX-2450 Data Sheet,” 2009. [Online]. Available: <ftp://ftp2.nearson.com/Drawings/Antenna/S131CL-L-XXX-2450S.pdf> 184
- [127] I. Rasool, H. K. Maheshwari, and A. H. Kemp, “Error distribution of range measurements in Wireless Sensor Networks (WSNs),” in *IEEE 21st International Symposium on Personal Indoor and Mobile Radio Communications (PIMRC), 2010*, sept. 2010, pp. 1990–1995. 237
- [128] X. Li, “RSS-Based Location Estimation with Unknown Pathloss Model,” *Wireless Communications, IEEE Transactions on*, vol. 5, no. 12, pp. 3626–3633, december 2006. 238
- [129] M. I. V. Martnez, B. T. Sieskul, F. Zheng, and T. Kaiser, “A hybrid SS-ToA wireless geolocation based on path attenuation under imperfect path loss exponent,” in *n Proc. 18th European Signal Processing Conference 2010*, ser. EUSIPCO 2010, August 2010, pp. 681–685. 238